EUROPEAN ORGANIZATION FOR NUCLEAR RESEARCH

CERN/AT/95-44 (ET)

CONCEPTUAL DESIGN OF A FAST NEUTRON OPERATED HIGH POWER ENERGY AMPLIFIER

C. Rubbia, J.A. Rubio, S. Buono[1], F. Carminati, N. Fiétier[2], J. Galvez, C. Gelès, Y. Kadi, R. Klapisch, P. Mandrillon[2], J.P. Revol and Ch. Roche

Abstract

The basic concept and the main practical considerations of an Energy Amplifier (EA) have been exhaustively described in Ref. [1]. Here the realisation of the EA is further explored and schemes are described which offer a high gain, a large maximum power density and an extended burn-up, well in excess of 100 GW × day/t corresponding to about five years at full power operation with no intervention on the fuel core. Most of these benefits stem from the use of fast neutrons, as already proposed in Ref. [2].

The EA operates indefinitely in a closed cycle, namely the discharge of a fuel load, with the exception of fission fragments, is re-injected in the sub-critical unit with the addition of natural Thorium to compensate for the burnt fuel. After many cycles an equilibrium is reached, in which the Actinide concentrations are the balance between burning and "incineration". The fuel is used much more efficiently, namely the power obtained from 780 kg of Thorium is roughly the same as the one from 200 tons of native Uranium and a PWR (33 GW × day/t of burn-up). The probability of a criticality accident is suppressed since the device operates at all times far away from it. Spontaneous convective cooling by the surrounding air makes a "melt-down" leak impossible.

An EA module consists of a 1500 MW_{th} unit with its dedicated 1.0 GeV proton accelerator of 12.5 mA. A compact, highly reliable and modular Cyclotron has been designed. A plant may be made of several such modules. For instance a cluster of three such modular units will produce about 2,000 MWe of primary electrical power. A relevant feature of our design is that it is based on natural convection to remove the heat generated inside the core. The EA is a large, passive device in which a proton beam is dumped and the heat generated by nuclear cascades is extracted, without other major elements of variability. The delivered power is controlled exclusively by the current of the accelerator. The fuel needs no access during the whole burn-up and it may be kept sealed up as a non-proliferation safeguard measure. Contrary to Fusion, there are no major technological barriers.

After ≈ 700 years the radio-toxicity left is about 20,000× smaller than the one of an ordinary Pressurised Water Reactor (PWR) for the same energy. Geological storage (10^6 years) is virtually eliminated or at least strongly reduced [≤ 500 Ci/(GW_e × y) after 1000 years]. It could be further reduced (< 35 Ci) "incinerating" some of the nuclides. Radioactivity dose to individuals truncated to 10,000 years and due to operation is about 1/330 of the one of PWR and about 1/33 of Coal burning.

Geneva, 29th September, 1995

---

[1] Sincrotrone Trieste, Trieste, Italy

[2] Laboratoire du Cyclotron, Nice, France

Contents

1.— Introduction.

The principle of operation of the Energy Amplifier (EA) has been described in detail in Refs. [1-3]. The present paper is aimed at the demonstration of the practical feasibility of an EA with power and power density which are comparable to the ones of the present generation of large Pressurised Light Water Reactors (PWR). This is only possible with fast neutrons [2].

Greenhouse induced Global Warming concerns related to a massive use of Fossil Fuels may lead to a new call for nuclear revival. But a much larger share of energy produced by conventional Nuclear methods (PWR) will sharpen concerns and enhance many of the problems which must be solved before extending its use. We believe that most of the criteria for a revival of nuclear power are very tough:

(1) Extremely high level of *inherent safety;*

(2)*Minimal production of long lived waste* and elimination of the need of the geologic repositories;

(3)*High resistance to diversion,* since latent proliferation is a major concern.

(4)*More efficient use* of a widely available natural fuel, without the need of isotopic separation.

(5)*Lower cost of the heat* produced and *higher operating temperature* than conventional PWRs in order to permit competitive generation of substitutes to fossil fuels [4]. Substitution fuels are necessary to allow a widespread utilisation of the energy source and to permit retrofitting of existing facilities, now operating with CO_2 producing fuels.

Our design of an EA has these objectives as goals and it is intended as proof that they can be met fully. The primary fuel is natural Thorium which is completely burnt after a number of fuel cycles through the EA. Actinides present in the fuel discharge at the end of a fuel cycle are re-injected in the EA and become the "seeds" for the subsequent cycle. This ensures a very efficient use of the primary fuel element[1]. This objective is identical to the one eventually met by Fast Breeders. Compared to the consumption of natural fuel material, the EA is about 250 times more efficient than the present PWRs based on an open fuel cycle.

Nuclear power has successfully developed the methods of retaining large amounts of radioactivity within the power plant and in isolation with the biosphere.

---

[1] The heat produced burning 70.3 kg of Thorium in the EA is equal to the one of 1 million barrels of oil

The limited amount of fuel material of the EA and the sealed, passive nature of the device further simplifies the realisation of such a concept. The fractions of radioactivity actually injected in the environment during (1) mining, (2) operation and (3) reprocessing and refuelling are considered first. Preventive measures to eliminate unwanted accidents and their possible consequences on the environment will be considered later on.

The radio-toxicity released by a Thorium driven EA is much smaller than the one of the PWR related throw-away cycle [1] [2]. In the phase of the fuel extraction and preparation, it is about $10^{-3} \div 10^{-4}$ for the same delivered energy, since a much smaller amount of Thorium is required (0.78 ton vs. 200 tons of Uranium for 3 $GW_{th} \times$ year) in the first place and which is much less toxic to extract [5]. The toxicity released in form of waste at the back-end of the cycle for Actinides is reduced to the very tiny fraction lost during fuel re-cycling and reprocessing. Among fission fragments, excluding the short lived and stable elements, there are a few elements which are medium lived ($\tau_{1/2} \approx 30$ years, ^{90}Sr- ^{90}Y, ^{137}Cs, etc.) and some others (^{99}Tc, ^{135}Cs, ^{129}I, etc.) which are truly long lived. The policy we propose to follow is to store in man-watched, secular repositories for several centuries the medium lived in order to isolate them from the biosphere and to promote a vigorous research and development of methods of incinerating the bulk of the long lived FFs with the help of a fraction of the neutron flux of the EA or with dedicated burners [6]. Therefore, and contrary to the PWR related throw-away cycle, the need for a Geologic Repository is virtually eliminated.

UNSCEAR [7] has estimated collective radioactivity doses to the population associated to various forms of energy production. Coal burning emits radioactivity in fumes and dust, resulting in a typical, *collective radiation exposure* of 20 man Sv $(GW_e\ y)^{-1}$. The practice of using coal ashes for concrete production adds as much as 2.5×10^4 man Sv $(GW_e\ y)^{-1}$. In the case of the PWR throw-away cycle the estimated dose is 200 man Sv $(GW_e\ y)^{-1}$, with the main contribution coming from the mining and preparation of the fuel[2]. Accidents which have plagued some of the present Nuclear Power stations and which are expected to be absent because of the new features of the EA, have added as much as 300 man Sv $(GW_e\ y)^{-1}$, bringing the toll of Nuclear Energy to about 500 man Sv $(GW_e\ y)^{-1}$. Translating the figures of Ref. [7] to the conditions of the EA, we arrive at much smaller collective doses, namely 2.75

[2]The main nuclide contributions in the nuclear fuel cycle are Radon from Mill Tailings (150 man Sv/GW/y) and reactor operation and reprocessing (50 man Sv/GW/y). The potential accumulation of collective radiation doses in the far future from the practice of disposing the long lived waste (geologic storage) is not included in the UNSCEAR estimates, since it is subject to major uncertainties.

man Sv $(GW_e\ y)^{-1}$ for the local and regional dose and 0.44 ÷ 1.42 man Sv $(GW_e\ y)^{-1}$ for the global dose, depending on the type of mineral used. The total radioactivity absorbed by the population *is about one order of magnitude smaller than if the same energy is produced by burning Coal,* even if the ashes are correctly handled. In the case of the Coal option we must add the emissions of pollutants like dust, SO_2 etc. and their toll on the Greenhouse effect.

A novel element of our design is the presence of the proton beam. A recent experiment has specified the required characteristics of such an accelerator [3]. The accelerated particles are protons (there is little or no advantage in using more sophisticated projectiles) preferably of a minimum kinetic energy of the order of 1 GeV. The average accelerated current is in the range of 10 ÷ 15 mA, about one order of magnitude above the present performance[3] of the PSI cyclotron [8]. This current is lower by one order of magnitude than the requirements of most of the accelerator-driven projects based on c-w LINAC [9]. In view of the present developments of high-intensity cyclotrons and the outstanding results obtained at PSI [8], we have chosen a three-stage cyclotron accelerator. In the design particular attention has been given to the need of a high reliability and simplicity of operation. The experience accumulated in the field at CERN, PSI and elsewhere indicates that this goal is perfectly achievable. The expected over-all efficiency, namely the beam power over the mains load is of the order of 40%. The penetration of the beam in the EA vessel is realised through an evacuated tube and a special Tungsten window, which is designed to sustain safely both radiation damage and the thermal stress due to the beam heating. As discussed in more detail later on, the passive safety features of the device can be easily extended to these new elements.

Since the accelerator is relatively small and simple to operate, if more current is needed, several of these units can be used in parallel, with a corresponding increase of the overall reliability of the complex. In this case, the beams are independently brought to interact in the target region of the EA.

For definiteness, in the present conceptual design of the EA we have chosen a nominal unit capacity of 1500 MW_{th}. This corresponds to about 675 MWatt of primary electrical power with "state of the art" turbines and an outlet temperature of the order of 550 ÷ 600 ^oC. The thermodynamical efficiency of ≈ 45% is substantially higher than the one of a PWR and it is primarily due to the present higher temperature of operation. The general concept of the EA is shown in Figure 1.1.

---

[3] An improvement programme is on its way to increase the average current to about 6 mA.

The nominal energetic gain[4] of the EA is set to G = 120 corresponding to a multiplication coefficient k = 0.98. The nominal beam current for 1500 MW_{th} is then 12.5 mA $\times$ GeV[5]. In practice the proton accelerator must be able to produce eventually up to 20 mA $\times$GeV in order to cope with the inevitable variations of performance during the lifetime of the fuel. Such accelerator performance is essentially optimal for a chain of cascading cyclotrons. A significantly smaller current may not provide the required accelerator energetic efficiency; a higher current will require several machines in parallel. Hence, this size of the module is related, for a given gain, to the state of the art of the accelerator. The electric energy required to operate the accelerator is about 5% of the primary electric energy production. The choice of k is not critical. For instance an EA with k = 0.96 (G = 60) can produce the same thermal energy but with a fraction of re-circulated power about twice as large, namely 10% of the primary electricity, requiring two accelerators in parallel.

An energy generating module consists of a 1500 MW_{th} unit with its own dedicated 12.5 mA $\times$ GeV accelerator. An actual plant may be made of several such modules. For instance a cluster of three such modular units will produce about 2,000 MWatt of primary electrical power. Beams from the accelerators can be easily transported over the site and switched between units: a fourth, spare, accelerator should be added in order to ensure back-up reliability.

The modular approach has been preferred in several recent conceptual designs [10] of Sodium cooled fast reactors in the USA (ALMR, American Liquid Metal Reactor), Japan (MONJOU) and in Russia (BMN-170), for reasons of cost, speed of construction and licensing. Such modularity permits the use of the devices in relatively isolated areas. The power plant can be built in a well developed country and transported to the target area. Decommissioning of the device is also simplified. The European approach (EFR, European Fast Reactor) is more conservative and is based on a single, large volume pool for a nominal power in excess of 3,000 MW_{th}. Such an approach is possible also for the EA. In this case, because of the larger power, the beams from two accelerators will be simultaneously injected in the core of the EA. Both designs are robust, cost-effective and they incorporate many features which are the result of the extensive experience with smaller machines. They are designed for a number of different fuel configurations and they can easily

---

[4]The energetic gain G is defined as the thermal energy produced by the EA divided by the energy deposited by the proton beam.

[5]This notation is justified, since the energetic gain of the EA is almost independent of the proton kinetic energy, provided it is larger than about 1 GeV.

accommodate those appropriate to the EA. We have taken as "model" for our design many of the features of the ALMR. The ALMR was designed to provide high reliability for the key safety, including shutdown heat removal and containment. We intend to follow the same basic design, with, however, the added advantages of (1) sub-critical operation at all times (2) negative void coefficient of molten Lead (3) convection driven primary cooling system and (4) non reactive nature of Lead coolant when compared to Sodium.

The coolant medium is molten natural Lead operated in analogy with our (Sodium cooled) "models" at a maximum temperature of 600 ÷ 700 ^{o}C. In view of the high boiling temperature of Lead (1743 ^{o}C at n.p.t.) and the negative void coefficient of the EA, even higher temperatures may be considered, provided the fuel and the rest of the hardware are adequately designed. For instance direct Hydrogen generation via the sulphur-iodine method [4] requires an outlet temperature of the order of 800 ^{o}C. A higher operating temperature is also advantageous for electricity generation, since it may lead to an even better efficiency of conversion. Evidently, additional research and development work is required in order to safely adapt our present design to an increased operating temperature. In particular the cladding material of the fuel pins may require some changes, especially in view of the increased potential problems from corrosion and reduced structural strength. With these additions the present design should be capable of operating at temperatures well above the present figures.

A most relevant feature of our design is the possibility of using natural convection alone to remove all the heat produced inside the core. Convection cooling has been widely used in "swimming pool" reactors at small power levels. We shall show that an extension of this very safe method to the very large power of the EA is possible because of the unique properties of Lead, namely high density, large dilatation coefficient and large heat capacity. Convection is spontaneously and inevitably driven by (any) temperature difference. Elimination of all pumps in the primary loop is an important simplification and a contribution towards safety, since unlike pumps, convection cannot fail. In the convective mode, a very large mass of liquid Lead (≈ 10,000 tons), with an associated exceedingly large heat capacity[6] moves very slowly (≤ 2.0 m/s inside the core, about 1/3 of such speed elsewhere) transferring the heat from the top of the core to the heat exchangers located some 20

---

[6] The heat capacity of liquid Lead at constant pressure is about 0.14 Joule/gram/^{o}C. For an effective mass of ≈ 10^4 tons=10^{10} grams and a power of 1.5 GWatt (full EA power), the temperature rise is of the order of 1.0 ^{o}C/s. The mass flowing through the core for $\Delta T \approx$ 200 ^{o}C is 53.6 tons/sec, corresponding to some 1.5 minutes of full power to heat up the half of the coolant in the "cold" loop, in case the heat exchangers were to fail completely.

metres above and returning at a lower temperature ($\Delta T \approx -200\ ^oC$) from the heat exchangers to the bottom of the core.

The geometry of the EA main vessel is therefore relatively slim (6.0 m diameter) and very tall (30 m). The vessels, head enclosure and permanent internal structures are fabricated in a factory and shipped as an assembled unit to the site[7]. The relatively slender geometry enhances the uniformity of the flow of the liquid Lead and of the natural circulation for heat removal. The structure of the vessel must withstand the large weight of the liquid Lead. There are four 375 MW_{th} heat exchangers to transfer the heat from the primary Lead to the intermediate heat transport system. They are located above the core in an annular region between the support cylinder and the walls of the vessel.

The vessel is housed below floor level in an extraordinarily robust cylindrical silo geometry lined with thick concrete which acts also as ultimate container for the liquid Lead in case of the highly hypothetical rupture of the main vessel. In the space between the main vessel and the concrete wall the Reactor Vessel Air Cooling System (RVACS) is inserted. This system [11], largely inspired from the ALMR design, is completely passive and based on convection and radiation heat transfer. The whole vessel is supported at the top by anti-seismic absorbers. Even in the case of an intense earthquake the large mass of the EA will remain essentially still and the movement taken up by the absorbers.

The fuel is made of mixed oxides, for which considerable experience exists. More advanced designs have suggested the use of metallic fuels or of carbides [12]. These fuels are obviously possible also for an EA. We remark that the use of Zirconium alloys is not recommended since irradiation leads to transmutations into the isotope ^{93}Zr, which has a long half-life and which is impossible to incinerate without separating it isotopically from the bulk of the Zirconium metal. The choice of the chemical composition of the fuel is strongly related to the one of the fuel reprocessing method. A relative novelty of our machine when compared to ordinary PWRs is the large concentration of ThO_2 in the fuel and the corresponding production of a small but relevant amount of Protactinium. A liquid separation method called THOREX has been developed and tested on small irradiated ThO_2 fuel samples [13]. The extrapolation from the widely used PUREX process to THOREX is rather straightforward and this is why we have chosen it, at least at this stage. Methods based on pyro-electric techniques [14], which imply preference to metallic

[7] The shipping weight is about 1500 tons. Removable internal equipment is shipped separately and installed through the top head.

fuels, are most interesting, but they require substantial research and development work. Since the destination of the Actinides is now well defined i.e. to be finally burnt in the EA, the leakage of Actinides in the Fission Fragment stream must be more carefully controlled, since they are the only Actinides in the "Waste". We have assumed that a "leaked" fraction of 10^{-4} is possible for Uranium. The recycled fuel has a significant radio-activity. We have checked that the dose at contact is similar to the one of MOX fuels made of Uranium and Plutonium, already used in the Nuclear Industry.

The average power density in the fuel has been conservatively set to be $\rho = 55$ *Watt/gr-oxide*, namely about 1/2 the customary level of LMFBR[8] (ALMR, MONJOU, and EFR). The nominal power of 1500 MW_{th} requires then 27.3 tons of mixed fuel oxide. The fuel dwelling time is set to be 5 years equivalent at full power. The average fuel burn-up is then 100 GWatt day/ton-oxide. Since the fissile fuel is internally regenerated inside the bulk of the Thorium fuel, the properties of the fuel are far more constant than say in the case of a PWR. As shown later on, one can compensate to a first order the captures due to fission fragments, operating initially with a breeding ratio below equilibrium. All along the burn-up, the growth of the fissile fuel concentration counterbalances the poisoning due to fission fragments. *Therefore neither re-fuelling nor fuel shuffling appear necessary for the specified duration of the burn-up.*

No intervention is therefore foreseen on the fuel during the five years of operation, at the end of which it is fully replaced and reprocessed. Likewise in the "all-convective" approach there are no moving parts which require maintenance or surveillance. In short the *EA is a large, passive device in which a proton beam is dumped and the generated heat is extracted, without other major elements of variability.*

Safety and nuclear proliferation are universal concerns. In the case of conventional Nuclear Power, accidents have considerably increased the radioactivity exposure of individuals and the population [7]. The total nuclear power generated, 2000 GW $\times$ year, is estimated to have committed an effective dose of 400,000 man Sv from normal operation. Accidents at Windscale, TMI and Chernobyl have added 2000, 40 and 600,000 man Sv respectively. These types of accidents are no longer possible with the EA concept: Chernobyl is a criticality accident, impossible in a sub-critical device and TMI, a melt-down accident, is made impossible by the "intrinsic" safety of the EA.

---

[8] This choice is motivated by the relative novelty of the "all-convective" approach and the relative scarce experience with ThO_2 , when compared with UO_2.

A thermal run-off is the precursory sign of a number of potentially serious accidents. The present conceptual design is based on a swimming pool geometry where the heat generated by the nuclear cascade is extracted from the core by convection cooling, completely passive and occurring inevitably because of temperature differences. Thermal run-off is prevented, since a significant temperature rise due for instance to an insufficiency of the secondary cooling loop and of the ordinary controls will inevitably produce a corresponding dilatation of the liquid Lead. Because of the slim geometry of the vessel, the level of the swimming pool will rise by a significant amount (≈ 27 cm/100 ^{o}C), filling (through a siphon) additional volumes with molten Lead, namely :

(1)The Emergency Beam Dump Volume (EBDV), a liquid Lead "beam stopper" sufficiently massive as to completely absorb the beam some 20 metres away from the core and hence bring the EA safely to a stop. In the unlikely event that the beam window would accidentally break, molten Lead will also rise, so as to fill completely the pipe and the EBDV, thus removing the incoming proton beam from the core.

(2)A narrow gap normally containing thermally insulating Helium gas, located between the coolant and the outer wall of the vessel, which in this way becomes thermally connected to the coolant main convection loop. The outer wall of the EA will heat up and bleed the decay heat passively through natural convection and radiation to the environment (RVACS) [11]. This heat removal relies exclusively on natural convection heat transfer and natural draught on the air side.

(3)A scram device based on B_4C absorbers which are pushed into the core by the liquid Lead descending narrow tubes. These absorbers anchor the device firmly away from criticality.

These passive safety features are provided as a backup in case of failure of the active systems, namely of the main feed-back loop which adjusts the current in order to maintain constant the temperature at the exit of the primary cooling loop. Multiply backed-up but simple systems based on current transformers and physical limitations in the accelerator (available RF power in the cavities, space charge forces, etc.) sharply limit the maximum current increase that the accelerator can deliver. Were these methods all to fail, the corresponding increase of temperature will dilate significantly the Lead, activating the ultimate shut-off of the proton beam from the accelerator, the emergency cooling and the scram devices, before any limit is exceeded in the EA.

Normally the EA is well away from criticality at all times, there are no control bars (except the scram devices) and the power produced is directly controlled by the injected beam current. However in some unforeseen circumstances the EA may become critical. In itself, this is not an unacceptable though exceptional operation mode, provided the amount of power produced does not exceed the ratings of the EA. Indeed even a quite large reactivity insertion is strongly moderated by the large negative temperature coefficient (Doppler) of the fuel. Since the operating temperature of the fuel is relatively low, even a rapid increase of the instantaneous power will increase the temperature of the fuel within limits, large enough, however, to introduce a substantial reduction of k as to exit from criticality. The safety of multiplying systems depends to a large extent on fast transients. A kinetic model dealing with fast transients due to accidental reactivity insertions and unexpected changes of the intensity of the external proton beam shows that the EA responds much more benignly to a sudden reactivity insertion than a critical Reactor. Indeed, no power excursions leading to damaging power levels are observed for positive reactivity additions which are of the order of the sub-criticality gap. Even if the spallation source is still active (the accelerator is not shut-off), the power changes induced are passively controlled by means of the increase of the natural convection alone (massive coolant response) thus excluding any meltdown of the sub-critical core.

Any very intense neutron source ($\geq 10^{13}$ n/s) could in principle be used to produce bomb grade Plutonium by extensive irradiation of some easily available depleted Uranium. This is true both for fission and fusion energy generating devices. We propose to prevent this possibility by "sealing off" the main vessel of the EA to all except a specialised team, for instance authorised by IAEA. This is realistic for a number of reasons. The energetic gain of the EA is almost constant over the lifetime of the fuel, though it changes significantly after a power level variation. Convection cooling is completely passive and occurring inevitably because of temperature differences. There are no active elements (pumps, valves etc.) which may fail or need direct access to the interior of the main vessel. In addition the fuel requires no significant change in conditions over its long lifetime of five years, since the fissile material is continuously generated from the bulk of Thorium. The only two maintenance interventions to be performed are the periodic replacement of the beam window about once a year and the possible replacement of some failing fuel elements, performed remotely with the pantograph. Both activities can be carried out without extracting the fuel from the vessel. We can therefore envisage conditions in which the EA is a sort of "off limits black-box" accessed very rarely and only by a specialised team, for instance authorised by IAEA. The ordinary user (and owner) of

the EA will have no access to the high neutron flux region and to the irradiated fuel, a necessary step towards any diversion which may lead to proliferation or misuse of the device.

Proliferating uses of the fuel are further prevented by the fact that the fissile Uranium mixture in the core is heavily contaminated by strong γ-emitter ^{208}Tl which is part of the decay chain of ^{232}U and by the fact that the EA produces a negligible amount of Plutonium. As shown later on, a rudimentary bomb built starting with EA fuel, in absence of isotopic separation, will be most impractical and essentially impossible to use or to hide.

The EA can operate with a variety of different fuels. Several options will be discussed in detail in the subsequent sections. A specialised filling can transform Plutonium waste into useful ^{233}U, for instance, in order to accumulate the stockpile required at the start-up of the EA. More generally one could envisage a combined strategy with ordinary PWRs. Presently operating PWRs represent an investment in excess of 1.0 Tera dollars. It is important to make every possible effort in order to minimise their impact on the environment and to increase their public acceptability. A specially designed EA could be used to (1) transform Plutonium waste into useful ^{233}U and (2) reduce the stockpile of "dirty" Plutonium waste. The EA will be initially loaded with a mixture of Actinide waste and native Thorium, in the approximate ratio 0.16 to 0.84 by weight. Other Actinides, like Americium, Neptunium and so on can also be added. The mixture is sub-critical and the EA can be operated with k = 0.96-0.98.

During operation, the unwanted actinides are burnt, while ^{233}U is progressively produced. The freshly bred ^{233}U compensates the drop of criticality due to the diminishing and deteriorating Actinide mixture and the one due to the build-up of Fission Fragments. A balanced operation over a very long burn-up of up to 200 GW day/t is thus possible without loss of criticality, corresponding to 5-10 years of operation without external intervention. The fuel of the EA is then reprocessed, the ^{233}U is extracted for further use. FFs are disposed with the standard procedure of the EA. The remainders of Plutonium[9] and the like, could either be sent to the Geological Repository to which they were destined or further burnt in the EA, topped with fresh Thorium. This combination of a PWR and an EA has several advantages:

---

[9] The discharge after ≈ 150 GWatt × day/t contains about 50% of the initial Pu, but is highly depleted of ^{239}Pu (1/5) and ^{241}Pu(1/4), while other Pu isotopes are essentially unchanged. Am and Cm isotopes stockpiles are essentially unchanged. Note that the Plutonium is "denatured" of the highly fissile isotopes, making it worthless for military diversions.

1) It eliminates permanently some of the Actinide waste of the PWR reducing the amount to be stored in a Geological Repository.
2) It produces additional power through the EA, thus increasing by about 50% the energetic yield of the installation.
3) The amount of fissile Uranium, which is by weight about 80% of the incinerated Plutonium is a valuable asset. It can be used either to start a new, Thorium operated, EA or it can be mixed with depleted Uranium to produce more fuel for PWRs. As is well known, ^{233}U is an almost perfect substitute for ^{235}U in a ratio very close to 1. The yearly Plutonium and higher Actinides discharge of a typical ≈ 1 GW_e PWR operated 80% of the time is of the order of 300 kg, thus producing via the EA 240 kg of ^{233}U, which in turn can be used to manufacture ≈ 8 tons of fresh fuel from depleted U with 0.3% ^{235}U and 3.0 % ^{233}U. This is $\approx 1/3$ of the supply of enriched Uranium fuel for the operation of the PWR.

We have also considered as an alternative a fast neutron driven EA operated on Plutonium only, namely without Thorium. Similar schemes, though mostly operated with thermal neutrons are under consideration at Los Alamos [15], JAERI [16] and elsewhere [17]. Such potential devices require frequent refills and manipulations of the fuel, since the reactivity of the Plutonium is quickly deteriorated by the burning and choked by the emergence of a large relative concentration of FF's. At the limit one is lead to the "chemistry on line" proposed by the Los Alamos Group [15]. Adding a large amount of fertile Thorium greatly alleviates such problems and the device can burn Plutonium and the like for very many years without intervention or manipulation of the fuel, since the bred ^{233}U is an effective substitute to Plutonium to maintain a viable and constant criticality. In addition FFs are diffused in a much larger fuel mass. Finally the ^{233}U recovered at the end of the cycle constitutes a valuable product.

In principle our method of a Th-Pu mixture could be extended to the operation of a Fast Breeder used as incinerator [18], however, probably at a much higher cost and complexity due to the higher degree of safety involved.

We have indicated Thorium as main fuel for the EA since the radio-toxicity accumulated is much smaller than Uranium and it offers an easier operation of the EA in a closed cycle. But there are also reasons of availability. Thorium is relatively abundant on earth crust, about 12 g/ton, three times the value of Uranium [19]. It ranks 35-th by abundance, just after Lead [20]. It is well spread over the surface of the planet. In spite of its negligible demand ($\approx$ 400 t/y) the known reserves in the

WOCA[10] countries are estimated [21] to about 4×10^6 tons (Table 1.1). Adding a guessed estimate from the USSR, China and so on, we reach the estimate of perhaps 6×10^6 tons, which can produce 15,000 TW $\times$ year of energy, if burnt in EAs, namely about a factor 100 larger than the known reserves of Oil or Gas and a factor 10 larger than Coal. This corresponds to 12.5 centuries at the present world's total power consumption (10 TW).

There are reasons to assume that this figure is largely underestimated. Firstly the demand is now very low and there has been very little incentive to date to search for Thorium "per se". Additional resources of any mineral have always been found if and when demand spurs a more active perspection. The presently exploited Thorium ores are richer, by a factor $10 \div 100$, than the ones which are exploitable at a price acceptable by market conditions applicable to the case of Uranium.

In view of the small contribution of the primary Thorium to the energy cost, one may try to estimate how the recoverable resources would grow if exploitation is extended to ores which have a content for instance an order of magnitude smaller, i.e. similar to the best Uranium ores. Such analysis has been performed for Uranium [22], assuming that the distribution in the crust follows a "log-normal" (Figure 1.2) distribution. Other metals for which a better mining history is known, show a similar trend, though the slope parameter may be different in each case (Figure 1.3). In the case of Thorium, in absence of better information, we may assume the same slope as in the case of Uranium. Then, a tenfold decrease in the concentration of the economically "recoverable" ores[11] would boost reserves of Thorium by a factor of 300, still a small fraction (3×10^{-5}) of what lies in the Earth crust. Reserves of Thorium energy would then be stretched to 4.5 million TW $\times$ year, *corresponding to $\approx$ 2200 centuries at twice the present world consumption level which can be considered truly infinite on the time scale of human civilisation.*[12].

Several other projects have sought the realisation of a "clean" Nuclear Energy. The project CAPRA [23] focuses on the incineration of Plutonium in a Fast Breeder. On a longer time scale, Fusion holds the promise of a "cleaner" energy. Amongst the various projects, Inertial Fusion offers the largest flexibility in design of the combustion chamber and hence the best potentials of reduction of the activation

---

[10]This stands for World Outside Centrally Planned Activities.

[11]We remark that even this 10-fold decrease would make these minerals somewhat more concentrated than the 2000 ppm "high content ores" used today for Uranium.

[12]In order to estimate the magnitude of the error in such a "prediction", we note that the somehow extreme cases of Tungsten and of Copper have boost factors of 500,000 and 40 respectively. But even the lower limit of Copper predicts ≥ 300 centuries at twice the today's world consumption.

effects due to neutrons [24]. But neither inertial nor magnetic fusion have so far achieved ignition[13]. We have compared the activity of the remnants (Ci) of the EA with the one of the CAPRA project and of two of the Inertial Fusion concepts, namely LIBRA [25] and KOYO [26] in which the greatest care has been exercised to reduce activation. In order to make the comparison meaningful we have to take into account that the published values of activation for fusion are given in Ci after shut-down and 40 years of operation. Therefore the activities quoted for the fission case (CAPRA, EA) have been normalised to the same scenario, namely counting the total activity of remnants (sum of all fuel cycles, in the case of EA excluding recycled fuel) after 40 years of continued, uninterrupted operation. Activities have been normalised 1 GW of electric power produced (Figure 1.4).

After the cool-down period in the secular repository ($\approx$ 1000 years) the activity of the remnants (40 years of operation) stabilises at levels which are : 1.7×10^7 Ci for CAPRA, 2.35×10^4 Ci for LIBRA, 900 Ci for KOYO and 1.3×10^4 Ci for the EA without incineration. With incineration we reach the level of 950 Ci, out of which about one half is due to ^{14}C. The activation for unit delivered power of the EA without incineration is comparable to the one of LIBRA concept whilst with incineration we reach a level which is close to the one of KOYO concept based on second generation design of the combustion chamber. The expected doses after 1000 years of cool-down from Magnetically Confined Fusion are typically three order of magnitude larger than the quoted values for Inertial confinement due to substantial differences in the neutron spectra. This improvement is mainly due to the moderation of neutrons in the blanket consisting of LiPb liquid circulating through SiC tubes, before they hit the first wall [24]. *Therefore we conclude that the EA concept can reach a level of "cleanliness" which is well in the range of the best Fusion conceptual designs.*

From the point of view of cleanliness, as well as for the other major goals — namely non-criticality, non-proliferation and inexhaustible fuel resources — the EA matches fully the expectations of Fusion. But like CAPRA — which however is about 1000 times less effective in eliminating radioactive remnants — the EA has no major technological barriers, while in the case of Fusion, major problems have to be solved.

---

[13] The project ITER is aimed at demonstrating Ignition in magnetically confined fusion, presumably circa 2005. The new large megajoule range optical LASERs in development at Livermore and in France have the potential for ignition with inertial fusion.

Table 1.1 - Thorium resources (in units of 1000 tons) in WOCA (World Outside Centrally Planned Activities) [21]

	Reasonably Assured	Additional Resources	Total
Europe			
Finland		60	60
Greenland	54	32	86
Norway	132	132	264
Turkey	380	500	880
Europe Total	566	724	1290
America			
Argentina	1		1
Brazil	606	700	1306
Canada	45	128	173
Uruguay	1	2	3
USA	137	295	432
America total	790	1125	1915
Africa			
Egypt	15	280	295
Kenya	no estimates	no estimates	8
Liberia	1		1
Madagascar	2	20	22
Malawi		9	9
Nigeria	no estimates	no estimates	29
South Africa	18	no estimates	115
Africa total	36	309	479
Asia			
India	319		319
Iran		30	30
Korea	6	no estimates	22
Malaysia	18		18
Sri Lanka	no estimates	no estimates	4
Thailand	no estimates	no estimates	10
Asia total	343	30	403
Australia	19		19
Total WOCA	*1754*	*2188*	*4106*

This compilation does not take into account USSR, China and Eastern Europe. Out of 23 listed countries, six (Brazil, USA, India, Egypt, Turkey and Norway) accumulate 80% of resources. Brazil has the largest share followed by Turkey and the United States.

Figure Captions.

Figure 1.1 General lay-out of the Energy Amplifier complex. The electric power generated is also used to run the Accelerator (re-circulated power ≤ 5%). At each discharge of the fuel (every 5 years) the fuel is "regenerated". Actinides, mostly Thorium and Uranium are re-injected as new fuel in the EA, topped with fresh Thorium. Fission fragments and the like are packaged and sent to the Secular repository, where after ≈ 1000 years the radioactivity decays to a negligible level (see Figure 1.4). For simplicity the option of incinerating long-lived fragments is not shown.

Figure 1.2 Estimated amount of Uranium mined as a function of the concentration of metal in the ores.

Figure 1.3 Cumulative amount of metal mined for different metals as a function of the ore concentration of metal.

Figure 1.4 Accumulated activity of Remnants as a function of the time elapsed after shutdown for a number of conceptual projects aiming at minimising the radio-active waste. CAPRA [23] is based on Fast-Breeders similar to Super-Phenix. LIBRA [25] and KOYO [26] are Inertial Fusion devices (ICF). The EA concept with and without incineration of long-lived FFs can reach a level of “cleanliness“ which is well in the range of the best Fusion conceptual designs. Activities in Ci are given for 40 years of operation. According to Ref. [24] Magnetically confined Fusion in general produces activation which are up to three order of magnitude larger than ICF.

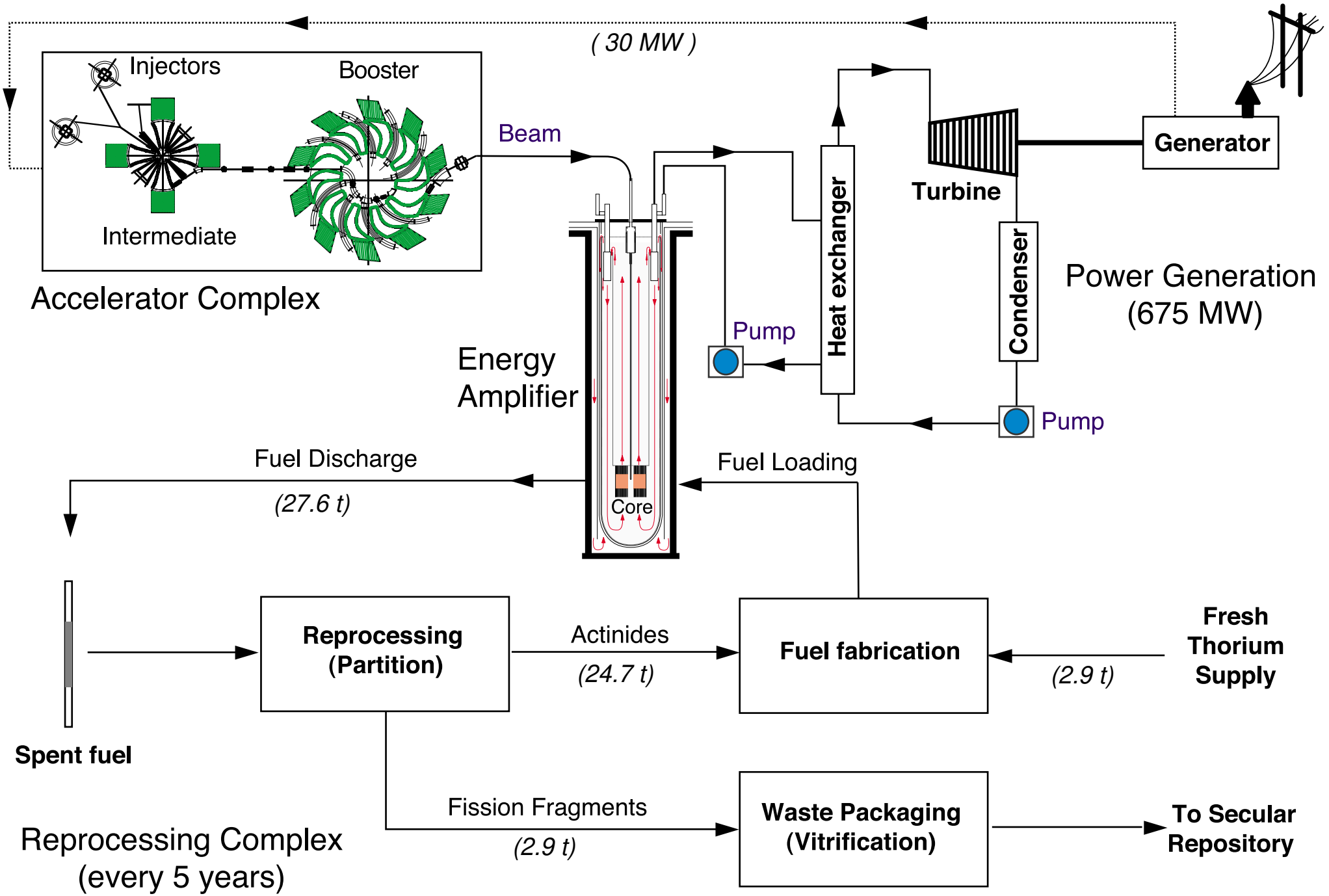
(30 MW)
Injectors
Booster
Intermediate
Accelerator Complex
Beam
Energy
Amplifier
Core
Pump
Heat exchanger
Turbine
Generator
Condenser
Power Generation
(675 MW)
Pump
Fuel Discharge
(27.6 t)
Fuel Loading
Spent fuel
Reprocessing
(Partition)
Actinides
(24.7 t)
Fuel fabrication
(2.9 t)
Fresh
Thorium
Supply
Fission Fragments
(2.9 t)
Waste Packaging
(Vitrification)
To Secular
Repository
Reprocessing Complex
(every 5 years)

Figure 1.1

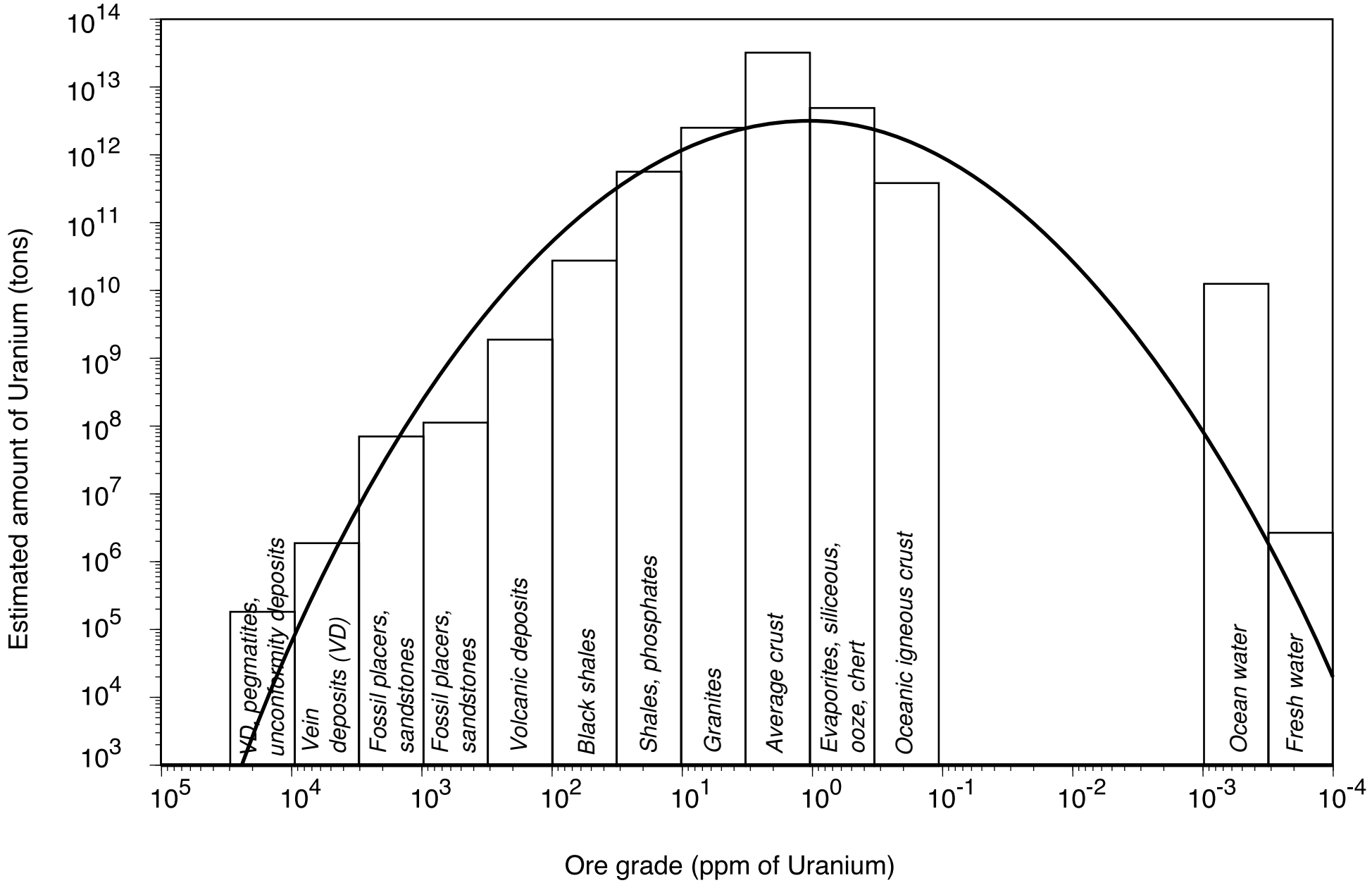
Estimated amount of Uranium (tons)
10^{14}
10^{13}
10^{12}
10^{11}
10^{10}
10^{9}
10^{8}
10^{7}
10^{6}
10^{5}
10^{4}
10^{3}
VD, pegmatites, unconformity deposits
Vein deposits (VD)
Fossil placers, sandstones
Fossil placers, sandstones
Volcanic deposits
Black shales
Shales, phosphates
Granites
Average crust
Evaporites, siliceous, ooze, chert
Oceanic igneous crust
Ocean water
Fresh water
10^{5}
10^{4}
10^{3}
10^{2}
10^{1}
10^{0}
10^{-1}
10^{-2}
10^{-3}
10^{-4}
Ore grade (ppm of Uranium)

Figure 1.2

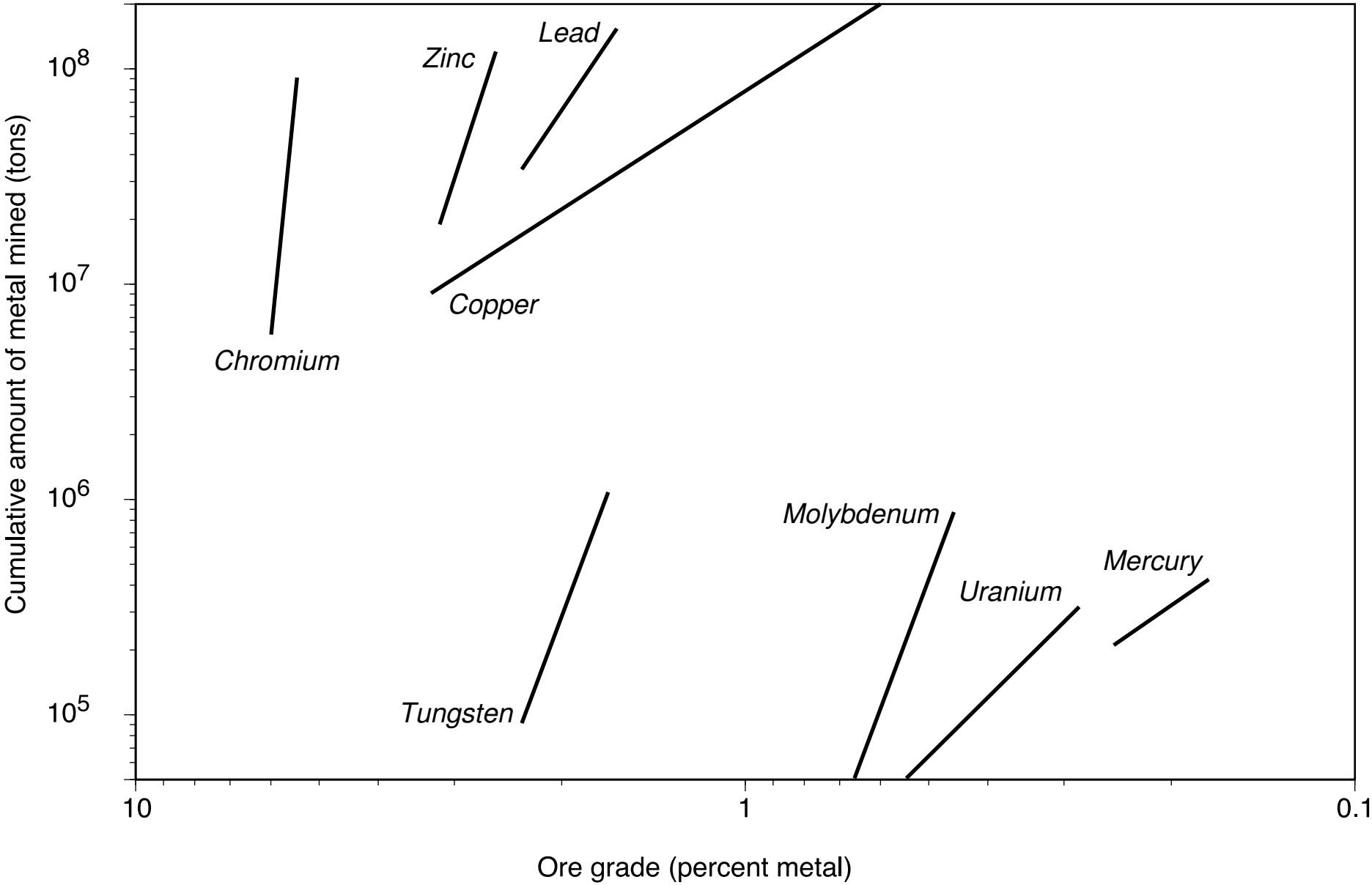
Cumulative amount of metal mined (tons)
10^8
10^7
10^6
10^5
Zinc
Lead
Copper
Chromium
Tungsten
Molybdenum
Uranium
Mercury
10
1
0.1
Ore grade (percent metal)

Figure 1.3

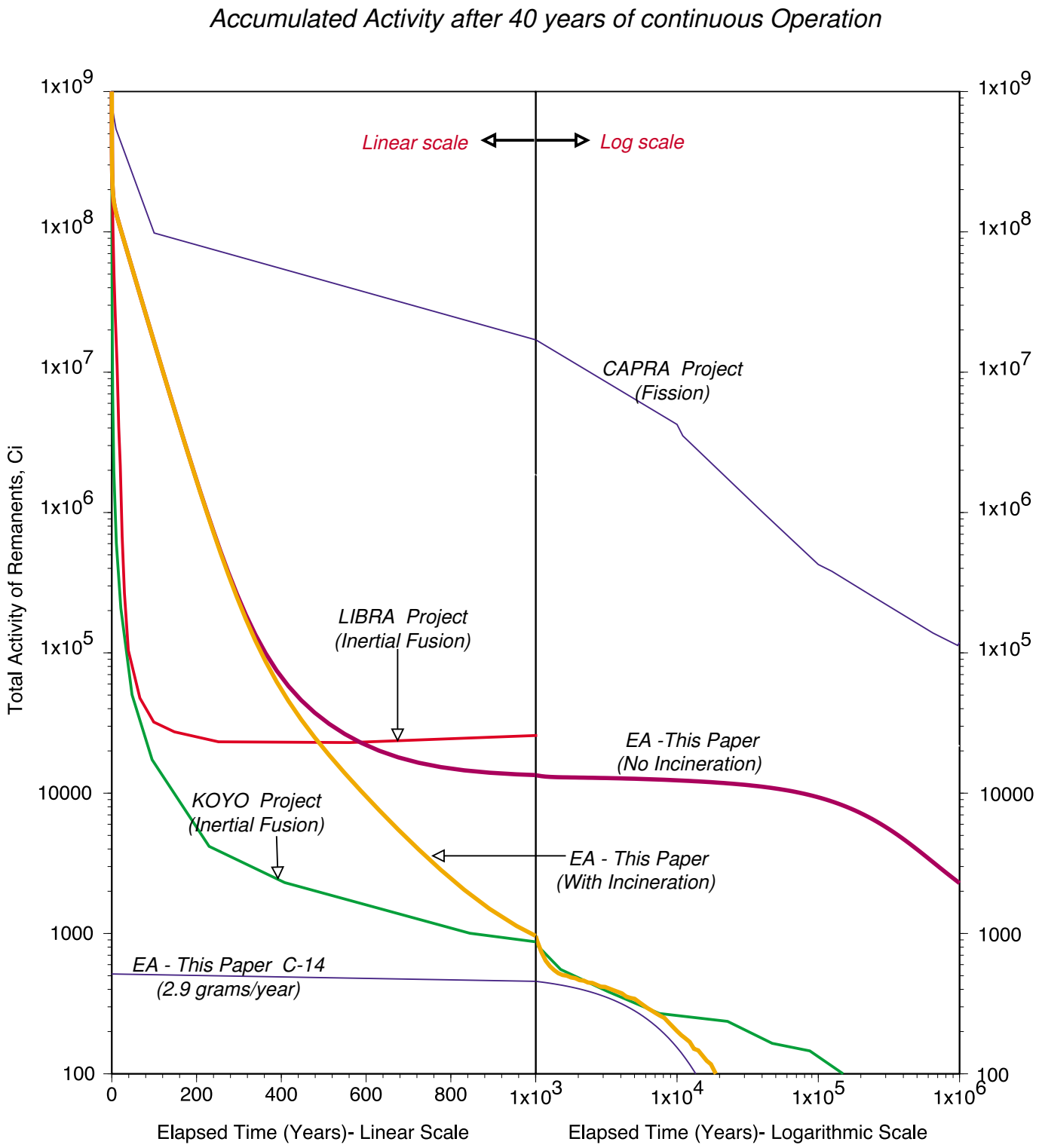
Accumulated Activity after 40 years of continuous Operation
Linear scale
Log scale
CAPRA Project
(Fission)
LIBRA Project
(Inertial Fusion)
EA -This Paper
(No Incineration)
KOYO Project
(Inertial Fusion)
EA - This Paper
(With Incineration)
EA - This Paper C-14
(2.9 grams/year)
Total Activity of Remanents, Ci
1x10^9
1x10^8
1x10^7
1x10^6
1x10^5
10000
1000
100
0
200
400
600
800
1x10^3
1x10^4
1x10^5
1x10^6
Elapsed Time (Years)- Linear Scale
Elapsed Time (Years)- Logarithmic Scale

Figure 1.4

2.— Physics considerations and parameter definition.

2.1 - Spatial Neutron Distribution. While the neutron distribution inside a Reactor is determined primarily by the boundary conditions, in the EA the geometry of the initial high energy cascade is dominant. The two spatial distributions are expected to differ substantially. The flux distribution is of fundamental importance in order to determine the generated power distribution and the uniformity of the burning of the fuel, both of major relevance when designing a practical device.

We shall consider first, in analogy to a Reactor a simple, uniform fuel-moderator medium operated away from criticality [27]. It turns out that in such "reactor like" geometry, the neutron flux non uniformity associated to sub-critical regime[14] may be so large as to hinder the realisation of a practical device. A radically different geometry, described in paragraph 2.2, can be used to solve this problem.

We neglect the fine structure of the sub-critical assembly and consider a fictitious material with uniform properties. We assume no reflector and therefore the EA is a uniform block of specified size. The high energy beam interacts directly with the fuel material. The basic diffusion equation for the neutron flux for mono-energetic or thermal neutrons in a steady state is

$$D\nabla^2\phi - \Sigma_a\phi + S = 0$$

where S is the source term, namely the rate of production of neutrons per cm^3 per second, $D = \Sigma_s / 3\Sigma^2$ is the diffusion coefficient and Σ, Σ_s and Σ_a respectively the macroscopic total, elastic and absorption cross sections, all homogenised over the fuel-moderator mixture. This formula is strictly applicable only to mono-energetic neutrons of velocity v and then only at distances greater than two or three mean free paths from boundaries.

Let k_∞ be the number of neutrons produced at each absorption in the fuel-moderator mixture. The source term is decomposed in two parts, namely $S = k_\infty\Sigma_a\phi + C$ where the first term is due to fission multiplication in the fuel and the second is the inflow of neutrons (per cm^3 and second) emitted by the high energy cascade. Upon dividing by D and rearranging terms the diffusion equation becomes

---

[14] As shown later on, a subcritical device far from criticality has a neutron flux distribution which is exponentially falling from the target region, while a critical reactor has the well known cos-like distribution. The exponential is obviously falling very fast and the burn-up is therefore highly non uniform and concentrated around the beam area.

$$\nabla^2\phi - \frac{1-k_\infty}{L_c^2}\phi + \frac{C}{D} = 0 \qquad [1]$$

where L_c^2 is equal to D/Σ_a. Boundary conditions are determinant. The neutron density at the outer boundary of the medium is quite small. It cannot be exactly zero because neutrons diffuse out of the medium. In analogy with Reactor theory [27] we shall use the boundary condition that at the extrapolated distance $d = 2/3\Sigma_S$ from the boundaries of the medium the flux must vanish, $\phi = 0$.

In order to solve Eq. [1] we find it useful to introduce a new function $\psi(\vec{x})$ where $\vec{x} \equiv (x, y, z)$ which is defined by the following differential equation, in which only the geometry of the device is relevant:

$$\nabla^2\psi(\vec{x}) + B^2\psi(\vec{x}) = 0 \qquad [2]$$

The boundary conditions $\psi(\vec{x}) = 0$ at the extrapolated edges introduce a quantization in the eigen-values of B^2 and the corresponding eigen-functions $\psi(\vec{x})$. Therefore we have a numerable infinity of solutions.

For instance in the case of rectangular geometry, namely a parallelepiped with dimensions a, b, c and origin at one edge, such as $\psi(\vec{x}) = 0$ for the planes x = a, x = 0, y = b, y = 0, and z = c, z = 0, we find

$$\psi_{l,m,n}(\vec{x}) = \sqrt{\frac{8}{abc}}\sin\left(l\frac{\pi x}{a}\right)\sin\left(m\frac{\pi y}{b}\right)\sin\left(n\frac{\pi z}{c}\right)$$

$$B_{l,m,n}^2 = \pi^2\left(\frac{l^2}{a^2} + \frac{m^2}{b^2} + \frac{n^2}{c^2}\right)$$

Analogue expressions can be given for different geometries. The eigen-functions $\psi(\vec{x})$ are normalised to one and constitute a complete ortho-normal set. Hence it is possible to express any function as the appropriate series of such eigen-functions, provided the boundary conditions are the same. In particular the high energy neutron source $C(\vec{x})$ produced by the beam interactions (zero outside, in order to satisfy boundary conditions) is expanded to

$$C(\vec{x}) = D\sum_{l,m,n} c_{l,m,n}\psi_{l,m,n}(\vec{x}) \qquad \text{where} \quad c_{l,m,n} = \frac{1}{D}\int_{volume}\psi_{l,m,n}(\vec{x})C(\vec{x})dV$$

It is then possible to express the neutron flux as a series expansion with the help of Eq. [1] and of Eq. [2]:

$$\phi(\vec{x}) = \sum_{l,m,n}\frac{c_{l,m,n}}{B_{l,m,n}^2 + \Gamma}\psi_{l,m,n}(\vec{x}) \qquad \text{where} \qquad \Gamma = \frac{1-k_\infty}{L_c^2} \qquad [3]$$

Note that the only parameter which is not geometry related is Γ. The criticality condition can be defined as a non zero flux for the limit of $c_{l,m,n} \to 0$. Therefore one of the denominators $B_{l,m,n}^2 + \Gamma$ of Eq. [3] must vanish, which of course implies $\Gamma < 0$ or equivalently $k_\infty > 1$. The smallest value of $B_{l,m,n}^2$ and therefore the smallest value of k_∞ which makes the system critical occurs for l = m = n = 1, namely the fundamental

mode of Eq. [2]. This result exhibits the well known sinusoidal distribution of the neutron flux of a Reactor and the classic condition for criticality, $k_\infty - 1 = B_0^2 L_c^2$, where B_0^2 is the "buckling" parameter.

The significance of $B_{l,m,n}^2$ is further illustrated if one considers the neutron absorption and escape rates or probabilities for the mode $i \equiv (l,m,n)$, $P_{abs}^{(i)}$ and $P_{esc}^{(i)}$ respectively. Let us consider a case in which the i-th eigen-mode of the wave function is dominant. It is easy to show that

$$P_{esc}^{(i)} = P_{abs}^{(i)} \frac{D}{\Sigma_a} B_i^2 = P_{abs}^{(i)} L_c^2 B_i^2$$

where L_c is the (already defined) diffusion length. The (small) escape probability for each mode $P_{esc}^{(i)}$ is then simply equal to B_i^2 in units of the inverse of the square of the diffusion length. Note that since B_i^2 is a rapid rising function of the mode i, higher modes escape much more easily from the volume. Therefore the containment of the cascade is improved if the source geometry is such as to minimise the excitation of the higher eigen-modes.

This interpretation of B_i^2 makes also more transparent the classic condition for criticality of a Reactor, $k_\infty - 1 = B_0^2 L_c^2$. Evidently in order to have criticality, the number of neutrons produced at each absorption k_∞ must exceed 1 precisely by $P_{esc} \approx L_c^2 B_0^2$, the fraction of neutrons escaping the active volume. To extend this formula to the EA it is then natural to introduce the mode dependent multiplication coefficient $k_i = k_\infty - L_c^2 B_i^2$, in which the escape probability has been taken into account. In the case of the fundamental mode, the corresponding *k*-value has the classic significance of the Reactor Theory. This makes even more transparent the significance of the denominator of Eq. [3], which becomes

$$B_i^2 + \Gamma = \frac{1}{L_c^2}\left(L_c^2 B_i^2 + 1 - k_\infty\right) = \frac{1}{L_c^2}\left(1 - k_i\right)$$

We can then re-write Eq. [3] as

$$\phi(\vec{x}) = L_c^2 \sum_{l,m,n} \frac{c_{l,m,n}}{1 - k_{l,m,n}} \psi_{l,m,n}(\vec{x})$$

where the "(1-k) enhancement" of each mode is further emphasised. The formula can be used to readily calculate the neutron flux distribution in the uniform EA starting from the known initial cascade distribution.

In contrast with the case of the critical reactor in which only the fundamental mode is active, any reasonable source configuration in an EA will excite a large number of different modes, each with its different criticality coefficient k_i. The neutron distribution will be wider than the source distribution only because $B_{l,m,n}^2$ grows with increasing order and therefore expansion coefficients are indeed different

from $c_{l,m,n}$. In general the distribution of neutrons inside a uniform medium operated as an EA reasonably far from criticality will remain strongly non uniform. One can show that far from the source it decays approximately exponentially rather than having the characteristic cos-like shape of a Reactor.

Since the neutron inventory is very critical, the neutron containment inside the EA must be as complete as possible. Inevitably this implies a large fraction of the volume with a low neutron flux and hence with a small specific energy production. An EA made of a uniform volume of fuel with the beam interacting in the central region will therefore be highly impractical.

2.2 - EA Uniformisation with a diffusive Medium. One can overcome this difficulty by embedding discrete fuel elements in a large, diffusing medium of high neutron transparency. In Figure 2.1 we show the capture cross sections at the typical energy of the neutrons in the EA as a function of the element number. One can remark very pronounced dips, which are due to the occurrence of closed shell in the nuclei. This is why their "nuclear reactivity" is minimal. These dips are somehow the equivalent of the Noble Gases in the atomic shell structure. The unique properties of the Lead and Bismuth are evident. The uniformisation of the fuel burn up is then ensured by the long migration length of the diffusing medium. Since the present design of the EA is based on fast neutrons, the medium must have also a very small lethargy, i.e. a high atomic number. Two elements appear particularly suited: Lead and Bismuth. In general Lead will be preferable because of its lower cost, smaller toxicity and smaller induced radioactivity. Both elements have the added advantage that the neutron yield of the high energy beam is large: the same medium can therefore be the high energy target and the diffuser at the same time.

While ^{209}Bi is a single isotope, natural Lead is made of ^{204}Pb (1.4 %), ^{206}Pb (24.1%), ^{207}Pb (22.1 %) and ^{208}Pb (52.4 %), which have quite different cross sections. Isotopically enriched ^{208}Pb would be very attractive because of its smaller capture cross sections. However, we shall limit our considerations to the use of natural Lead.

Assume a large, uniform volume made of Lead, initially without fuel elements. The proton beam is arranged to interact in the centre, producing a relatively small, localised source of spallation neutrons. The solution of the diffusion equation (Eq. (2) in the case of an infinite diffusing medium and a small source of strength Q(n/s) is given by [27]:

$$\phi(r) = \frac{Q}{4\pi D}\frac{e^{-\kappa r}}{r} = \frac{Q\kappa}{4\pi D}\frac{e^{-\kappa r}}{\kappa r}$$

where D is the diffusion coefficient and κ the reciprocal of the diffusion length with ($\kappa^2 = \Sigma_{abs} / D$). In the case of Lead, D is very small (D ≈ λ_s/3 ≈ 1.12 cm) and $1/\kappa$ very large, about 1 metre, the exact values depending on the energy dependent cross sections. Neutrons will then fill a very large volume of few $1/\kappa$ units and they will execute a brownian motion, stochastically "stored" in the medium by the very large number of diffusing collisions.

Spallation neutrons above a few MeV are rapidly slowed down because of the large (n,n') cross section. Once below threshold (≈ 1 MeV), the well known slowing-down mechanism related to elastic collisions takes over. The logarithmic average energy decrement for Pb and Bi is very small $\xi = 9.54 \times 10^{-3}$ and the mean number of collisions to slow down the neutron for instance from 1 MeV to 0.025 eV (thermal energies) is very large, $n_{coll} = \ln(1\text{ MeV}/0.025\text{ eV})/\xi = 1.8 \times 10^3$. The elastic cross section, away from resonances is about constant, around 10 b corresponding to a scattering mean free path of λ_s = 3.38 cm (700 °C). The total path to accumulate n_{coll} is then the enormous path of 62 metres! The actual average drift distance travelled is of course much smaller, of the order of 1 metre, since the process is diffusive.

During adiabatic moderation, the neutron will cross in tiny energy steps a resonance region, located both for Pb and Bi in the region from several hundred KeV to few KeV. We introduce the survival probability $P_s(E_1, E_2)$, defined as the probability that the neutron moderated through the energy interval $E_1 \rightarrow E_2$ is not captured. The probability that a neutron does *not* get captured while in the energy interval between E and E + dE is $[1 - (\Sigma_{abs}/(\Sigma_{abs}+\Sigma_{sc}))\ (dE/E\xi)]$ where Σ_{sc} and Σ_{abs} are the macroscopic elastic scattering and absorption cross sections. Evidently such probability is defined for a large number of neutrons in which the actual succession of energies is averaged. Combining the (*independent*) probabilities that it survives capture in each of the infinitesimal intervals, $P_s(E_1, E_2)$ is equal to the product over the energy range:

$$P_s(E_1, E_2) \cong \prod_{E_1}^{E_2}\left(1 - \frac{\Sigma_{abs}}{\Sigma_{sc}+\Sigma_{abs}}\frac{dE}{\xi E}\right) = \exp\left[-\frac{1}{\xi}\int_{E_2}^{E_1}\frac{\Sigma_{abs}}{\Sigma_{sc}+\Sigma_{abs}}\frac{dE}{E}\right] = \exp\left(-\frac{I_{res}}{\xi}\right)$$

where the resonance integral I_{res} is defined as

$$I_{res} = \int_{E_2}^{E_1}\frac{\Sigma_{abs}}{\Sigma_{sc}+\Sigma_{abs}}\frac{dE}{E}$$

If the cross sections are constant, the integral is easily evaluated

$$P_s(E_1, E_2) = \exp\left[-\frac{\Sigma_{abs}}{\Sigma_{sc}+\Sigma_{abs}}\frac{1}{\xi}\ln\left(\frac{E_1}{E_2}\right)\right]$$

which evidences the large enhancement factor due to the slow adiabatic process, $\ln(E_1/E_2)/\xi = 104.8\ln(E_1/E_2)$ with respect to a single scattering. For instance, if $E_1/E_2 = 50$, the effective value of the absorption cross section Σ_{abs} is increased by a factor 410. The values of the resonance integral I_{res} for the Lead isotopes are given in Table 2.1 for E_1= 1.0 MeV and several final energies E_2. Natural Lead and Bismuth have similar properties, while a pure ^{208}Pb will be vastly superior. The temperature coefficient of the survival probabilities is (slightly) negative, since Doppler broadening increases the extent of the resonances. About 20% of the fission neutrons are absorbed in pure diffusing medium before they reach an energy of 100 keV, which is the typical energy in a practical EA. In reality the presence of a substantial amount of fuel in the EA will reduce such a loss: typically one expects that about 5% of the neutrons will end up captured in the diffusing medium.

Let us assume that a localised, strongly absorbing fuel element is introduced in the diffusing medium. The effects on the flux due to its presence will extend over a volume of the order of the migration length, as one can easily see describing the localised absorption as a "negative source". Hence one can in a good approximation use averaged properties for a diffuser-fuel region.

In a fuel-diffuser mixture with a relatively small concentration η of fissile material, $\Sigma_{sc} \approx \Sigma_{sc}^{diff}$ whilst $\Sigma_{abs} \approx \eta\Sigma_{abs}^{fuel} = \eta(\Sigma_{n,\gamma}^{fuel} + \Sigma_{fiss}^{fuel}) >> \Sigma_{abs}^{diff}$. The survival probability is therefore strongly reduced, namely due to the large probability of absorption in the fuel. Adding fuel elements in the otherwise "transparent" medium makes it "cloudy". Evidently a large fraction of the absorptions will occur in the fuel even if in relatively small amounts, because of the very high transparency of the pure medium.

Once the capture in the added materials becomes dominant, a larger fuel concentration with respect to the diffuser concentration implies an earlier neutron capture and hence a higher average neutron energy. This leaves a large freedom in the quantity of fuel to be used, depending on the power required for the application. An analytical analysis of such a composite system is necessarily approximate, lengthy and outside the scope of the present paper. For more details we refer to Ref. [28]. (The actual behaviour of some specific designs will be derived with the help of numerical calculations).

The conceptual design of the diffuser driven EA consists of a large volume of diffusing medium in which one can visualise a series of concentric regions around the centre, where the proton beam is brought to interact (Figure 2.2):

i) A *spallation target* region, in which neutrons are produced by the high energy cascade initiated by the proton beam. This region is made of pure diffuser. The proton beam is brought in through an evacuated pipe and a thin window.

ii) A *buffer* region, again of pure diffuser in which neutrons are migrated and the energy spectrum is softened by the (n,n') reactions. This ensures that the structural elements (fuel assembly) is not exposed to high energy neutrons from the proton beam which may produce an excessive radiation damage.

iii) A *fuel* region in which a series of discrete fuel elements are widely interspersed in the diffusing medium. The outer part of the fuel region can be loaded with non-fissile materials to be bred (breeder region).

vi) A *reflector* region made of pure diffuser, with eventually an outer retaining shield, which closes the system, ensuring durable containment of neutrons.

In order to ensure appropriate containment, the Lead or Bismuth volume must be of the order of 2000÷3000 tons, arranged in a sort of cylinder or cube of some 6 m each side. Since the neutron containment is essential, this order of magnitude of diffuser volume is required in all circumstances. The amount of fuel to ensure dominance of the capture process needs instead to be much smaller. A realistic EA is already possible with 6-7 tons of fuel, corresponding to a ratio fuel/diffuser $\eta \geq 2.5\ 10^{-3}$. On the other hand larger fuel amounts are possible for large power applications. From the point of view of the neutronics, $\eta \leq 0.01$ is ideal. The neutron leakage out of the diffuser is then typically less than 1% and the fraction of captures in the Lead nuclei of the order of 4 ÷ 6%, i.e. much smaller than in the case of a pure diffuser.

2.3 - Numerical example of spatial distributions. .In order to evaluate the actual neutron flux distribution in practical cases, analytic calculations are either too approximate or too cumbersome. It is preferable to use the Montecarlo computer method described in paragraph 2.6. The burn-up radial distribution for three different values of *k* and a typical EA geometry[15] of Figure 2.2 has been calculated with the full Montecarlo method (see paragraph 2.6) and it is shown in Figure 2.3. The value of *k* has been varied changing the pitch of the hexagonal fuel lattice and hence the fuel density. One can see clearly how the neutron flux distribution changes from exponential for k=0.95 (pitch 1.40 cm) to an almost perfect cos-like distribution

[15]The outer radius are as follows: Spallation Target and Buffer: 40 cm, Main core and Breeder : 1.67 m. The height of the core is 1.5 m and the containment box a cylinder of 6 m diameter and 6 m high. The fuel is a compact hexagonal lattice with fuel pins as described in Table 4.4. The fuel is made of ThO_2 with 10% by weight of $^{233}UO_2$. The cladding is made of HT-9, low activity steel.

for k = 0.99 (pitch 1.138 cm), indicating the emerging dominance of the fundamental mode. At k = 0.98 (pitch 1.243 cm) which is the chosen working point for our conceptual design, one is somehow in a transitory region. The concavity of the curve passes through a zero and a linear fit is a good approximation.

A number of different machine geometries have been explored in order to assess the effects of higher modes in a more general way. In general one can say that lowering the k produces a faster decay in the exponential mode, in agreement to what is found in the elementary theory. The actual transition value of k from pure exponential to linear and eventually to cos-like depends on the geometry of the spallation source and of the core. A geometry with several spallation sources (beams) or a widely diffused source can be beneficial in order to improve the uniformity, especially if the source distribution follows a symmetry pattern such as to cancel the contribution of the most offending higher modes.

2.4 - Fuel breeding. For many reasons illustrated for instance in Ref. [1], the by far preferred fertile material is ^{232}Th, although applications based on other Actinides are of interest for burning Plutonium, depleted Uranium and similar surpluses. Neutron captures in the fertile element lead to production of fissile material. The main chain of events for ^{232}Th is then

$$^{232}Th + n \xrightarrow{\gamma} {}^{233}Th \xrightarrow{\beta^-,22m} {}^{233}Pa \xrightarrow{\beta^-,27.0days} {}^{233}U$$

In steady neutron flux conditions, the chain will tend to an equilibrium, namely in a situation in which each fissioned ^{233}U nucleus is replaced by a newly bred fuel nucleus. To a first order, the equilibrium condition can be summarised by the equations:

$$N(^{232}Th)\sigma_{\gamma}(^{232}Th)\phi = N(^{233}Pa) \,/\, \tau(^{233}Pa \rightarrow {}^{233}U) = N(^{233}U)\sigma_{fiss+\gamma}(^{233}U)\phi$$

where cross sections are averaged over the neutron spectrum of integrated flux ϕ. Such a "breeding" equilibrium is naturally attained with a specific value of the fuel/breeder concentration ratio determined solely by the ratio of cross sections

$$\xi = \frac{N(^{233}U)}{N(^{232}Th)} = \frac{\sigma_{\gamma}(^{232}Th)}{\sigma_{fiss+\gamma}(^{233}U)}$$

This equation assumes no alternatives besides the main chain, justified as long as the rate of neutron captures by ^{233}Pa competing with natural decay is kept negligible with a sufficiently low neutron flux. This is the "decay dominated" regime [1] in contrast with the high flux, "capture dominated" regime investigated by Bowman et al [15] where the ^{233}Pa must be quickly extracted to avoid capture.

The breeding ratio at equilibrium is about $\xi = 1.35\times10^{-2}$ for thermal energies and it rises to ξ = 0.126 for fast neutrons and cross sections of Table 2.2. An EA based on

fast neutrons (F-EA) will then require a fuel concentration which is about nine times the one of a device based on fully thermalised neutrons (T-EA). However, it can operate with much higher burn-up rates and hence the total mass of fuel is correspondingly reduced: for the same *output power*, the stockpiles of ^{233}U are in general comparable.

During the actual burn-up of the fuel following an initial fuelling, the equilibrium equation above is only approximately attained, since the concentration of the bulk, fertile material is decreasing with time. Solving the related Bateman equations with an initial breeding material exposed to a constant neutron flux shows that correction terms have to be introduced to the asymptotic value of the breeding ratio[16]:

$$\xi_{lowflux} = \frac{N(^{233}U)}{N(^{232}Th)} = \frac{\sigma_\gamma(^{232}Th)}{\sigma_{fiss+\gamma}(^{233}U)}\left(1 + \frac{\sigma_\gamma(^{232}Th)}{\sigma_{fiss+\gamma}(^{233}U)}\right)$$

$$\xi = \frac{N(^{233}U)}{N(^{232}Th)} = \xi_{lowflux}\left(1 + \phi\sigma_\gamma(^{232}Th)\,\tau(^{233}Pa \rightarrow ^{233}U)\right)$$

The first correction is negligible for a T-EA, but it increases significantly (by 10%) the breeding equilibrium of the F-EA. The second, flux dependent term is smaller but not negligible ($\Delta\xi = 0.31\times 10^{-3}$ for a burn-up rate ρ = 60 W/g and cross sections of Table 2.2) and it compensates partially the flux dependent losses due to captures of the intermediate state ^{233}Pa.

The energetic gain G, namely the energy produced in the EA relative to the energy dissipated by the high energy proton beam is given by the expression [1]

$$G = \frac{G_o}{1-k} = \frac{2G_o}{2-\overline{\eta}(1-L)}$$

where G_0 is the gain proportionality constant, typically 2.4 ÷ 2.5 for a well designed EA; k is the fission-driven multiplication coefficient $k = \overline{\eta}(1-L)/2$; L is the sum of fractional losses of neutrons (absorbed in a variety of ways, like captures in structures and coolant, in fission-product poisons, diffused outside the EA and so on); $\overline{\eta}$ is the (spectrum averaged) number of fission neutrons produced by a neutron absorbed in the fissile isotope[17]. The parameter $\eta(E)$ has a rather complicated neutron energy dependence, with a somewhat lower value in some parts of the resonant region, before rising to larger values for fast neutrons.

---

[16]In our treatment we do not include the captures in ^{233}Pa, which of course are also a rate dependent effect. These losses are instead counted in L.

[17]This equation is easily worked out realising that *at the breeding equilibrium* the number of neutron captures in ^{233}U and in ^{232}Th at each generation must be the same and normalised to 1 neutron are equal to (1–L)/2, since, by neutron conservation, [captures in ^{233}U] + [captures in ^{232}Th] + [Losses]= 1 = (1–L)/2+(1–L)/2+L = 1. As the number of next generation neutrons η(1–L)/2 generated by ^{233}U fissions is also, by definition, the multiplication coefficient k, we conclude that k = η(1–L)/2.

As is well known, in order to achieve criticality the denominator must become zero, $\overline{\eta} = 2/(1-L)$. More precisely, criticality is achieved when neutron losses are reduced to the value $L_{crit} = 1 - 2/\overline{\eta}$. Note that since L > 0 in order to reach criticality $\overline{\eta} > 2$, one neutron being required to maintain the chain reaction and the second being absorbed by the fertile material.

The F-EA has the advantage, when compared to a T-EA that it operates in a region where $\overline{\eta}$ is significantly larger. In addition because of the higher energies, additional neutrons are produced at each generation by different processes, like for instance fast fissions in the fertile material ^{232}Th and (n,2n) reactions in the fuel and the moderator. In order to take into account these contributions it is customary to replace the parameter $\overline{\eta}$ with $\overline{\eta}\varepsilon$ where ε (fast fission factor) is the ratio of all neutrons produced to the ones from the main fission reaction. For a F-EA we expect $\overline{\eta}\varepsilon \approx 2.4 \leftrightarrow 2.5$, conveniently and significantly larger than 2 and larger than $\overline{\eta}\varepsilon \approx 2.1 \leftrightarrow 2.2$ [2] appropriate for a T-EA. The larger allowance for losses (f.i. $L_{crit} = 1 - 2/\overline{\eta}\varepsilon = 0.167 \leftrightarrow 0.200$ vs. $L_{crit} = 0.048 \leftrightarrow 0.091$) is an important asset of the F-EA, even if operation is always with $L > L_{crit}$. As discussed in more detail later on, these extra neutrons do not necessarily have to be thrown away: they may for instance be used to breed additional fuel or to eliminate radio-toxic substances [6]. It is also convenient to start operation of a F-EA with a ^{233}U concentration smaller than the one corresponding to the breeding equilibrium. During operation, the increase of criticality due to the build-up of the ^{233}U relative concentration can be used to compensate growing neutron losses due to captures by fission fragments, thus ensuring a more uniform gain during a longer period of operation without interventions.

2.5 - Flux dependent effects. It has been pointed out [1] that there are sharp limitations to the neutron flux at which an EA can operate in acceptable conditions. The power produced is directly proportional to the neutron flux. We define with ρ the specific power, in units of thermal Watt produced by one gram of Thorium in fuel[18]. At the breeding equilibrium the fluxes for thermal and fast neutrons are given by

$$\phi_{thermal} = 1.80 \times 10^{12} \times \left[\frac{\rho}{W/g}\right] cm^{-2}s^{-1} \; ; \; \phi_{fast} = 3.88 \times 10^{13} \times \left[\frac{\rho}{W/g}\right] cm^{-2}s^{-1}$$

[18] In this chapter we define the power density with reference to the main Thorium content, unlike the rest of the paper where we have taken as reference the unit weight of the actual chemical mixture of the fuel.

where for the latter we have used the cross sections of Table 2.2. Let us estimate some orders of magnitude. For thermal neutrons (E = 0.025 eV), a power of ρ = 15.0 W/g corresponds to a flux $\phi = 2.7 \times 10^{13}$ cm^{-2} s^{-1}, which is considered optimal for a T-EA [1]. In practice the flux in a T-EA will depend somewhat on the energy spectrum of the neutrons, which in turn depends on the operating temperature of the device and on the choice of the moderator. For the same power yield, the neutron flux in a F-EA is approximately 20 times larger. As is well known, it simply reflects the fact that at higher energies cross sections are generally smaller. A practical burn-up rate of a F-EA is about ρ = 60 W/g : the flux will then be $\phi = 2.33 \times 10^{15}$ cm^{-2} s^{-1}, about 80 times larger than the one optimal for a T-EA.

There are several flux dependent effects which have a direct influence on the value and the stability during operation of the multiplication factor k, and hence on the gain:

1) Neutron capture by the intermediate elements of the breeding process and specifically by the ^{233}Pa which destroys a nascent ^{233}U atom at the price of an extra neutron. Such a loss involves a competition between neutron capture and radioactive decay, and it is proportional to the total flux ϕ through the parameter $\Delta\lambda_1 = \sigma_a(^{233}Pa) \times \tau(^{233}Pa \rightarrow ^{233}U) \times \phi << 1$ where τ is the mean life. The absorption cross section $\sigma_a(^{233}Pa)$ is about 43 b at thermal energies, it has a resonance integral of 850 b and it is equal to 1.12 b for fast neutrons (Table 2.2). The corresponding value for a T-EA is $\Delta\lambda_1 \approx 1.45 \times 10^{-16} \phi$, corresponding to a contribution to L of $\Delta L = (1 - L)\overline{\eta\varepsilon}\Delta\lambda_1 / 2 \approx 3.78 \times 10^{-3}$ for the typical flux of 2.7 $\times 10^{13}$ cm^{-2} s^{-1}. For fast neutrons the cross section is much smaller but the flux is correspondingly larger: for a given burn-up rate ρ, $\Delta\lambda_1$ is 0.56 times the value for thermal neutrons. Note however that the allowance for neutron losses is much greater for the F-EA and therefore larger burn-up rates are practical: for ρ = 60 W/g, $\Delta\lambda_1 = 8.81 \times 10^{-3}$ which is quite acceptable.
2) A consequence of the relatively long mean life of ^{233}Pa (1/e decay after τ = 39 days) is that a significant reactivity increase occurs during an extended EA shut-down. Conversely, any prolonged increase in burn-up rate produces a temporary reduction of reactivity until the ^{233}Pa inventory has been re-established. The magnitude of such a reactivity change following a shut-down need not be a problem, but appropriate measures would be required to correct its effects. The density of ^{233}Pa is given by

$$N(^{233}Pa) = \tau(^{233}Pa \rightarrow ^{233}U)\overline{\sigma_{\gamma+fiss}(^{233}U)}N(^{233}U)\phi =$$
$$= (1 + \alpha)\tau(^{233}Pa \rightarrow ^{233}U) \times \left[N(^{233}U)\overline{\sigma_{fiss}}(^{233}U)\phi\right]$$

where α is the ratio of the non-fission (n,γ) to fission reactions and the last term $N(^{233}U)\overline{\sigma_{fiss}}(^{233}U)\phi$ is directly proportional to the ^{233}U burn-up rate, ρ. If the accelerator beam is shut down, following the characteristic decay lifetime $\tau(^{233}Pa \rightarrow ^{233}U)$, the concentration of ^{233}U will increase by an amount asymptotically equal to $N(^{233}Pa)$, essentially independent of the mode of operation of the EA for a given equilibrium burn-up rate. However since in the case of the F- EA the equilibrium concentration ξ of ^{233}U is about nine times larger, its effect on reactivity $\max(\Delta k/k) = N(^{233}Pa) / N(^{233}U)$ will be only 1/9 of the one for a T-EA. For the chosen examples of burn-up rates, $\max(\Delta k/k) \approx 5.2 \times 10^{-2}$ for the T-EA and only $\max(\Delta k/k) \approx 2.08 \times 10^{-2}$ for the F-EA, in spite of the factor four in ρ in favour of the present option.

3) Neutron losses due to the high cross section fission product ^{135}Xe are well known [29]. The Xenon poison fraction is neutron flux dependent, since it relates, like in the case of ^{233}Pa to an equilibrium between captures and decays. For thermal neutrons and at the breeding equilibrium, the fraction of neutrons captured by ^{135}Xe is given by $\Delta\lambda_3 \approx 0.9 \times 10^{-19}\phi / (2.1 \times 10^{-5} + 3.5 \times 10^{-18}\phi)$ which tends to an asymptotic value $\Delta\lambda_3 \approx 0.021$ for a flux $\phi \approx 2.7 \times 10^{13}$ cm^{-2} s^{-1}. Following a reactor shutdown or reduction in power, the Xenon poisoning temporarily increases even further [29] because decays producing Xe continue to occur, passing through a maximum 10 to 12 hours after the shutdown. The magnitude of this transient additional poisoning is also dependent on the neutron flux. Although the temporary loss is not significant, a reactivity reserve, if normally compensated by control rods, would represent a permanent loss of neutrons. The Xenon type poisoning effect is essentially absent in the case of F-EA, since there is no fission fragment nucleus which has the required features in the energy domain of importance.

As one can see in a F-EA the importance of these effects is much smaller. The estimated effects at the burn-up rate $\rho = 60$ W/g are given in Table 2.3.

The reactivity increase due to ^{233}Pa decays is quoted for a 10 day cooling period, since such a time is largely sufficient to overcome any imaginable technical problem, assuming that the "scram" system fails in blocking the reactivity. The most direct consequence of this fact is that a larger value of *k* is operationally conceivable, with a consequently higher energetic gain, (see paragraph 2.6). As discussed further on, the temperature coefficient of criticality is negative, corresponding to $\Delta k = + 0.01$ for a temperature drop of 700 ^{o}C. Adding linearily the effect of such a large temperature swing to the 10 day intervention limit suggests that the largest, practical

maximum value of operational reactivity of a subcritical F-EA is about $k \leq 0.98$. It should be noted however that already for $k = 0.96$ the recirculation power through the accelerator is less than 10% of the delivered, useful electric power.

2.6 - Computing methods. The exact definition of the parameters of the F-EA implies an appropriate account of the resonance or otherwise complex energy behaviour of the cross sections of the many elements which intervene in the cascade reactions.

As in Ref. [1] we have adopted a Montecarlo method in which a large number of individual neutrons are followed from their birth to absorption. We make use of the concept of neutron generation and introduce the effective multiplication coefficient k_{eff}, the fraction of neutrons which are regenerated at each generation. Both fissions and (n, 2n) reactions are considered. Cross sections are finely interpolated from the most complete sets of cross section data available today [30] and include all main channels, like for instance inelastic (n,n') scattering. Thermal movement of the target nuclei (Doppler broadening) is included in the simulation.

The elementary structure of the EA is subdivided in a number of different regions, which reflect the geometrical properties of the device. The composition of each of these regions is allowed to change as a function of time taking into account the changes in concentrations of the newly produced elements due to (1) the nuclear transformations and (2) the spontaneous decay chain. A complete database of all known elements with their decay modes and rates is used [31] and new elements are introduced to the list whenever a decay or a reaction channel justifies it.

Particular attention has been given to fissions, since they are the dominant, driving process for the multiplication. The energy dependence of the neutron multiplicity has been parametrized from existing data [30].

One important feature of the programme is the one of calculating the evolution of the (poisoning) fission fragments. In order to do so effectively many hundreds of different elements must be followed during the calculations. This very complete method of simulation has been made possible only recently due to the availability of more powerful computers. It is still somewhat limited in the statistical accuracy due to lack of computing power [32].

In practice, the computer programme requires that one defines the different geometrical regions, their initial composition and their operating temperatures. One

has to define then the scale of time and of reaction activity. The programme then calculates the time evolution of the system — based of course on a much smaller random neutron population but with changes of concentrations scaled to the actual flux — and calls on further elements whenever required. The calculation can be coupled with a Montecarlo programme which simulates the high energy cascade. Hence the Montecarlo emulates the whole process initiated by an incoming beam of specified characteristics. More often it is used as a stand-alone module to determine the multiplication coefficient k_{eff}, starting from an initial spectrum due to fission neutrons.

The Montecarlo method has the advantage over other methods that in principle it provides a very realistic evolution of the system. However the computing time is long and the results affected by statistical errors. Therefore it has been coupled with another, simpler evolution programme, which permits a faster exploration of the main features of an EA. This programme makes use of some of the information from the full Montecarlo, namely

1) the averaged cross sections for all relevant elements are extracted as the average over the energy and the fuel volume of the flux as computed by the Montecarlo. Since (see paragraph 2.2) the flux is rather uniform over the fuel elements, the spatial average is a good approximation. The averaging over energy may introduce some approximations in presence of strong resonances, where the flux may be locally affected. The extent of this approximation has been checked comparing true Montecarlo with the evolution programme and found acceptable for our purposes.
2) the parameter *L*, namely the sum of fractional losses of neutrons (absorbed in a variety of ways, like captures in structures and coolant, diffused outside the EA and so on) is divided into two components, namely a term which is constant, but geometry dependent and another (mainly due to fission-product poisons, spallation and activation nuclei etc.) which is linear in the burn up. This parametrization is in excellent agreement with the Montecarlo results. Actual values to be used in the evolution programme are fitted from the Montecarlo simulation. Hence they take into account all burn-up dependent neutron losses.

The time evolution in a slab of material subject to a neutron flux and with spontaneous decays cannot be calculated following the classic Bateman evolution equations [33]. This is due to the fact that the Bateman's description assumes an open, successive chain of decay nuclei, eventually leading to the final stable isotopes, namely a specific path in the (A,Z) plane. Under the simultaneous action of neutrons

and decays, nuclei can both rise (neutron induced reactions) and fall in the atomic A, Z number (spontaneous decays). Hence the decay paths in the (A,Z) plane perform loops which may bring back the same nucleus an arbitrary number of times and imply products of an infinite number of terms, although with a decreasing probability. For this reason our time evolution programme is based on numerical step-wise methods. In our analysis both programmes are used and give consistent results. Furthermore the neutron flux and criticality predicted by the Montecarlo programme is in good agreement with the results of standard, non evolutionary programmes [34].

2.7 - Cumulative fission fragment poisoning. One of the most serious limitations in the T-EA comes from the losses of neutrons due to slowly saturating or non saturating fission fragments (FFs). In contrast to ^{135}Xe and ^{149}Sm, which have a very large neutron cross section and therefore reach saturation in a short time, the majority of the fission products have cross sections which are comparable or smaller than the one of the fuel itself. Hence the aggregate poisoning effect of such fission products is roughly proportional to the fractional burn-up of the fuel. The accumulated effect depends significantly on the past history of the fuel. Computer calculations have been used to analyse the poisoning as a function of the integrated burn-up for a variety of different conditions.

One important result is that losses due to fission fragment poisoning are much less important for a F-EA, when compared to a T-EA (Figure 2.4). In both cases however the build up of FFs implies a progressive reduction of criticality.

An important feature of the F-EA is that it is possible to operate the device for a long time (several years) without intervention on the fuel. In order to enhance such a feature we have investigated the possibility of starting with a ^{233}U concentration smaller than at the breeding equilibrium ξ and thus compensate as much as possible the drop of criticality due to fission fragment poisoning with the help of the increasing fraction of bred ^{233}U.

In Figure 2.5 we have considered with the help of the evolution programme the criticality coefficient k for the EA device described in paragraph 2.3 as a function of burn-up for a constant neutron flux and given initial ^{233}U concentration. Since the neutron flux will in practice depend on time, the criticality coefficient will be slightly affected also by the dependence of the ^{233}Pa concentration with flux. The initial criticality coefficient is adjusted "ad hoc" to $k = 0.965$ by slightly increasing the

neutron losses *L*. The initial filling of ^{233}U is set to $\xi = 0.117$, significantly lower than the breeding ratio at equilibrium. The graph shows three different fluxes and hence power yields, ρ. The general behaviour of the curves shows an initial drop related to ^{233}Pa production, followed by a rise due to the increment of ξ due to breeding. Fission fragment captures eventually become important and bring down *k*. A higher ρ gives lower *k* values since early captures in ^{233}Pa reduce the breeding yield. Curves without fission fragment poisoning are also shown. One can conclude that (1) a very smooth running is possible up to a burn up of the order of 150 GW day/ton, essentially without intervention and (2) a power yield of the order of $\rho \approx 100$ W/g is perfectly acceptable[19]. An extended shut-down will move to the curve for $\rho \to 0$, still sufficiently far away from criticality. Of course, as already pointed out, in view of the long ^{233}Pa lifetime, there is plenty of time to introduce corrective measures.

For a fixed beam power the flux is time dependent, and will vary proportionally to gain. Since gain is related to the ^{233}Pa concentration and in turn to its capture probability, the dependence of *k* as a function of burn up is even smoother. In Figure 2.6 we show the typical *k* behaviour for a somewhat larger initial value of *k*. Almost constant conditions can be ensured without intervention over a burn up of $100 \div 150$ GW day/t, namely over several years.

2.8 - Higher Uranium isotopes and other actinides. Higher Uranium isotopes and higher Actinides are produced by successive neutron captures. The time evolution of an initially "pure" ^{232}Th and ^{233}U fuel mixture can be easily calculated and is given in Ref. [1] for a T-EA. The build-up of the several isotopes introduces more captures and some fissions. Hence in principle the multiplication coefficient *k* is also modified. It was shown in Ref. [2] that the asymptotic mixture preserves an acceptable value of k for initial ^{232}Th both in thermal and fast neutron conditions, while for initial ^{238}U only fast neutrons preserve an acceptable gain.

In the EA the initial fuel is *completely* burnt in a closed, indefinite cyclic chain in which Actinides of the spent fuel become the "seeds" of the next fuel cycle [1]. At each discharge an appropriate amount of fresh fuel is added to compensate for the burn-up and the accumulated nuclear species, products of the fission (fission fragments, FFs) are removed. The initial fuel nuclei (either Th^{232} or U^{238} or

[19]Note that in the present design, we have conservatively set the power density to about one half of this value.

eventually a mixture of both) undergo a series of transformations induced by neutron captures and spontaneous decays, until they achieve ultimate fission. The first of these transformations is the initial "breeding" reactions which continue to be the dominant source of fissions (^{233}U or ^{239}Pu respectively) even after a long burn-up. However a rich hierarchy of secondary processes builds up at all orders. These secondary processes become essential in determining the atomic concentration vector $c_{(A,Z)}$ of Actinides and hence the neutron economy of the cascade. For stationary conditions the atomic concentration vector $c_{(A,Z)}(\phi)$ tends asymptotically, (i.e. after long burn-ups) to a limiting equilibrium value.

In order to estimate the actual evolution of $c_{(A,Z)}(\phi)$ we have studied the time evolution of some fuel exposed to the average flux of an F-EA with the help of the evolution programme and using the cross sections of Table 2.2. Results have been checked with the full Montecarlo programme. The chain of many successive re-fillings has been simulated. Although the results are widely independent of the power density, for definiteness the value ρ = 100 W/g has been used. After a pre-assigned burn-up of 150 GW day/t, Actinides are discharged and the fuel topped-up with fresh ^{232}Th. Since the amount of fuel burnt is not negligible the stockpile of ^{233}U is affected by the over-all reduction of the fuel mass, even if the relative concentration with respect to ^{232}Th has remained constant (at the breeding equilibrium) or significantly increased (if initially below the breeding equilibrium). It is therefore necessary in general to add to the renewed fuel an amount of ^{233}U which is larger than what is recovered at the discharge. For this reason a small breeder section has to be added to the EA: initially made of pure Thorium, it is designed to supply such a needed difference. The total ^{233}U stockpile as a function of burn up has been calculated with the full Montecarlo for the geometry given in paragraph 2.3 and shown in Figure 2.7. With the help of such an extra breeding, it is realistic to expect that the initial volume of ^{233}U can be made available at the end of the cycle. Therefore in our simulation of the evolution of $c_{(A,Z)}(\phi)$ we assume that both ^{232}Th and ^{233}U are topped up to the initial values at each filling. The new fuel will contain in addition all the remaining Actinides produced by the previous combustion.

In Figures 2.8a, 2.8b and 2.8c we show the Actinide distribution at discharge, as a function of the discharge number. The relative concentrations are listed in Table 2.4. All elements clearly reach an asymptotic concentration, in which production and incineration are in equilibrium. Concentrations of higher actinides tend to a stable equilibrium condition which is a fast decreasing function of A and Z. This is due to the fact that almost at each step of the neutron induced evolution ladder, fissions subtract a significant fraction of nuclei. The most offending isotopes, because of their

amount and their radio-toxicity, namely ^{231}Pa and ^{232}U are practically close to the asymptotic values of 1.06×10^{-4} and 1.30×10^{-4} already at the first discharge. Note also the large concentration of ^{234}U which quickly reaches an asymptotic concentration which is about 38% of ^{233}U. The Uranium composition at (asymptotic) discharge is therefore 9.354×10^{-4} of ^{232}U, 63.88 % of ^{233}U, 24.12 % of ^{234}U, 5.870 % of ^{235}U, 6.01 % of ^{236}U and 1.03×10^{-4} of ^{238}U, which constitutes about 14% of the spent fuel mass. Likewise the Neptunium and Plutonium, produced in negligible amounts during the first fillings grow to asymptotic values of 0.2% and 0.1 % respectively. Plutonium is dominated by the isotope ^{238}Pu which has the short half life of 87.7 years and therefore has no practical military application. Higher Actinides, Americium and Curium, never reach concentrations of significance. Note that for instance after 20 refilling the fuel seeds have produced an integrated burn up of the order of 3000 GW day/t and therefore these contaminating amounts, once normalised to the produced energy are totally negligible. For instance the Plutonium concentration at the discharge of an ordinary PWR is about 1.1% for 33.0 GW day/t. The amount of trans-uranic Actinides produced per unit of energy delivered is about three orders of magnitude less than in an ordinary PWR.

We have compared the evolution of k as a function of burn-up obtained with the simple evolution programme and the "exact" calculations of the Montecarlo programme. As shown in Figure 2.9, the agreement is excellent.

The behaviour of the multiplication coefficient *k* as a function of the burn-up during successive refills is given in Figure 2.10. One can see that in spite of the significant change of the fuel composition, the value of *k* remains remarkably constant.

We conclude that the fuel can be indefinitely used in an open ended chain of cycles. Indeed the fuel can survive the lifetime of the installation and be re-used as long as there is demand for EAs, with very small or no loss of performance. In contrast with an ordinary reactor the EA produces no "Actinide Waste" to speak of, but only valuable "Seeds" for further use and once the asymptotic concentrations have been reached, there is no significant increase with operation of the radio-toxicity of the Actinide stockpile (see next paragraph).

2.9 - Elementary, analytic formulation of Actinide evolution. A number of simplifying assumptions permits calculating analytically the essential features of the evolution of the concentration vector $c_{(A,Z)}(\phi)$. We ignore the discontinuity of the

refills and assume a constant inflow of the father element and neglect the (n,2n) and other channels which may introduce "loops" in the (A,Z) evolution plane, as already mentioned. We assume that in the presence of the neutron flux ϕ, for all elements there is only one transformation channel (either with neutron capture averaged cross section $\sigma_{capt}^{(i)}$ or radioactive decay with decay rate $\lambda^{(i)}$, whichever is dominant) and a dissipative, fission channel with spectrum averaged cross section $\sigma_{fiss}^{(i)}$. For very high values of A spontaneous fission and other forms of nuclear instability will contribute to such dissipative terms. The rate of transformation in a neutron flux ϕ is $\phi\sigma$ and the total rate $\mu^{(i)} = \phi(\sigma_{capt}^{(i)} + \sigma_{fiss}^{(i)})$ or $\mu^{(i)} = \phi\sigma_{fiss}^{(i)} + \lambda^{(i)}$ if the transformation is decay dominated. The survival, chaining coefficient, which represents the probability of continuation to the next step of the evolution chain is defined as $\alpha^{(i)} = \sigma_{capt}^{(i)} / (\sigma_{capt}^{(i)} + \sigma_{fiss}^{(i)})$ or $\alpha^{(i)} = \lambda^{(i)} / (\lambda^{(i)} + \sigma_{fiss}^{(i)} \times \phi)$ respectively. The procedure is schematically shown below:

Chain	$P \rightarrow \quad N_1 \rightarrow$ $\downarrow$	$N_2 \quad \rightarrow$ $\downarrow$	$N_3 \quad \rightarrow$ $\downarrow$	$N_i \quad \rightarrow$ $\downarrow$
Initial amount	$N_1(0)$	0	0	0
Removal rate	$\phi\sigma_{fiss}^{(1)}$	$\phi\sigma_{fiss}^{(2)}$	$\phi\sigma_{fiss}^{(3)}$	$\phi\sigma_{fiss}^{(i)}$
Transfer rate	$\phi\sigma_{capt}^{(1)}, [\lambda^{(1)}]$	$\phi\sigma_{capt}^{(2)}, [\lambda^{(2)}]$	$\phi\sigma_{capt}^{(3)}, [\lambda^{(3)}]$	$\phi\sigma_{capt}^{(i)}, [\lambda^{(i)}]$
Survival coeff. $\alpha^{(i)}$	$\frac{\sigma_{capt}^{(1)}}{\sigma_{capt}^{(1)} + \sigma_{fiss}^{(1)}}$	$\frac{\sigma_{capt}^{(2)}}{\sigma_{capt}^{(2)} + \sigma_{fiss}^{(2)}}$	$\frac{\sigma_{capt}^{(3)}}{\sigma_{capt}^{(3)} + \sigma_{fiss}^{(3)}}$	$\frac{\sigma_{capt}^{(i)}}{\sigma_{capt}^{(i)} + \sigma_{fiss}^{(i)}}$
Total rate $\mu^{(i)}$	$\phi\sigma_{fiss}^{(1)} + \lambda^{(1)}$	$\phi\sigma_{fiss}^{(2)} + \lambda^{(2)}$	$\phi\sigma_{fiss}^{(3)} + \lambda^{(3)}$	$\phi\sigma_{fiss}^{(i)} + \lambda^{(i)}$

Assuming first no refill ($P = 0$) and an initial number of nuclei $N_1(0)$, the time evolution is given according to the Bateman equation (i >1):

$$N^{(i)}(t) = N^{(0)}(t)\left(\prod_{j=1}^{j=i-1}\alpha^{(j)}\right)\times\left[\left(\prod_{j=1}^{j=i-1}\mu^{(j)}\right)\times\sum_{j=1}^{j=i}\frac{\exp(-\mu^{(j)}t)}{\prod_{\substack{k=1\\k\neq j}}^{k=i}(\mu^{(k)}-\mu^{(j)})}\right]$$

If alternatively, there is refill at the constant rate P per unit time and no initial nuclear sample, i.e. $N_1(0) = 0$, the formula becomes (i > 1)

$$N^{(i)}(t) = P\left(\prod_{j=1}^{j=i-1}\alpha^{(j)}\right)\times\left[\left(\prod_{j=1}^{j=i-1}\mu^{(j)}\right)\times\sum_{j=1}^{j=i}\frac{1-\exp(-\mu^{(j)}t)}{\mu^{(j)}\prod_{\substack{k=1\\k\neq j}}^{k=i}(\mu^{(k)}-\mu^{(j)})}\right]$$

In practice, both refilling and initial nuclei are present and the actual number of nuclei will be simply the sum of the two above terms. Note that for ρ ≈ 100 W/g, $\phi \approx 5\times10^{15}$ cm^{-2} s^{-1} and that the sum of cross sections is of the order of magnitude of $\approx 2\times10^{-24}$ cm^2, leading to an evolution time constant $1/\mu^{(i)}$ of the order of ≈ 3 years.

The asymptotic distribution is reached at the limit $t\to\infty$. At this stage the process is dominated by the refill term *P* and one can easily calculate the equilibrium amounts:

$$N^{(i)}(t\to\infty) = P\frac{\left(\prod_{j=1}^{j=i-1}\alpha^{(j)}\right)}{\mu^{(i)}} = N^{(1)}(t\to\infty)\frac{\mu^{(1)}}{\mu^{(i)}}\left(\prod_{j=1}^{j=i-1}\alpha^{(j)}\right)$$

The time required by $N^{(i)}$ to grow to $N^{(i)}(t\to\infty)(1-1/e)$is approximately given by $\sum 1/\mu^{(j)}$ where the sum is extended up to i. Since the order of magnitude of the time constant is typically 3 years, equilibrium is reached after ≈ 3 (i-1) years where we have used i-1 to take into account that the step through the ^{233}Pa is fast. The fast decrease of $N^{(i)}(t\to\infty)$ with the rank in the chain is due to the product of the $\alpha << 1$ terms. To a fast decreasing degree of concentrations, the whole table of elements is eventually involved. As already pointed out, in practice the chain is not open-ended since spontaneous fissions and other instabilities ensure very small α–values toward the end.

2.10 - Practical considerations. Strictly speaking, continuing operation of the EA requires merely the recycling of the Uranium isotopes. However at each refill of the fuel, inevitably, individual Actinides are separated during the reprocessing. Furthermore their relative incineration rate is independent of the concentration. Therefore, although their elimination requires permanence in the EA for a long time, it is not mandatory to dilute these extra products in every fuel refill of each EA. They can be accumulated and inserted instead in a dedicated device. Whichever strategy is chosen, the already calculated evolution of the trans-uranic stockpile as a function of the integrated burn up (Figures 2.8a-c) remains valid.

In order to positively destroy such trans-uranic Actinides, the exposure time is long, extending over many refilling steps. Since their relative amount is very small it is possible to concentrate them in a few, dedicated fuel bars, to be inserted

somewhere in the bundles of ordinary fuel, which is then made of Uranium and Thorium only. After irradiation, such dedicated bundles do not need further reprocessing, since even if the local Fission Fragment concentration becomes very high, it will not affect the over-all criticality of the device which is not appreciably different than if they were generally distributed. Therefore it may be sufficient at each refill of the main fuel to bleed the gaseous fragments produced and to add a new protecting sleeve or otherwise ensure the continuing mechanical strength of such specialised fuel bars: it will make sense not to reprocess them any more, until all actinides are positively transformed into fission fragments and their incineration completed.

Therefore a practical scenario will consist in (1) reprocessing of the bulk of the spent fuel at each refill, with separation of Thorium and Uranium which are to be used to fabricate the next fuel refill and (2) separation at each reprocessing stage of the trans-uranic Actinides and of Protactinium in a small stockpile which is then introduced in the neutron flux of the EA once and for all and up to its total incineration, with gas bleeding and strengthening of the cladding at each refill.

The amount of elements at the discharge depends critically on the concentration of ^{236}U, which acts as the gateway to ^{237}Np. Therefore we have considered the production of trans-uranic elements after 150 GW day/t, starting from the asymptotic mixture of Uranium in the fuel. Much smaller amounts will be produced during the early fillings, as seen from Figures 2.8a-2.8c. Results are listed in Table 2.5. The discharge consists primarily of ^{237}Np (66.0 %), ^{231}Pa (4.24 %), medium lived ^{238}Pu (26.1 %, half-life of 87.7 years) and 239Pu (3.3%) and it is ridiculously small, namely 276 grams/ton of fuel, or 4.14 kg for a 15 ton discharge. The radioactive heat of this discharge is ≈ 600 W, primarily due to ^{238}Pu, and quite manageable. The relative radio-toxicity of such trans-uranic products is also very modest, when normalised to the produced energy. The volume is only a few percent of the production of a PWR for the same energy. As already pointed out, once inserted in an appropriate fuel containment rod, they will not be handled again until fully incinerated. In view of the simplicity of such a procedure, geologic storage of trans-uranic waste from an EA is unnecessary. Clearly the best place to put the unwanted long lived waste is the EA itself, where an incineration lifetime of years is at hand.

2.11 - Proliferation issues. A great concern about Nuclear Power is that military diversions may occur with the spent fuel. The present EA scheme offers much better guarantees against such a potential risk. We assume that the procedure of fuel loading and reprocessing is the one described in the previous section. Critical

Masses (CM) and other relevant parameters for bare spheres of pure metal are listed in Table 2.6. The addition of a neutron reflector, a few inches thick may be used to reduce the CM by a factor two or so.

One can see that three chemical elements of the discharge, namely the asymptotic Uranium Mixture, Neptunium and Plutonium exhibit potential nuclear explosive features. However several other features limit the feasibility of an actual explosive device. We consider them in turn, following the arguments given in Ref. [35]:

1) Decay heat produced by the α-decays of the material in some instances is much larger than the eight watts emitted from the approximately three kilograms of weapon grade plutonium which is suggested to be in a modern nuclear warhead. Since the high-explosive (HE) around the fuel would have insulating properties (≈ 0.4 W m $^{o}C^{-1}$), only 10 cm of HE could result in an equilibrium temperature of about 190 ^{o}C for 100 W of heat. Apparently the breakdown rate of many types of HE becomes significant above about 100 ^{o}C. Although methods could be envisaged to add heat sinks to the device, we assume that α-heat yield much larger than 1000 W will not be acceptable.
2) Gamma activity from some of the decay products of the chain are making the handling of the device during construction and deployment very risky and eventually impossible. In particular the hard γ-ray emitted by ^{208}Tl is very hazardous. The corresponding dose rate of 30 kg of Uranium mixture with 10^3 ppm of ^{232}U contamination is asymptotic after 10^3 days [36] and is about 3.6×10^4 mSv/hour which corresponds to a 50% lethal dose after 10 minutes exposure to the bare mass.
3) Spontaneous fissions produce neutrons which could cause the pre-initiation of the chain reaction and thus dramatically reduce the potential yield of the device. Gun-type implosion systems, which are the easiest to realise, are particularly sensitive to pre-ignition. This effect for instance discourages the use of such simple systems in the case of weapon grade Plutonium, which has a yield of 66 n g^{-1} s^{-1}, where high power explosives providing an implosion speed of one order of magnitude larger must be used. We assume therefore that fuels with a neutron yield much larger than 1000 n g^{-1} s^{-1} are not practical, leading to a too small "fizzle yield", namely the smallest possible yield resulting from pre-initiation.

As already mentioned, the total discharge of Neptunium and Plutonium is of the order of 4 ÷ 5 kilograms after a long burn-up (5 years of operation) of a typical

EA. Hence in order to accumulate the amount of explosive to reach a single CM the full discharges of many decades of operation, and the result of the reprocessing of hundreds of tons of spent fuel must be used. Note that according to our scenario, this is impossible since the spent fuel is re-injected in the EA right after reprocessing and completely incinerated. Clearly the accumulation of a CM demands suspending such a procedure for decades. In addition it will be a very poor explosive, since as one can see from Table 2.6, both cases will have a very small "fizzle yield" which will require HE ignition. This effect is particularly large in the case of Neptunium, since the CM will produce 10^{10} n/s! In the case of Plutonium, this effect is also large, but the ignition method will be heavily hampered by the large heat production of the short-lived (half-life 87.7 y) ^{238}Pu isotope, 4.4 kW for the CM.

Therefore the main concern stems from the possible diversion of the Uranium Mixture, which is abundantly produced. It has been suggested to denature the Uranium adding a significant amount of ^{238}U. In our view such a method is not foolproof since the ^{238}U will quickly produce ample amounts of ^{239}Pu which is a well proven, widely used explosive and which could be extracted maliciously during reprocessing, as is the case of ordinary PWRs. Instead we believe that the very strong γ-radiation from the ^{208}Tl contaminant constitutes a strong deterrent and an excellent way to "denature" the fuel. A new technology in constructing, assembling and handling the weapon must be developed, which we believe is highly self-discouraging, with respect to other ways of achieving such a goal.

2.12 - Burning of different fuels. As one can see from Table 2.2 the majority of Actinides have a large cross section for fission. Therefore the required level of sub-criticality can be attained with a very large variety of different fuels. Clearly the choice is application dependent and an almost infinite number of alternatives are possible. In this report we shall limit ourselves to a number of specific cases.

1) Fuel based on ^{238}U, in which the fissile element bred is Plutonium, which might be of interest in view of the huge amount of unused depleted Uranium. The main draw-back of this fuel, when compared with Thorium is the large amount of Plutonium and higher Actinides produced. However they are eventually incinerated and the stockpile remains constant, just as in the case of the previous example based on Thorium.
2) Initial mixture of Thorium and "dirty" Plutonium from the large amount ($\geq$ 1000 tons) of the surplus Plutonium stockpile, presently destined to the geologic storage. In this way one can actually "transform" Plutonium into ^{233}U with about 85% efficiency, to be used for instance to start-up other EAs,

besides incinerating the unwanted ashes and producing a considerable amount of useful energy.

We shall briefly review the basic properties of the breeding cycle based on ^{238}U, $^{238}U + n \xrightarrow{(n,\gamma)} {}^{239}U \xrightarrow{\beta^-} {}^{239}Np \xrightarrow{\beta^-} {}^{239}Pu$. Such a burning cycle is of interest in view of the huge amount of surplus of depleted Uranium, but it implies a major concern in view of the larger radio-toxicity of the spent fuel and of the possible military diversion of the large amounts of Plutonium. It has been shown in Ref. [1] that the thermal EA cannot use this fuel, since the asymptotic fuel has a reactivity k_∞ which is smaller than the one of Thorium. With fast neutrons, however, this cycle has "per se" some advantages over the Thorium cycle, namely an even higher reactivity k_∞ which in principle could permit envisaging even a critical device and a shorter half-life (2.12 days) of the intermediate ^{239}Np which considerably reduces the reactivity changes with power, as shown in Table 2.7.

Cross sections have been integrated over the neutron spectrum calculated with Montecarlo methods on a realistic model (see paragraph 2.6). The breeding ratio ξ is somewhat larger than the one for Thorium, while the amount of intermediate state ^{239}Np is much smaller, mainly because of its shorter lifetime. The main consequence is that the variation $Max(\Delta k)$ subsequent to an extended shutdown and the breeding loss due to premature captures in ^{239}Np are much smaller. Note that the value of k_∞ at breeding equilibrium is for the binary mixture ^{238}U – ^{239}Pu. As we shall see the Plutonium mixture will rapidly evolve in a mixture of several isotopes, which reduce the value of k_∞ at the asymptotic limit.

Notwithstanding, as already pointed out in the introduction, the large value of k_∞ at first sight would indicate that for instance a traditional Fast Breeder might suffice to exploit the fuel cycle [37][18]. But in the case of an EA the excess criticality could be used to extend the burn up, typically in excess of 200 GW day/t, in presence of fission fragments, starting the EA with a mixture well below the breeding equilibrium. The radiation damage of the fuel sleeves and the gas pressure built up have to be periodically taken into account, for instance by a periodic renewal of the fuel encapsulation and gas bleeding. These procedures are much simpler than a full reprocessing and in principle do not have to be exposed to the full radio-toxicity of the fuel.

Reprocessing and in general the fuel handling strategy implies that several components of the spent fuel are assembled into a renovated fuel, eventually with the external supply of additional fuel (i.e. "dirty" Plutonium) and/or with additional fissile material produced in the breeder section. A simplified, elementary method of

estimating the relevant multiplication coefficient can be formulated assuming that the neutron spectrum in the EA is not appreciably affected by the variations in the mixture. This is only approximately valid in the case of strong resonances which may produce "screening", namely local "dips" in the spectrum. Also large variations of fuel concentration will affect the spectrum and hence the performance of the system since the fraction of captures and the lethargy effects in the Lead diffuser will change. Notwithstanding, such a treatment could be very useful to understand at least qualitatively the general evolution during burn-up and refills.

The multiplication coefficient k_∞ of a small amount of element mixture of two components exposed to an "external" neutron flux ϕ(E) is given by

$$k_\infty^{(1+2)} = \frac{\sum_1^n N_i \sigma_{fiss}^{(i)} \nu^{(i)}}{\sum_1^n N_i \left(\sigma_{fiss}^{(i)} + \sigma_{capt}^{(i)}\right)} = \frac{\phi \sum_1^k N_i \sigma_{fiss}^{(i)} \nu^{(i)} + \phi \sum_{k+1}^n N_i \sigma_{fiss}^{(i)} \nu^{(i)}}{\phi \sum_1^k N_i \left(\sigma_{fiss}^{(i)} + \sigma_{capt}^{(i)}\right) + \phi \sum_{k+1}^n N_i \left(\sigma_{fiss}^{(i)} + \sigma_{capt}^{(i)}\right)} = \frac{n_1 k_\infty^{(1)} + n_2 k_\infty^{(2)}}{n_1 + n_2}$$

where $\nu^{(i)}$ is the spectrum averaged neutron multiplicity due to fissions and the multiplication coefficients for the two media are, as obvious

$$k_\infty^{(1)} = \frac{\sum_1^k N_i \sigma_{fiss}^{(i)} \nu^{(i)}}{\sum_1^k N_i \left(\sigma_{fiss}^{(i)} + \sigma_{capt}^{(i)}\right)}; \text{ and } \quad k_\infty^{(2)} = \frac{\sum_{k+1}^n N_i \sigma_{fiss}^{(i)} \nu^{(i)}}{\sum_{k+1}^n N_i \left(\sigma_{fiss}^{(i)} + \sigma_{capt}^{(i)}\right)}$$

The weights are given simply by the relative absorption rates (per unit time) in the two media

$$n_1 = \phi \sum_1^k N_i \left(\sigma_{fiss}^{(i)} + \sigma_{capt}^{(i)}\right) \quad \text{and} \quad n_2 = \phi \sum_{k+1}^n N_i \left(\sigma_{fiss}^{(i)} + \sigma_{capt}^{(i)}\right)$$

In order to simplify the algebra we have limited our consideration to the dominant contribution due to fission. The discussion can be easily extended to other processes, like (n,2n) and so on. Generalising, the multiplication coefficient of a mixture of n-elements is simply given by the "stoichiometric" weight of the coefficients of the components. In particular, after n cycles with refills of fuel with no external additions (each after a predetermined flux exposure $\beta = \int \phi dt$) the multiplication coefficient can be easily estimated as stoichiometric sum of the same fuel which is subject to a series of successive exposures corresponding to $n\beta, (n-1)\beta, (n-2)\beta \cdots\cdots, \beta$. If at each cycle some fresh amount of fuel is added or eventually some component is removed, its contribution must obviously be added or subtracted stoichiometrically.

Linearization of the problem permits using simple "chemistry" considerations which are very useful for instance in defining the strategy of the refills. The definition of the elements of the mixture is of course dependent on the problem one wants to

solve. They can be either the refill mixture or even single isotopes. Each of the elements will then independently evolve inside the fuel i.e. N_i will change with time. In our approximation the total number of nuclei $\sum N_i$ will decrease because of fissions. Clearly the gain G is not a linearized quantity and it must be estimated with the help of the parameter k. In order to calculate k, one has to introduce the effect of the losses L as discussed in the previous paragraphs, starting from the value of k_∞.

The total burn up of the fuel is the sum of the burn-ups of the elements, since the power produced is the sum of the power delivered by each of the elements, $\rho = \sum \rho^{(i)} = \phi \varepsilon_{fiss} \sum N_i \sigma_{fiss}^{(i)}$, where $\varepsilon_{fiss} = 3.2 \times 10^{-11}\, joules$ is the energy produced by each fission.

We have estimated the evolution of some of the primary ingredients of the fuel strategy. Spectra are taken from the exemplificative designs of section 2.3. They should be a good representation of the actual situation, with the above mentioned provision. We have considered sub-fuel elements made of pure ^{232}Th, ^{233}U, ^{235}U, ^{239}Pu and the typical trans-uranic discharge of a PWR after 33 GW day/t of burn-up, in which Np, Pu, Am and Cm isotopes have been included. In Figure 2.11 we have plotted k_∞ as a function of the days of exposure to a flux $\phi = 4.0 \times 10^{15}$ n cm^{-2} s^{-1}. One can distinguish the difference between the fissile elements which have a k_∞ decreasing with the isotopic evolution of the mixture and the breeder elements in which k_∞ starts very small (some fission is present even for pure elements) and grows because of the progressive breeding of fissionable elements.

In order to estimate the value of k_∞ for a mixture of such elements as a function of the burn-up one has to introduce the stoichiometric weights n_i. In Figure 2.12 we plot $r_{abs}^{(i)}$ the relative absorption rates (per unit time) for 1 initial gr/cm^3 of each element, which must then be multiplied by the actual initial concentration of each element d_i to compute n_i.. Likewise the power produced for 1 gram of the mixture by the flux ϕ is easily calculated with the help of Figure 2.13, in which ρ_i, the power/gram of each element is given as a function of the integrated flux. The irradiation dependence and the power/gram of the mixture are then

$$k_\infty = \frac{\sum k_\infty^{(i)} r_{abs}^{(i)} d_i}{\sum r_{abs}^{(i)} d_i} \quad \text{and} \quad \rho[W/gr] = \frac{\sum \rho_i d_i}{\sum d_i} \frac{\phi\left[cm^{-2} s^{-1}\right]}{4 \times 10^{15}}$$

Note that in practice one might prefer to set the more relevant parameter ρ and derive the consequent flux, which is trivially done with the above formula. Finally in Figure 2.14 we give the disappearance rate of nuclei due to fissions as a function of the integrated flux. Note that the burn-up for full disappearance is about 950 GW day/t and therefore the burn-up for a given integrated exposure can be calculated

with the appropriate weights directly from the Figure 2.14, rather than integrating ρ. Fission fragment captures must be evaluated in order to calculate k from k_∞. An approximate formula has been derived from the full Montecarlo calculation and gives a linear dependence of the fraction of neutrons vs. burn-up, with L = 0.065 for 100 GW day/t.

As one can see from Figure 2.11 to Figure 2.14, the features amongst the various fissionable elements on one hand and of the two main breeding materials on the other are surprisingly similar. This means that a large flexibility exists in substituting a fissionable material for another or in building a convenient mixture of them: a wide spectrum of choices is possible, depending on the availability of fuels and on the application. The same EA can be used (even simultaneously) (1) to produce energy (2) to transform fuels, like for instance Plutonium discharge into ^{233}U and (3) to incinerate unwanted Actinides. In general using mixtures other than ^{232}Th/^{233}U would, however, produce fuel discharges with a much greater radio-toxicity.

2.13 - Conclusions. In order to ensure a practical utilisation of the fuel, the neutron distribution in an EA must be sufficiently uniform. This in turn requires abandoning the classic homogeneous fuel-moderator mixture geometry of an ordinary reactor and instead inserting sparse fuel elements in a strongly diffusive medium. Lead or Bismuth appear to be ideal materials for such purposes, at least for a F-EA. Other media with similar properties, like for instance Graphite or Heavy Water could be used for a T-EA.

The energetic gain of a T-EA, as discussed in Ref. [1] is of the order of G = 30÷50. In practice this is realised operating the EA at an effective multiplication k in the range 0.92 < k< 0.95. Fission poisoning limits the burn-up of the T-EA to some 30-50 GW day/t. There are other reasons which suggest operation of the T-EA with relatively small values of k, namely its relatively large variations due to decay mechanisms after shut-down or power variations (^{233}Pa and ^{135}Xe) so as to leave enough margin from risk of criticality.

The same type of considerations would however suggest a much greater gain for a F-EA [2], for which an operating point in the vicinity of k = 0.98 is an optimal operating point, corresponding to an energetic gain in the interval G= 100÷150. A first reason for this choice stems from the much larger value of $\overline{\varepsilon\eta} \approx 2.5$, which implies $k_\infty \geq 1.20$ and ΔL = 8.6 10^{-3} for k = 0.980. On the other hand the fission poisoning is much smaller and linearly growing with the burn-up, amounting to

about ΔL = 0.05 after 100 GW day/t. The flux dependent ^{135}Xe effect is absent and the time dependent k variation due to ^{233}Pa decays is much smaller for a given power density. All these considerations suggest k ≈ 0.98 as quite appropriate for a F-EA.

The multiplication factor k_∞ is such as to permit to reach such a k value with a ^{233}U concentration below the breeding equilibrium, thus permitting to compensate the growth due to fission fragment captures during operation with the increase of k_∞. In this way, very long burn-ups are possible without intervention and in exceptionally stable conditions.

At the end of each of these very long cycles, reprocessing is necessary in order to remove Fission Fragments and replace the burnt fuel mass with fresh Thorium. Uranium isotopes are chemically recovered and reused as seeds for the next fuel load. The rest of the trans-uranic Actinides are of modest amount (few kilograms) and they should be stored indefinitely in the EA where they are progressively incinerated. Thus, Geological Storage of Actinides is unnecessary.

Although the optimal performance of the EA is ensured with the Thorium cycle, a variable amount of other isotopes could be used instead, with very little or no change in performance. For instance depleted Uranium (^{238}U) of which vast amount of surplus exists, could be used to replace ^{232}Th. The fissionable ^{233}U could be replaced in part or totally with ^{235}U, ^{239}Pu or even the trans-uranic discharge mix of a PWR. Burning such unwanted "ashes" of the present PWR power plants is not only providing a very large amount of extra energy from an otherwise useless waste destined to geologic storage, but also helps to eliminate permanently materials that nobody wants.

Table 2.1 - Resonance Integral and Survival Probability for Lead and Bismuth (E_1 = 1 MeV, T = 20 ^{o}C)

Element	^{204}Pb	^{206}Pb	^{207}Pb	^{208}Pb	Nat Pb	^{209}Bi
Integral I_{res}						
E_2=1 eV	.0781	.00787	.0272	.000685	.00974	.00621
E_2=10 eV	.0649	.00728	.0125	.000676	.00626	.0054
E_2=100 eV	.0607	.0071	.00783	.000673	.00516	.00512
E_2=1 keV	.0568	.00706	.00635	.000672	.00475	.00331
E_2=10 keV	.0287	.0065	.00516	.000671	.00283	.00223
E_2=100 keV	.0124	.00435	.00395	.000636	.0018	.00195
Surv.prob.,$P_s(E_1, E_2)$						
E_2=1 eV	.000278	0.438	0.0578	0.930	0.360	0.521
E_2=10 eV	.00111	0.466	0.269	0.931	0.519	0.567
E_2=100 eV	.00172	0.475	0.440	0.931	0.582	0.584
E_2=1 keV	.00259	0.477	0.514	0.931	0.607	0.706
E_2=10 keV	.04940	0.506	0.582	0.932	0.743	0.791
E_2=100 keV	0.272	0.633	0.661	0.935	0.828	0.815

Table 2.2 - Averaged cross sections (barn) of Actinides relevant to the fast EA.

Element	Capture	Fission	Elastic	(n->2n)	(n->n')	Total
^{230}Th	0.198672	0.018918	14.060925	0.000598	0.989135	15.268245
^{232}Th	0.386855	0.005966	10.923501	0.000560	0.699221	12.016131
^{231}Pa	3.309176	0.179791	9.133289	0.000398	1.110933	13.733619
^{233}Pa	1.121638	0.038989	8.093003	0.000162	1.754808	11.008615
^{232}U	0.731903	2.096317	9.368297	0.000281	0.433875	12.630690
^{233}U	0.289003	2.783923	8.919141	0.000211	0.280445	12.272738
^{234}U	0.615564	0.248950	10.031339	0.000054	0.718069	11.613976
^{235}U	0.574071	1.972008	8.858968	0.000457	0.640860	12.046378
^{236}U	0.490142	0.068786	11.125422	0.000294	0.855951	12.540620
^{237}U	0.492199	0.610042	9.189025	0.000920	0.491900	10.784104
^{238}U	0.428265	0.025351	11.254804	0.000529	0.832077	12.541045
^{237}Np	1.674921	0.233176	9.157094	0.000115	0.759934	11.825250
^{238}Np	0.089278	0.595202	10.439487	0.000000	0.000000	11.123966
^{239}Np	2.083201	0.353837	9.184162	0.000135	0.865835	12.487206
^{238}Pu	0.756840	1.025175	11.046388	0.000152	0.342888	13.171463
^{239}Pu	0.557041	1.780516	9.156214	0.000237	0.770227	12.264245
^{240}Pu	0.667103	0.288079	10.331735	0.000083	0.573045	11.860045
^{241}Pu	0.425030	2.577470	8.104389	0.000880	0.801986	11.909761
^{242}Pu	0.535288	0.190578	11.024648	0.000229	0.667679	12.418422
^{243}Pu	0.403097	0.810772	9.283313	0.002254	0.623218	11.122661
^{244}Pu	0.236048	0.157011	10.805879	0.000808	0.813081	12.012833
^{241}Am	1.963967	0.190469	9.580900	0.000004	0.565741	12.301095
^{242}Am	0.079728	0.530819	10.233513	0.000462	0.073528	10.844059
^{243}Am	1.582431	0.146245	10.003948	0.000028	0.935282	12.667938
^{242}Cm	0.372092	0.105767	10.362508	0.000007	0.724242	11.564615
^{243}Cm	0.265210	2.655223	10.012800	0.000456	1.005476	13.939172
^{244}Cm	0.909153	0.318102	10.515990	0.000135	0.540912	12.284297
^{245}Cm	0.335178	2.475036	8.750109	0.000831	0.862513	12.423669
^{246}Cm	0.230261	0.181669	10.844025	0.000174	0.780190	12.036336
^{247}Cm	0.348536	1.926754	9.117731	0.001353	0.372127	11.766518
^{248}Cm	0.265514	0.218438	11.295776	0.000234	0.813142	12.593122
^{249}Bk	1.447988	0.113146	10.220059	0.000052	1.186927	12.968192
^{249}Cf	0.667223	2.707975	9.064980	0.000189	0.425589	12.865973
^{250}Cf	0.614795	0.944213	8.927651	0.000406	0.468860	10.955943
^{251}Cf	0.368920	2.488528	8.815815	0.001573	0.417832	12.092679
^{252}Cf	0.320039	0.573875	11.865360	0.000335	0.414425	13.174031
^{253}Cf	0.180410	0.716114	9.940411	0.000000	0.000000	10.836935

Table 2.4 - Relative concentrations of Actinides at the discharge after 150 GW day/t of burn up. The power density was ρ = 100 W/g, corresponding to a cycle of about 5 years. Concentrations are normalised to the fuel mass which is made of corresponding oxides.

Element	First discharge	5th discharge	10th discharge	15th discharge	Asymptotic limit
^{230}Th	1.408 E-7	1.378 E-6	2.586 E-6	3.271 E-6	3.642 E-6
^{232}Th	7.637 E-1	7.637 E-1	7.637 E-1	7.637 E-1	7.637 E-1
^{231}Pa	9.246 E-5	1.055 E-4	1.059 E-4	1.061 E-4	1.061 E-4
^{232}U	7.942 E-5	1.298 E-4	1.304 E-4	1.305 E-4	1.306 E-4
^{233}U	8.919 E-2	8.919 E-2	8.919 E-2	8.919 E-2	8.919 E-2
^{234}U	1.403 E-2	3.102 E-2	3.340 E-2	3.365 E-2	3.368 E-2
^{235}U	1.851 E-3	7.242 E-3	8.101 E-3	8.185 E-3	8.196 E-3
^{236}U	2.420 E-4	4.475 E-3	7.428 E-3	8.214 E-3	8.395 E-3
^{238}U	3.239 E-8	3.145 E-6	9.390 E-6	1.296 E-5	1.440 E-5
^{236}Np	2.626 E-10	1.047 E-7	5.787 E-7	1.228 E-6	1.924 E-6
^{237}Np	1.669 E-5	9.127 E-4	1.832 E-3	2.104 E-3	2.168 E-3
^{238}Pu	3.163 E-6	5.975 E-4	1.545 E-3	1.875 E-3	1.958 E-3
^{239}Pu	2.274 E-7	1.422 E-4	4.706 E-4	6.029 E-4	6.374 E-4
^{240}Pu	1.172 E-8	3.709 E-5	2.144 E-4	3.307 E-4	3.703 E-4
^{241}Pu	5.192 E-10	5.084 E-6	3.756 E-5	6.172 E-5	7.034 E-5
^{242}Pu	1.694 E-11	9.800 E-7	1.536 E-5	3.508 E-5	4.572 E-5
^{244}Pu	2.494 E-17	8.631 E-12	3.155 E-10	1.163 E-9	1.999 E-9
^{241}Am	2.924 E-11	7.003 E-7	7.218 E-6	1.316 E-5	1.547 E-5
^{243}Am	5.577 E-13	1.406 E-7	3.575 E-6	9.807 E-6	1.372 E-5
^{243}Cm	1.647 E-14	4.741 E-9	7.930 E-8	1.646 E-7	2.010 E-7
^{244}Cm	4.859 E-14	5.683 E-8	2.479 E-6	8.489 E-6	1.303 E-5
^{245}Cm	2.185 E-15	9.850 E-9	6.417 E-7	2.550 E-6	4.158 E-6
^{246}Cm	3.693 E-17	9.783 E-10	1.519 E-7	1.023 E-6	2.329 E-6
^{247}Cm	3.660 E-19	4.102 E-11	1.038 E-8	8.604 E-8	2.166 E-7
^{248}Cm	5.510 E-21	3.492 E-12	2.011 E-9	2.743 E-8	9.618 E-8

Table 2.3 - Neutron flux dependent effects in the F-EA based on the ^{232}Th cycle. The parameter ρ is the power density produced per unit fuel mass at breeding equilibrium.

Quantity		Values for ρ = 60 W/gr
Ratio $N(^{233}\mathrm{Pa})/N(^{233}\mathrm{U})$		0.0208
Variation of the breeding ratio, ξ	$\Delta\xi$	$+ 0.388 \times 10^{-3}$
Neutron Flux $cm^{-2}\ s^{-1}$	ϕ	2.33×10^{15}
Effects of ^{135}Xe, ^{149}Sm etc.	$Max(\Delta k)$	$< 10^{-4}$
Breeding loss due to premature capt. in ^{233}Pa	Δk	– 0.00480
Criticality rise after 10 days shut-down (^{233}Pa)	Δk	+ 0.00413
Criticality rise after infinite shut-down (^{233}Pa)	$Max(\Delta k)$	+ 0.0203

Table 2.5 - Trans-uranic and Protactinium from discharge for asymptotic fuel concentration. Integrated burn up is 150 GW day/t.

Element		Partial density (gr/cm^3)
^{231}Pa		0.9179 E-04
	Total Pa	0.9179 E-04
^{236}Np		0.5469 E-07
^{237}Np		0.1428 E-02
	Total Np	0.1428 E-02
^{238}Pu		0.5640 E-03
^{239}Pu		0.7141 E-04
^{240}Pu		0.6185 E-05
^{241}Pu		0.3924 E-06
^{242}Pu		0.1887 E-07
	Total Pu	0.6420 E-03
^{241}Am		0.2638 E-07
^{243}Am		0.8461 E-09
	Total Am	0.2722 E-07
^{242}Cm		0.4182 E-09
	Total Cm	0.5500 E-09
	Total discharge	2.1618 E-3

Table 2.6 - Some properties of Actinides from EA discharge having relevance to possible military diversions of fuel.

Element from EA	Uranium Mix	Neptunium	Plutonium
Critical mass (CM),kg	28.0	56.5	10.4
Decay Heat for CM,Watt	24.3	1.13	4400
Gamma Activity, Ci/CM	790	small	small
Neutron Yield, n g^{-1} s^{-1}	very small	$2.1\ 10^5$	$2.6\ 10^3$

Table 2.7 - Neutron flux dependent effects in the F-EA base on ^{238}U cycle. The parameter ρ is the power density produced per unit fuel mass at breeding equilibrium.

Quantity		Values for $\rho = 120$ W/gr
Neutron Flux cm^{-2} s^{-1}	ϕ	5.967×10^{15}
Breeding ratio, zero flux $N(^{239}\text{Pu})/N(^{238}\text{U})$	ξ	0.190
Rate variation of the breeding ratio, ξ	$\Delta\xi$	-6.00×10^{-4}
Ratio $N(^{239}\text{Np})/N(^{239}\text{Pu})$		3.66×10^{-3}
Fuel intrinsic mult. factor at breeding equil.	k_∞	1.250
Effects of ^{135}Xe, ^{149}Sm etc.	$Max(\Delta k)$	$< 10^{-4}$
Breeding loss due to premature capt. in ^{239}Np	Δk	-3.816×10^{-3}
Criticality rise after infinite shut-down (^{239}Np)	$Max(\Delta k)$	3.256×10^{-3}

Figure Captions.

Figure 2.1 Capture Cross sections at 65 keV, as a function of the element number.

Figure 2.2 Conceptual design of the diffuser driven EA.

Figure 2.3 The burn-up radial distribution for different criticality coefficients, namely for (a) for k=0.99, (b) for k=0.975 and (c) for k=0.950. Open points have not been included in the fits.

Figure 2.4 Fraction of neutrons capture by the fission fragments as a function of the integrated burn-up, for thermal and fast EA.

Figure 2.5 Criticality coefficient k as a function of the integrated burn-up for different power yields. The effect on k due to the neutron captures by the fission fragments is also shown.

Figure 2.6 Behaviour of k as a function of the integrated burn-up.

Figure 2.7 ^{233}U stockpile as a function of the integrated burn-up.

Figure 2.8a ^{231}Pa and ^{232}U stockpile as a function of the discharge number (integrated seeds burn-up).

Figure 2.8b Other actinides stockpile as a function of the discharge number (integrated seeds burn-up).

Figure 2.8c Trans-uranic production/unit energy relative to ordinary PWR as a function of the discharge number (integrated seeds burn-up).

Figure 2.9 Comparison of k_{eff} calculated analytically and by Montecarlo.

Figure 2.10 Behaviour of k as a function of the burn-up for different fillings.

Figure 2.11 Behaviour of k_{∞} as a function of the irradiation time at a constant flux of 4.0×10^{15} neutrons s^{-1} cm^{-2}.

Figure 2.12 Relative absorption rates for different isotopes as a function of the irradiation time at a constant flux of 4.0×10^{15} neutrons s^{-1} cm^{-2}.

Figure 2.13 Power delivered per gram of different isotopes as a function of the irradiation time at a constant flux of 4.0×10^{15} neutrons s^{-1} cm^{-2}.

Figure 2.14 Rate of disappearance of different isotopes as a function of irradiation time at a constant flux of 4.0×10^{15} neutrons s^{-1} cm^{-2}.

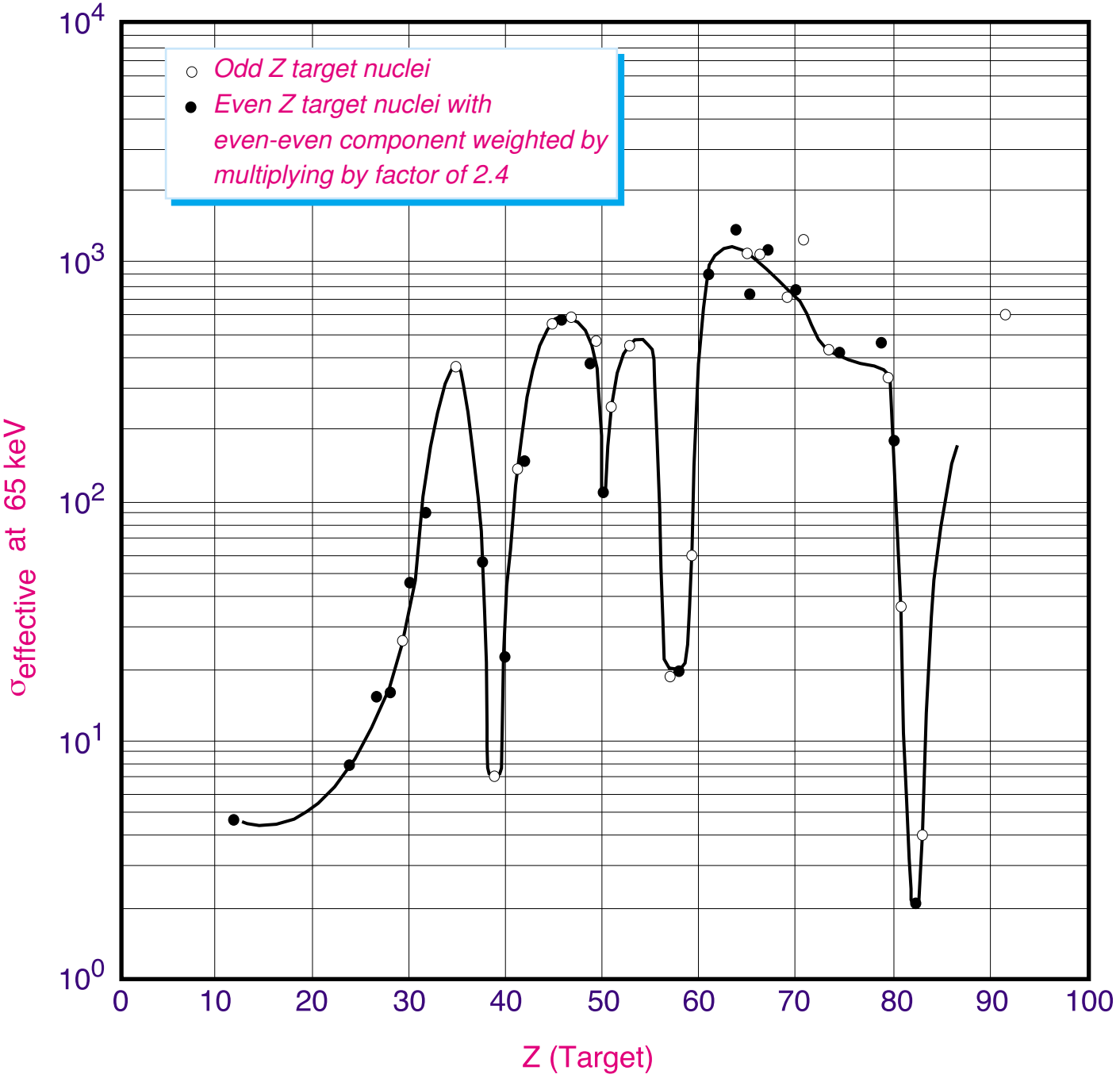
Odd Z target nuclei
Even Z target nuclei with even-even component weighted by multiplying by factor of 2.4
10^4
10^3
10^2
10^1
10^0
$\sigma_{effective}$ at 65 keV
0
10
20
30
40
50
60
70
80
90
100
Z (Target)

Figure 2.1

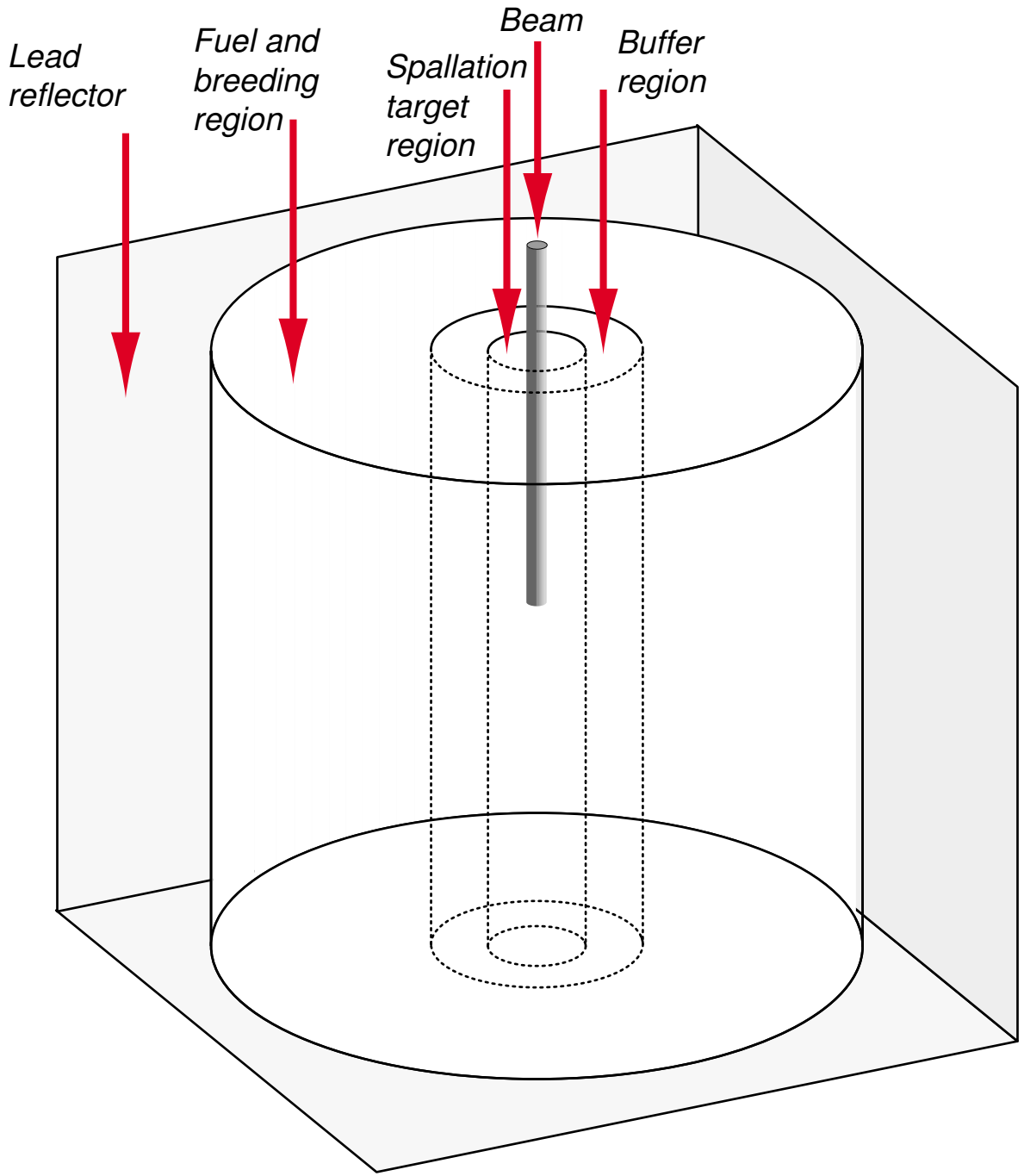
Lead reflector
Fuel and breeding region
Spallation target region
Beam
Buffer region

Figure 2.2

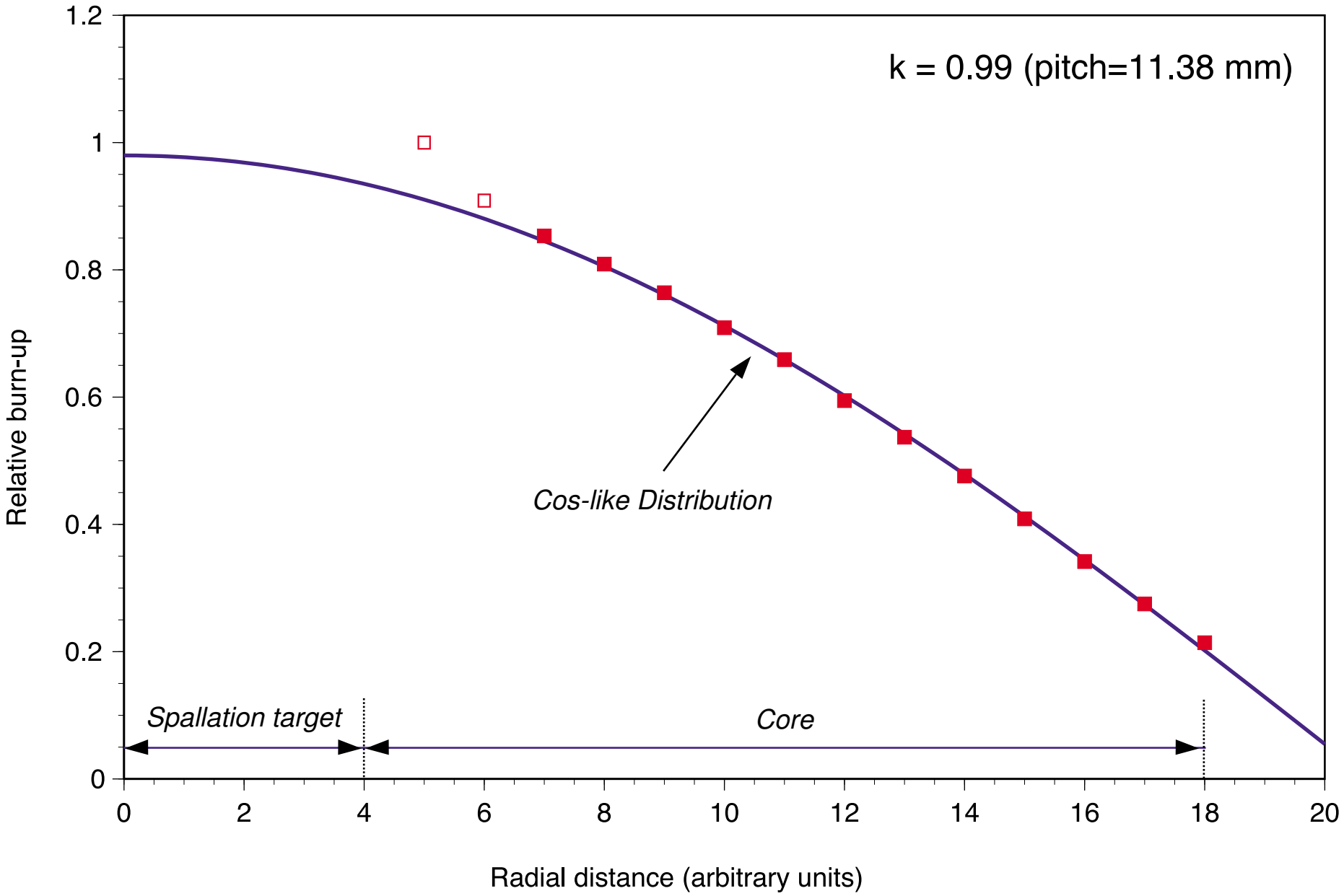
k = 0.99 (pitch=11.38 mm)
Relative burn-up
Radial distance (arbitrary units)
Cos-like Distribution
Spallation target
Core
1.2
1
0.8
0.6
0.4
0.2
0
0
2
4
6
8
10
12
14
16
18
20

Figure 2.3a

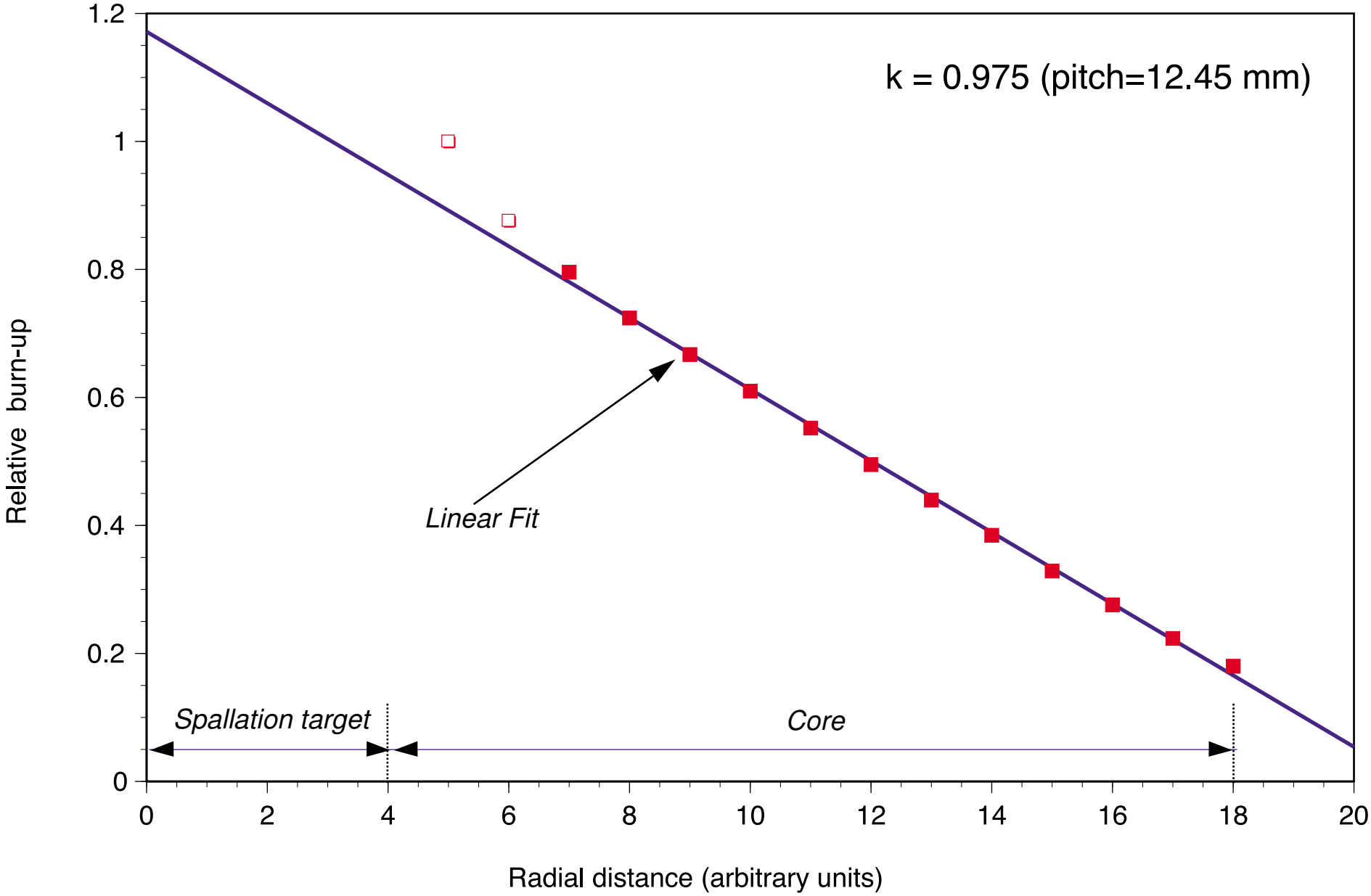
k = 0.975 (pitch=12.45 mm)
Linear Fit
Spallation target
Core
Relative burn-up
Radial distance (arbitrary units)
1.2
1
0.8
0.6
0.4
0.2
0
0
2
4
6
8
10
12
14
16
18
20

Figure 2.3b

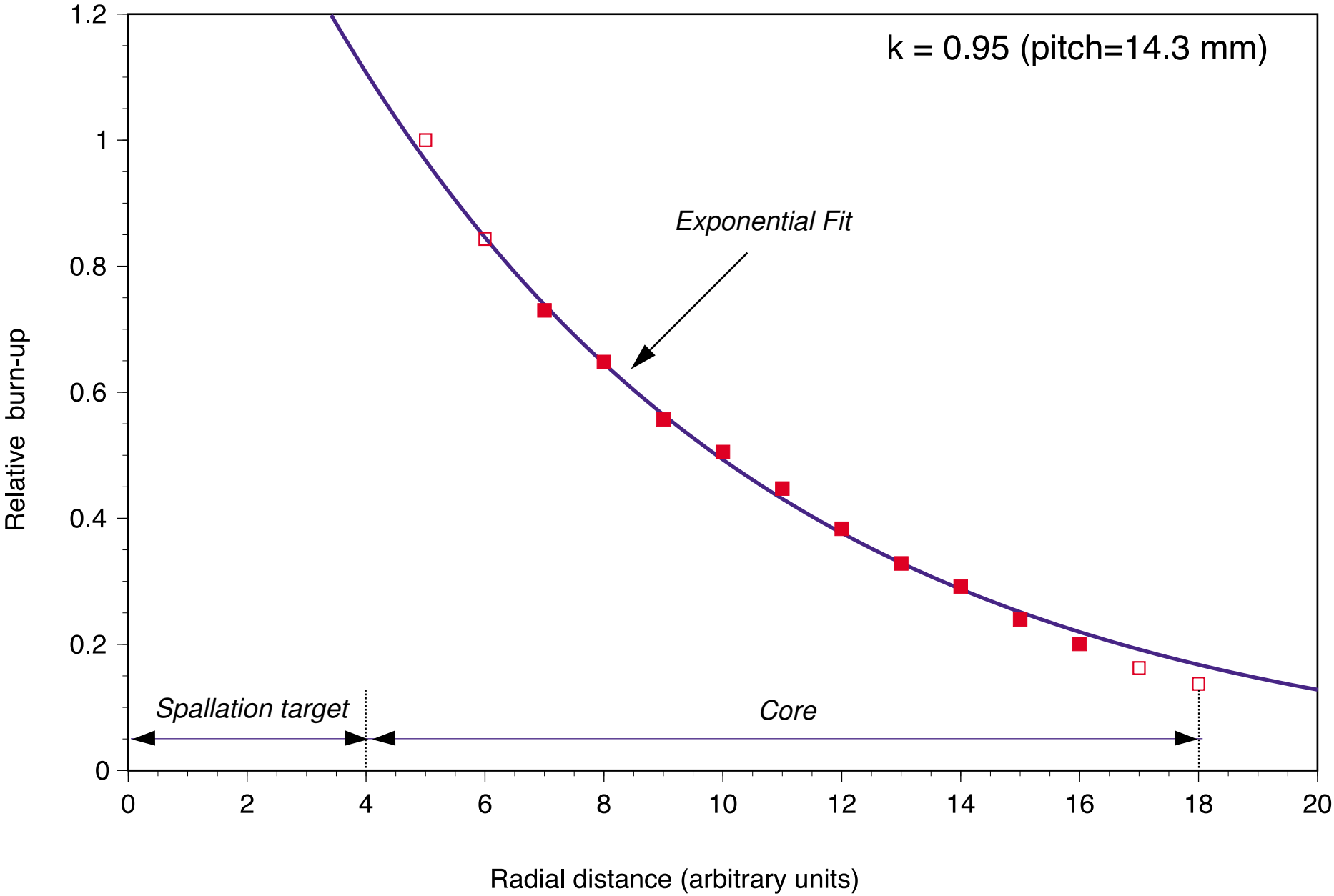
k = 0.95 (pitch=14.3 mm)
Exponential Fit
Spallation target
Core
Relative burn-up
Radial distance (arbitrary units)
1.2
1
0.8
0.6
0.4
0.2
0
0
2
4
6
8
10
12
14
16
18
20

Figure 2.3c

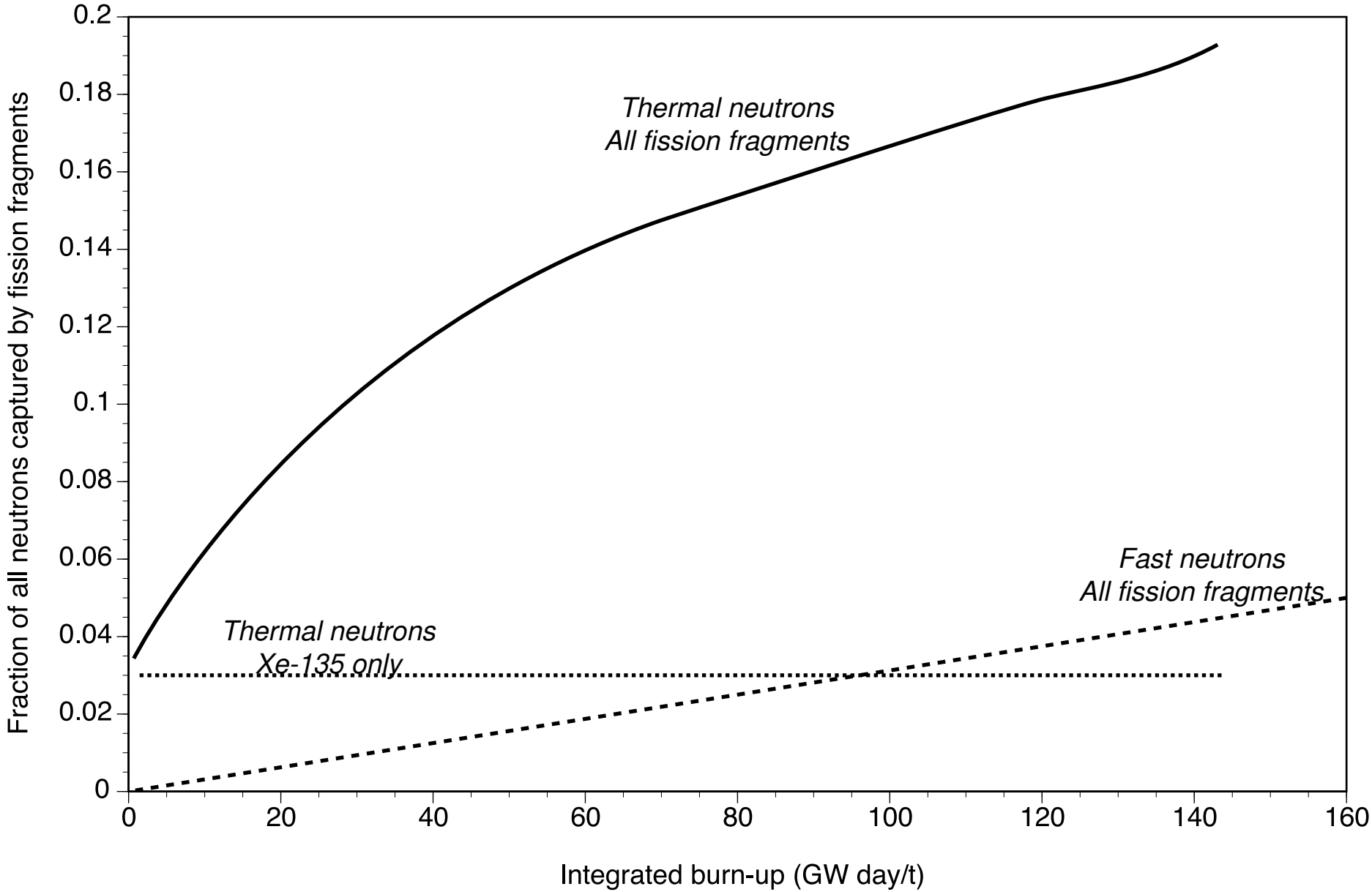
Fraction of all neutrons captured by fission fragments
0.2
0.18
0.16
0.14
0.12
0.1
0.08
0.06
0.04
0.02
0
0
20
40
60
80
100
120
140
160
Integrated burn-up (GW day/t)
Thermal neutrons
All fission fragments
Fast neutrons
All fission fragments
Thermal neutrons
Xe-135 only

Figure 2.4

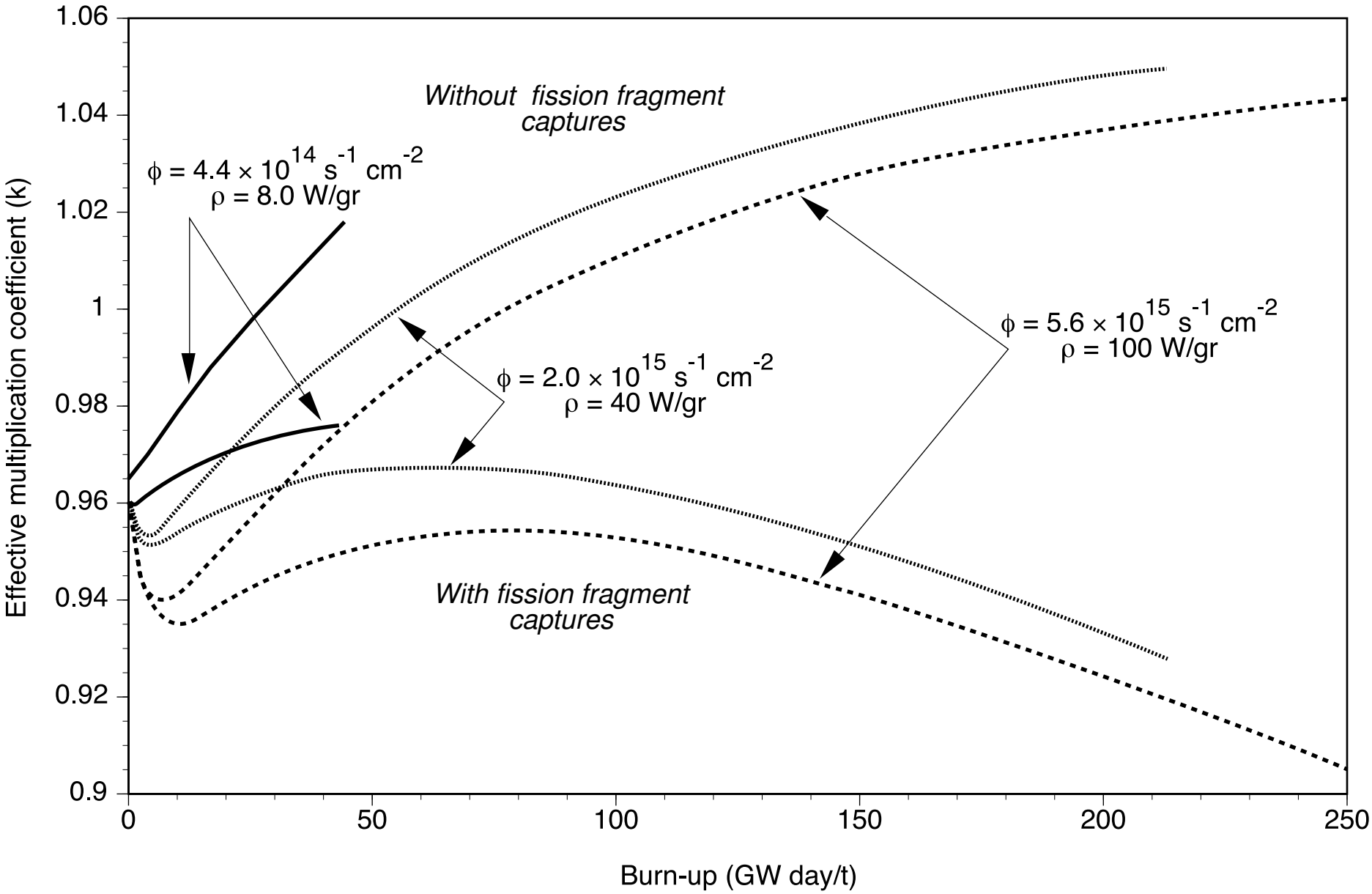
1.06
1.04
1.02
1
0.98
0.96
0.94
0.92
0.9
Effective multiplication coefficient (k)
0
50
100
150
200
250
Burn-up (GW day/t)
Without fission fragment captures
With fission fragment captures
ϕ = 4.4 × 10^14 s^-1 cm^-2
ρ = 8.0 W/gr
ϕ = 2.0 × 10^15 s^-1 cm^-2
ρ = 40 W/gr
ϕ = 5.6 × 10^15 s^-1 cm^-2
ρ = 100 W/gr

Figure 2.5

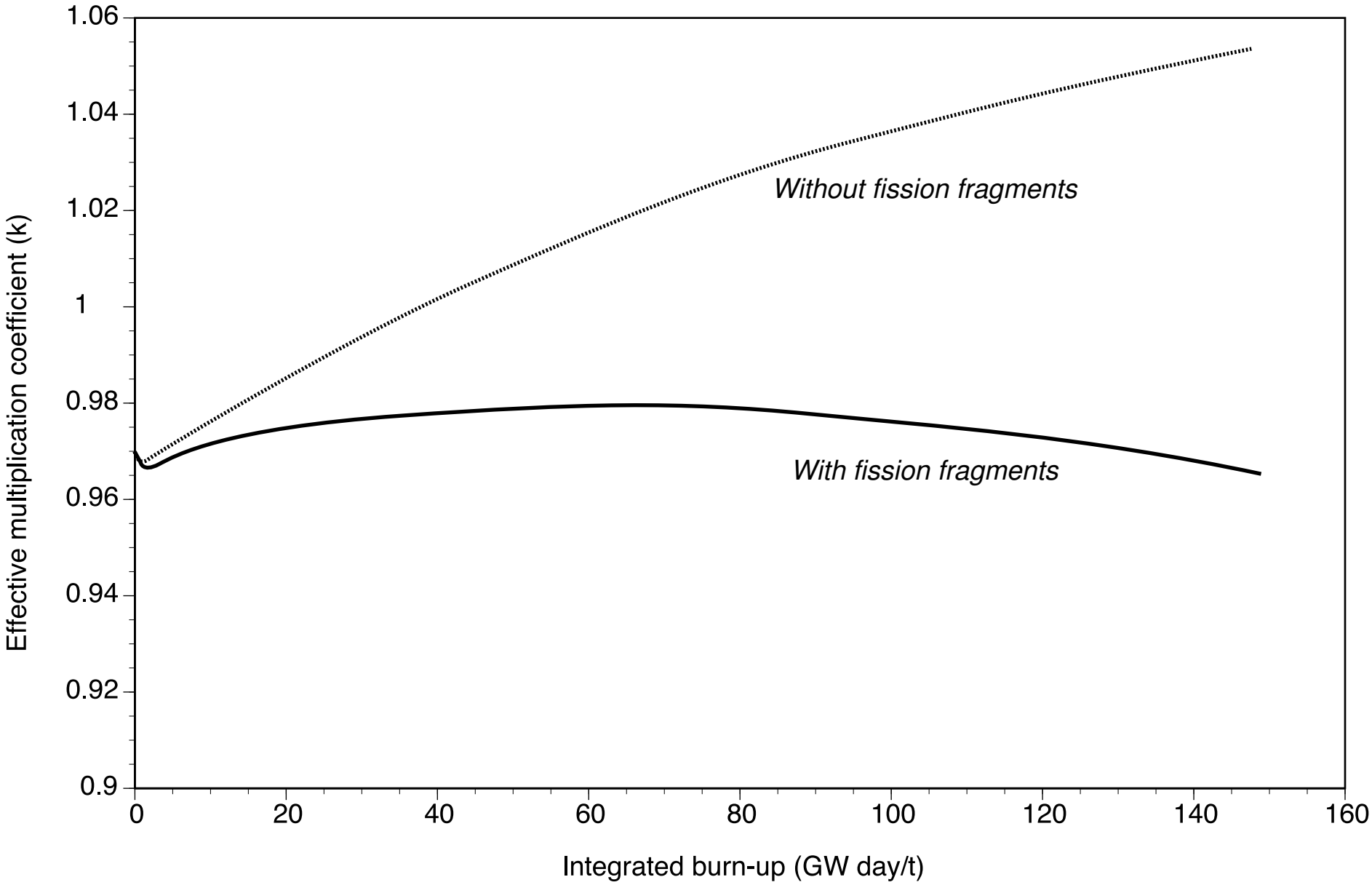
1.06
1.04
1.02
1
0.98
0.96
0.94
0.92
0.9
Effective multiplication coefficient (k)
Without fission fragments
With fission fragments
0
20
40
60
80
100
120
140
160
Integrated burn-up (GW day/t)

Figure 2.6

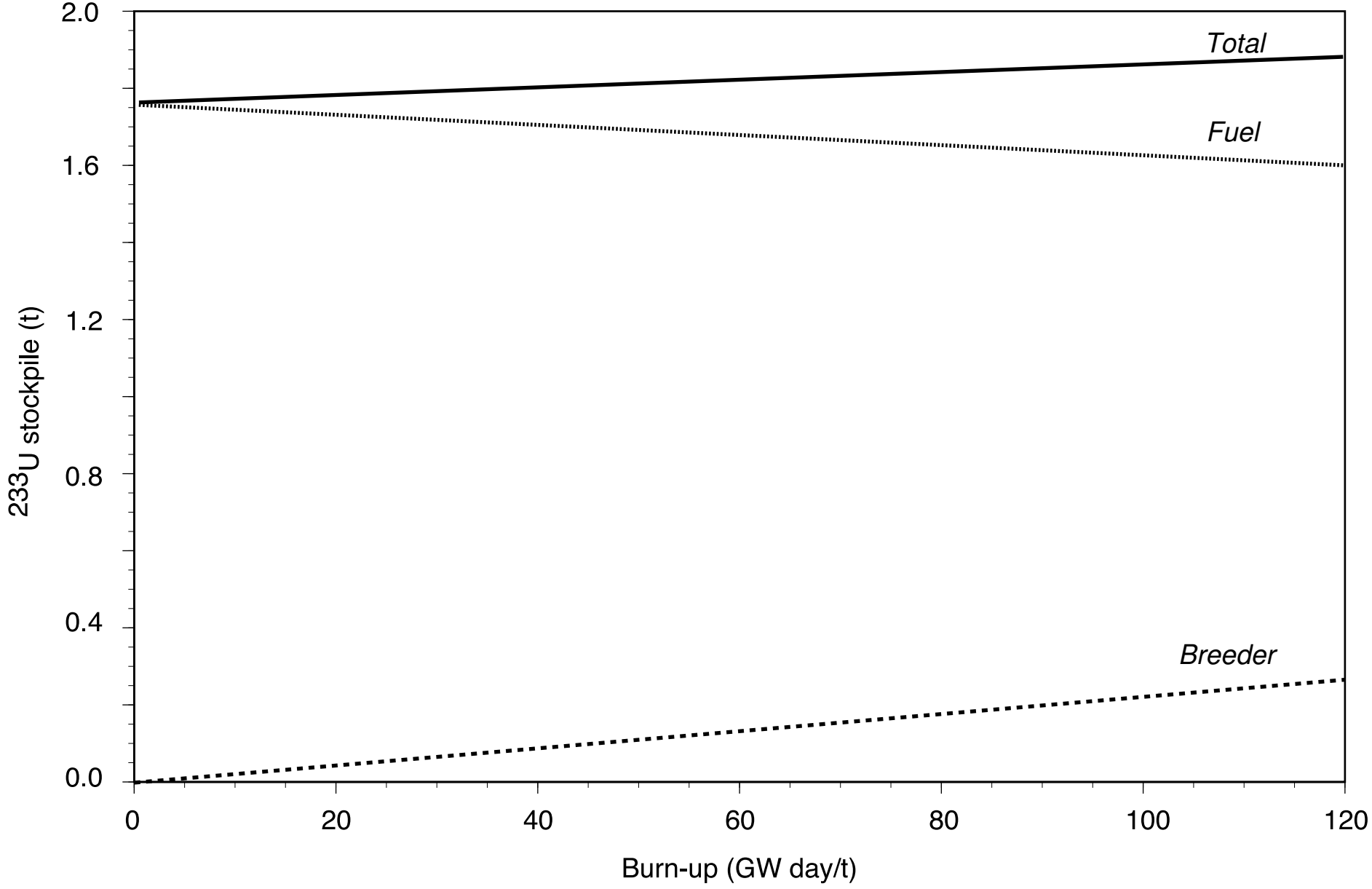
2.0
1.6
1.2
0.8
0.4
0.0
^{233}U stockpile (t)
Total
Fuel
Breeder
0
20
40
60
80
100
120
Burn-up (GW day/t)

Figure 2.7

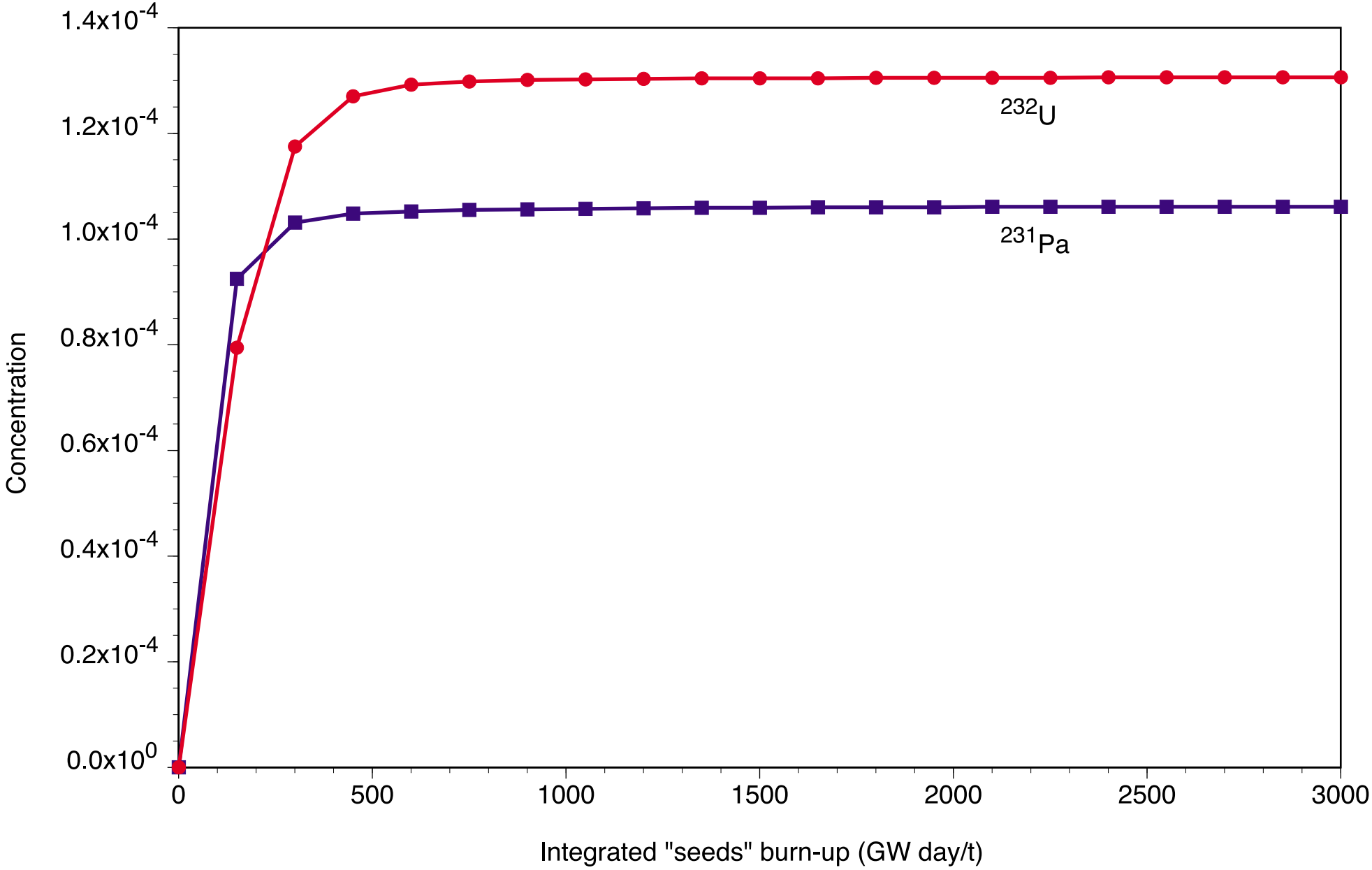
1.4x10-4
1.2x10-4
1.0x10-4
0.8x10-4
0.6x10-4
0.4x10-4
0.2x10-4
0.0x100
Concentration
232U
231Pa
0
500
1000
1500
2000
2500
3000
Integrated "seeds" burn-up (GW day/t)

Figure 2.8a

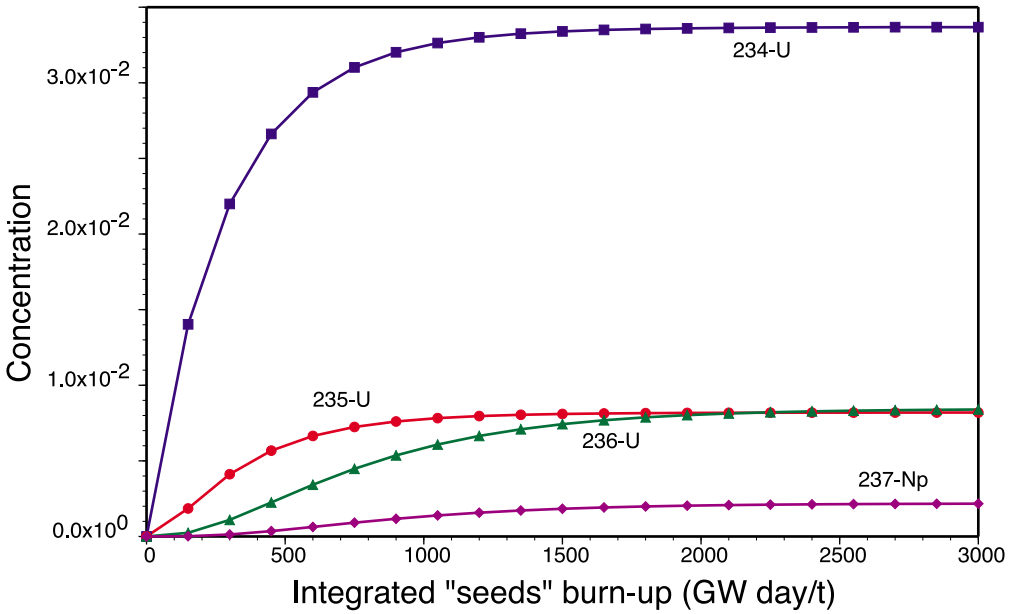
Concentration
3.0x10-2
2.0x10-2
1.0x10-2
0.0x100
234-U
235-U
236-U
237-Np
0
500
1000
1500
2000
2500
3000
Integrated "seeds" burn-up (GW day/t)

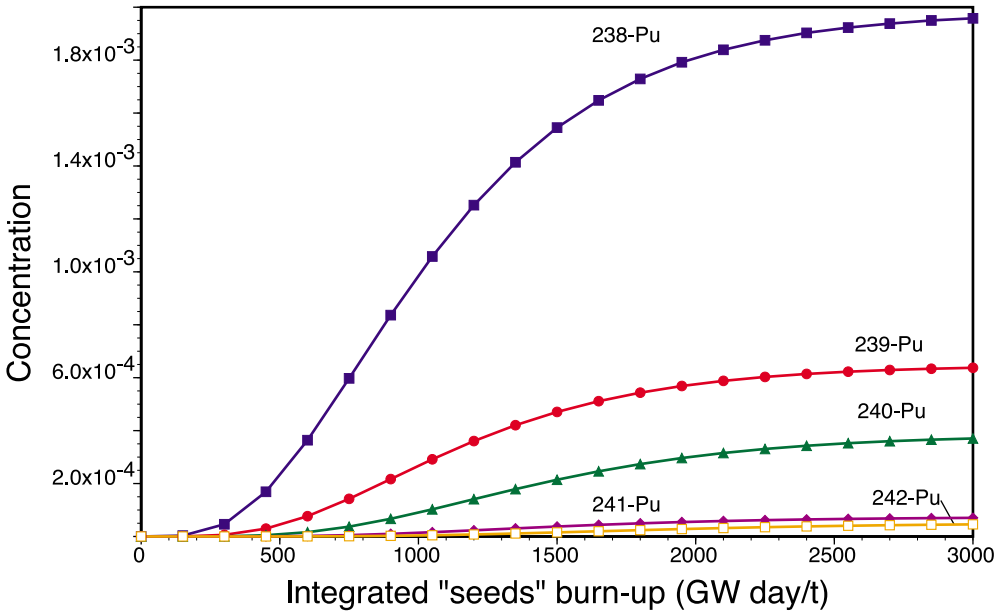
Concentration
1.8x10-3
1.4x10-3
1.0x10-3
6.0x10-4
2.0x10-4
238-Pu
239-Pu
240-Pu
241-Pu
242-Pu
0
500
1000
1500
2000
2500
3000
Integrated "seeds" burn-up (GW day/t)

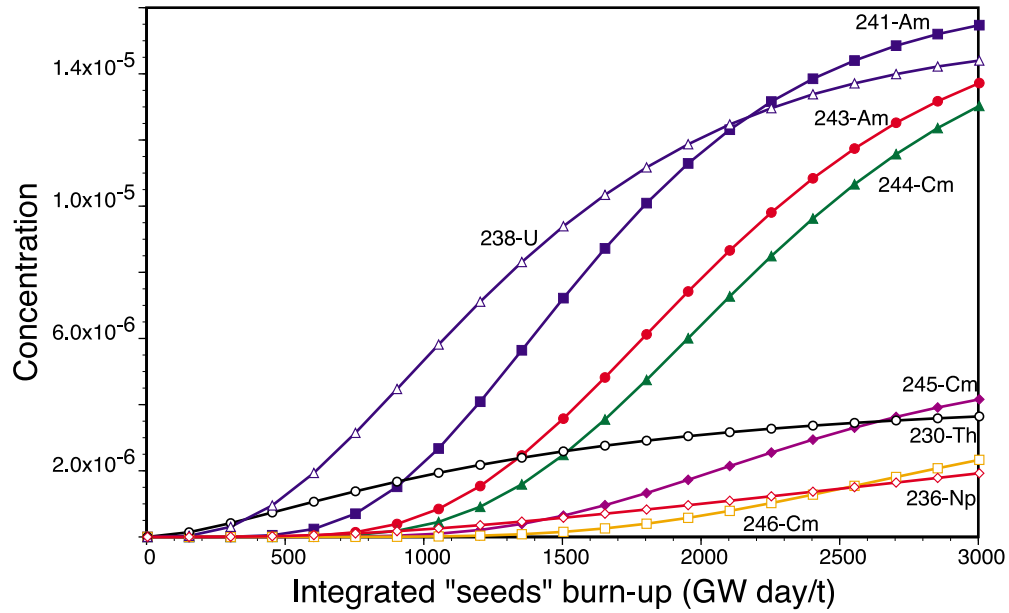
Concentration
1.4x10-5
1.0x10-5
6.0x10-6
2.0x10-6
241-Am
243-Am
244-Cm
238-U
245-Cm
230-Th
236-Np
246-Cm
0
500
1000
1500
2000
2500
3000
Integrated "seeds" burn-up (GW day/t)

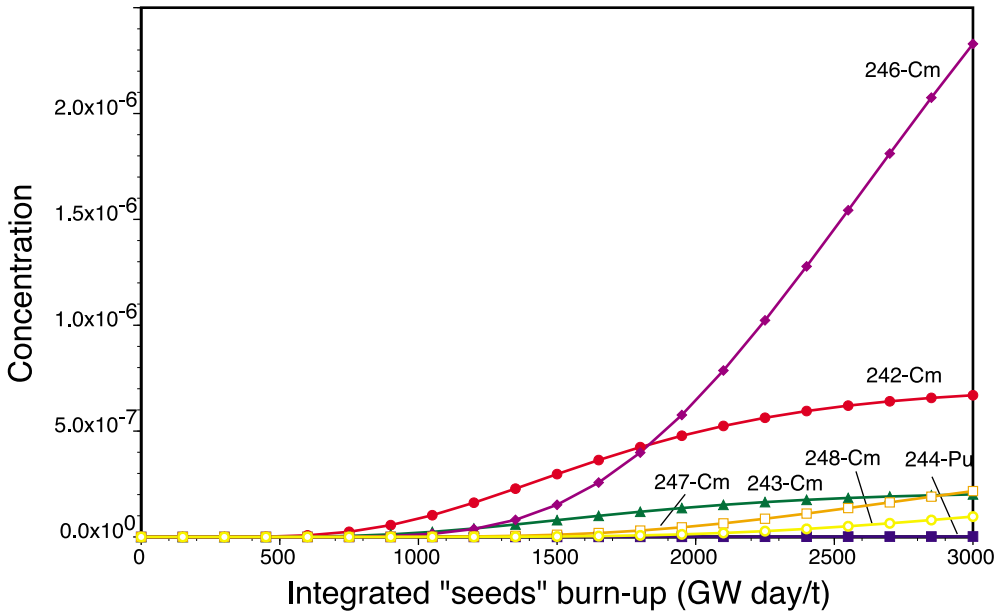
Concentration
2.0x10-6
1.5x10-6
1.0x10-6
5.0x10-7
0.0x100
246-Cm
242-Cm
248-Cm
244-Pu
247-Cm
243-Cm
0
500
1000
1500
2000
2500
3000
Integrated "seeds" burn-up (GW day/t)

Figure 2.8b

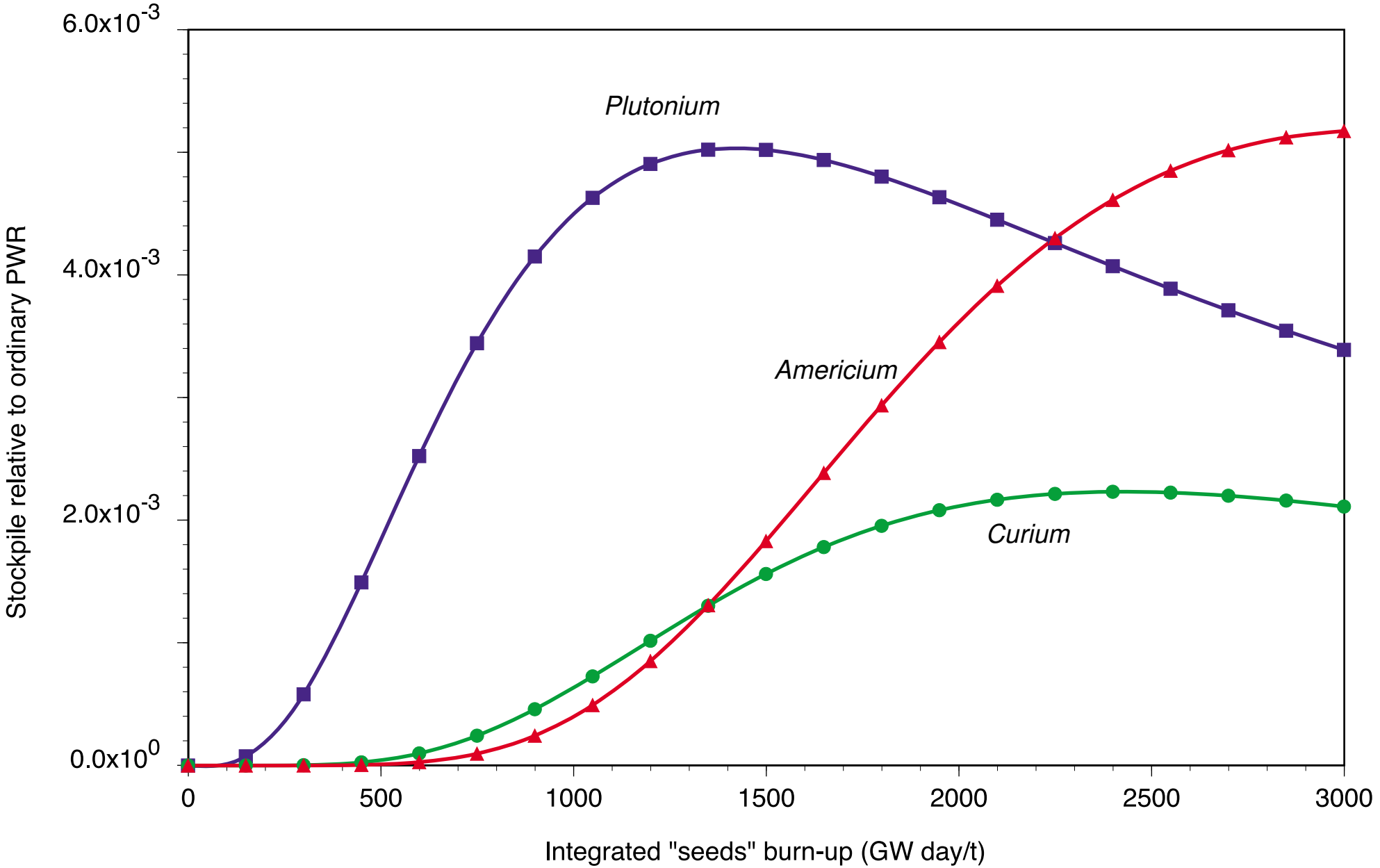
6.0x10-3
4.0x10-3
2.0x10-3
0.0x100
Stockpile relative to ordinary PWR
Plutonium
Americium
Curium
0
500
1000
1500
2000
2500
3000
Integrated "seeds" burn-up (GW day/t)

Figure 2.8c

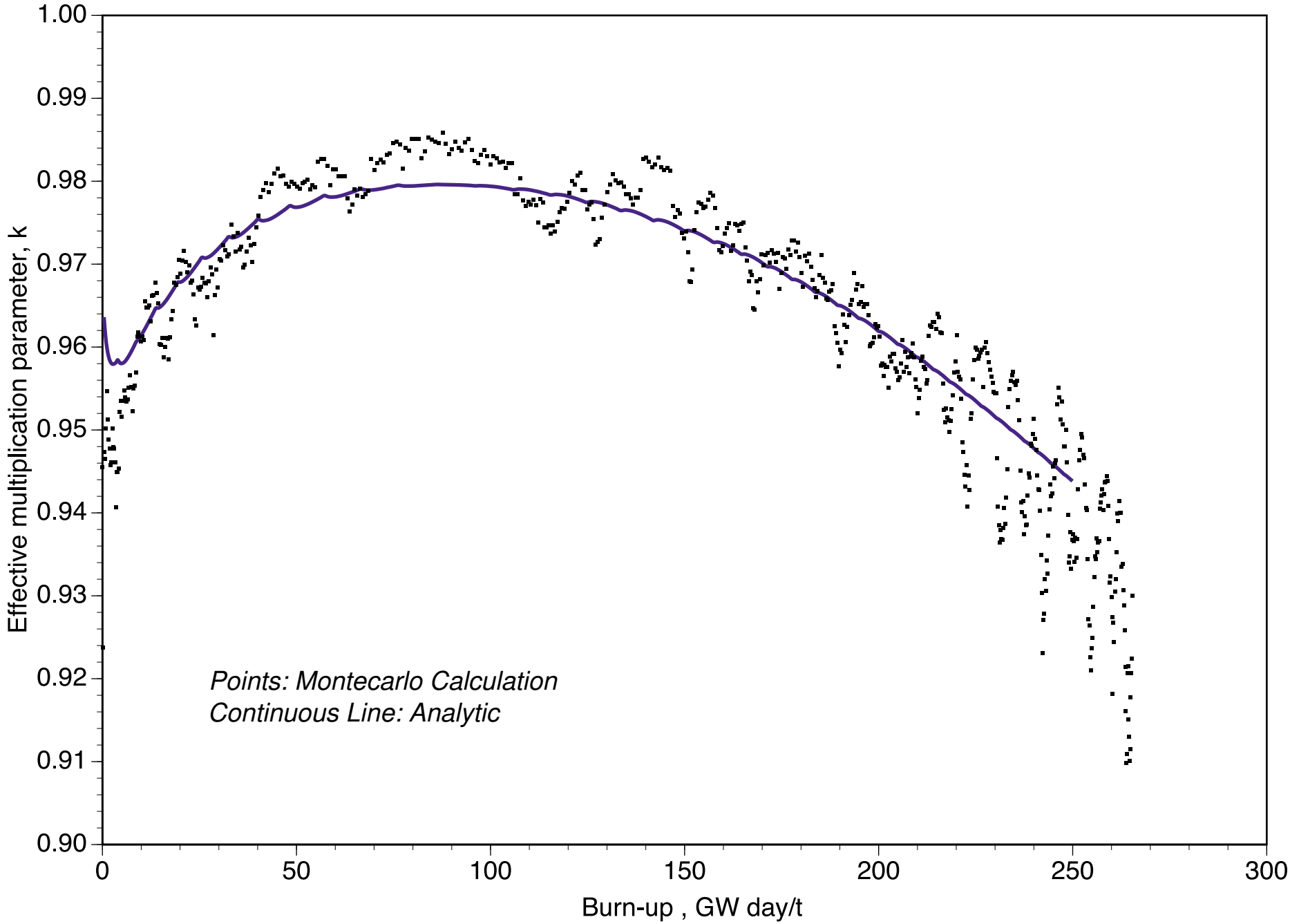
1.00
0.99
0.98
0.97
0.96
0.95
0.94
0.93
0.92
0.91
0.90
Effective multiplication parameter, k
0
50
100
150
200
250
300
Burn-up , GW day/t
Points: Montecarlo Calculation
Continuous Line: Analytic

Figure 2.9

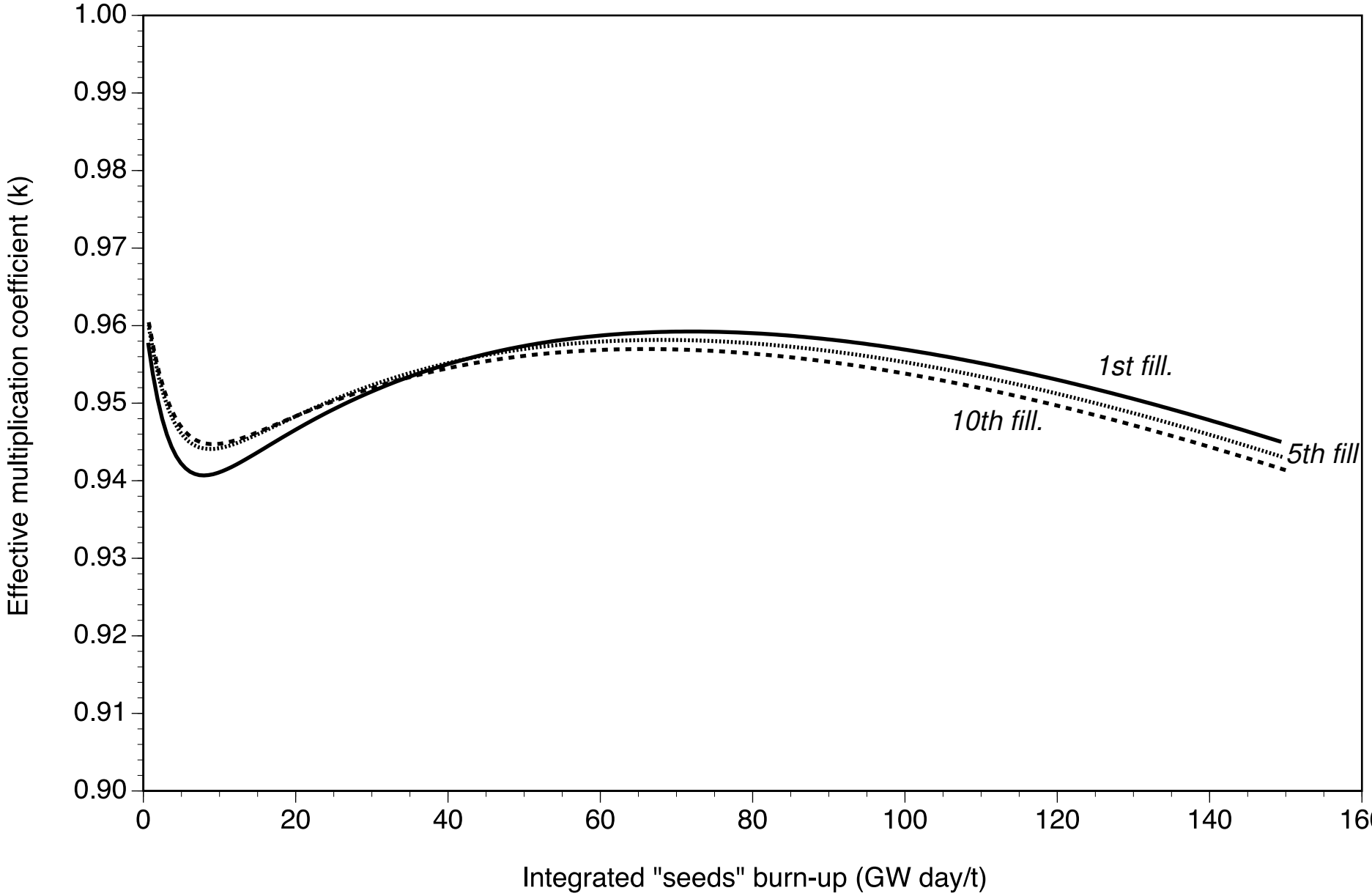
1.00
0.99
0.98
0.97
0.96
0.95
0.94
0.93
0.92
0.91
0.90
Effective multiplication coefficient (k)
0
20
40
60
80
100
120
140
160
Integrated "seeds" burn-up (GW day/t)
1st fill.
10th fill.
5th fill

Figure 2.10

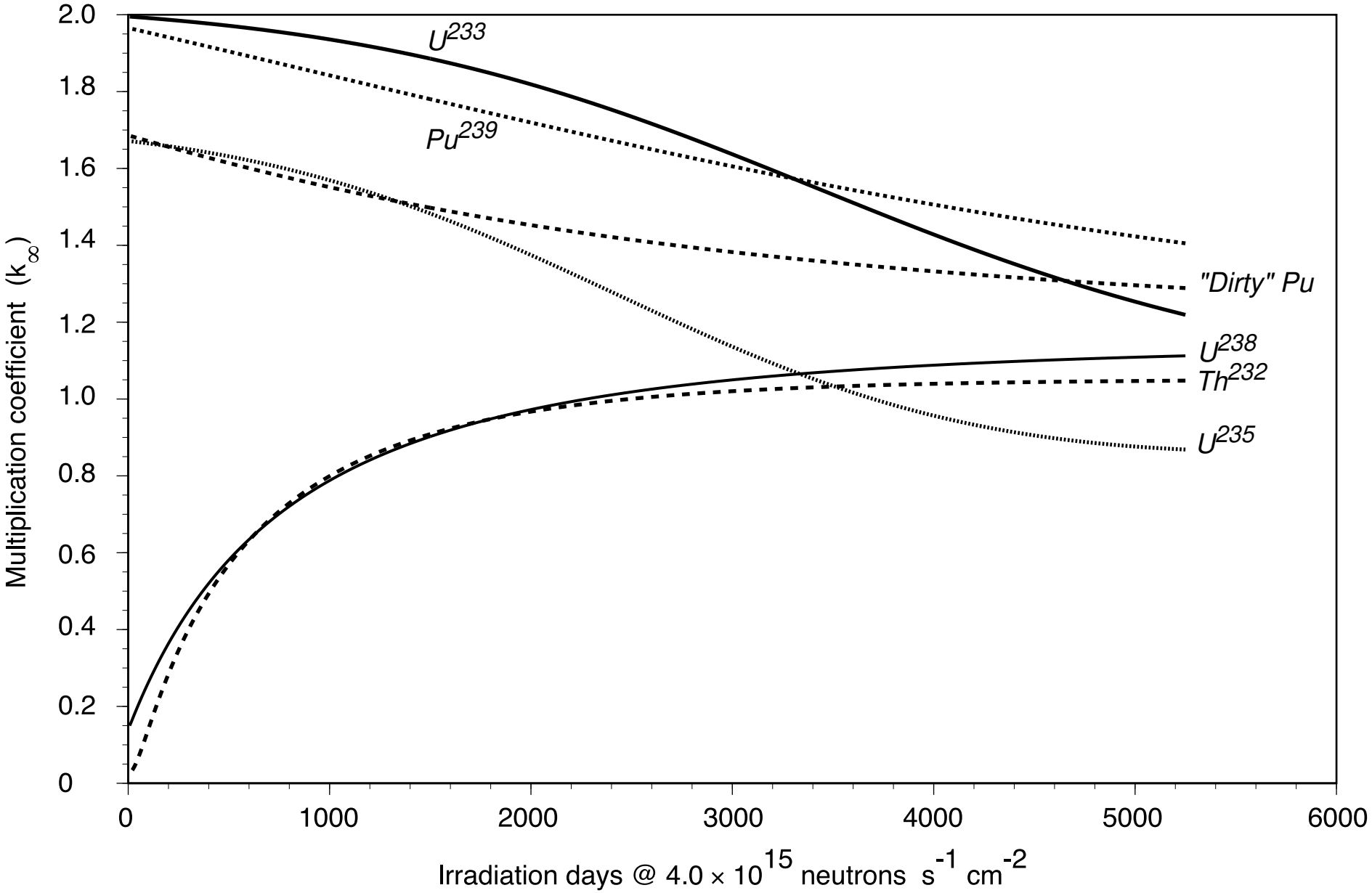
2.0
1.8
1.6
1.4
1.2
1.0
0.8
0.6
0.4
0.2
0
Multiplication coefficient (k∞)
U233
Pu239
"Dirty" Pu
U238
Th232
U235
0
1000
2000
3000
4000
5000
6000
Irradiation days @ 4.0 × 10^15 neutrons s^-1 cm^-2

Figure 2.11

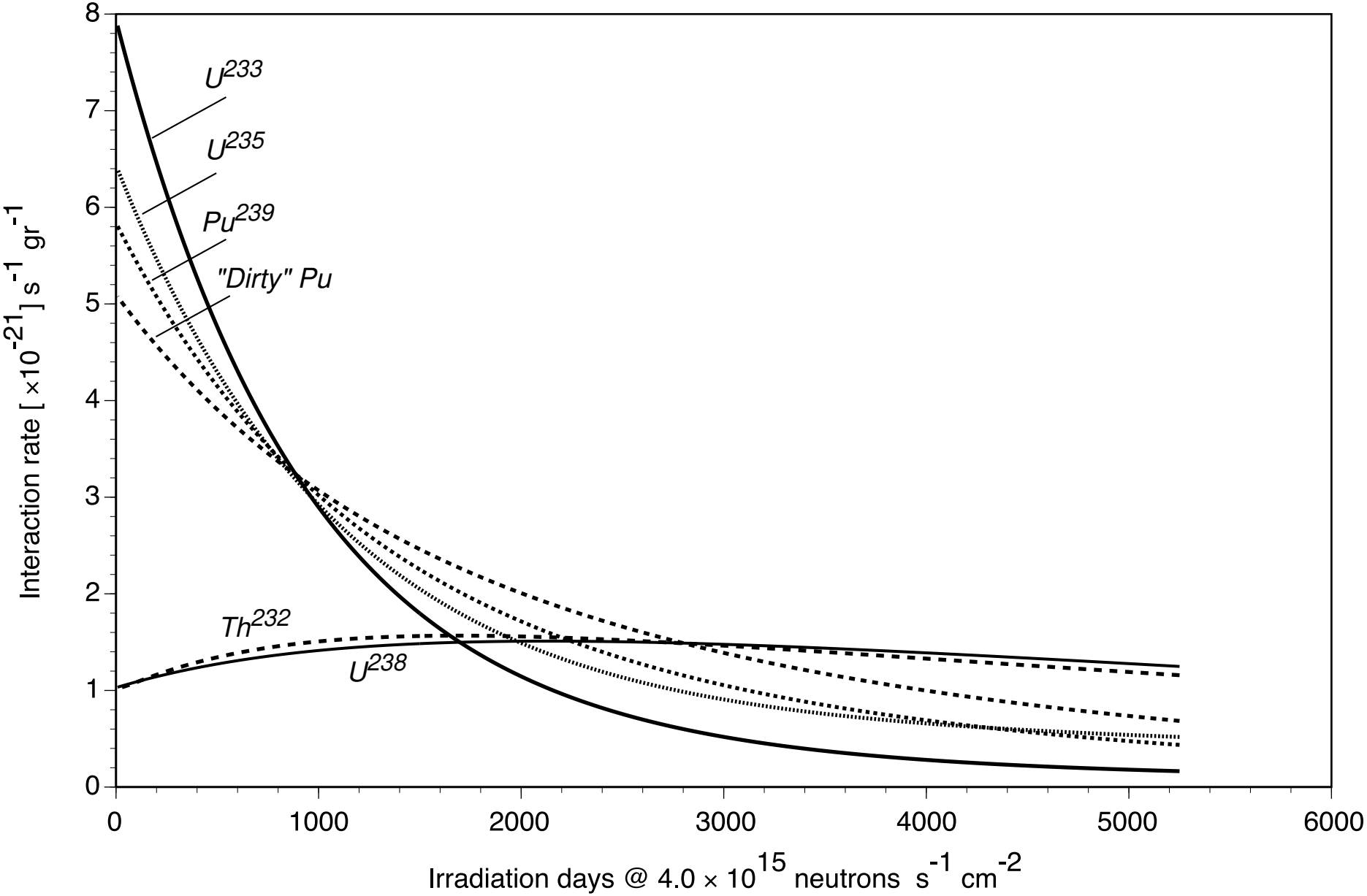
8
7
6
5
4
3
2
1
0
0
1000
2000
3000
4000
5000
6000
U233
U235
Pu239
"Dirty" Pu
Th232
U238
Interaction rate [×10-21] s-1 gr-1
Irradiation days @ 4.0 × 1015 neutrons s-1 cm-2

Figure 2.12

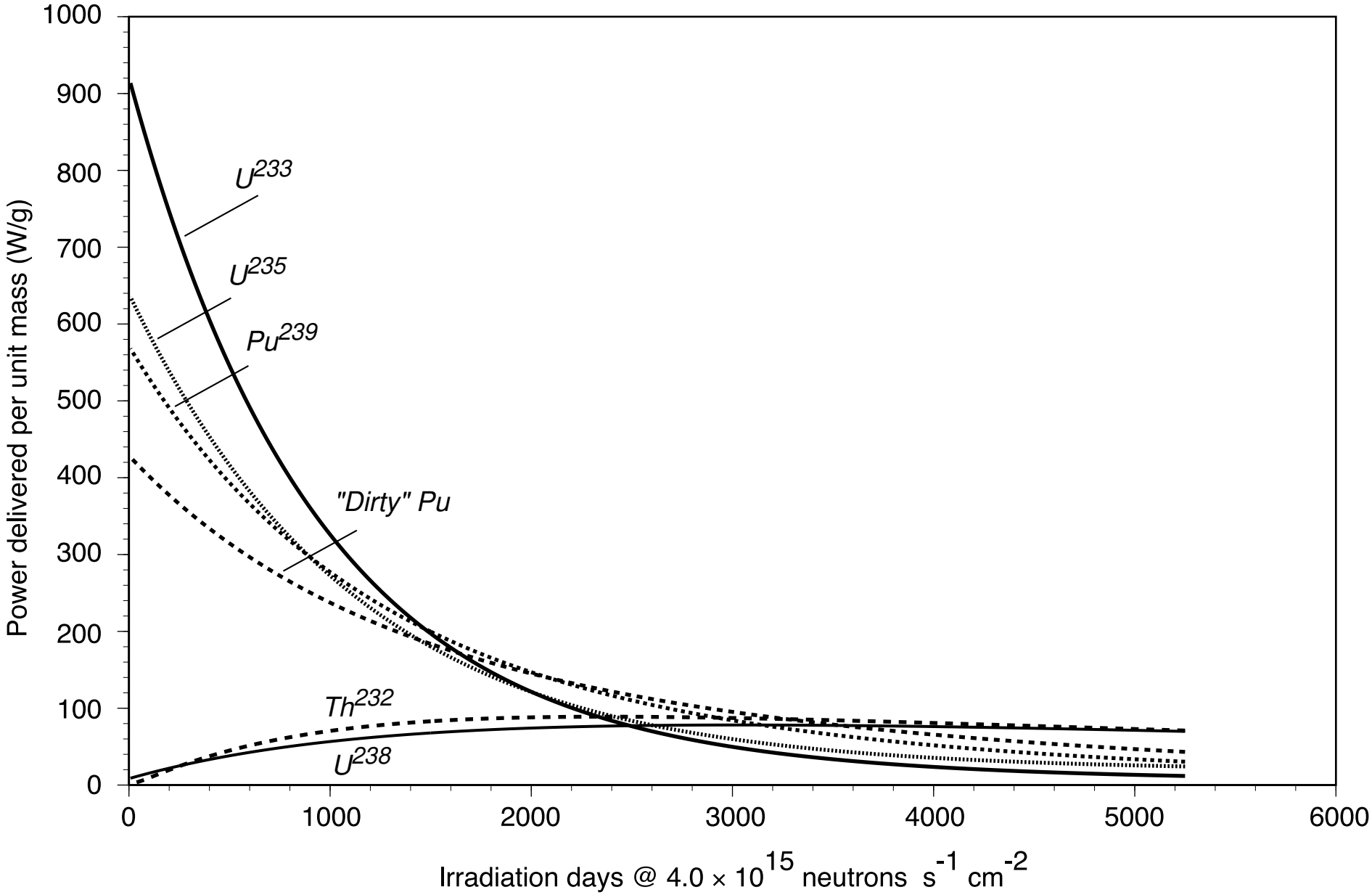
1000
900
800
700
600
500
400
300
200
100
0
Power delivered per unit mass (W/g)
U233
U235
Pu239
"Dirty" Pu
Th232
U238
0
1000
2000
3000
4000
5000
6000
Irradiation days @ 4.0 × 10^15 neutrons s^-1 cm^-2

Figure 2.13

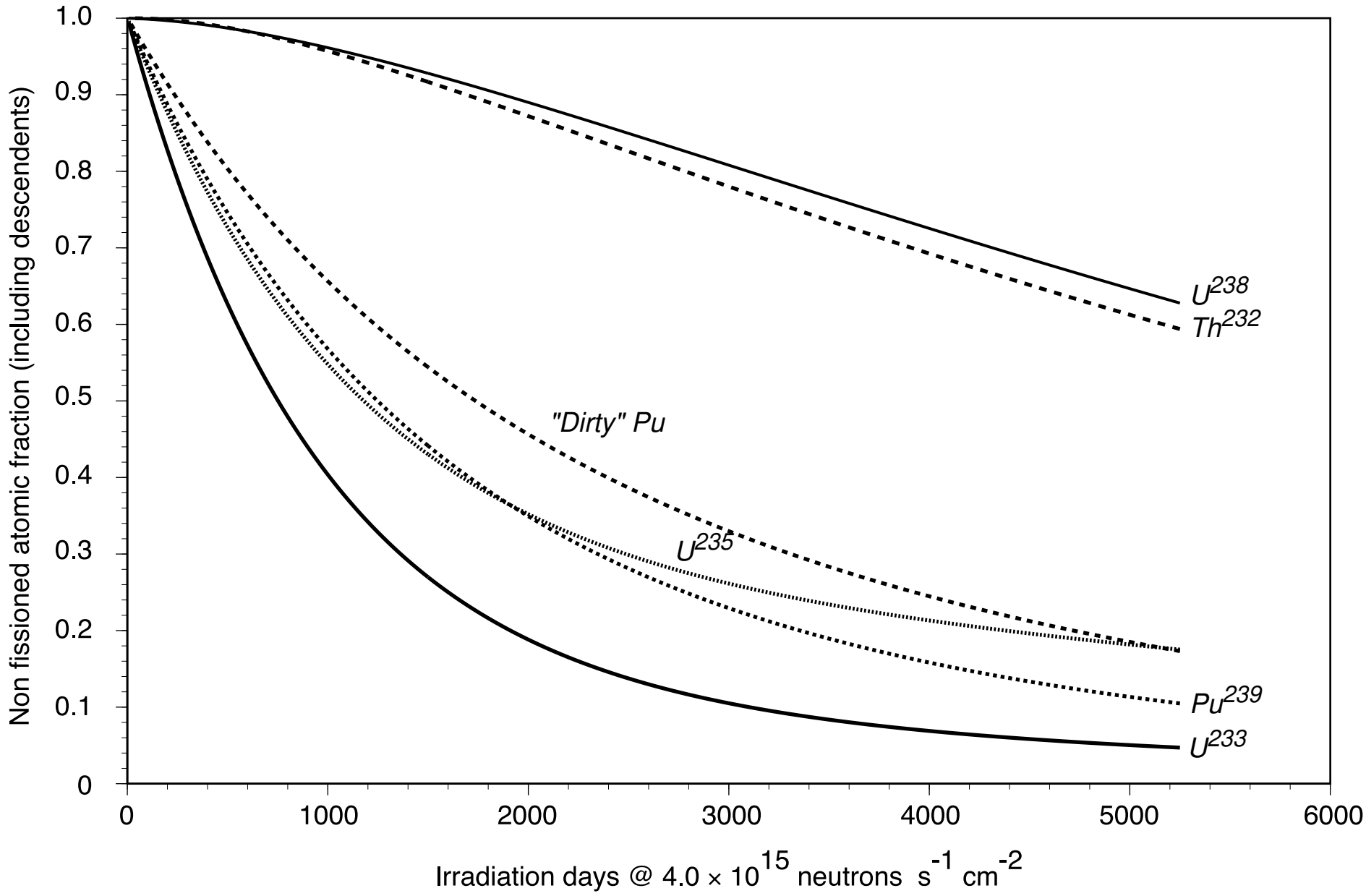
1.0
0.9
0.8
0.7
0.6
0.5
0.4
0.3
0.2
0.1
0
Non fissioned atomic fraction (including descendents)
0
1000
2000
3000
4000
5000
6000
Irradiation days @ 4.0 × 10^15 neutrons s^-1 cm^-2
U238
Th232
"Dirty" Pu
U235
Pu239
U233

Figure 2.14

3. —The accelerator complex.

3.1 - A three-stage cyclotron facility. The accelerator has to provide a proton beam of 10 ÷ 15 mA, one order of magnitude lower than the one of most of the accelerator-driven incineration projects based on continuous-wave (c-w) LINAC [9]. The relatively modest requirement of the present application, primarily related to the high gain of the F-EA, allows alternative and much simpler solutions based on circular machines producing a continuous beam, such as ring cyclotrons [38] [39] which have a lower cost and a much smaller size.

Taking into account the recent development of high-intensity cyclotrons and the outstanding results obtained at PSI [8], we have chosen a scheme based on a three-stage cyclotron accelerator (Figure 3.1), namely in succession: (1) the injector, made of two 10 MeV, Compact Isochronous Cyclotrons (CIC). Beams are merged with the help of negative ion stripping; (2) the intermediate stage, a cyclotron with four separated sectors (ISSC) bringing the beam up to 120 MeV; (3) the final booster with ten separated sectors and six cavities (BSSC), raising the kinetic energy up to about 1 GeV.

The main novelty of our design, besides the about tenfold increase of the accelerated current, well within the expectations of the present knowledge of space charge effects and beam instabilities, is the increased power efficiency. This extrapolation can be made with confidence and relies primarily on the performance of the RF cavities, which is confirmed by specific model studies that we have made. In particular we believe that the increased beam loading can be adequately handled. This conclusion has been confirmed by a similar study of the PSI Group [8].

The main parameters of the two separated sector cyclotrons are given in Table 3.1. An essential aspect of the accelerator complex is the overall efficiency which depends mainly on the RF performances. Power estimates have been made assuming a 70 % yield of the RF power amplifiers and taking into account measurements on cavity models for the RF losses. Further optimisations of the cavity shape which are in progress show that a global efficiency slightly greater than 40 % is within the reach.

An important aspect of the Accelerator complex when used in conjunction with the EA is the high level of reliability required. Based on previous experience with

similar machines and possible improvements within reach we believe that the unscheduled down-time of the accelerator can be kept to the level of 3÷5 %.

3.2 - Overall design considerations. Acceleration of intense beams requires a very efficient extraction. To this effect, the main parameters of the accelerators should follow several design criteria:

1) Injection energy should be high enough in order to reduce the longitudinal space charge effects especially during the first turns after injection in the intermediate stage.
2) Separated sectors magnets with small gap (5 cm) to obtain good vertical focusing and to provide plenty of free space between sectors for accelerating structures, injection and extraction devices. A high energy gain per turn is important in order to reduce the number of turns to reach the extraction radius. The number of sectors is mainly determined by engineering considerations (number of RF cavities as well as extraction channel problems).
3) Flat-topping RF cavities: in order to decrease the energy spread flat-topping accelerating cavities are added, namely, two additional RF resonators working on a harmonic of the main RF cavity frequency in order to obtain an "as flat as possible" accelerating voltage wave form. These cavities operate on a third (or fifth) harmonic mode with a peak voltage between 12 and 14% (or 4 and 5%) of the main RF cavities.
4) Single turn extraction: In order to get a high extraction efficiency, it is necessary to achieve a large radial separation of the last turns. In turn this requires choosing a large extraction radius, i.e. a low average field and a high energy gain per turn. The effective turn separation depends somewhat also on the phase width of the beam; for 20 º (30 º) it is 12.9 mm (12.4 mm) in the intermediate (ISSC) cyclotron and 9.0 mm (8.4 mm) for the final booster (BSSC).
5) Matching the three stages: in order to avoid any beam loss, matching conditions must be satisfied between the different stages. To simplify the overall design of the RF system, a good choice is to operate all three machines at the same frequency, i.e. 42 MHz in the proposed design, and to accelerate protons on the same harmonic number at least in the ISSC and BSSC, since at the same time the magnetic fields can be kept sufficiently far away from saturation.

The main parameters of the Accelerator complex for the RF option at 42 MHz are given in Table 3.2. Equilibrium orbits and related properties have been calculated numerically using realistic magnetic field maps.

3.3 - The injector cyclotron. It consists of a four sector isochronous cyclotron capable of delivering 5 mA in the acceptable phase width of the intermediate stage. The beams of two such injectors working at the same frequency are then merged before injecting them into the intermediate stage (ISSC) and the final booster. Commercial compact cyclotrons accelerating negatively-charged H^- ions [40] operate routinely with an internal ion source (i.e. an injection at low energy, about 30 KeV) at about 2 mA intensities. In our case a higher current is required and therefore the injection energy must be increased to about 100 keV in order to avoid space charge limitations in the source-puller gap. Taking into account the possibility to inject large currents from an external source at high voltage [41], we have chosen an axial injection system at about 100 kV for various reasons :

1) A high extraction voltage for the source.
2) A multicusp ion source for the production of negatively charged ions. This source is cumbersome and therefore it could not be installed in the central region of the cyclotron.
3) A high brightness beam accelerated by the cyclotron requires a careful 6D matching (the two transversal and the longitudinal phase space); in particular, it is necessary to use a buncher in a way to avoid too strong effects of the space charge.
4) Increasing the reliability of the cyclotron: the absence of an internal source assures a better vacuum in the cyclotron, which allows higher RF peak voltages.
5) Refined 3-D computations of the magnetic field have been carried out, in particular in the injection and extraction regions. As opposed to the intermediate and booster cyclotrons, a closed magnet configuration with a return yoke is used in order to make the cyclotron more compact.
6) The RF system consists of two accelerating and two flat-topping cavities. The fourth harmonic of the particle frequency has been chosen to make the cyclotron rather compact. In order not to worsen space-charge effects by phase compression, a constant voltage distribution along the cavity gaps is desired.

Table 3.3 summarises the main parameters of the injector cyclotrons. A general view of the injector cyclotron is visible in Figure 3.2. Bunches of the two 5 mA beams produced by each of the two injectors are merged in order to obtain a single 10 mA beam to be injected in the ISSC. Both injectors operate with negative ions (H^-). A H^+ beam extracted by stripping H^- ions and an H^- beam, extracted by a conventional channel, are synchronised so that bunches are superposed (in phase space) in a straight portion of the ISSC injection line. A stripper is installed at the end of the injection line, before the beam enters the ISSC magnetic field to convert the H^- beam into a H^+ beam. As a result the particle density in the phase space injected in the ISSC is about doubled, leading to an injected current of 10 mA at no increase of the single beam emittance. The method can be easily extrapolated to the merging of currents of even a larger number of injector cyclotrons.

3.4 - The intermediate separated-sector cyclotron (ISSC). The general view of the ISSC is given in Figure 3.3. A four-separated-sector cyclotron has been chosen as the intermediate stage because of the following reasons :

1) the acceleration to a sufficiently-high injection energy for the booster can be achieved in about 100 turns due to the possibility to install, between the sectors, cavities providing a high accelerating voltage without prohibitive losses.
2) the flat-topping of the RF voltage is easy to achieve.
3) the strong magnetic focusing provided by the four identical C-shaped sector magnets with a constant small magnetic gap (5 cm).
4) the possibility to install an efficient extraction channel in the field-free valleys.

The choice of the injection energy into the ISSC is certainly one of the most important parameters which influences the overall performances of the cyclotron complex. The space charge effects are strong at low energy. They are present in both transversal and longitudinal directions of the beam. Figure 3.4 shows the simulation of the evolution of the accelerated beam in the radial-longitudinal plane during the first 16 turns under the following conditions: intensity 20 mA, injection energy 10 MeV, energy spread 0.05 MeV, normalised emittances π mm.mrad in both radial and vertical directions. Flat-topping with a third harmonic voltage and a shift in phase (-10 RF deg.) with respect to the accelerating voltage have been used in order to compensate the linear effects of the space charge and increase the longitudinal acceptance (± 15 RF deg.) of the bunch. It has been observed that the beam shape in the r-ϕ plane seems to stabilize after a certain number of turns (cf. Figure 3.4). The

beam radial spread is about ± 15 mm in the extraction region. The result of these simulations is that a nominal 10 mA beam can be handled at an injection energy of the order of 10 MeV.

Acceleration of the beam is provided by two main resonators located in opposite valleys giving an energy gain per turn of 0.6 MeV at injection and 1.2 MeV at extraction, increasing the beam energy from 10 MeV to 120 MeV. The RF frequency of the accelerating (main) cavities has been chosen equal to 42 MHz, which corresponds to the sixth harmonic of the particle revolution frequency in the cyclotron. Due to the large (30 RF deg.) beam phase width, flat-topping cavities would operate on the third harmonic of the main cavities i.e. on the eighteenth harmonic of the revolution frequency.

Double-gap cavities have been selected (as opposed to single-gap) because their radial extension is much smaller, thus leaving more space in the centre of the machine for the bending and injection magnets and the beam diagnostics. A voltage (or phase compression) ratio of 2.0 is used between injection and extraction. In order to reduce the number of turns in the cyclotron and to have sufficient turn separation, accelerating voltages of 170 kV and 340 kV are required at injection and extraction. The main characteristics of the RF cavities are given in Table 3.4.

The shape of the cavities has been defined with the help of the 3D electromagnetic code MAFIA [42]. Models of the main and flat-top cavities have been respectively built at 1:3 and 1:1 scales in order to check the computations with MAFIA. These models are of the low-power type and are mainly made of wood and copper. Photographs of the accelerating and flat-topping cavity model during assembling and measurements are shown in Figure 3.5.

For a current of 10 mA, the power to be delivered to each main cavity of the ring cyclotron is estimated to be about 770 kW (550 kW beam power and 220 kW cavity loss), which correspond to about 1.1 MW electrical power load (assuming a 70% DC to RF conversion efficiency). The beam power to be absorbed by each cavity is 65 kW, which is about seven times the power dissipated in the walls (9 kW).

The injection channel of the ISSC cyclotron brings the beam from outside the cyclotron to the first RF cavity gap where it is accelerated. It starts after the stripper which is located at the end of the beam line that transports the combined H^+/H^- beam from the injectors. The stripped H^+ beam is injected in the cyclotron through a valley along a flat-top RF cavity as shown in Figure 3.6. When it reaches a radius lower than the injection radius it is deflected in a first bending magnet BMI1 in the

clockwise direction (seen from above). It is then deflected counter-clockwise, first by a second bending magnet BMI2 and by a electromagnetic channel EMDI located in one of the cyclotron sector gap so that it reaches the first RF cavity gap where beam acceleration starts. Injecting at 10 MeV allows to take benefit of enough room to locate the deflecting magnets and use a simple set of deflecting elements with moderate magnetic field requirements. The main parameters of the injection channel are given in Table 3.5. The location of the injection and extraction channel elements of the ISSC are given in Figure 3.6.

The extraction channel allows deflecting the accelerated beam outside the cyclotron. In order to achieve an extraction efficiency of nearly 100% so as to reduce induced radioactivity, the extracted orbit at the channel entrance should be fully separated from the last internal orbit. It consists of an electrostatic deflector (ESDE), an electromagnetic deflector (EMDE) and a bending magnet (BME). The three channel components are located in two successive valleys. After the beam is kicked outwards from the last internal orbit, by the electrostatic deflector located at the exit of a main RF-cavity it passes through the magnet sector. It is then further deflected to the entrance of the next valley by the electromagnetic deflector. The last section is a conventional bending magnet which is located in the valley behind the RF flat topping cavity as shown on Figure 3.6. Table 3.6 gives the main parameters of the extraction channel.

3.5 - The separated-sector booster cyclotron (BSSC). A general view of the booster can be seen in Figure 3.7. The magnet of the final booster consists of 10 identical C-shaped sector magnets with a strong spiral needed in order to obtain sufficient vertical focusing at high energies. Each sector is made of a pair of spiral pole tips whose angular aperture is increasing with the radius. The width of the sector at low energies fixes the magnetic field level Bs needed in the magnet for isochronism and the value of the vertical focusing frequency ν_z. The sector width should not be too large so that devices like the RF cavities and the extraction channel elements can be installed in the valleys. All these considerations have led us to select a 10 degree sector angle width at low radii. The corresponding values of the vertical focusing frequency and sector field are respectively 1.2 T (without space-charge) and 1.8 T. As in the ISSC cyclotron design, no trimming coils are used for generating the radial magnetic field increase required by isochronism. This effect is obtained by increasing the sector width with radius. The characteristics of the magnet are presented in Table 3.7.

Acceleration of the beam is provided by 6 main resonators located in the valleys. They should provide an energy gain per turn of 3.0 MeV at injection and 6.0 MeV at extraction, increasing the beam energy from 120 MeV to 990 MeV. In order to compensate the effects of the space charge forces, two flat-topping cavities are needed. The RF frequency of the accelerating (main) cavities has been fixed equal to 42 MHz, which corresponds to the sixth harmonic of the particle revolution frequency in the cyclotron. Since the beam phase width can be reduced to 15 degrees at the intermediate cyclotron exit, fifth harmonic operation has been selected for the flat-top cavities. This enables to decrease the flat-top cavity power compared to operation on the third harmonic. Single-gap cavities are the most suitable candidates because azimuthal space is restricted and they have high quality factors. This type would be used for both accelerating and flat-topping cavities. A voltage (or phase compression) ratio of 2.0 is used between injection and extraction in order to reduce the number of turns in the cyclotron and to have sufficient turn separation at extraction. The main characteristics of the accelerating cavities are given in Table 3.8. Measurements on the accelerating cavity model (1:3 scale) which can be seen on Figure 3.8 where the upper part has been removed, have been carried out in order to check and determine precisely the cavity characteristics. A very good agreement has been found between theoretical calculations and experimental results.

The power to be delivered to each main cavity of the ring cyclotron is estimated to be about 2.05 MW (1.45 MW beam power and 0.60 MW cavity loss), which corresponds to about 2.9 MW electrical power (assuming a 70% DC to RF conversion efficiency). The beam power to be absorbed by each flat-top cavity is 220 kW, which is about 20 times the power dissipated in the walls (10 kW). Operating on the fifth harmonic allows to reduce the power absorption in flat-top cavities by a factor slightly larger than 2. All the figures above are given for a current of 10 mA.

The injection channel of the BSSC cyclotron is the system that allows to bring the beam from outside the cyclotron to the first RF cavity gap where it is accelerated. Its layout can be seen in Figure 3.9, where both injection and extraction channel components are visible. The main parameters of the injection channel are given in Table 3.9. The main parameters of the extraction channel are given in Table 3.10.

3.6 - Beam Transport to the EA. The beam extracted from the cyclotron complex has a typical transverse invariant emittance of $\varepsilon_{inv} = 2\ \pi\ 10^{-6}$ rad m (the true emittance is $\varepsilon = \varepsilon_{inv} / \beta\gamma$ where $\beta\gamma$ is the usual relativistic factor), and a momentum spread of the order of a few 10^{-4}. The current density is roughly uniform in the

transverse phase-space, leading to an approximately parabolic current density in a focal point. It is not difficult to transport such a beam over significant distances and to the EA. This can be accomplished with the help of standard bending magnets and quadrupoles. The momentum of a 1.0 GeV kinetic energy protons is 1.696 GeV/c corresponding to a magnetic curvature radius of 3.77 metres in a field of 1.5 Tesla and to $\beta\gamma = 1.807$. In particular the "goose neck" required to bend the beam from horizontal to vertical into the EA requires a total bending strength of 8.88 Tesla × metre. This magnet is also used to separate the beam transport from the neutrons escaping the EA through the beam pipe. An appropriate beam catcher is used to remove them far away from the proton beam path.

As is well known, the beam transverse radial dimensions in each plane are determined by the so-called betatron function $\Delta x(z) = \sqrt{\beta(z)\varepsilon/\pi}$. Over the beam transport channel, typically $\beta(z) \approx$ 20 m and the beam radius is $\Delta x \approx$ 5.0 mm. At the EA beam window we want $\Delta x \approx 7.5$ cm and therefore $\beta(z) \approx$ 4000 m. This is realised by creating a focal point some L = 30 meters away from the window and letting the beam spread-out naturally because of its emittance. In absence of magnetic fields, the evolution of the β-function at a distance L from the focal point is given by the well known formula $\beta(z) = \beta(0) + L^2/\beta(0) \approx L^2/\beta(0)$. Setting $\beta(z) = 4000$ m we find $\beta(0) \approx L^2/\beta(z) = 0.225$ m, which is within reach with the help of an ordinary quadrupole triplet[20]. The beam radius at the focal point is very small, $\Delta x(0) = \sqrt{\beta(0)\varepsilon/\pi} = 0.70$ mm. In short the idea is the one of enhancing the angular divergence of the beam by making a very tiny focal spot[21]. A long drift space following such a focal point will traduce this angular divergence into a large spot.

An appropriate collimator is limiting the aperture available to the beam in this point to about 10 times its nominal radial size, large enough in order to let the beam through with no loss in ordinary conditions. In case of the accidental mis-steering of the beam or of a malfunctioning of the focusing lenses, the spot will grow in size and the beam will be absorbed by the collimator. In this way the beam window can be protected against accidental "hot spots" caused by the wrong handling of the beam. It has been verified that the defocusing forces due to the beam current do not appreciably affect the beam optics[22].

---

[20]It may not seem entirely obvious to obtain such a low beta value with a beam transport if the actual emittance from the accelerator were less than what is quoted. If so, one could easily increase the emittance of the beam through the beam transport with the help of multiple scattering or with a pair of orthogonal small steering magnets operated at high frequencies (Lissajous pattern).

[21]From phase-space conservation in fact through the beam transport the product of the beam size and angular divergence is a constant.

[22]For instance the CERN-PS Booster routinely handles and transports peak currents of the order of 100 mA, about one order of magnitude larger than the present case.

The beam must be transported under a reasonable level of vacuum. In our design the last part of the beam tube is filled with Pb vapour at the pressure of about 5×10^{-4} Torr, the vapour tension of the coolant at the operating temperature. Differential pumping and a cold trap will remove these vapours which may be radioactive before they reach the accelerator. There are no appreciable effects of this residual pressure on the beam propagation. The need of clearing electrodes will be further studied, but it appears unnecessary at this level.

The extracted beam current and positions are carefully monitored with non-destructive probes, beam profile monitors and pick-up electrodes. In case of a malfunctioning of the beam, the accelerator current can be cut-off very easily on the axial injection line of the injectors in times of the order of microseconds (the transition time from the ion source to the final focus), thus avoiding any damage of the hardware due to beam mis-steering. An alternate beam dump should be provided to which the beam could be dumped during accelerator tuning and the like.

3.7 - Conclusions. The above preliminary studies have shown that a 3-stage Cyclotron facility could provide a solution for a $\approx$ 10 GeV $\times$ mA beam to drive the Energy Amplifier. Detailed design studies are now being undertaken in order to clarify the following points in beam dynamics:

1) detailed calculations on the beam dynamics in the injectors in order to assess the intensity limits of this kind of injector.
2) more refined calculations of the merging of the 2 beams (H^+ and H^-) coming out of the injectors in order to define the beam characteristics at injection in the ISSC.
3) detailed beam dynamics in the ISSC with space charge effects taking into account the particle distribution after stripping.

Besides this, technical design studies on the three accelerators have to be started, in particular mechanical design studies (vacuum chamber of the large SSCs, optimisation of the shape of the main cavities of the SSCs, etc.). Finally, a conceptual study aiming at increasing the final energy towards 1200 MeV is in progress.

Tables and Figures relevant to Section 3.

Table 3.1 - Main parameters of the two ring cyclotrons

Accelerator	ISSC	BSSC
External diameter	10.5 m	16 m
Magnet iron weight	1000 tons	3170 tons
Magnet power	0.6 MW	2.7 MW
RF power	1.54 MW	12.5 MW

Table 3.2 - Main parameters for the 42 MHz design

Accelerator type	Injector	Intermediate	Booster
Injection	100 KeV	10 MeV	120 MeV
Extraction	10 MeV	120 MeV	990 MeV
Frequency	42 MHz	42 MHz	42 MHz
Harmonic	4	6	6
Magnet gap	6 cm	5 cm	5 cm
Nb. sectors	4	4	10
Sector angle (inj/ext)	15 /34 deg	26/31 deg	10/20 deg
Sector spiral extraction	0 deg	0 deg	12 deg
Nb. cavities	2	2	6
Type of cavity	delta	delta	single gap
Gap Peak Voltage injec.	110 KVolt	170 KVolt	550 KVolt
Gap Peak Voltage extrac.	110 KVolt	340 KVolt	1100 KVolt
Radial gain per turn ext.	16 mm	12 mm	10 mm

Table 3.3 - Main parameters of the injector cyclotrons

Injection energy	100 keV
Extraction energy	10 MeV
Number of sectors	4
Pole radius	0.75 m
Total yoke height	1.2 m
Maximal field in the sectors	1.5 T
Number of main RF cavities	2
RF frequency	42 MHz
Harmonic number	4
Peak Voltage	113 kV
Losses per cavity	17 kW
Number of flat-top cavities	2
RF frequency of flat-top cavities	126 MHz
Peak Voltage of flat-top cavities	13 kV
Axial Deflector field	15 kV/cm

Table 3.4 - Main characteristics of the ISSC cyclotron RF cavities

	Main cavities	Flat-top cavities
Number of cavities	2	2
Type of cavity	λ/2, double-gap, tapered walls	λ/2, double-gap, tapered walls
Frequency	42.0 MHz	126.0 MHz (h=3)
Cavity height	2.6 m	1.0 m
Cavity length	2.6 m	2.45m
Voltage at injection	2×170 kV	2×20 kV
Voltage at extraction	2×340 kV	2×40 kV
Quality factor	13000	11000
Losses/cavity	220 kW	9 kW
Beam power/cavity	550 kW	-65 kW
Total power/cavity	770 kW	-56 kW
Total electric power/cavity (70% efficiency)	1.1 MW	13 kW

Table 3.5 - ISSC Injection channel characteristics

Element	Length (m)	Magnetic field DB (T)
BMI1	0.4	0.4
BMI2	0.6	1.0
EMDI	0.8	0.25

Table 3.6 - ISSC Characteristics of the extraction channel elements

Element	Length (m)	Electric field (kV/cm)	Magnetic field DB (T)
ESDE	0.4	80	0
EMDE	0.9	0	0.25
BME	1.2	0	1.0

Table 3.7 - Main characteristics of the booster magnets

Number of sectors	10
Angular aperture at injection	10 deg
Angular aperture at extraction	20 deg
Spiral angle at extraction	12.0 deg
Magnetic gap in the sector	50 mm
Overall external diameter	15.8 m
Total iron weight	3170 tons
Maximum field in the sector	1.8 T
Total electric power	2.7 MW

Table 3.8 - Main characteristics of the booster cyclotron accelerating cavities

Frequency (MHz)	42.0
Number of cavities	6
Type of cavity	$\lambda/2$, double-gap, curved walls
Voltage at injection	550 kV
Voltage at extraction	1100 kV
Quality factor	31000
Losses (estimated)	600 kW

Table 3.9 - BSSC Injection channel characteristics

Element	Length (m)	Field drop DB (T)
BMI1	0.90	1.70
BMI2	0.50	1.30
BMI3	0.50	1.70
BMI4	0.50	1.70
BMI5	0.50	1.30
EMDI	0.90	0.25

Table 3.10 - BSSC Extraction channel characteristics

Element	Length (m)	B-Field drop (T)	E-Field (kV/cm)
ESDE	0.80	-	55
EMDE	0.30	0.16 T	-
BME	1.30	1.0 T	-

Figure Captions.

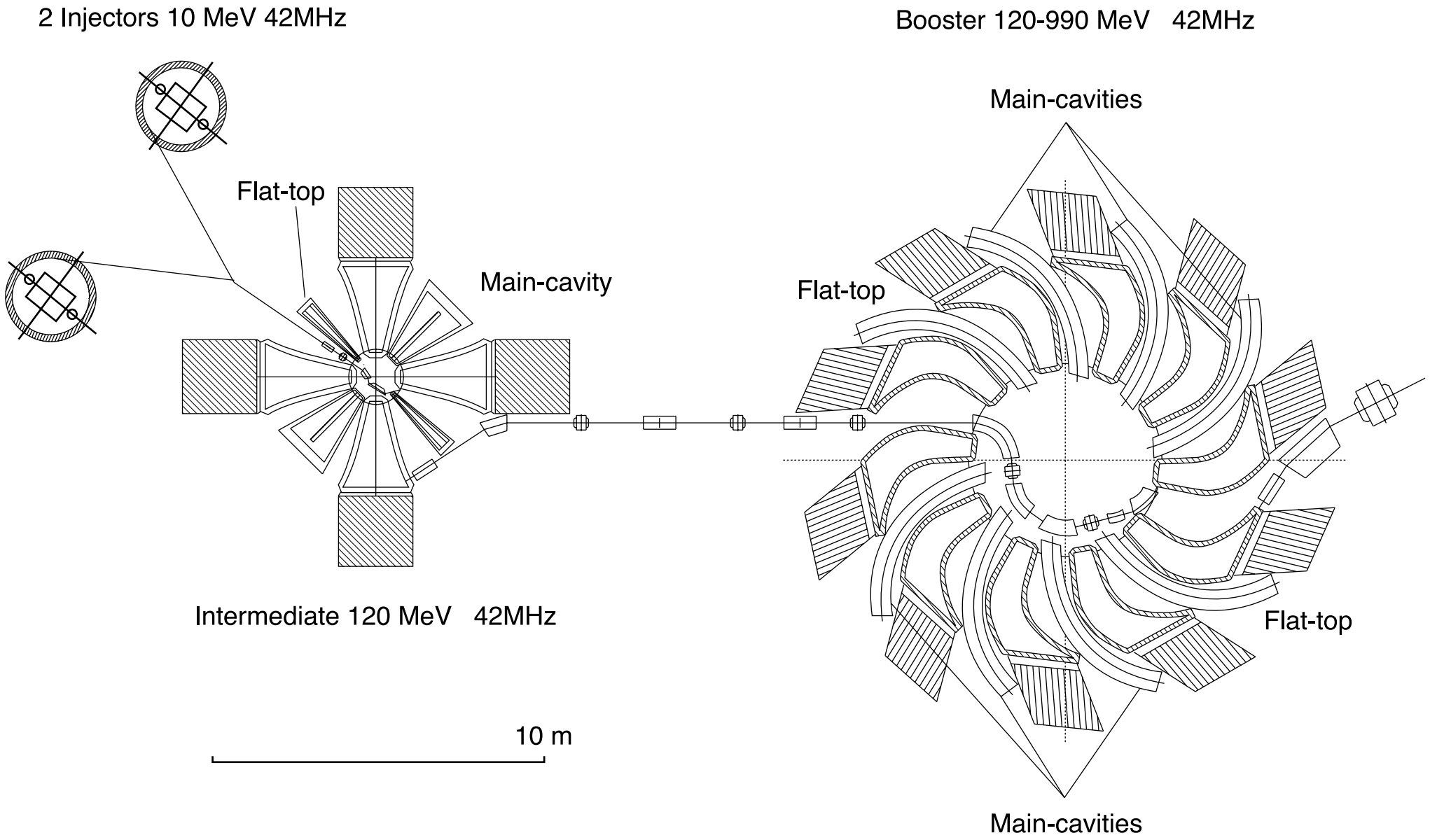
2 Injectors 10 MeV 42MHz
Booster 120-990 MeV 42MHz
Main-cavities
Flat-top
Main-cavity
Flat-top
Intermediate 120 MeV 42MHz
Flat-top
10 m
Main-cavities

Figure 3.1

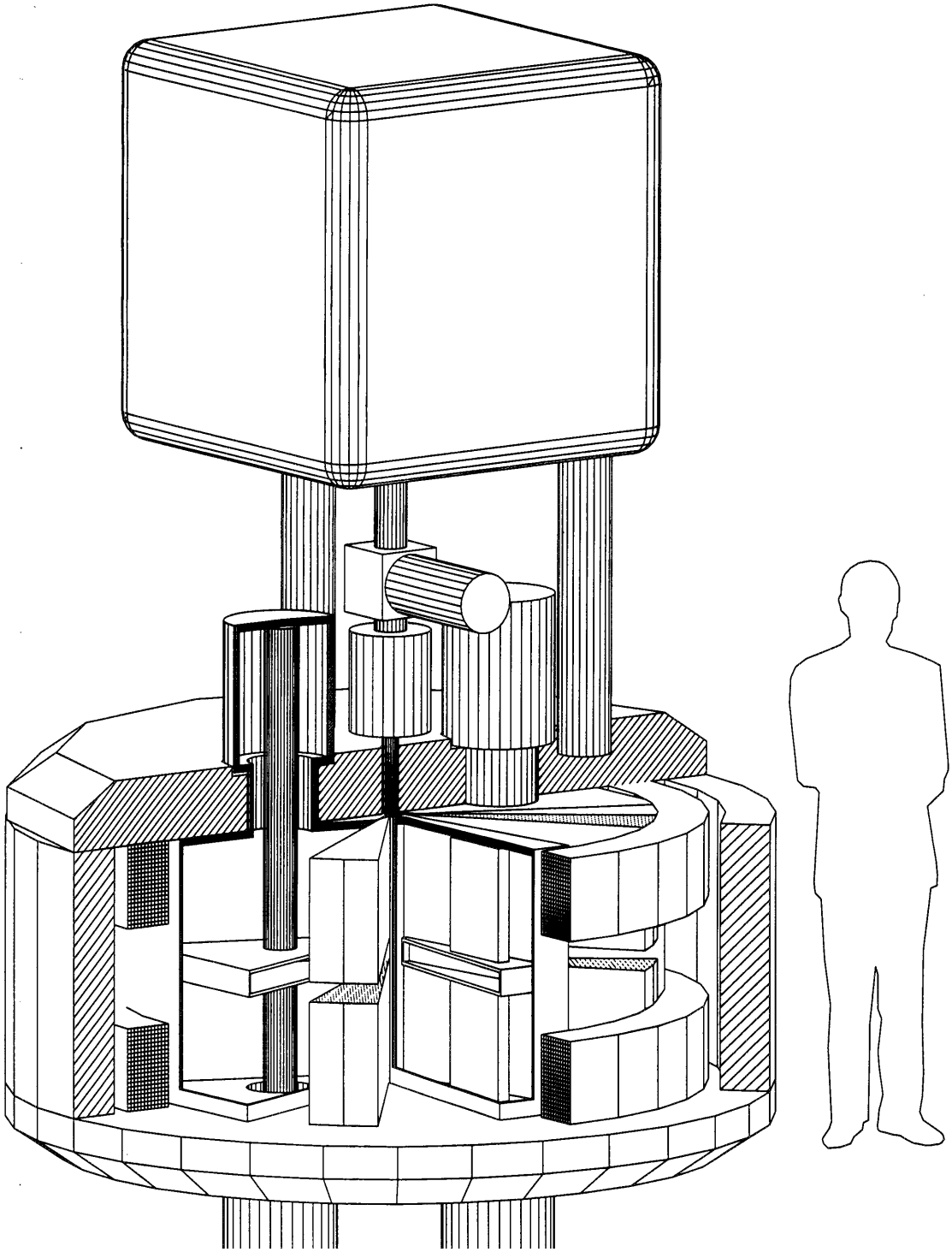

FIG. 3.2 General view of the injector cyclotron

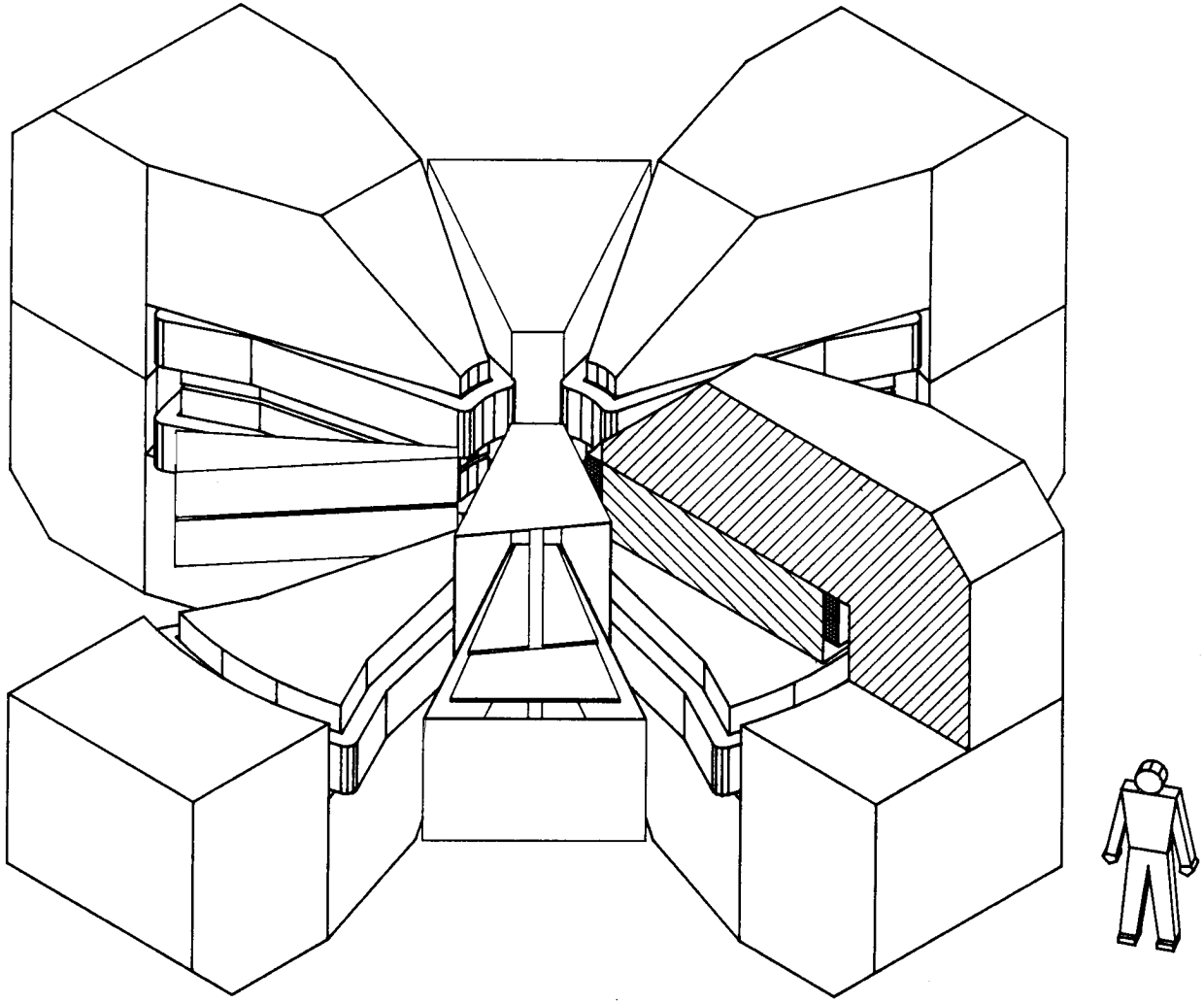

Figure 3.3

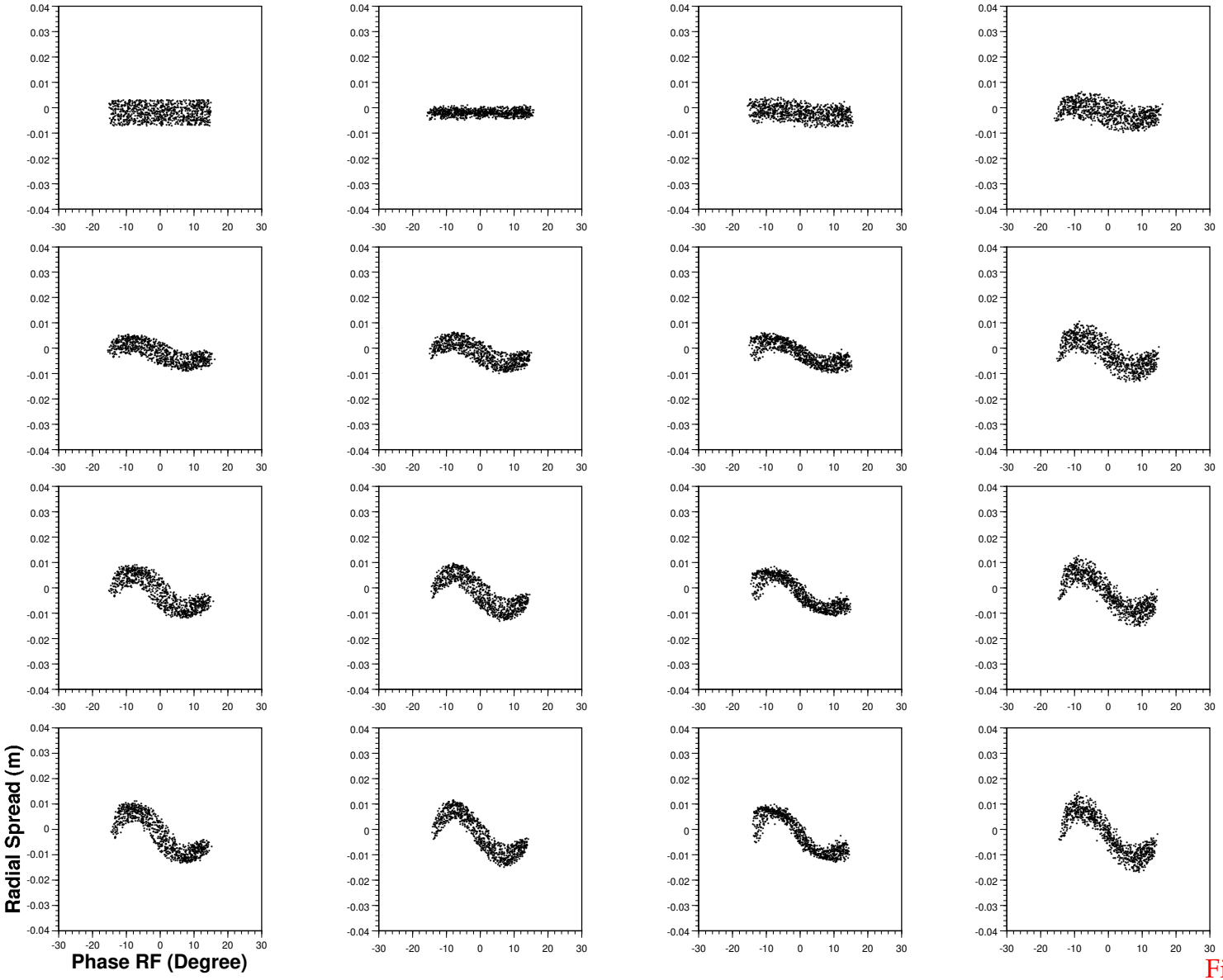

Figure 3.4

FIG. 3.5 Photographs of the cavity models (top : flat-topping cavity during assembling ; bottom : main cavity during assembling.)

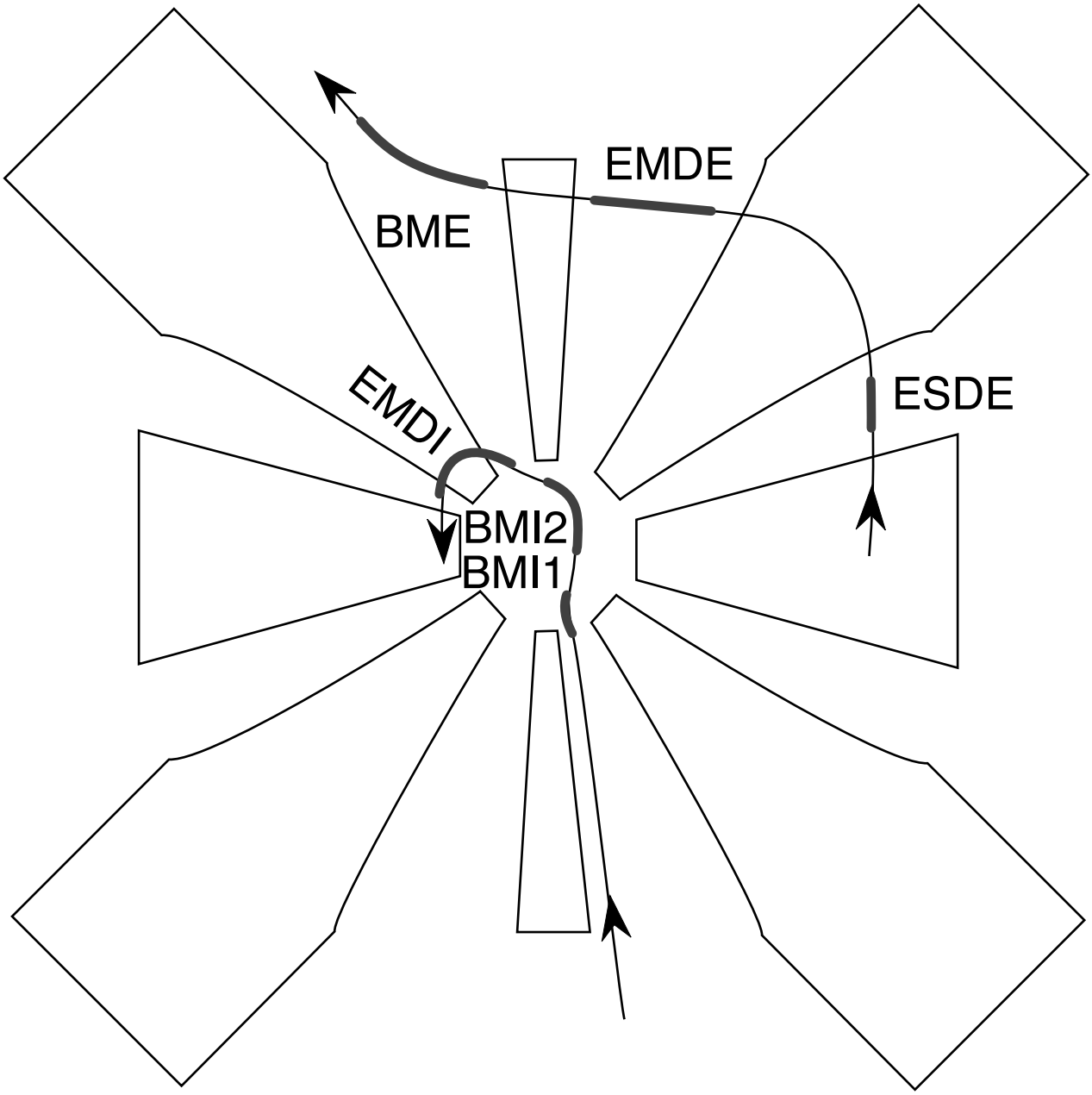

FIG. 3.6 Location of the injection and extraction channel elements of the ISSC

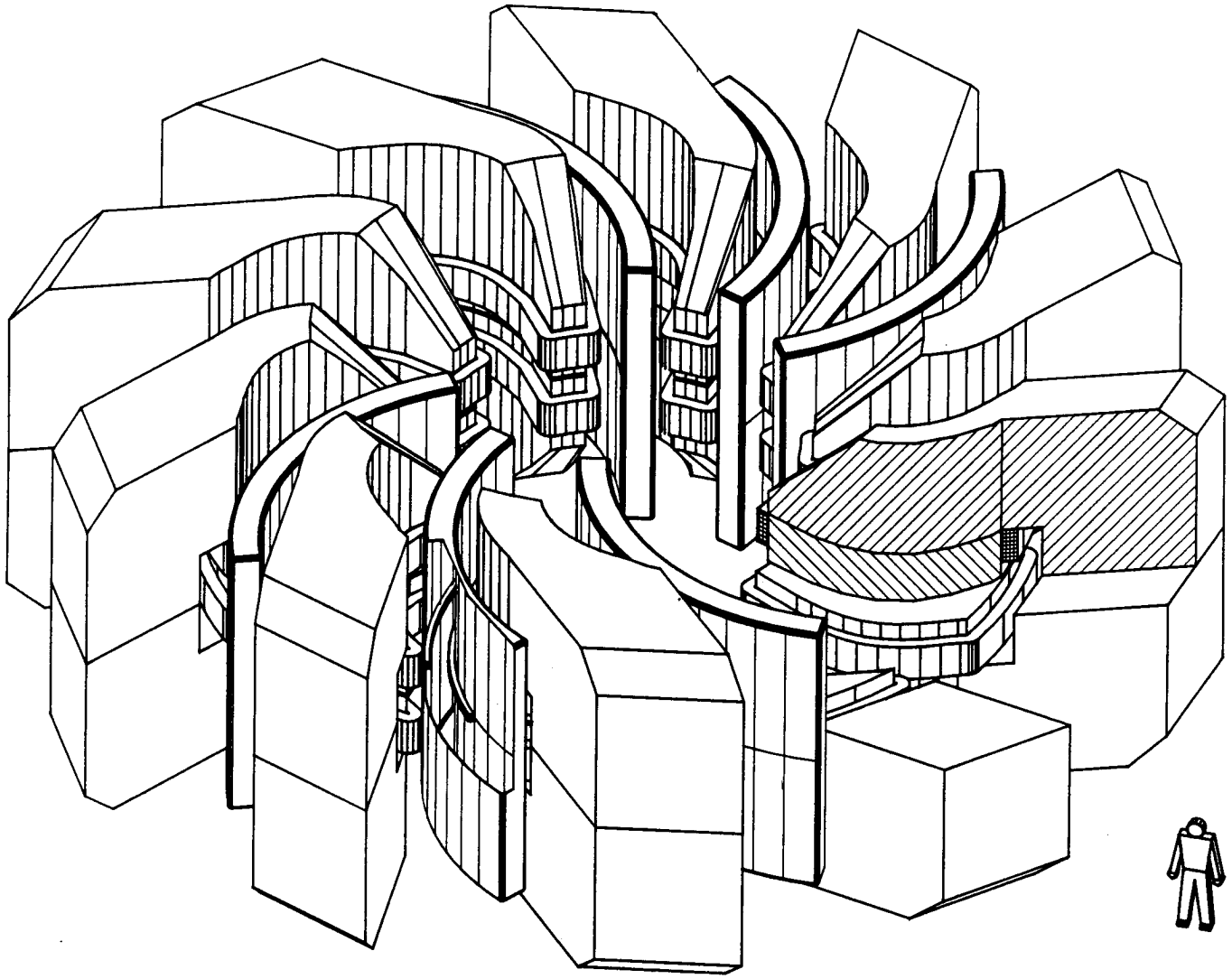

Figure 3.7

FIG. 3.8 View of the model of the accelerating cavity of the booster

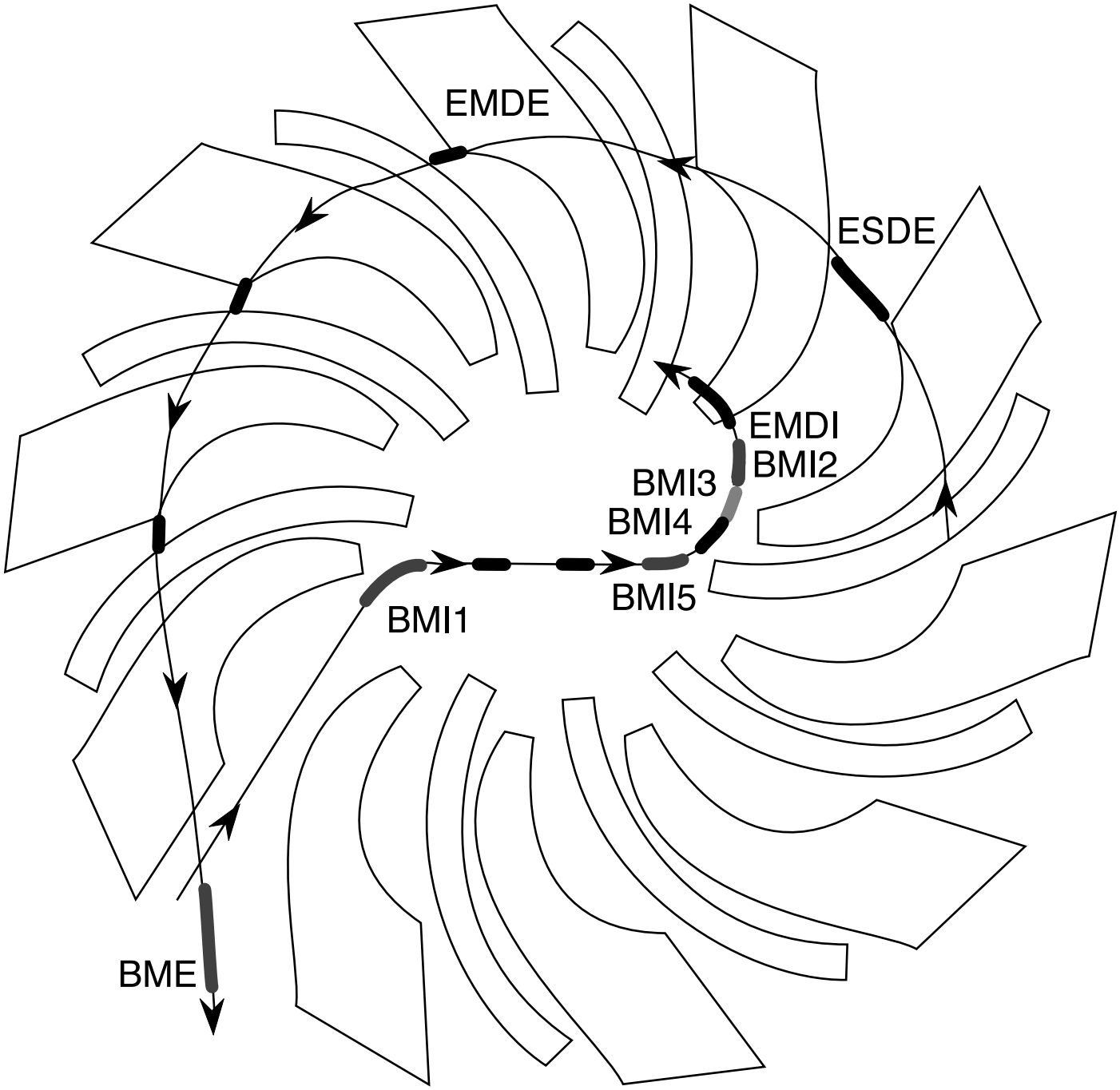

FIG. 3.9 Location of the injection and extraction channel elements of the booster ring cyclotron

4. —The Energy Amplifier Unit.

4.1 - Introduction. The general layout of the EA unit is shown in Figure 4.1a-b. The main design parameters are given in Table 4.1. In short it consists of a main vessel, about 6 m in diameter and 30 m tall, filled with molten Lead. The vessels, head enclosure and permanent internal structures are fabricated and shipped as an assembled unit to the site. The shipping weight is then about 1500 tons. Removable internal equipment is shipped separately and installed through the top head. The relatively slender geometry enhances the uniformity of the flow of the molten Lead and of the natural circulation for heat removal.

A high energy beam is injected through the top and made to interact in the Lead near the core. The heat produced by the nuclear cascade is extracted by the Heat Exchangers. Most of the inside of the vessel is free of obstructions, in order to permit a healthy circulation of the cooling liquid. The circulation of the Lead in the vessel is ensured exclusively by natural convection. There are four 375 MW_{th} heat exchangers to transfer the heat from the primary Lead to the intermediate heat transport system. They must be designed in such a way as to introduce a small pressure drop in order not to slow down too much the convective cooling flow. The liquid once cooled by the heat exchangers, descends along the periphery and feeds the lower part of the core and the target region. A thermally insulating wall separates the two flows. In order to have an effective circulation at the chosen power level (1500 MW_{th}), the temperature gradient across the Core must be of the order of 250 ^{o}C. Consequently the volume inside the vessel can be ideally divided in three separate regions, namely (1) the target/core/breeder region, (2) the convection draft generating region and (3) the heat exchangers region. A remotely controlled pantograph transfer machine is used to transfer fuel between the core, storage racks located in the convection generating region and the transfer station, where they can be inserted or removed from the EA vessel by a transfer cask[23]. The fuel storage region can be used also as a cooling down region for spent fuel. Fuel bundles can be extracted or introduced into the vessel with the help of appropriate tooling through the top cover of the vessel[24]. According to previous experience with such

[23]Refuelling machines of this type have been applied in the UK's PFR, Italy's PEC and Japan's MONJOU. The conceptual design for the ALMR transfer machine was provided by Ansaldo (Italy).

[24]As already pointed out, in order to reduce the proliferation risk, the fuel extraction or injection operation may be restricted to the user (owner) of the plant and allowed only to specialized team. This is possible since refuelling occurs only once about every 5 years and there are no major, active elements which need access during operation.

pantographs, widely used in existing Fast Reactors, the refuelling time may require of the order of 1-2 weeks. As described in the text, it is to be performed about once every five years or so.

The proton beam enters the vessel through a long cylindrical evacuated tube of about 30 cm diameter, which restricts to 20 cm before entering the core region. The beam diameter at the window is about 15 cm. The life expectancy of the beam penetration window is estimated to be about 1 year, namely it requires periodic replacement, performed extracting the full beam tube. The window is cooled by the main Lead circulation in the vessel. Accidental breaking of the window will fill the beam tube with molten Lead. This will bring the Energy Amplifier to a halt, since the injected lead will act as a beam stopper. The design of the beam penetration channel is more amply discussed further on.

There are no control bars and the power produced is controlled with the beam current. A feed-back system ensures that the inlet temperature of the heat exchangers is maintained to the specified value. For further safety however the ultimate shut down assembly which drops CB_4 by gravity, is retained, following the ALMR design, but slightly modified since the buoyancy of the Lead is much greater than the one of Sodium. This simple scram system is however used to anchor the EA solidly away from criticality when not operating. In contrast with an ordinary Reactor, in the EA there are no main elements of variability in the neutronics of the device.

Accidental thermal run-off is ultimately prevented using the natural expansion of the coolant. In case of an overheating of the EA, its lead level rises at the rate of 27 cm/100 ^{o}C. Such a level rise (see Figure 4.1b) is used to activate an overflow path which

(1) fills through a siphon a cavity located about 25 m above the Core, in which the proton beam is safely absorbed. Natural convection is sufficient to remove the residual power of the proton beam, which represents about 1/6 of the amount of the initial decay heat.

(2) fills with molten Lead the narrow gap between the vessel liner and the containment vessel, ordinarily filled with Helium[25] gas at normal pressure (Figure 4.1b). The thermal conductivity increases from the 0.03 W/m/K of Helium at 1 bar pressure to 16 W/m/K for Pb. This allows the surplus heat to be dissipated away into the environment through air convection and radiation (RVACS),

[25] The choice of helium gas is justified by the fact that the more commonly used Argon will mix with the radio-active nuclide ^{42}Ar produced by the spallation cascade.

(3) scrams the EA to a low k- value. Safety is also enhanced by the strong negative void coefficient and the negative temperature coefficient (Doppler) of the fuel which operates at relatively low temperatures.

These passive safety features are provided as a backup in case of failure of the active systems, based on the ultimate shut-off of the proton beam from the accelerator, which brings to an immediate stop the fission generated power of the Amplifier. These functions are achieved by passive means without operator action. The key processes underlying these functions are governed by thermal expansion, natural circulation of molten Lead, natural air circulation on the outer containment surface, and thermal radiation heat transfer which becomes very effective at elevated temperatures. Our design integrates all these effects into an efficient passive safety system which can accommodate primary coolant flow loss and loss of heat removal of secondary transport system with benign consequences on the Core, which can survive with no damage.

The various main components constituting the EA will be separately discussed.

4.2 - Molten Lead as Spallation Target and Coolant. Lead constitutes an ideal spallation target, since its neutron yield is high, and it is very transparent to neutrons of energies below 1 MeV. It has also excellent thermodynamical properties which make it easy to dissipate the intense heat produced by the beam. As illustrated in the previous sections, Lead has also the required properties in terms of small lethargy and small absorption cross sections to perform the function of main coolant. Its very high density and good expansion coefficient make convection sufficient even for large power production. Finally it is an excellent shielding material and most of the radiation produced by the EA core is readily and promptly absorbed. There is no need to add additional internal shields or reflectors like in the case of Liquid Sodium to protect structurally important elements inside the vessel. The radiation dose transmitted to the outer Main vessel is very small. Hence, unlike for instance in PWRs, its active life is very long since the neutron fluence is about 10^{20} n/cm^2/ year its radiation damage is negligibly small (see Table 5.5).

Molten Lead when compared to Sodium, has considerable advantages on safety. The void coefficient of Sodium is notoriously positive, namely creation of bubbles increases the reactivity. In Lead the void coefficient is negative. The absence of void coefficient problem allows for instance a less flattened shape of the fuel core. Hence the fuel pins in our design are substantially longer. The boiling point of Lead

(1743 ^{o}C) is also much higher than the one of Sodium (880 ^{o}C) and it does not react like Sodium in contact with air. Thermodynamic properties of both molten metals are given in Table 4.2. Saturation vapour pressure and evaporation rate against vacuum are shown in Figure 4.2. Since these quantities are very small (respectively 5×10^{-4} Torr and 10^{-5} g cm^{-2} s^{-1}) it is possible to keep molten Lead in an evacuated region: this feature is very important to ensure safety for the proton beam. In general, in order to have the same pressure and temperature changes through the core for a given specific power production, the speed of circulating Lead must be about 0.38 times the one of Sodium and the pitch in the fuel lattice must be enlarged in order to provide a flow area which is 1.8 times larger. The flow speed of Lead in the core is typically of the order of few m/s. The mass flow through the core is approximately doubled with respect to Sodium. Once these changes are easily implemented the two fluids become essentially equivalent.

Notwithstanding there is little or no experience in the use of Lead as a coolant in Reactors, with the exception of Military applications in the former USSR. For instance the use of molten Lead requires further studies to overcome corrosion. As discussed further on, such a problem appears fully manageable.

Natural Lead exposed to an intense neutron flux in the EA will become activated. Since the Lead is circulating in the EA this activity will spread from the core to the rest of the device. Fortunately the main activation channels are benign. Natural Lead is made of several isotopes, ^{208}Pb (52.4%), ^{206}Pb (24.1%), ^{207}Pb (22.1%) and ^{204}Pb(1.4%). If the target is ideally made of pure ^{208}Pb, a neutron capture will produce ^{209}Pb, which quickly ($t_{1/2}$ = 3.25 h) decays into the stable ^{209}Bi (with a β^- decay of 645 keV end point and no γ-ray emission) which will remain as eutectic mixture with the target material. Reactions of type (n, 2n) occur at a level which is few percent of captures and create ^{207}Pb, also stable. Both daughter nuclei are stable elements and excellent target material themselves. A target with natural Lead will produce an appreciable amount of ^{205}Pb from captures of ^{204}Pb and to a smaller level from (n, 2n) of ^{206}Pb. This element is long lived ($t_{1/2}$ = 1.52 10^7 y) and decays into stable ^{205}Tl by electron capture (i.e. by neutrino emission) and no γ-ray emission. The Q of the decay is only 51 keV. Therefore its presence is relatively harmless. Neutron capture properties of ^{205}Pb are unknown and therefore it is impossible to estimate the possibility of further transformations. However it is likely that the main channel will be neutron capture, leading to the stable ^{206}Pb. Finally ^{203}Pb from (n, 2n) of ^{204}Pb is short lived ($t_{1/2}$ = 51.8 h) and decays into stable ^{203}Tl by electron capture and γ-ray emission. Reactions of the type (n,p) which are very rare since they occur only for high energy neutrons, transform Pb isotopes into the corresponding

Thallium isotopes (^{208}Tl, ^{207}Tl, ^{206}Tl and ^{204}Tl) which all β-decay quickly into Pb nuclei again.

The situation is more complex in the case of a Bismuth target. Neutron captures lead to short lived ^{210}Bi which decays ($t_{1/2}$ = 5.0 d) in ^{210}Po which, in turn, decays with $t_{1/2}$ = 138 days to stable ^{206}Pb. There is a long lived ($t_{1/2} = 3\times10^6$ y) isomeric state ^{210m}Bi, also excited by neutron capture, which decays by α-decay to short lived ^{206}Tl (RaE), which in turn β-decays in stable ^{206}Pb. Reactions of the (n,2n) type would produce the long lived ($t_{1/2} = 3.68\ 10^5$ y) ^{208}Bi, which ends up to stable ^{208}Pb via internal conversion. Therefore a Bismuth moderator may present significant problems of radio-toxicity which must be further examined before seriously considering such material as target. Consequently the use of Bismuth or of Bismuth-Lead eutectic mixtures is not considered as main coolant, since Bismuth via the leading single neutron capture produces sizeable amounts of Polonium which is radio-toxic and volatile at the temperatures considered for the present study. However such mixture is envisaged for secondary cooling loops because of its lower boiling point (125 ^{o}C).

Additional fragments are produced by the spallation processes due to the high energy beam (see Table 5.10). The toxicity problem is investigated later on, although there is expectation that no major problems should arise, provided the appropriate precautions are taken.

4.3 - Corrosion effects due to molten Lead. Molten lead has a significant solubility for many metals (Ni and Mn > 100 ppm; Fe, Cr, Mo, 1 ÷ 10 ppm at 600 ^{o}C), which is a rising function of temperature (Figure 4.3). As a consequence, after prolonged immersion some metals and alloys exhibit a significant deterioration. This is a relevant problem and it must be mastered. Some experience on the use of Lead and Bismuth coolants in Nuclear Reactors exists in the former Soviet Union. Extensive studies of corrosion of Lead-Lithium mixtures have been carried out in the context of Fusion, where a neutron multiplying, Tritium breeding blanket is necessary. For instance a steel type HT-9 immersed in liquid Lead for 50,000 hours exhibits a corrosion loss of about 80 μm at about 500 ^{o}C [43]. In general Ferritic steels are moderately corroded by lead and in particular they do not exhibit inter granular damage (typically 30 μ after some 3000 hours at 575 ^{o}C for EM 12). The effect is more pronounced for austenitic steels (typically 120 μ after the same period at 700 ^{o}C for 800 H, where also mass transfer from the hot to cold regions is observed). Several

successful methods have been devised and demonstrated effective in order to suppress corrosion due to prolonged hot Lead Immersion:

1) *Purification and additives to the liquid metal.* When a de-oxidant (225 ppm Mg) is added to lead, no corrosion (0 µ) is observed [44] for 15 CD 9-10 loops after 28000 hours (3.2 years) of tests at 550 °C. In comparison, the same conditions and no additive would result in a corrosion in excess of 300 µ. Similar results are obtained with Titanium or Zirconium additions to the liquid Lead, where no corrosion is observed after 750 hours at 950 °C [45], in contrast to a 400 µ for an uncoated steel. Their beneficial effect is probably related to the formation of nitrides at the interface Steel/Lead. The nitrogen is contained in the Steel, if not treated beforehand. If the Zirconium is maintained constantly the film is self-healing and its long term effectiveness is preserved.

2) *Coating materials.* Amongst all the coated materials which have been tested, some seem to give the best results (i) 15 CD 9-10 low chromium steel coated with plasma sprayed Molybdenum [46][47], where no cracking or dissolution is observed after 1500 hours at 720 °C; (ii) Aluminium on low Chromium steel [46] where no evolution of the specimen is observed after 1500 hours at 750 °C. The coated material is prepared by heating the specimen in contact with a mixture of aluminium oxide and Aluminium. The coating probably reacts with traces of Oxygen to form a self-healing protective Alumina film; (iii) Z6 CN 91-9 coated with ZrN: this coating is self-healing if Zirconium is added to Lead. These last two possibilities are considered the most promising in view of to their self-healing capacity.

A small amount of embrittlement may also occur for some alloys (45 CD 4 and 35 CD 7) mostly around the melting point of Lead. Liquid metal embrittlement is a reduction of the fracture strength of a metal stressed in tension while in contact to a surface active liquid metal. This effect is enhanced when some elements such as Sn, Sb and Zn are added to the Lead. As for 15 CD 9-10, no significant embrittlement effect has been evidenced, even in the 320-350 °C temperature range. Hence specifications on the maximum concentration of certain elements in Lead must be established.

In conclusion there is no doubt that some type of additives and/or coating can effectively stop corrosion in the domain of interest [37]. *But an important experimental work has to be done (non isothermal experiments, effects of cyclic load and so on).*

4.4 - The Proton beam. The proton beam (≈ 10 mA) after acceleration and beam transport is brought to the Amplifier by conventional beam transport and a 90 degrees bending on top of the vessel. The amount of power of the beam is comparable to the one envisaged in Neutron Spallation sources under design [48]. The magnetic bending helps also in separating leakage neutrons, which are absorbed in an appropriate beam dump. By switching off the bending magnets of the last bending, the beam can be safely diverted to an appropriate beam dump. An appropriate but conventional design of the beam channel allows to perform the switch to the beam dump in a time of the order of 1 millisecond, which is extremely short in view of the thermal inertia of the Amplifier. The beam, focused by conventional quadrupoles, traverses the whole beam penetration tube and enters in the lead coolant and target through a window made of Tungsten ≈ 3 mm thick. The material has been chosen for its high melting temperature (3410 ^{o}C), its excellent thermal conductivity, its high mechanical strength[26] and acceptable activation properties. In addition it exhibits a negligible corrosion by molten Lead [49].

The beam spot size is determined by the physical distance from the focal point (≈ 30 m), where a narrow collimator has been installed (see paragraph 3.6). This arrangement ensures that the beam size at the window cannot become abnormally small, for instance as the result of a miss-steering or a failure of the beam transport. The proton beam window has a spherically curved profile and it is cooled by the bulk of the Lead coolant circulating in the target region at a speed of the order of a few m/sec. At the window the proton beam spot size has a parabolic profile, $2I_p / \pi r_o^2\left[1 - r^2 / r_o^2\right]$ with $2r_o = 15cm$ corresponding to a peak current density of 113.2 μA/cm^2 for I_0 = 10 mA. Montecarlo calculations show that the beam deposits about 1% of its kinetic energy in passing through the window, mostly due to ionisation losses, namely ≈ 95 kWatt, with a peak power density in the centre of 113 W/cm^2, which is comparable to the peak power density of the fuel rods. The same Montecarlo calculations, in excellent agreement with experimental data [50] have been used in conjunction with a fluid-dynamic code to predict the temperature and flow of the coolant and the conditions of the window[27]. The maximum temperature rise for the Tungsten and the surrounding Lead is respectively ΔT = 137 ^{o}C and ΔT =

---

[26]The use, for example, of alloys like Tungsten-Rhenium can further enhance the mechanical resistance of the window and its weldability. In particular such an alloy has a higher re-crystallisation Temperature (1650 °C vs. 1350 °C for pure Tungsten). However it has a considerable disadvantage, namely the thermal conductivity is about a factor 2 lower. Note that the operating temperature of the window is about 540 °C and the incipient re-crystallisation temperature is considerably higher (1150 °C)

[27]The thermal hydraulic model has been built using the code STAR-CD [51] and describes at the same time, the thermal behaviour of the lead (liquid) and of the beam window (solid).

107 ^{o}C. Thermal stresses associated with beam intensity variation have been estimated and found largely within the limits set by the properties of the material[28]. We have reduced such thermal stresses by reducing the thickness of the window from 3 mm in the welding of the pipe to 1.5 mm in the centre of the hemisphere, along the beam axis and were most of the energy is released (see Figure 4.4). More generally the energy deposited by the beam predicted by the Montecarlo calculations is pictured in Figure 4.5. The temperature profiles of the window and of the surrounding Lead are shown in Figure 4.6 for a local Lead speed of 5 m/s. The main parameters of the final beam transport in the Vessel are listed in Table 4.3.

The window should safely withstand accidental power densities which are more than one order of magnitude larger than the design value. The expected peak radiation damage in the window after 6000 hours at full beam intensity is of 171.1 d.p.a. and the associated gas production are of 1.1×10^4 He (appm) and 9.97×10^4 H (appm). These values are reasonable but suggest that the window should be periodically replaced. A high quality vacuum ($\leq 10^{-4}$ Torr) in the final beam transport and in the Accelerator is easily ensured by differential pumping and a Cold Trap in which Lead vapour will condense. The low Lead vapour pressure in the last part of the beam transport ($\approx 5 \times 10^{-4}$ Torr at 600 °C) has no appreciable influence on the proton beam which has a high rigidity and penetrating power.

In the unlikely possibility that the proton beam will persist even for instance if the main cooling system of the Amplifier would fail, a totally passive system (Figure 4.7), driven by the thermal dilatation of the Lead coolant will ensure that an enlarged volume region, sufficiently massive to stop the proton beam will be automatically filled with liquid Lead, the Emergency Beam Dump Volume (EBDV). A shut-off valve at the bottom of the volume ensures that the whole beam pipe is not filled with Lead. This measure has no character of necessity, but only of convenience. Indeed in the unlikely case that the Tungsten window would break, liquid Lead will rise, such as to fill completely the pipe and the Emergency Beam Dump Volume, though at a slightly lower level, but still sufficient to kill the beam and bring the Amplifier safely to a halt. It has been verified that convection cooling can safely transfer the heat produced in the EBDV (10 MW) to the main Lead coolant. This method is applicable because of the high density (10.55 g/cm^3) and the low vapour pressure ($\approx 5 \times 10^{-4}$ Torr at 600 ^{o}C) of the molten Lead (Table 4.2).

---

[28] The static structural analysis of the window has been performed using the code ANSYS [52]. The model developed used detailed pressure and temperature maps coming from the thermal hydraulic calculations.

4.5 - Fuel design and Burn-up goals. Fuel and Breeder elements are loaded in the form of thin rods (pins). Pins are clustered in sub-assemblies, each with a pre-determined number of pins, arranged at constant pitch roughly in an hexagonal configuration. Pins are made of small oxide pellets inserted in a robust steel cladding. Each pin has two extended void regions, called "plenums", one at each end, intended to accumulate the gaseous fission fragments. The pins are kept separate by a wire wrapped around the pin, which also improves the coolant flow. The main parameters of the fuel assemblies are listed in Table 4.4. They are quite similar to the ones used in Fast Breeders (FB). But in order to adapt these well proven designs to our case we must (1) modify the pitch between pins to the different thermodynamical properties of the Lead coolant when compared to Sodium and (2) reduce the coolant pressure losses through the plenum region. The temperature and pressure drop across the core must be adjusted to the requirements of convective cooling. We have chosen two different sub-assemblies with different pitches: a wider pitch is used in the central part of the core where the specific power is larger. The flat to flat distance is the same for all sub-assemblies but the number of pins is slightly different to accommodate the two different pitches.

The burn-up of an ordinary reactor varies from the 7 GW × day/t of a natural Uranium fuel of CANDU reactors to the 30 ÷ 50 GW × day/t of enriched Uranium in PWRs. The fuel burn-up of the EA is of the order of 100 GW × day/t, averaged over the fuel volume. The most exposed pins, if no intermediate shuffling is performed will accumulate about 200 GW × day/t. The practical final burn-up is determined not only by the losses of fuel quality due to FF captures, but also by (1) radiation damage of the supporting structures; and (2) pressure build-up of gaseous fission fragments. These two effects are briefly reviewed:

1) Radiation damage of the pins. Note that for a given power yield, the flux in the case of ^{233}U is smaller than the one of ^{239}Pu in a FB by a factor 0.64 due to the difference in cross sections. Therefore 150 GW × day/t for a Thorium based EA produce an integrated neutron fluence through the cladding $\int \phi dt$ equals to the one after about 96 GW × day/t in a FB. Considerable experience exists in burn-up tests for fuel pins in FB. Based on this extensive experience, a limit of about 100 ÷ 120 GW × day/t is a current goal value for most of these designs. A reasonable goal for the radiation damage in the Amplifier will then be 160 ÷ 180 GW × day/t for the most exposed pins. A burn-up of 100 GW × day/t in our case corresponds to an integrated neutron fluence through the cladding of $\int \phi dt$

$= 3.3 \times 10^{23}$ n/cm^2. The most exposed pins will accumulate about twice such a fluence. The effects on the properties of the HT-9 steel used have been examined [53]. The conclusion is that we expect ≈ 34 d.p.a./year for the most exposed pins. A reasonable ultimate limit applicable to this material is 225 d.p.a. A five year lifetime is therefore reasonable. Likewise other effects, namely He production and embrittlement appear fully acceptable.

2) The fuel material in form of (mixed) Oxides will undergo considerable damage and structural changes in view of the considerable fraction which is burnt and transformed into FFs. The behaviour of ThO_2 is not as well known as the one of the UO_2 which is presently universally used. However, the thermal conductivity, the expected mechanical properties and the melting point of ThO_2 are more favourable than in the case of UO_2 and we do not anticipate any major problem. For these reasons we have chosen at least at this stage the rather conservative average power density of $\rho = 55$ W/g[29]. The most exposed pins will operate at $\rho = 110$ W/g. The temperature of the fuel averaged over the core is then 908 ^{o}C. The average temperature of the most exposed pins is then 1210 ^{o}C and its corresponding hottest point 2350 ^{o}C, well below the melting point of ThO_2 which is 3220 ^{o}C.

3) Some space must be provided for the fission fragments, which have in general a significant mobility, especially at high temperatures. The pressure build-up is not very different for different fissionable fuels and therefore the volume of the plenum for the gases due to FFs has been calculated taking into account the mechanical properties of the cladding under a specified pressure increase, assuming that all gaseous products escape the fuel. The plenum fractional volume turns out to be essentially the same as the one of the conventional pin designs for Fast Breeders (ALMR, EFR etc.). The hottest point of the cladding is 707 ^{o}C, well below the structural limits of the steel of the cladding[30]. Note also that, when compared to Sodium cooled pins, we are dealing with a single phase coolant with negative void coefficient.

We have therefore taken as reference parameters for our design pins (Figure 4.8) which are essentially the same as those used in our " FB-models" designs with, however, the following changes:

(1) longer fuel pins to improve neutron containment in the core (1.5 m);

---

[29]This value is about one half of what is currently used in SuperPhenix and Monjou.

[30] The corresponding value for Monjou is 675 ^{o}C.

(2) a larger, variable pitch to accomodate the differences in hydraulics of molten Lead in a convective regime. Two different pitches have been used, a wider one for the Inner Core and a tighter one for the Outer Core;
(3) an appropriate "plenum" to ensure the required burn-up, but with smaller diameter and correspondingly more elongated in order to reduce the pressure drop through the core;
(4) cladding made of steel with low activation and small corrosion rate by molten lead (HT-9). More research work is still required to ensure an effective protection against corrosion (see paragraph 4.3).

The general layout of the two fuel subassemblies is shown in Figure 4.9. Many of these subassemblies which have all the same flat to flat dimensions are arranged in a continuous, quasi circular geometry with an empty central region for the Spallation Target assembly and the molten Lead diffusing region. A few hexagonal elements are left empty for the scram device and other control functions.

The Breeder is designed to compensate for the reduction of the ^{233}U stockpile during the long burn-up and the inevitable losses due to reprocessing. Especially if the EA is started well below the breeding equilibrium, such an additional amount is small. Hence the breeder mass is typically some 20% of the total fuel mass. For simplicity, the pin and subassembly geometry have been taken to be the same as in the case of the Fuel elements. Toward the end of the fuel cycle, some significant power is produced also by the Breeder (ρ = 3.0 W/g), though much smaller than in the Fuel.

During successive fuel cycles, the isotopic composition of the Uranium changes, especially due to the production of a substantial amount of ^{234}U. In order to accomodate the extra mass some additional 20 cm of the fuel pin are left initially empty and progressively filled. Hence for asymptotic fuel composition, the active length of the fuel pins may be increased to as much as 1.70 m.

Small amounts of Trans-uranic elements (Np, Pu and Am) and long lived ^{231}Pa are separated out during each reprocessing and re-injected in the EA for final incineration. It is convenient to insert these materials in special "incineration" pins which undergo no successive periodic reprocessing at least until a major fraction of the isotopes is incinerated. These pins have a much shorter fuel section and a much larger "plenum" section, to allow build-up of fission fragments. The lifetime of the cladding is limited by radiation damage. We have already estimated that the ordinary fuel exposure accumulates ≈ 34 d.p.a./year. Assuming an ultimate cladding lifetime of 250 d.p.a. these pins may last 7/8 years. After this time they

must be reinforced with a second, fresh cladding or equipped with a new one. In order to ensure the fastest incineration these pins must be located where the flux is the highest, namely near to the target region.

The operating temperature of the plant is application dependent. In our basic design we have retained the choices of the reference design, which calls for a fuel outlet temperature of about 600 ºC. It must be noted however that in principle the Lead coolant could permit a somewhat higher operating temperature, which is advantageous to increase the efficiency of the conversion into electricity and eventually to produce synthetic Hydrogen [4]. Evidently additional research and development work is required in order to safely adapt our present design to an increased operating temperature. In particular the cladding material of the fuel pins may require some changes, especially in view of the increased potential problems from corrosion and reduced structural strength[31].

4.6 - Core lay-out and main parameters. The EA is based on a highly diffusive structure (molten Lead) in which a number of fuel elements are inserted. In absence of fuel, spallation neutrons produced roughly in the centre of the device will diffuse and loose adiabatically energy until either they are captured or they escape. If fuel is inserted gradually in the molten Lead medium, both the captured fraction in Lead and the escape probability will decrease. The fuel properties will gradually influence the neutronics. We consider as reasonable design parameter an escape probability ≤ 1% and captures in the Lead moderator of the order of 5-6% (Table 4.5). Note that in an EA the neutron inventory is of primary importance and that these losses must be as small as possible. While in an ordinary PWR losses can be easily compensated with a more enriched fuel, the necessity of full breeding does not offer much degrees of freedom in an EA. On the other hand the void coefficient for molten Lead is negative and therefore the rather awkward measures ordinarily taken in a Sodium cooled device are no longer necessary. In particular one does not need to make the shape of the fuel core "pancake" like. A more spherical profile improves the neutron containment and hence the losses in the moderator.

Because of the long migration length in the Lead medium, these parameters are largely independent on the detailed geometry of the fuel and depend primarily on the fuel and diffuser masses. The core can be ideally divided into three concentric

[31] Titanium based alloys have been studied for the Fast Breeder and may be an interesting development for our application. In particular the corrosion of molten Lead on Titanium is very low.

regions. The first region (the *Spallation Target*) has no fuel and it is naturally filled by the molten lead. In this volume beam particles interact to produce primary neutrons. The radial size of such a volume has to be sufficiently ample in order to ensure that the neutron spectrum is made softer by the occurrence of (n,n') inelastic interactions in Lead. In this way the spectrum at the first fuel element is softened sufficiently as to ensure a minimal radiation damage to the structural materials and to uniformise by diffusion the vertical illumination of the fuel pins. We have chosen a radial distance of the order of ≥ 40 cm. With this choice, the calculated spectrum at the edge of the target region is not appreciably different from the one in the core. The second region is the *Main Fuel* region, in which a variety of fuels can be inserted (generally subdivided in two parts, the Inner Core and the Outer Core with different pitches), followed by a third region, the *Breeder* region, initially loaded with pure ThO_2 breeding material.

The nominal power of 1500 MW_{th} requires 27.3 tons of mixed fuel oxide at the average power density of 55 W/g. The duration of the fuel is set to be 5 years equivalent at full power. The average fuel burn-up is then 100 GWatt day/ton-oxide. The main parameters of the Fuel/Breeder core are listed in Table 4.4. As already pointed out the breeding equilibrium concentration of ^{233}U, referred to ^{232}Th is ξ = 0.126. With such a high concentration there is obviously no problem in setting the wanted value of k and eventually even of reaching criticality. However with continued burn-up the fraction of captures due to FFs, ΔL_{ff} will grow linearly with time, absorbing for instance about 6% of all neutrons at 100 GW × day/t and causing a corresponding reduction in the criticality. The reduction of the multiplication coefficient $\Delta k_{ff} = -\left(\overline{\eta}\varepsilon / 2\right)\Delta L_{ff}$ will be very large. For instance, if initially we have k = 0.98 and G= 120, after 100 GW × day/t, k = 0.908 and G = 26.0. Such fivefold decrease of gain would be completely catastrophic. It is therefore preferable to start with a ^{233}U concentration lower than the breeding equilibrium and let it grow toward such a limit during burn-up. As already pointed out in paragraph 2.7 one can realise a first order cancellation between the approximately linear rise of the FF captures and the exponentially approaching breading equilibrium. This leads to a much smaller initial ^{233}U concentration, x = 0.105.

4.7 - Convective Pumping. Convection pumping is realised with the help of a sufficiently tall Lead column in which the warm coolant from the Core rises as a result of the large value of the Lead expansion coefficient, 1.32 kg m^{-3} K^{-1}. The coolant returns to the Core after being cooled down to the initial temperature by the

heat exchangers. The pressure difference generated in the loop by the convective pumping action is given by $\Delta P = K \Delta T h g$, where ΔT is the temperature change, K is the coolant expansion coefficient, h is the height of the column and g the gravity acceleration constant. Typically for $\Delta T =$ 200 ^{o}C, h = 25 m, we find ΔP = 0.637 bars! Such a pressure difference is spent in order to put into movement the coolant and in stationary conditions it is equal to the sum of the pressure drops in the loop, primarily the pressure drops across the Core and the Heat exchangers. The pumping power required to move a volume V = 10 m^3/s of coolant with a pressure difference ΔP across the Core is $W_{pump} = V \Delta P =$ 0.647 MWatt. Such power must evidently be produced by the convective pump.

In order to dissipate a power q produced by nuclear reactions in the pin with a resulting temperature difference ΔT, the coolant must traverse the core with a speed v given by

$$\upsilon = \frac{q}{f_a \Delta T \rho c_p}$$

where f_a is the flow area and ρ and c_p are respectively the density and specific heat of the coolant. For cylindrical pins of radius $r \equiv [r_f ; r_p]$ of the fuel and the plenum respectively arranged in an infinite hexagonal lattice of pitch p, the flow area is $f_a = \sqrt{3} p^2 / 2 - \pi r^2$. Neglecting end effects and the temperature dependence of the parameters, the pressure drop through the core ΔP consequent of a given flow speed v in the fuel which the pump must supply is given by

$$\Delta P = \frac{2 \chi \eta l \rho \upsilon^2}{d_e}; \quad \eta = 0.079 \times \left(\frac{\rho \upsilon d_e}{\mu} \right)^{-0.25}; \quad d_e = \frac{4 f_a}{2 \pi r}; \quad \chi = \frac{l_f}{l} + \frac{l_p}{l} \left(\frac{d_{e,f}}{d_{e,p}} \right)^{1.25} \left(\frac{f_f}{f_p} \right)^{1.75}$$

where χ is a geometry dependent factor, $l = l_f + l_p$ the pin length, divided in the fuel section and the plenum section; η is the friction factor, function of the Reynolds number, which in turn depends on the viscosity μ; $d_e \equiv [d_{e,f} ; d_{e,p}]$ is the effective diameter of the fuel and the plenum and, function of the coolant flow area $f_a \equiv [f_f, f_p]$ and of the so-called wetted perimeter. Additional corrections which typically amount to a maximum of 8% are due to the abrupt changes of the coolant flow area:

$$\Delta P = \frac{2 \chi \eta l \rho v^2}{d_e} + \frac{\rho v^2}{4} \left[\left(1 - \frac{f_p}{f_o} \right) \left(\frac{f_f}{f_p} \right)^2 + \left(1 - \frac{f_f}{f_p} \right) + 2 \left(1 - \frac{f_p}{f_f} \right)^2 + 2 \left(1 - \frac{f_0}{f_p} \right)^2 \left(\frac{f_f}{f_p} \right)^2 \right]$$

where f_o is the free flow area. With these corrections, the results of the formula [54] are in excellent agreement with the full hydrodynamic code COBRA [55].

In practice we take the temperature difference ΔT as an input design parameter, which determines the primary pressure difference ΔP_{pump} for a given convective pump column of length L. Such pressure difference must get the coolant through the

Core, the heat exchangers and the full loop (> $2L$ long) at a sufficiently high speed as to transfer the large amount of heat produced from the Core to the secondary loop. In order to provide sufficient margin for the other pressure drops, somewhat arbitrarily we have set the pressure drop across the core to 0.7 ΔP_{pump}, setting in this way the pressure and the temperature differences across the core. The pitch size of the lattice can be adjusted next in order to set the coolant speed v through the core to the value required by the actual power density and by ΔT. The resulting pitch and coolant speed as a function of the power density in the pins is given in Figure 4.10a and Figure 4.10b for L= 25 m and different temperature differences in the range 150 ^{o}C to 250 ^{o}C. They appear quite acceptable.

Since the power density produced in the fuel rods is falling about linearly with the inverse of the radius, the resulting pitch will be a smooth function of the core radial co-ordinate, leading to a pitch size decreasing with radius. In practice and in order to permit the same flat to flat dimensions for the fuel bundles across the core and a given fuel pin radius, we have actually quantified the pitch into discrete values corresponding to different number of integer rounds of hexagonal shape. This leads to some residual radial dependence of ΔT, which is partially absorbed by natural mixing along the convective column and it should be compensated restricting the flow for instance at the entry of the fuel bundles. Evidently a radial pitch variation affects also the neutronics of the core, which in turn has effects onto the power density. Hence, all these parameters have to be recurrently adjusted to their optimal values.

The motion of the warm coolant in the convective column is the key to the convective pumping and it has been carefully simulated with help of the full hydrodynamic code. The actual temperature and speed distributions at the exit of the core have been used as input in a simulation of the rising liquid. The speed and temperature of the coolant gently homogenise along the path through the column as shown in Figure 5.12 in the following section. The programme described in paragraph 5.5 to which we refer for more details reproduces the main results of our simpler analysis.

The previous calculations are made for the nominal power of the EA and stationary conditions. It has been verified that correct cooling conditions persist over the full range of conceivable powers, including decay heat and major transients. In general, convective cooling has “self-healing” features, namely the pumping action is directly related to the amount of power to be transported.

In stationary conditions and at the nominal power, the ≈ 10,000 tons of coolant will flow through the core at the rate of some 52 t/s, corresponding to a turn-around time of the order of 200 seconds for a total length of the loop of the order of 50 metres. In view of the large mass of the coolant, a considerable momentum is stored in the coolant during normal operation and it has considerable effect in (fast) changes of conditions.

4.8 - Seismic Protection. As already pointed out in order to reduce capital costs and increase flexibility large portions of the EA plant should be standardised. Furthermore, to gain public acceptance, the plant must be reliable and should have passive inherent features. Seismic design can play a major role in achieving a standardised design which could accommodate a range of seismic conditions. One approach to standardisation would be to design a plant using traditional methods for a Safe Shutdown Earthquake (SSE) which envelopes the responses of 90 percent of existing nuclear sites in the USA. This is the present licensing seismic basis (RC 1.60) and it calls for a maximum horizontal and vertical acceleration (PGA) of 0.30 g.

This approach, however, would lead to high seismic loads, especially in components and equipment, and would still exclude for instance California sites and limit the export potential of these plants to high seismic countries such as in the Pacific Rim region. Liquid Metal designs which consist of thin walled vessels designed to accommodate large thermal transients under low operating pressures are more sensitive to seismic loads and thus the EA would be particularly penalised by this approach. An appropriate design of a modular EA requires to be able to accomodate a variety of seismic conditions expected at a wide range of sites, from deep soil sites with a minimum shear wave velocity to stiff rock sites.

The alternative is to seismically isolate the plant. Several studies performed in Japan have shown that it would not be possible to design large LMR plants which are economical in areas of high seismicity without incorporating seismic isolation [56]. In an isolated plant, the design and qualification of equipment and piping and their supports become a simpler task than it is today and the impact of seismic design on preferred equipment layouts is minimised. Since the response of isolated structures is highly predictable, the risk of accidents due to uncertainties in the input motions is reduced, safety margin is increased, and plant investment protection is enhanced. Additionally, if seismic design criteria are upwardly revised, for example due to the discovery of unexpected geo-tectonic conditions, the standard plant design would

probably not have to be altered and only the isolation system would need to be upgraded.

Seismic isolation is a significant development in earthquake engineering that is gaining rapid world-wide acceptance in the commercial field [57]. This approach introduces a damped flexible mechanism between the building foundation and the ground to decouple the structure from the harmful components of earthquake induced ground motion, thus resulting in significant reductions in seismic loads on the structure and more significantly on equipment within the structure. In recent years, seismic isolation of nuclear structures has been receiving increased attention. To date, six nuclear power plant units in France and South Africa have been isolated. It is expected that seismic isolation will play a major role in the design of the advanced nuclear plants of the future in the US as well as in Japan and Europe.

Several technological advancements are responsible for making seismic isolation a practical alternative. These include the development of highly reliable elastomeric compounds used in seismic bearings which are capable of supporting large loads and accommodating large horizontal deformations during the earthquake without becoming unstable. Additionally, the development of high damping elastomers and other mechanical energy dissipators has provided the means to limit the resulting displacements in the isolators to manageable levels. Other factors include the availability of verified computer programmes, the compilation of reliable test results of individual seismic isolators under extreme loads, shake table tests for evaluating system response, and validation of computer programmes and confirmation of the response of isolated buildings during earthquakes [58].

Seismic isolation has been included in the EFR and in the ALMR designs. Most of this work is relevant also to our case. The ALMR design calls for a seismically isolated platform which supports the reactor module, containment, the reactor vessel auxiliary cooling system and the safety related reactor shut-down and coast-down equipment. The total mass to be insulated is of the order of 25,000 tons. The fragility of components appears greatly improved by insulation [59]. Some model tests have confirmed the results of these estimates [60]. Our present design can include most of the features of the ALMR design.

4.9 - Decay heat removal by natural air convection. Nuclear industry has developed a number of passive natural convection air cooling systems to remove decay heat in the unlikely event that all active cooling systems of a reactor fail [11]

[61]. We have applied the design made for the ALMR (RVACS) to the EA, in order to study the behaviour of our system in case of such an event[32].

The application of the RVACS to the Fast Energy Amplifier is illustrated in Figure 4.1b.

In the unlikely case of a scram event in which all the active cooling systems fail to operate, the heat produced by the fission products decay in the core increases the average temperature of the lead contained in the vessel. Lead expands (the level rising at the rate of 27 cm/100 ˚C) and when its temperature exceeds a determined safety margin, it overflows into a narrow gap between the main vessel and the containment vessel. This gap is normally filled with Helium which ensures a reasonable thermal isolation during normal operations.

The containment vessel is in contact with ambient air entering the system through a cooling channel. Air reaches the bottom of the vessel through a downcomer channel which is thermally isolated from a riser channel, in direct contact with the vessel.

When the lead fills the gap, a good thermal contact is established between the main and the containment vessels, and heat can be transferred to the air in the riser channel. Air temperature increases, and a natural circulation starts. Air draft is enhanced if a long chimney (about 30 m) is added at the end of the riser channel. The downcomer and riser channels consist of two annular regions around the vessel of respectively 18 and 57 cm thickness. In such conditions, for a vessel temperature of 500 ˚C, the air velocity attained in the hot channel is of the order of 10 m/s, corresponding to a flow rate of 53 m^3/s. The average outlet temperature of the air is about 177 ˚C and the heat removal rate of the order of 6.5 MW, which is linearly dependent on the vessel temperature.

Decay heat is therefore extracted by a simultaneous process of internal (lead) and external (air) natural convection, conduction (through the steel of the vessels) and radiation (from the external vessel into the riser channel).

The core decay heat generation and the RVACS heat removal rates during a scram event are shown in Figure 4.11. At the beginning the decay heat generation is at a much higher rate than the heat removal. Consequently, the lead heats up very

[32]We built a thermal-hydraulic model using the code STAR-CD [51]. The numerical model simulates the natural convection of air in the system, by taking into account convective and radiative heat transfer from the surface of the vessel to the air cooling channel.

slowly, thanks to the large thermal capacitance of the F-EA. The RVACS heat removal rate increases slowly with the gradual increase in the reactor vessel temperature. When the decay heat generation rate and the heat removal rate are equal, the system reaches its highest temperature. From then on, the removal rate exceeds the decay heat generation rate, and the average temperature of the vessel slowly decreases.

The thermal transient experienced by the F-EA vessel for different starting temperatures is shown in Figure 4.12. It consists of a slow increase over many hours to a peak temperature followed by a gradual cool down. The peak temperature is reached much earlier (and has a lower value compared to the starting temperature) in the case of higher starting temperatures, since the heat removal rate is higher.

The RVACS is based on the natural mechanism of lead dilatation and air convection. It is therefore completely independent on active components or operator actions, and insensitive to human errors.

4.10 - Miscellanea. The on-line, continuous determination of the multiplication coefficient k is essential in order to monitor the correct operation of the EA. The method we propose is based on the lifetime of the fast neutrons after a sudden shut-off of the proton beam (source). This is easily performed gating-off the ion source for a period of time of the order of a few hundred microseconds. The effects on the RF-cavities of suddenly removing the beam load is still being investigated, but it should be manageable by the control system. The time of the neutron activity is roughly exponential, with a time constant proportional to 1/(1-k). Monitoring of the k-value can be performed continuously as a part of the standard operation mode of the Accelerator.

Scram devices are used to anchor the k of the EA to a sufficiently low value during shutdowns, emergencies, etc. This is performed with the help of a series of blocks of CB_4, conveniently located throughout the Core. This material is very effective : about 20 kg of CB_4 diffused uniformly throughout the core produce a reactivity change $\Delta k = -0.04$. There are three types of such devices: (1) ordinary scram, performed with an appropriate, fast-moving mechanical device, (2) emergency scram, based on the design of the ALMR "ultimate shut-off" in which many small spheres of CB_4 are dropped by gravity inside an evacuated tube which descends to the Core, and (3) the Molten Lead Activated Scram (MLAS), associated with the siphon overflow triggered by the excessive expansion of the Lead and

consequent level increase in the vessel. As already amply discussed, this trigger activates also the RVACS to convey the extra heat to the surrounding air and blocks the proton beam from entering in the core region, filling with Lead the emergency beam dump volume (EBDV).

The conceptual design of the MLAS is shown in Figure 4.13. If the molten Lead is penetrating through the siphon, RVACS dedicated volume etc., a small fraction fills the long thin tube descending down to well below the core region. At this depth the pressure of the liquid will be of the order of 30 atm, which is amply sufficient to push upwards the CB_4 blocks well inside the core. A second tube is used to exhaust the neutral gas (Helium) which is normally filling the tubes. The CB_4 blocks, in presence of Lead, will be held firmly in place by the buoyancy of the liquid.

A lead purification unit is needed to remove impurities from the liquid and to ensure that the required additives against corrosion are effective. The detailed parameter list of this device is for the moment largely unknown, pending the results of the corrosion studies (see paragraph 4.3). Some way as to heat-up the Lead whenever appropriate is also necessary.

The heat exchangers are relatively conventional, except that they must be designed in order to introduce a small pressure drop across the primary circuit in order not to hamper natural convective cooling. At this stage we have assumed that the pressure drop is about 1/3 of the one across the main Core. We have verified that this choice is not critical to the performance of the convective cooling. We have indicated that the primary coolant should not contain an appreciable amount of Bismuth because of activation problems. This precaution does not apply of course to the secondary loop which can be filled with a Lead-Bismuth eutectic mixture. The Pb-Bi eutectic mixture has a boiling point in the vicinity of 125 ^{o}C and it has been chosen to avoid freezing of the coolant in the transmission line.

The EFR design has foreseen a convection driven cooling loop which performs a function similar to the RVACS. If considered necessary it could be added also to our design, although it is introducing a duplication which may be redundant. It could be considered as an alternative to the RVACS system. In the EFR design the decay heat is extracted by six additional heat exchangers of 15 MW each which reject excess heat directly in the environment. These Direct Cooling Systems (DCS) consist each of a (Lead-Bismuth eutectic mixture) filled loops. These loops extract heat from the hot pool of the primary molten metal by immersed Pb/Pb-Bi heat exchangers and reject the heat to the environment with Pb-Bi/air heat exchangers located well above the pool level. One of these DRC units relies exclusively on natural convection heat

transfer and natural draught on the air side. The other is normally operated with forced flow. Each loop is equipped with an electromagnetic pump and two fans in parallel on the air side. These active loops possess passive heat removal, if pumps and fans are off to about 2/3 of that of the active flow mode. A special Pb-Bi heat exchanger freezing protection insures that the temperature in individual pipes cannot fall below 140 ºC.

A large number of monitoring devices are required to follow the radiation monitoring, neutronics, the hydraulics (speed and temperatures) and the potential corrosions due to molten Lead.

4.11 - Conclusions In this section, we have presented the conceptual design of an EA with a power rating (1500 MWth, 675 MWe) that is of direct relevance to the modules presently considered by nuclear industry to meet the needs of utilities. Such a machine represents in our view a real breakthrough in the prospects of nuclear energy in setting the highest standards for safe and economical operation, coupled with realistic solutions for waste disposal and non-proliferation issues.

The machine is always subcritical. There are no control bars and in normal operation, the level of power is controlled entirely by the accelerator beam via a feed-back loop. The separation between the accelerator vacuum and the active medium (a "frequently asked question") appears entirely solved by a specially designed window that would be routinely changed once a year. Even if the window broke, which is unlikely, there would be no serious consequence and the EA would be brought to a safe halt, even without human intervention.

Conspicuous in our design is the absence of coolant pumps: the heat is evacuated by convection alone and transferred to the outside world through heat exchangers via a secondary cooling loop. Convection cooling is a unique feature for such a large power, and is only made possible by the use of molten Lead as coolant. The absence of pumps has advantages from the safety and maintenance point of view (no moving parts). In fact the whole vessel could be sealed during the long interval (five years) between refuelling as the owner utility has no valid reason to intervene inside. Obviously this offers an extra means of monitoring, by the controlling bodies of non-diversion of fissile material. The economical aspect is also important. Suppressing the pumping system is a substantial simplification in construction as well as a sizeable economy in capital costs.

The burn-up of the fuel is a key parameter in the economic performance of the EA. The EA achieves an average burn-up of 100 GW-day/t, whilst maintaining during that time a practically constant gain at the nominal value of G=120, corresponding to k = 0.98 with no external control devices. This is possible because one can compensate the loss of reactivity due to FF accumulation by starting the EA with less ^{233}U than the amount which would correspond to breeding equilibrium. Such a burn-up is matched to the radiation damage and the pressure build-up of fission product gases of the fuel pins. The average power density has been set to the conservative value of 55 W/g which is one half the value considered in Fast Breeders. This necessitates of course having a larger fuel load (for the nominal power of 1500 MWth one requires a 27. 3 tons load of mixed fuel oxide) which has no serious consequence since the fuel is inexpensive. On the other hand, the low burn-up rate translates into a rather long time between refuelling (5 years). This long time between access to the fuel has the important consequence of minimising the radiation dose absorbed by workers. There is no need to have a permanent crew on site devoted to fuel changes and this could probably be the task of travelling crews of specialists, conceivably under some kind of international supervision to insure no possibility of fuel diversion.

A machine designed today should put strong emphasis on safety issues. This has been a prime consideration during our design. First of all, the machine is safely subcritical, since any reactivity excursion leading to an increase in power output, will be immediately corrected by a strong negative temperature effect. The main difference with a Sodium based FB here is the absence of a positive void coefficient which could cause the latter to become prompt critical. Then, in the unlikely case of an accident that would not be corrected by human intervention or electronic feedbacks, passive measure would be implemented relying on basic properties such as thermal expansion of Lead, gravity, natural convection in molten Lead, circulation of air, and radiation. The result would be to bring the machine quickly to a halt and safely bleed the radioactive decay heat to the environment. At no point could a temperature increase occur that would cause the core to melt or otherwise lead to a radioactive release in the environment.

Molten Lead has in our view considerable advantages over Sodium, and its choice has been essential to us, not only in the physical principle of a Fast Neutron EA, but also for the inherent safety features which we have just discussed. Objections against the use of Lead have often been raised in the past on the grounds of its supposedly corrosive action on steel. We believe that up to the 550 °C - 600 °C region, on which we have based the present model, there is enough experience (or

reasonable extension of known facts) to plan safely on using a known material such as HT-9 for fuel cladding. However, we believe it would be desirable in the future to go to higher temperatures (800 °C), for processes such as Hydrogen production or in order to increase the efficiency of electricity production. For that temperature range, R&D would be needed.

Table 4.1 - Main parameters of the Energy Amplifier

Gross Thermal Power/unit	1500	MW
Primary Electric Power	625	MW
Type of plant	Pool	
Coolant	Molten Lead	
Sub-criticality factor k, (nominal)	0.98	
Doppler Reactivity Coefficient, ($\Delta k/\Delta T$)	-1.37×10^{-5}	
Void coefficient (coolant) $\Delta k/(\Delta\rho/\rho)$	+ 0.010	
Nominal energetic Gain	120	
Accelerator re-circulated Power	30	MW
Fraction Electric Power recirculated in Accel.	0.0465	
Control Bars	none	
Scram systems(3)	CB_4 rods	
Seismic Platform	yes	
Main Vessel		
Gross height	30	m
Diameter	6 m	m
Material	HT-9	
Walls thickness	70	mm
Weight (excluding cover plug)	2000	ton
Double Liner	yes	
Proton Beam and Spallation Target		
Accelerator type	Cyclotron	
Number of beams	1	
Accelerator overall efficiency[33]	43%	
Kinetic energy	1.0	GeV
Nominal current	12.5	mA
Nominal beam Power	12.5	MW
Maximum current	20	mA
Spallation Target material	Molten Lead	
Beam radius at spallation target	7.5	cm
Beam window	Tungsten, 3.0 (1.5)	mm
Max. power density in window	113	W/cm^2
Max. Temp. increase in window	137	°C
Window expected lifetime	≥ 1	year
Fuel Core		

[33]Beam power/Mains Load

Initial fuel mixture	ThO_2 +0.1$^{233}UO_2$			
Initial fuel mass	28.41			ton
Cladding material	low act. HT-9			
Specific power	52.8			W/g
Power density	523.			W/cm^3
Average Fuel Temperature	908			°C
Maximum Clad Temperature	707			°C
Dwelling time (eq. @ full power)	5.0			years
Average Burn-up	100.0			GW d/t
Breeder Core				
Initial fuel mixture	ThO_2			
Initial fuel mass	5.6			ton
Cladding material	low act. HT-9			
U^{233} stockpile at discharge	242.7			kg
Power density at end cycle	3.0			W/g
Primary cooling system				
Approximate weight of the coolant	10,000			ton
Pumping method	Nat. Convection			
Height convection column	25			m
Convection generated primary pressure	0.637			bar
Heat exchangers	4 × 375			MW
Decay heat removal	RVACS			
Inlet temperature, Core	400			°C
Outlet temperature, Core	600			°C
Coolant Flow in Core	53.6			ton/s
Coolant speed in Core, average	1.5			m/s
Decay Heat Passive Cooling (RVACS)				
Riser channel gap width		18		cm
Downcomer channel gap width		57		cm
Trigger Temperature	500	600	700	°C
EA Coolant max Temperature rise	110	83.5	64.5	°C
Time to max.Temperature rise	17.5	11.2	9.5	hours
Outlet air Temperature (@ max. temp.)	273	302	334.3	°C
Outlet air Speed (@ max. temp.)	13.4	14.2	15.2	m/s
Air flow Rate (@ max. temp.)	52.8	56.1	60	m^3/s
Extracted Heat (@ max. temp.)	8.57	9.65	10.84	MW

Table 4.2 - Main Properties of Molten Sodium and Lead.

	Sodium	**Lead**	
Melting Temperature	98	328	^oC
Boiling Temperature	880	1743	^oC
Values at 600 ^oC			
Vapour pressure	24.13	5×10^{-4}	Torr
Density	0.81	10.33	gr/cm^3
Heat capacity (by mass)	1.30	0.15	$J/gr\ ^oC$
Heat capacity (by volume)	1.053	1.5495	$J/cm^3\ ^oC$
Volumic dilatation coeff. ($\times 10^4$)	3.1938	1.3935	$^oC^{-1}$
Therm. conductivity	62.24	16.45	$W/m\ ^oC$
Heat transfer coeff ($\times 10^4$)	3.6	2.3	$W/m^2\ ^oC$
Dynamic viscosity ($\times 10^{-3}$)	0.206	1.55	$N\ s/m^2$
Surface tension ($\times 10^{-3}$)	146	431	N/m
Electric conductivity (e.m. pumps)		9.4×10^{-7}	Ω m

Table 4.3 - Main parameters of the final Beam Transport to the Vessel

Beam pipe material	HT9	
Beam pipe shape	cylindrical	
Beam pipe length	~ 30	m
Beam pipe external diameter	20	cm
Beam pipe thickness	3	mm
Window material	Tungsten	
Window shape	hemispherical	
Window external diameter	20	cm
Window thickness (edge, centre)	3.0, 1.5	mm
Beam radius at spallation target	7.5	cm
Values for 1 GeV, 10 mA beam		
Lead coolant nominal speed	5.0	m/s
Heat deposition in the lead	6.97	MW
Max. Temperature increase of Lead	107	˚C
Heat deposition in the window	95	kW
Max. Temperature increase of window	137	˚C
Max. power density in window	113	W/cm^2
Max. thermal window stress[34] (britt, duct)	48.2, 82.2	MPa

Table 4.4 - Main design parameters of the Fuel-Breeder Assemblies

[34]Tensile strength of Tungsten at 550 ˚C: 380 MPa

Pins	FFTF	EFR	Monjou	F-EA	
Outer diameter	5.84	8.2; 11.5[37]	6.5	8.2	mm
Cladding thickness	0.38	0.52; 0.6[37]	0.47	0.35	mm
Wrapper wire thickness	1.42	1.75	1.75		mm
Cladding material	HT-9	many	SUS316	HT-9	
Active length	91 (+?)	100 (+24)	93 (+65)	150	cm
Void length (total)	162	120		180	cm
Void outer diameter	5.84	8.2	6.5	5.0	mm
Void Cladding thickness	0.38	0.52	0.47	0.35	mm
Max. clad Temperature	700		675	692	°C
Average Power/met. fuel	100		121	60	W/g
Max. Radiation Damage		≈ 120	≈ 100	≈ 34	dpa/y

Sub-Assemblies	FFTF	EFR	Monjou	F-EA		
Configuration	Hexag.	Hexag.	Hexag.	Hexag. (IC)[35]	Hexag. (OC)[36]	
No hexagonal rounds	8	10		10	11	
No of pins	217	331,169[37]		331	397	
Total length	4.7	4.8		5.3		m
Flat to Flat	120	188		234		mm
Pitch between pins	7.26	9.95	8.25	12.43	11.38	mm
No units-fuel(IC+OC)	192	387		120		
No units-breeder		78		42		

[35]Inner Core
[36]Outer Core and Breeder
[37]The two values correspond to the fuel and breeder respectively.

Table 4.5 - Typical neutron capture inventory of a EA.

Zone-Wise			Fraction
Core			0.8879
Blanket			0.0456
Plenum			0.0277
Diffuser			0.0309
Beam Tube + Window			0.0005
Main Vessel			0.0073
Leakage			0.0012

Material-Wise			Fraction
Fuel (Th + U)			0.8493
Breeder (Th)			0.0427
Lead of which	percentage	Abs. Fraction	
Diffuser	(48.75 %)	0.0305175	
Plenum	(12.11 %)	0.00758086	
Core	(37.13 %)	0.02324338	
Blanket	(2.01 %)	0.00125826	
Lead Total			0.0626
Structures of which	percentage	Abs. Fraction	
Cladding	(83.28 %)	0.03780912	
Window	(1.03 %)	0.00046762	
Main Vessel	(15.69 %)	0.00712326	
Structures Total			0.0454
Leakage			0.0012

Figure Captions.

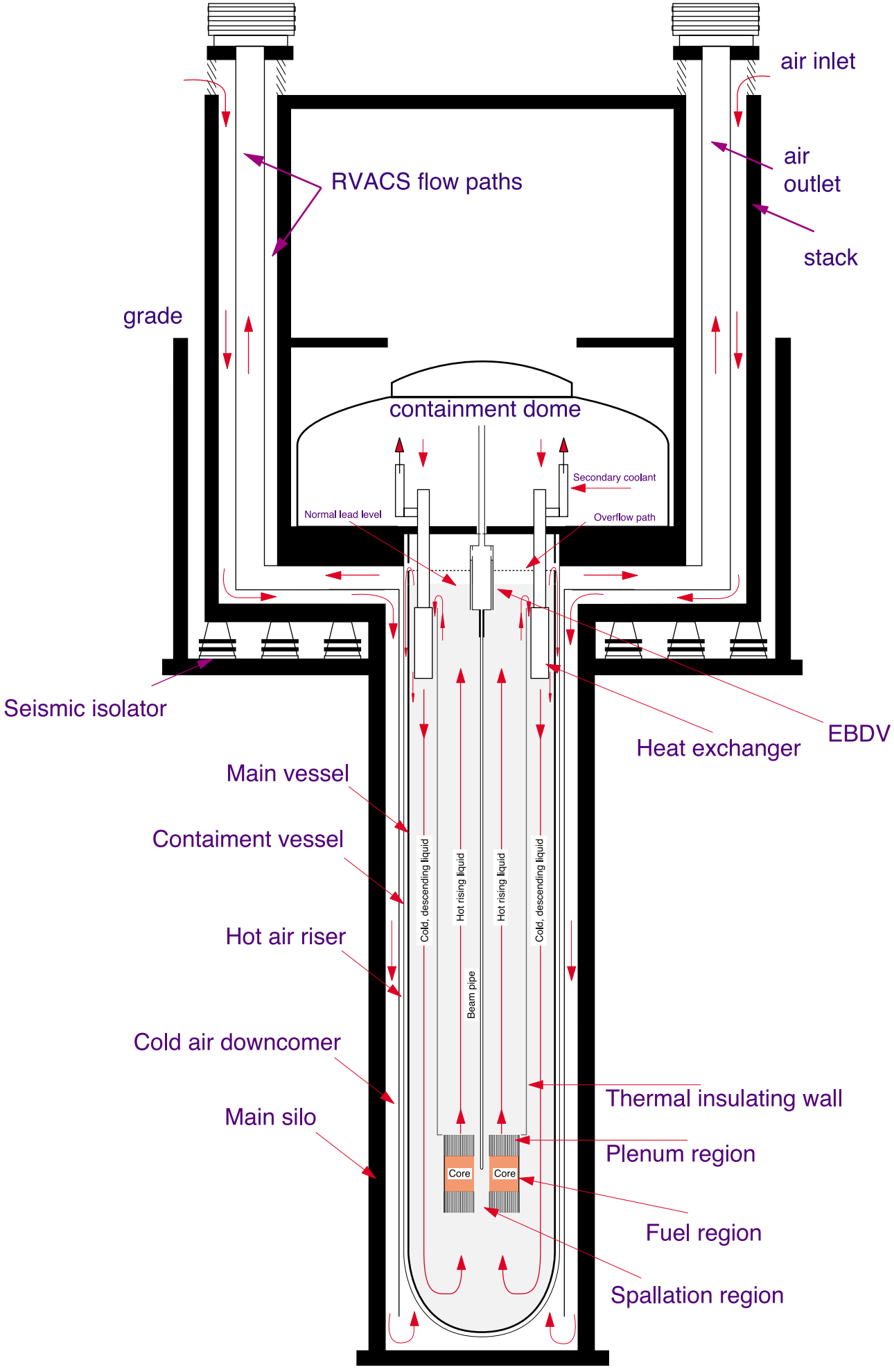
air inlet
air outlet
stack
RVACS flow paths
grade
containment dome
Secondary coolant
Normal lead level
Overflow path
Seismic isolator
EBDV
Heat exchanger
Main vessel
Containment vessel
Hot air riser
Cold air downcomer
Main silo
Cold, descending liquid
Hot rising liquid
Hot rising liquid
Cold, descending liquid
Beam pipe
Core
Core
Thermal insulating wall
Plenum region
Fuel region
Spallation region

Figure 4.1a

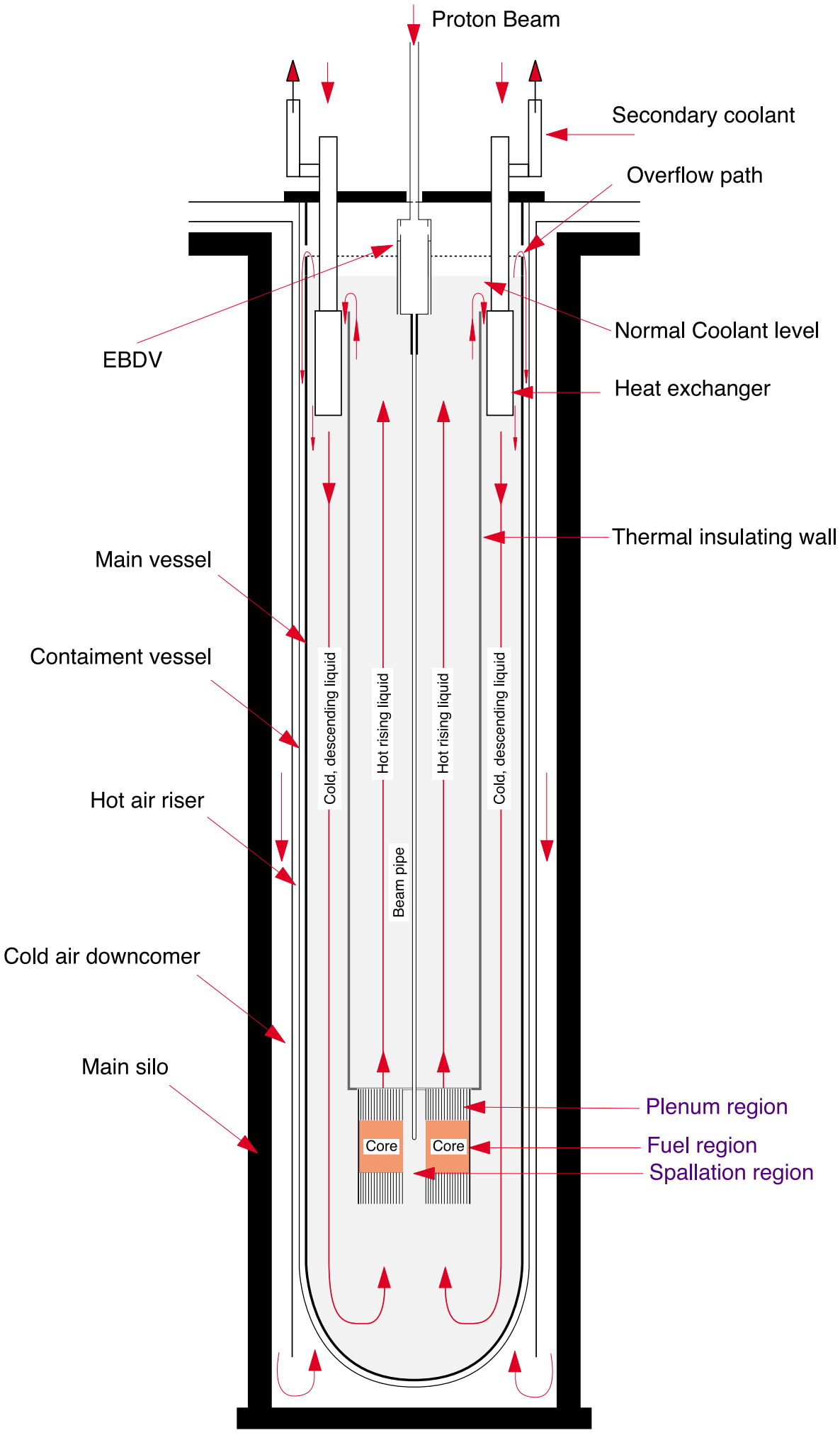
Proton Beam
Secondary coolant
Overflow path
EBDV
Normal Coolant level
Heat exchanger
Thermal insulating wall
Main vessel
Containment vessel
Hot air riser
Cold air downcomer
Main silo
Cold, descending liquid
Hot rising liquid
Hot rising liquid
Cold, descending liquid
Beam pipe
Core
Core
Plenum region
Fuel region
Spallation region

Figure 4.1b

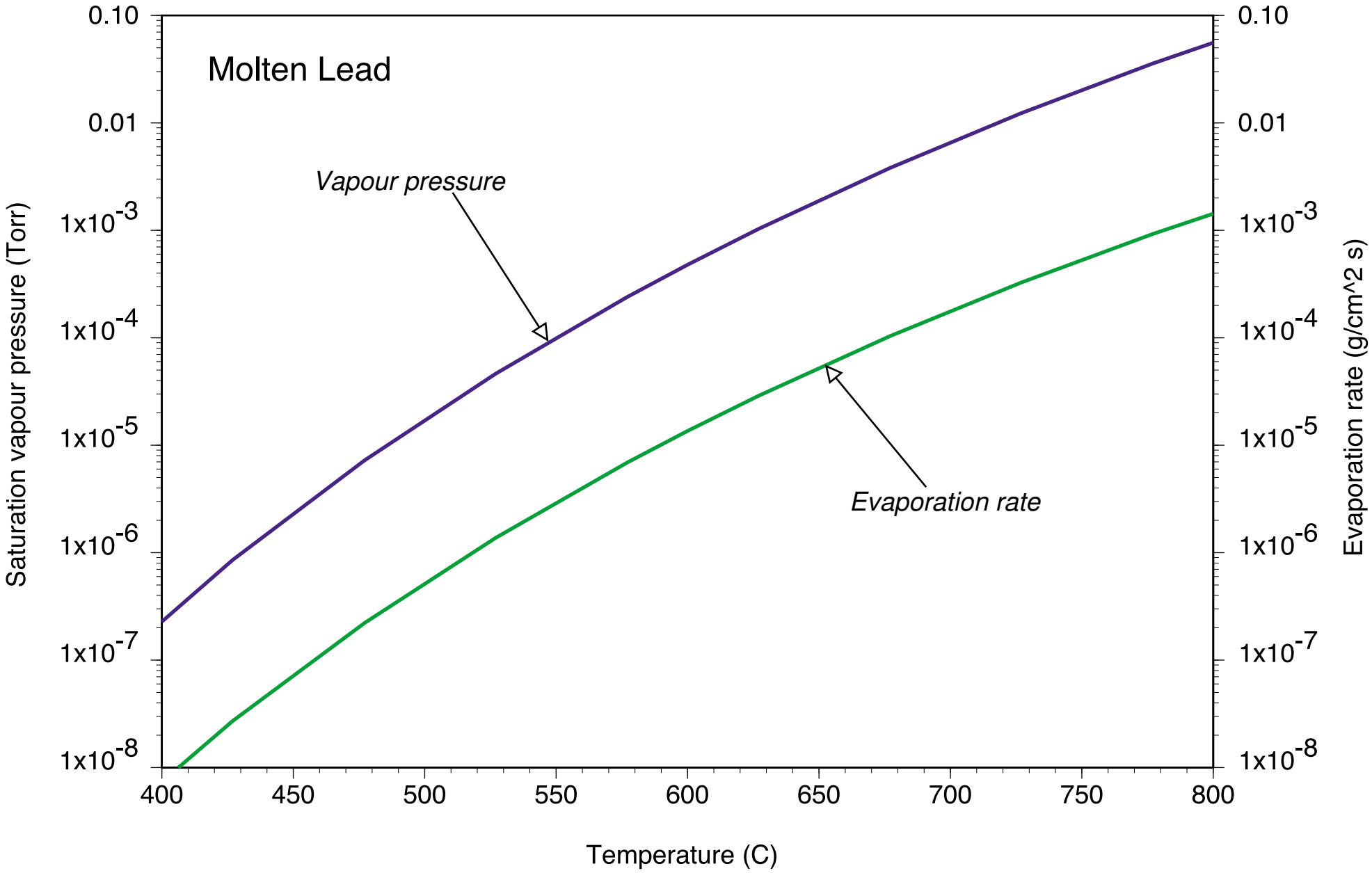
Molten Lead
Vapour pressure
Evaporation rate
Saturation vapour pressure (Torr)
Evaporation rate (g/cm^2 s)
Temperature (C)
0.10
0.01
1x10-3
1x10-4
1x10-5
1x10-6
1x10-7
1x10-8
400
450
500
550
600
650
700
750
800

Figure 4.2

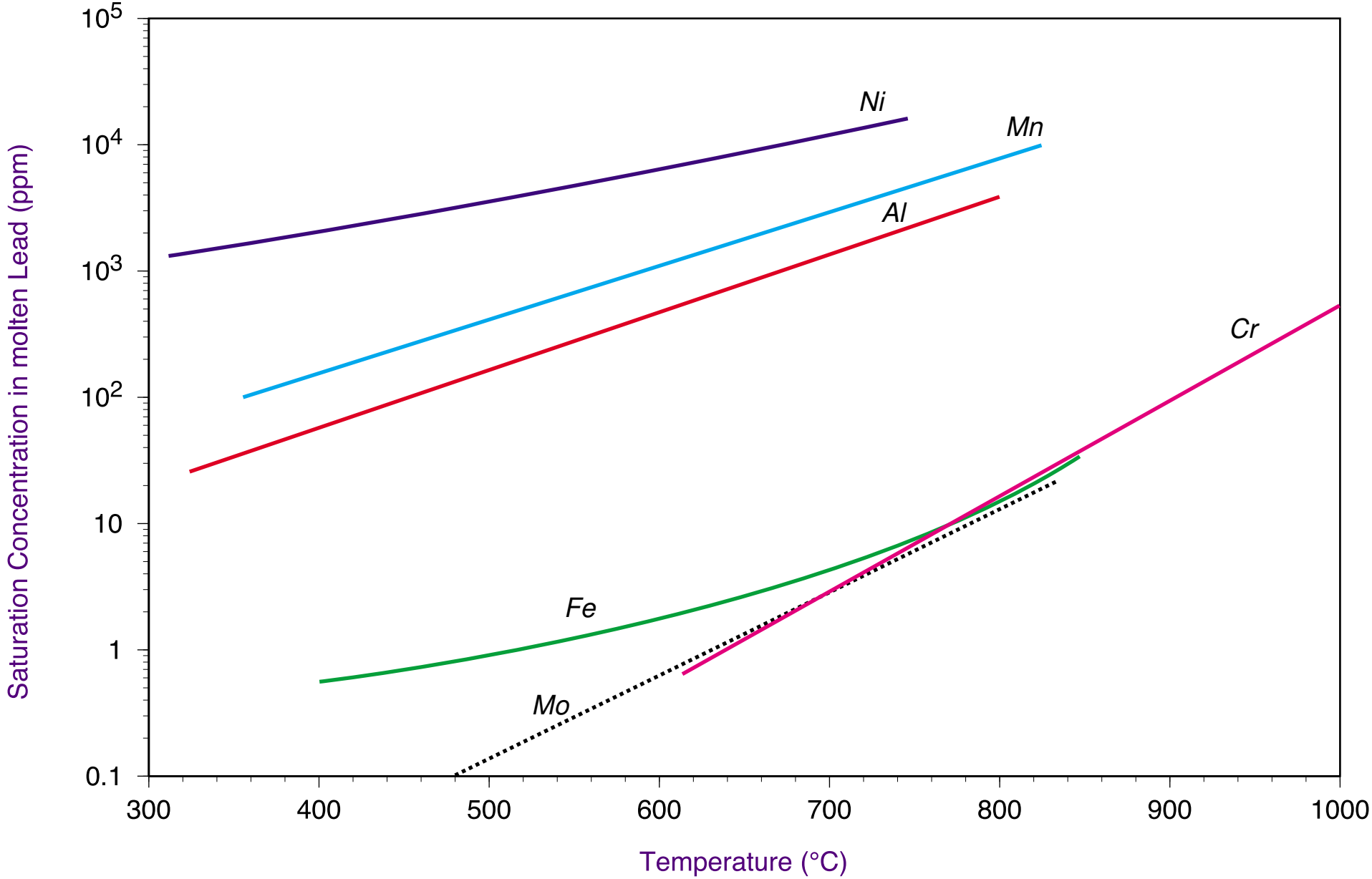
Saturation Concentration in molten Lead (ppm)
10^5
10^4
10^3
10^2
10
1
0.1
300
400
500
600
700
800
900
1000
Temperature (°C)
Ni
Mn
Al
Cr
Fe
Mo

Figure 4.3

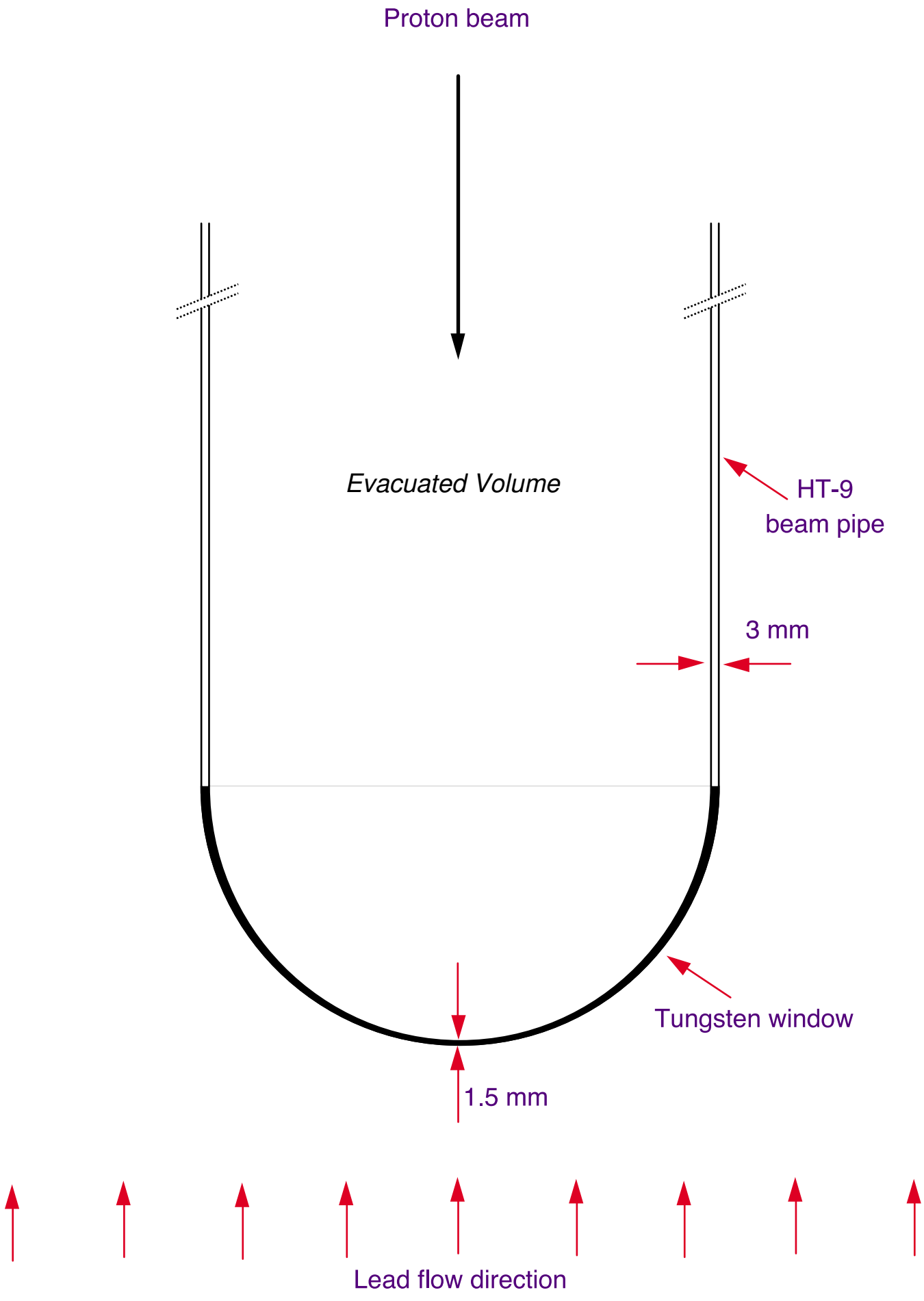
Proton beam
Evacuated Volume
HT-9
beam pipe
3 mm
Tungsten window
1.5 mm
Lead flow direction

Figure 4.4

Map of the energy deposit of a 1 GeV proton into the FEA target

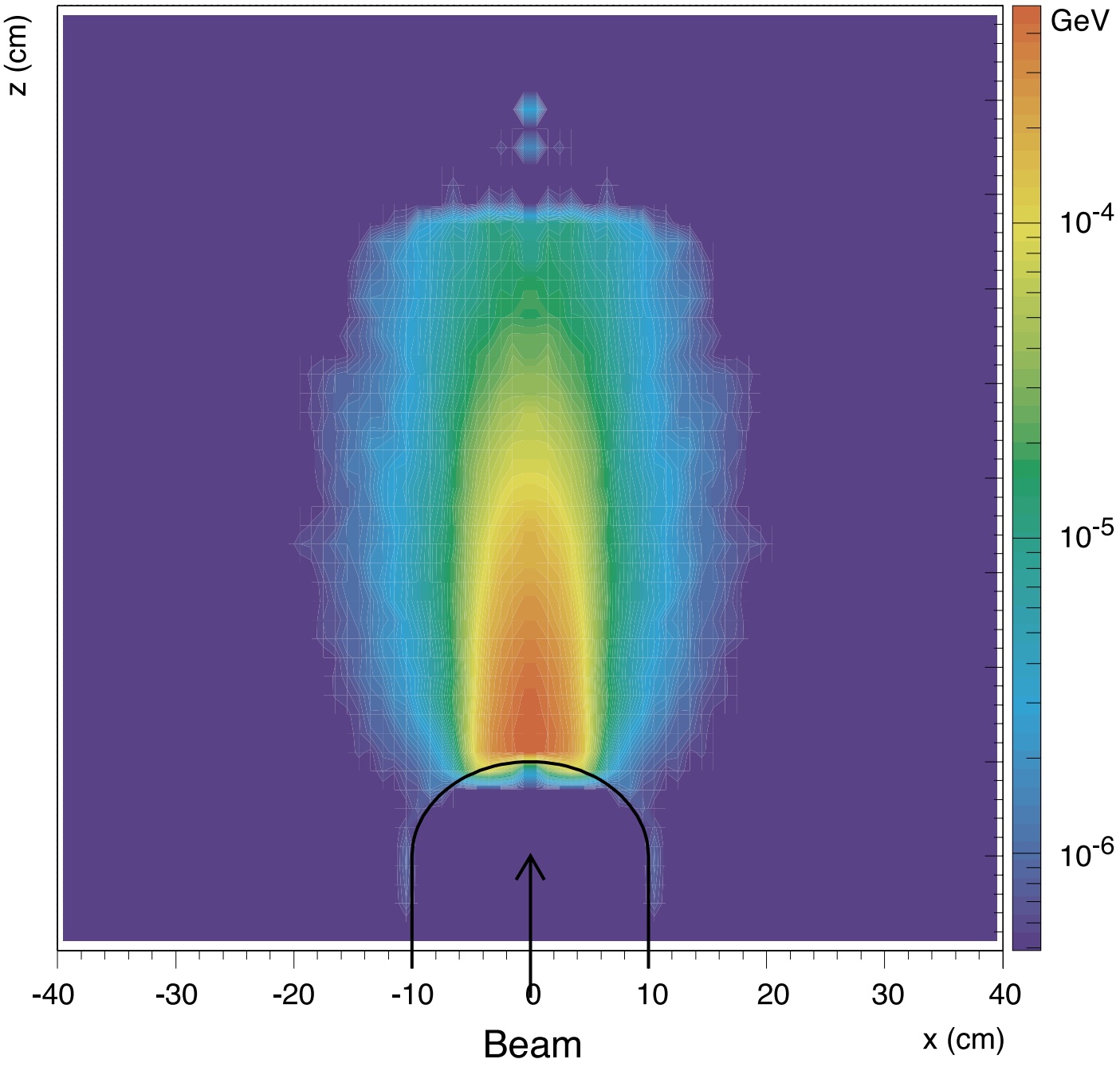

Figure 4.5

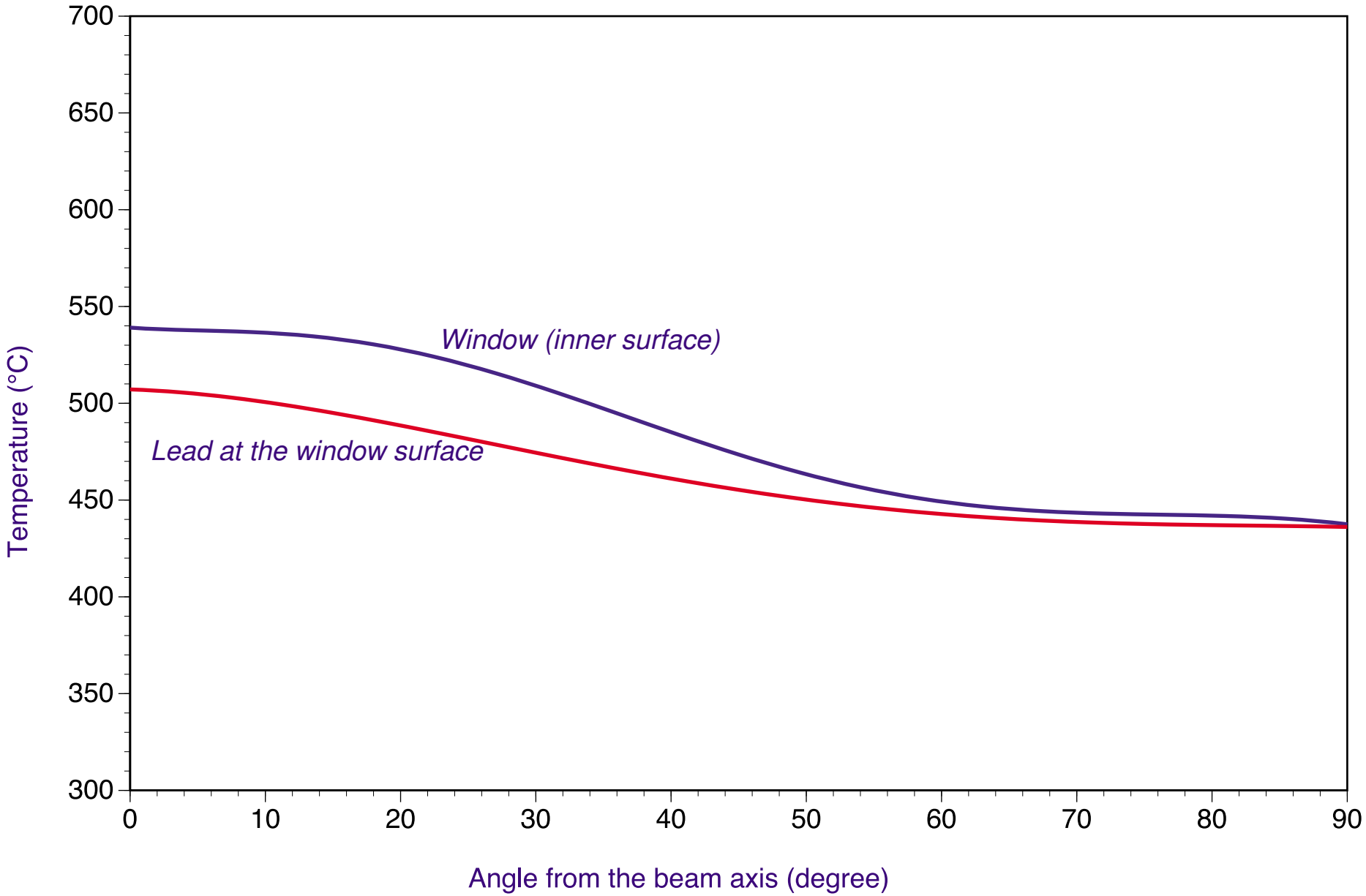
700
650
600
550
500
450
400
350
300
Temperature (°C)
Window (inner surface)
Lead at the window surface
0
10
20
30
40
50
60
70
80
90
Angle from the beam axis (degree)

Figure 4.6

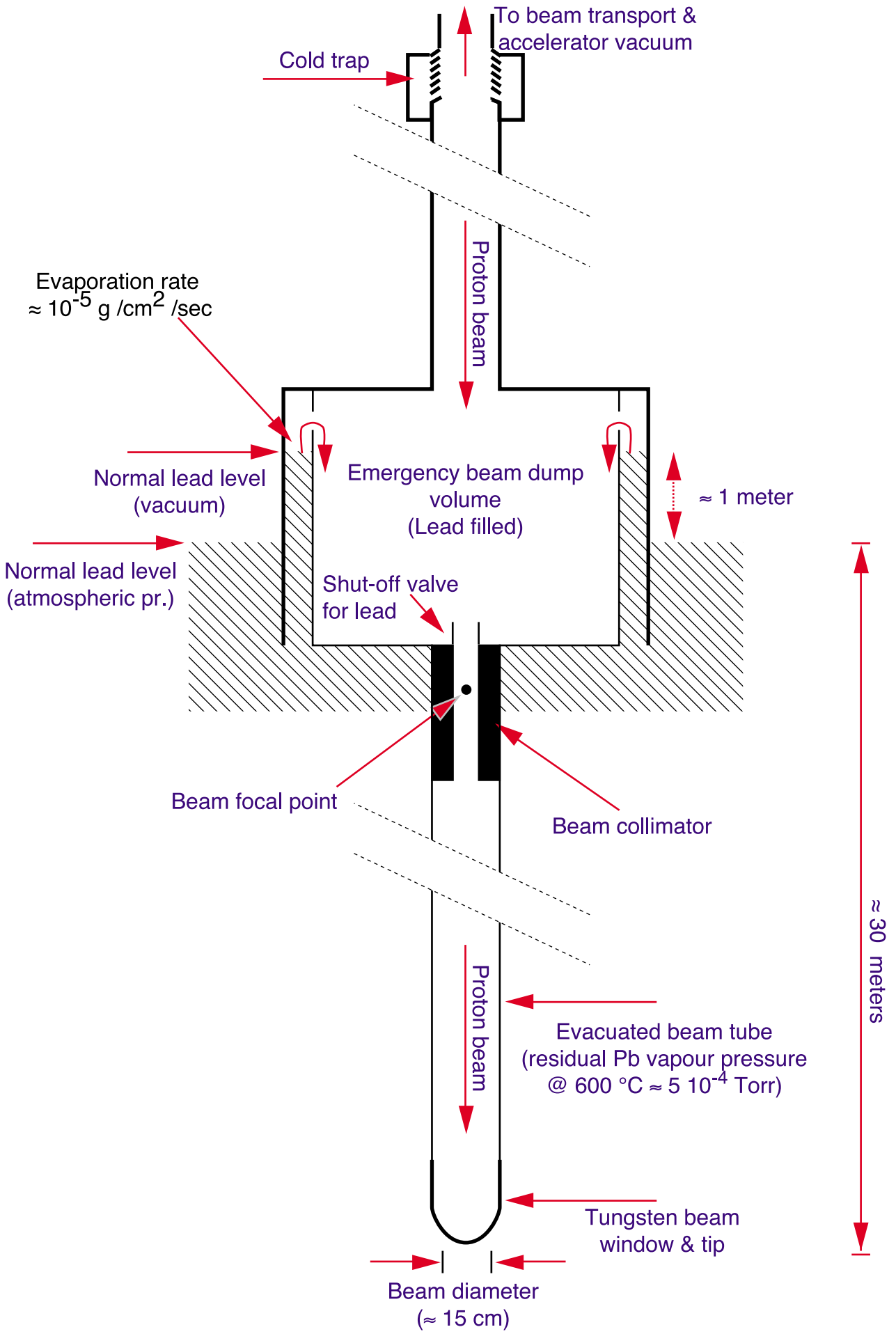
To beam transport &
accelerator vacuum
Cold trap
Proton beam
Evaporation rate
≈ 10-5 g /cm2 /sec
Normal lead level
(vacuum)
Emergency beam dump
volume
(Lead filled)
≈ 1 meter
Normal lead level
(atmospheric pr.)
Shut-off valve
for lead
Beam focal point
Beam collimator
≈ 30 meters
Proton beam
Evacuated beam tube
(residual Pb vapour pressure
@ 600 °C ≈ 5 10-4 Torr)
Tungsten beam
window & tip
Beam diameter
(≈ 15 cm)

Figure 4.7

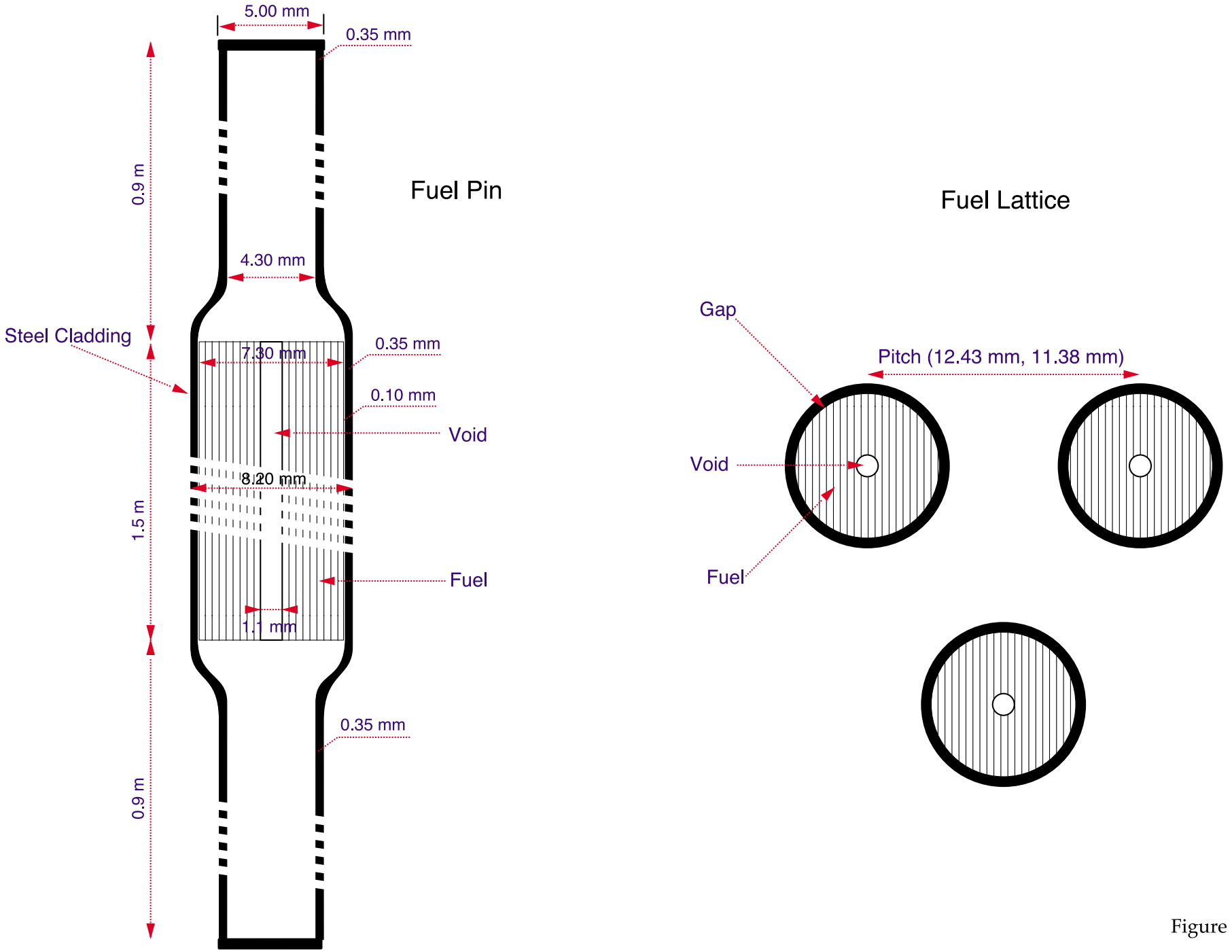
Fuel Pin
5.00 mm
0.35 mm
0.9 m
4.30 mm
Steel Cladding
7.30 mm
0.35 mm
0.10 mm
Void
8.20 mm
1.5 m
Fuel
1.1 mm
0.35 mm
0.9 m
Fuel Lattice
Gap
Pitch (12.43 mm, 11.38 mm)
Void
Fuel

Figure 4.8

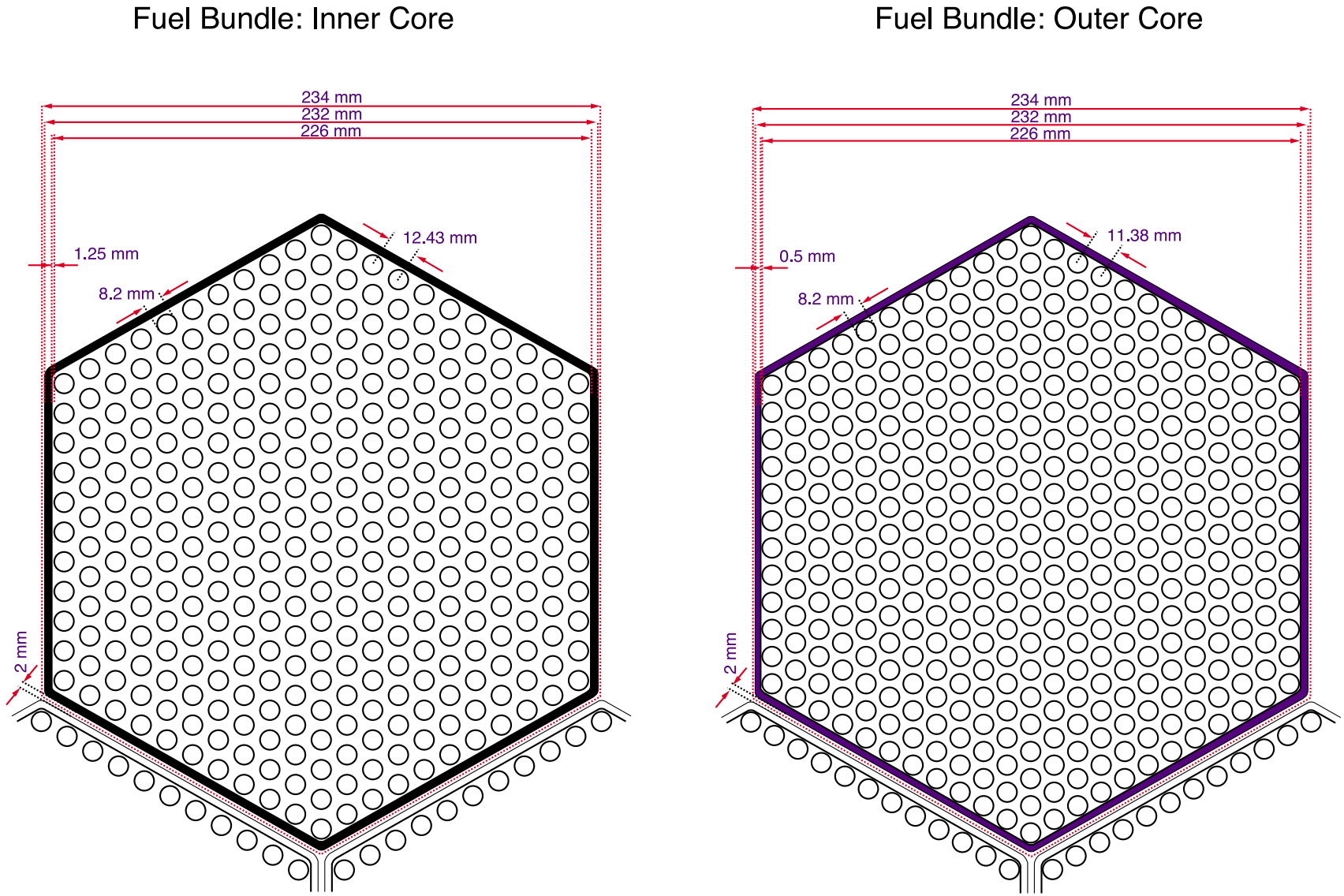
Fuel Bundle: Inner Core
234 mm
232 mm
226 mm
12.43 mm
1.25 mm
8.2 mm
2 mm
Fuel Bundle: Outer Core
234 mm
232 mm
226 mm
11.38 mm
0.5 mm
8.2 mm
2 mm

Figure 4.9

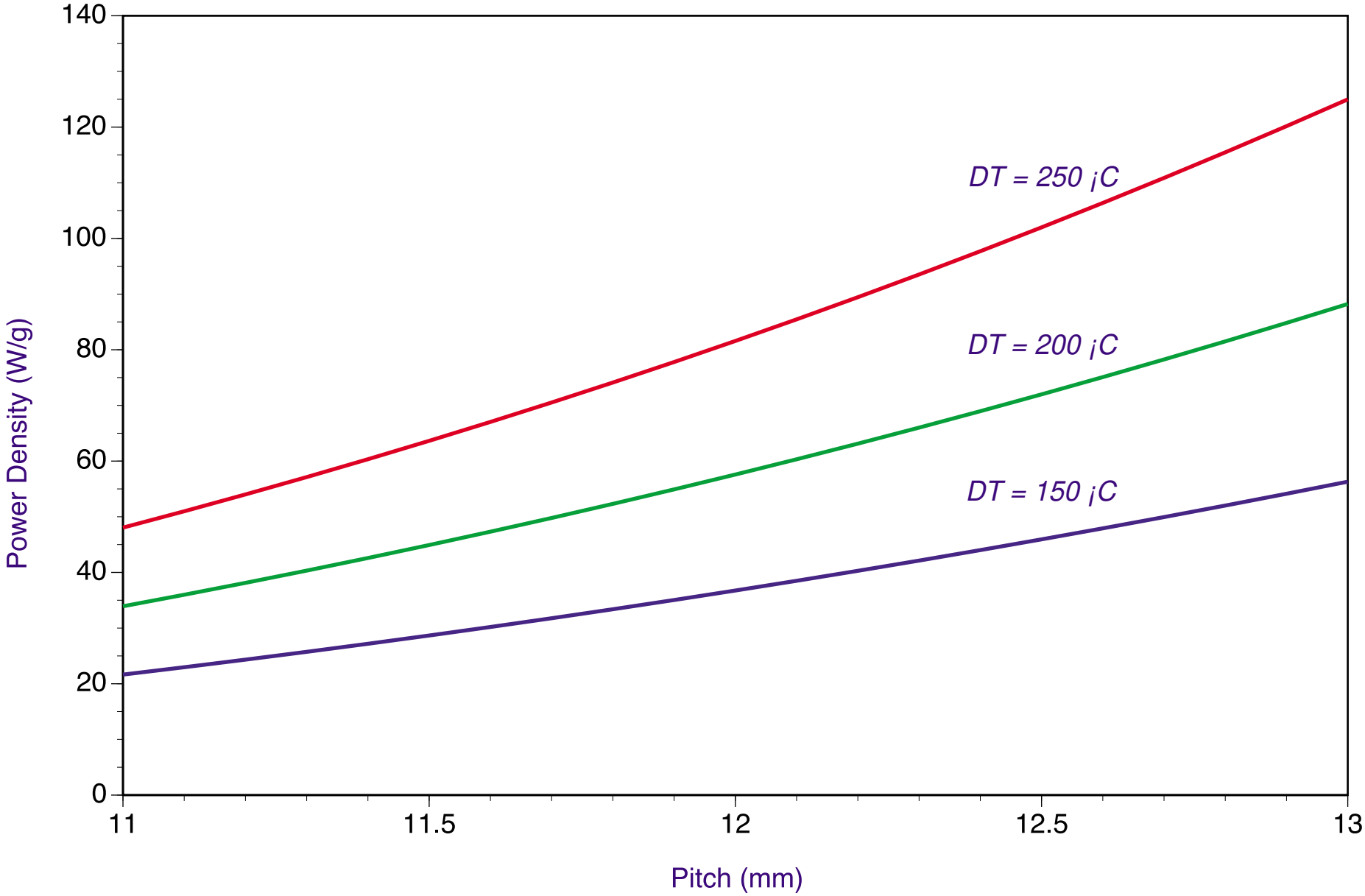
140
120
100
80
60
40
20
0
Power Density (W/g)
DT = 250 ¡C
DT = 200 ¡C
DT = 150 ¡C
11
11.5
12
12.5
13
Pitch (mm)

Figure 4.10a

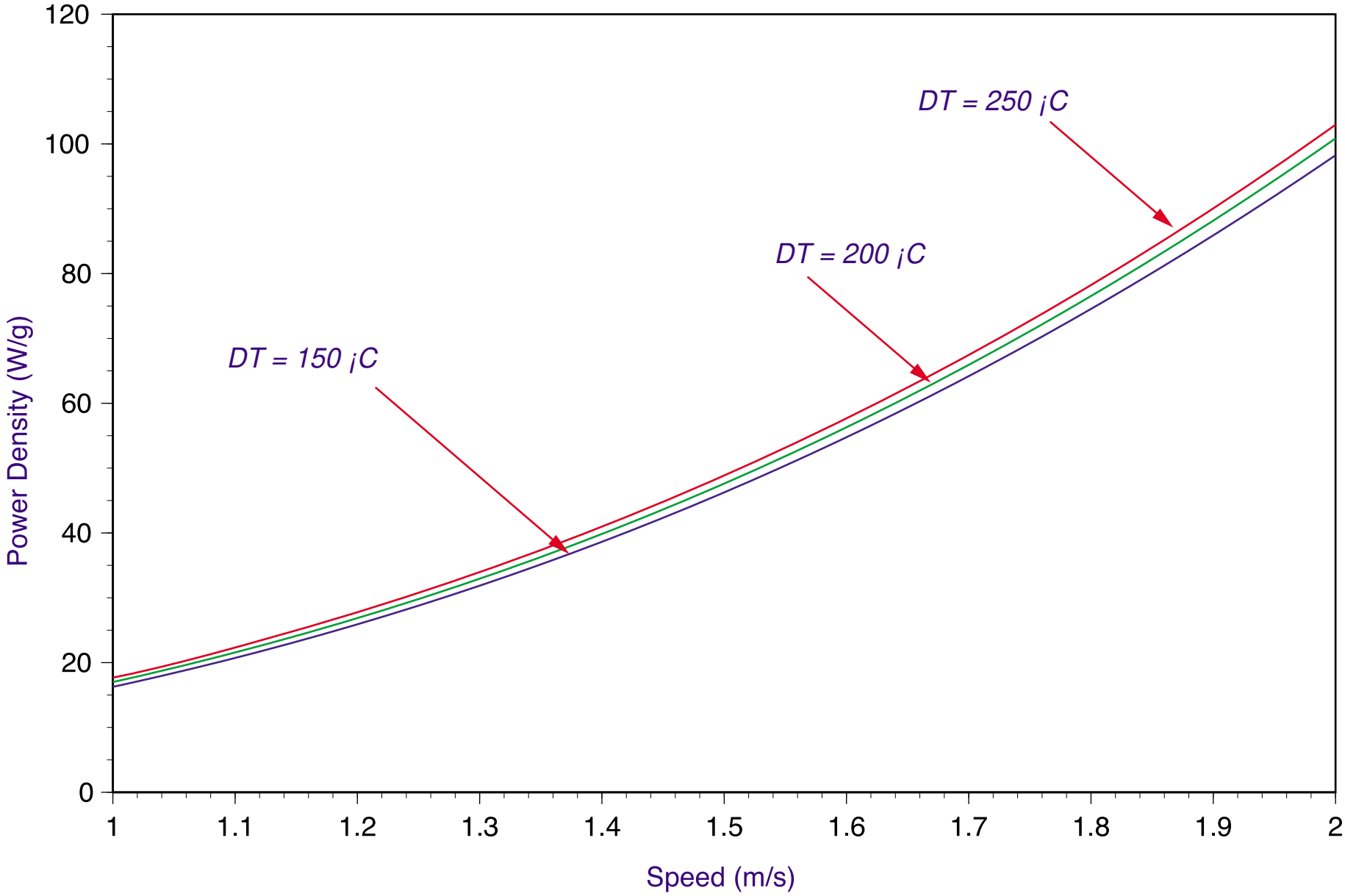
120
100
80
60
40
20
0
Power Density (W/g)
DT = 250 ¡C
DT = 200 ¡C
DT = 150 ¡C
1
1.1
1.2
1.3
1.4
1.5
1.6
1.7
1.8
1.9
2
Speed (m/s)

Figure 4.10b

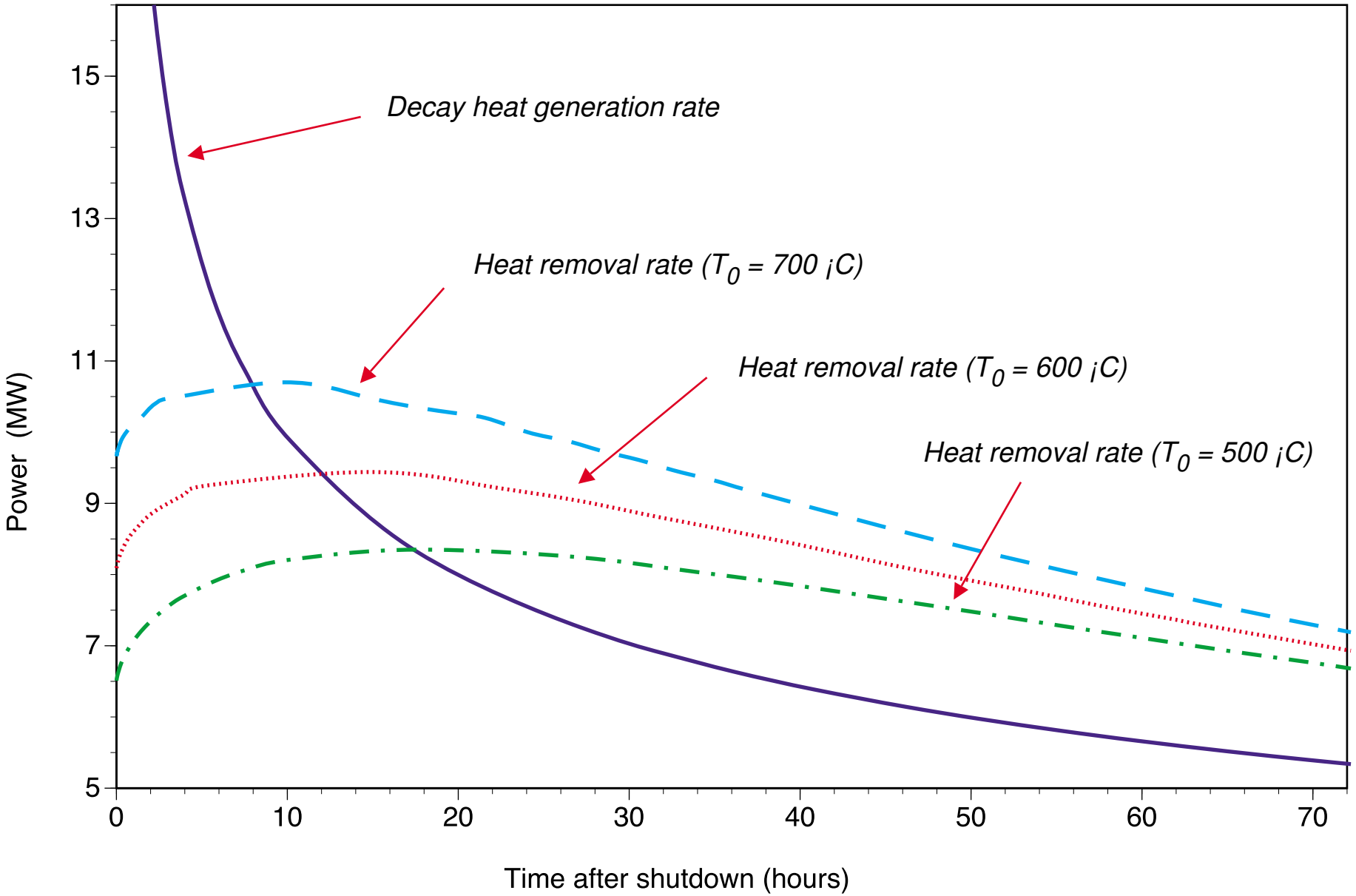
Decay heat generation rate
Heat removal rate (T_0 = 700 ¡C)
Heat removal rate (T_0 = 600 ¡C)
Heat removal rate (T_0 = 500 ¡C)
Power (MW)
15
13
11
9
7
5
0
10
20
30
40
50
60
70
Time after shutdown (hours)

Figure 4.11

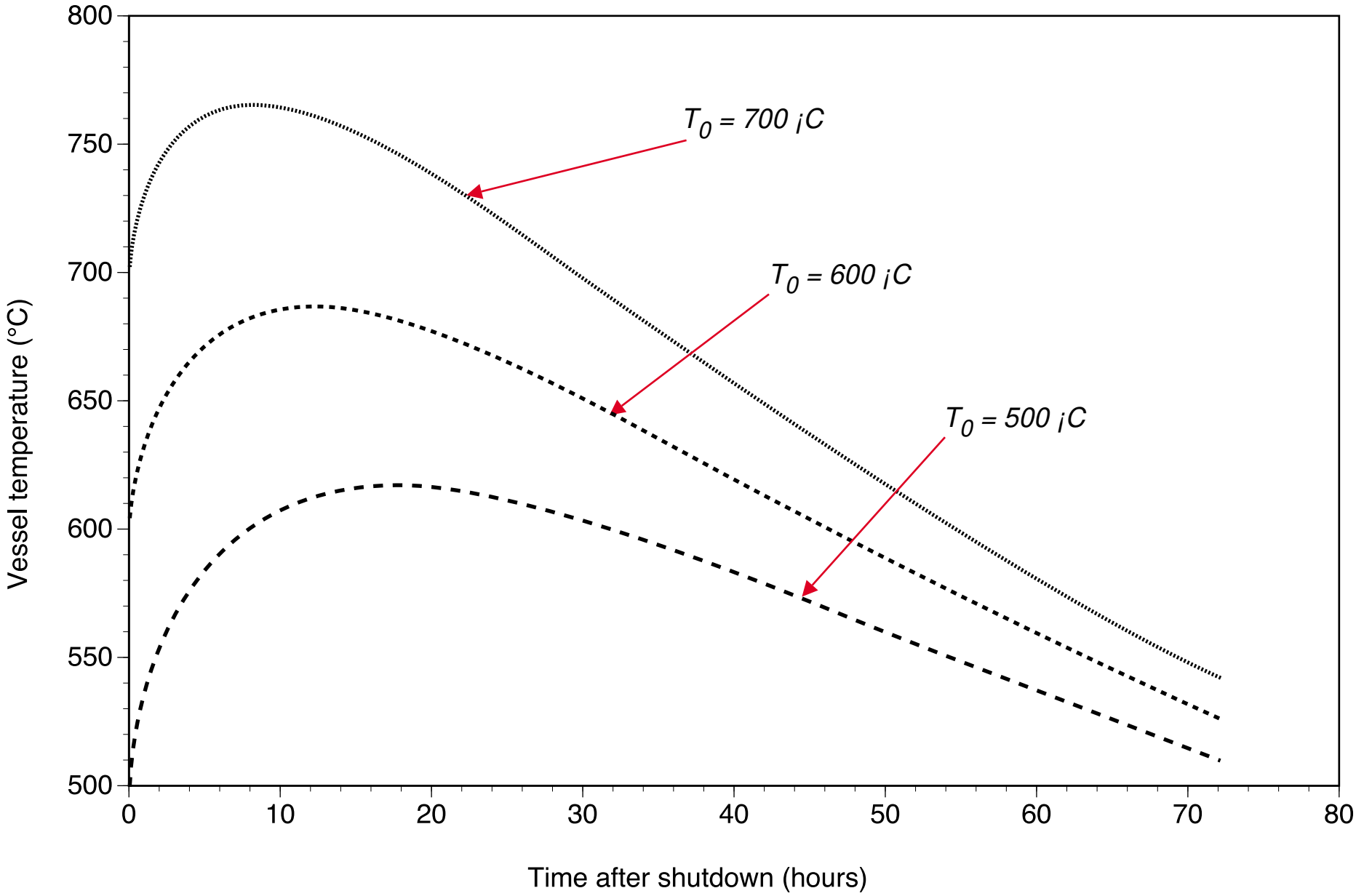
800
750
700
650
600
550
500
Vessel temperature (°C)
0
10
20
30
40
50
60
70
80
Time after shutdown (hours)
T_0 = 700 ¡C
T_0 = 600 ¡C
T_0 = 500 ¡C

Figure 4.12

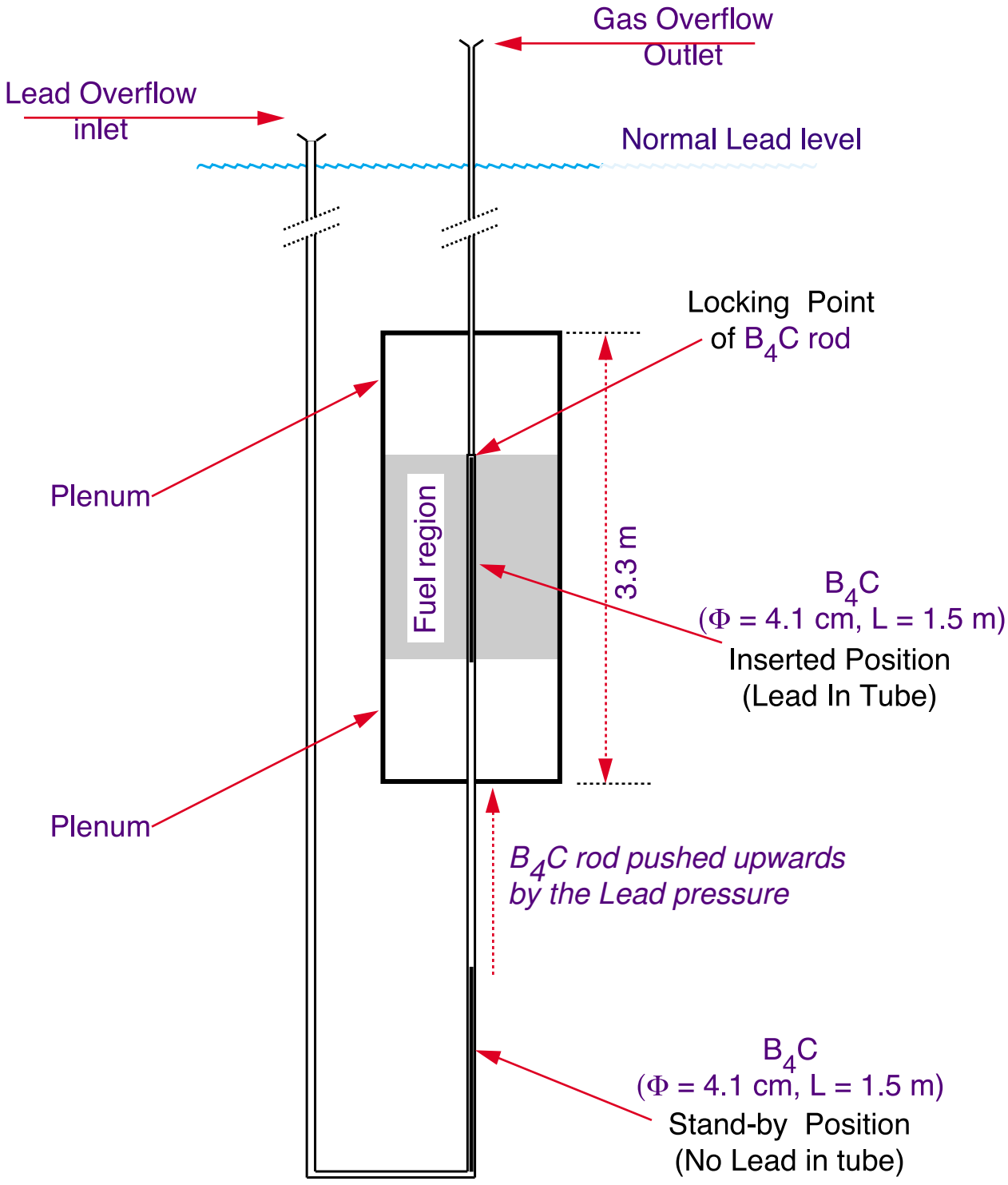
Gas Overflow
Outlet
Lead Overflow
inlet
Normal Lead level
Locking Point
of B_4C rod
Plenum
Fuel region
3.3 m
B_4C
(Φ = 4.1 cm, L = 1.5 m)
Inserted Position
(Lead In Tube)
Plenum
B_4C rod pushed upwards
by the Lead pressure
B_4C
(Φ = 4.1 cm, L = 1.5 m)
Stand-by Position
(No Lead in tube)

Figure 4.13

5. — Computer simulated operation.

5.1 - Simulation methods. Many classic programmes [34] exist which can calculate the neutronic behaviour of a sub-critical system. However such programmes have major limitations, namely (i) they operate on a given concentration of isotopes, while in our Amplifier the concentration of elements varies dynamically during burn-up or (ii) they are based on multi-group calculation methods and therefore take only approximately into account the narrow resonances in the Lead Moderator and in the Fuel. Finally the proton initiated cascade involves many reactions (spallation etc.) which have important effects on the composition of materials, especially at discharge. Therefore, appropriate Montecarlo methods have been developed in which the full evolution with time of the Amplifier is simulated.

The high energy cascade has been simulated with the help of the programme FLUKA [50] which is known to give a very realistic representation of the many processes in the energy interval of interest. The spallation neutron yield predicted by FLUKA has been compared with experimental data collected at CERN, where a proton beam of different kinetic energies in the interval of interest has been made to interact with Lead targets of different dimensions [3]. The neutron flux emitted has been measured after thermalization in water. The results show an excellent agreement between the experimental results and the predictions of FLUKA [62]. The agreement is typically better than a few percent.

The FLUKA cascade development is, however, still insufficiently accurate to emulate the complex neutronic behaviour below a few MeV. A second programme has been written, based on the ENDF-6 cross sections [30], which follows with Montecarlo technique the fate of neutrons in the Amplifier and the corresponding evolution of the local composition of the fuel elements. The volume of the Amplifier is segmented in a large number of separate regions with independently evolving concentrations and an accurate model of the geometry has been used. The validity of our calculations has been cross-verified with more classic programmes [34]. However all programmes rely on the same cross section data.

While the basic Nuclear Data used in the calculations on the $^{238}U/^{239}Pu$ cycle have been repeatedly checked and improved over the years, some uncertainties have persisted on the cross section data required to predict the Thorium based cycle. Fortunately a rather precise integral experiment has been carried out in the PSI zero-

power reactor facility, PROTEUS [63]. These results indicate that the breeding characteristics of heterogeneous ^{232}Th-containing fast reactor cores are predictable to an accuracy comparable to that of ^{238}U-containing systems. Measured and calculated spectra appear in general agreement with calculations based on cross section data [30]. We believe that the underlying physics information is sufficiently well known and verified to predict the behaviour of the EA.

Neutrons spend a considerable fraction of their life span in molten Lead. Lead cross sections have been well measured, but very little experience exists to date on the behaviour of neutrons in a Lead Moderator/Reflector. An experiment in which a spallation neutron source is imbedded in a large Lead block is in progress at CERN in order to compare predictions and experimental data [6].

The Montecarlo simulation starts with a proton beam of specified geometry and a given initial composition of elements in the Amplifier. The geometry of the EA is realistically represented. Various geometrical components are segmented in smaller units that we denominate as "pixels", in order to be able to record the differences in composition as a function of the location during burn-up. In the case of mixing liquids, like for instance the molten Lead, a common concentration table is used. The continuous proton beam is replaced with a limited number of protons which enter the EA at a specified event rate $f_p = 1/t_p$. The fate of these protons is initially determined by FLUKA in a phase in which a number of spallation neutrons are generated. These neutrons are subsequently followed inside the EA to their final destiny by our dedicated programme. Each particle is given a "weight" w in order to scale up the event rate to the number of protons actually introduced by the Accelerator, namely $w = i\ t_p/e$, where obviously i is the proton current and e its elementary charge. Wherever available, a set of 35 possible reaction channels [30], which include inelastic processes like n-n', n-2n, n-p, n-α and so on, are used to construct the development of the cascade. Secondary neutrons produced by these reactions become the source of additional cascades.

As a consequence of the cascade produced by each proton, the chemical composition of the target pixels is significantly affected. We therefore change the composition of each relevant pixel according to the nature of the interaction, replacing the initial nucleus with the fragments of the reaction and, in the case of fission, with the appropriate fission fragments, but with a weight w, namely as if all the protons over the time t_p had produced the same reaction. Clearly this approximation will vanish over a large number of events. Spallation products generated by FLUKA are also included.

After the full cascade of a given proton has been followed to its finish line and all pixel concentrations have been changed accordingly, concentrations of all pixels are evolved over the time interval t_p with the help of a full Bateman formalism, in preparation for the next proton shot. In particular the complete decay chain for each element is followed up to the stable elements with the corresponding concentrations in the pixels of the relevant new elements, whenever appropriate. The decay schemes for all known elements, including all possible branching ratios is provided by an appropriate database [31].

Typically the programme will operate with some 1200 different nuclear species (mostly fission and spallation fragments) and up to 256 different pixels of a variety of shapes and sizes. The computing speed on an ALPHA computer is of 50 neutron histories/sec. About one week of computer time is needed in order to obtain adequate statistics on a typical burn-up of 100 GW $\times$ day/t, corresponding to about 3 $\times$ 10^6 neutron histories.

The Montecarlo technique and the evolutive nature of the programme permits to introduce quite realistic simulations of the operation of the EA. For instance it is possible to adjust the beam current in order to ensure a specified power output or to simulate power variations and transients. The relevant parameters of the neutronics, (multiplication coefficient, k, neutron spectrum, fission fragment poisoning, fuel/breeder ratio and so on) are in this way accurately followed over a specified burn-up. Periodically, the fuel pin location may be shuffled to improve uniformization of burning. At the end of the calculation, the complete list of elements in the various parts of the Amplifier is provided and used to study reprocessing and refuelling. The refuelling can also be simulated, introducing appropriate changes in the pixel concentrations. The asymptotic concentrations after many refuelling and the overall performance of the device can be realistically simulated. The activation of the various parts of the EA can be accurately studied.

We have verified that the values of the main parameters of a sub-critical device obtained with our programme are in excellent agreement with the results of more classic programmes [34]. In particular the value of the multiplication coefficient k in the two methods typically agree to better than a fraction of a percent.

5.2 - Simulation of the standard operating conditions. We consider first the simulation of an initial load of fuel made of ^{232}Th-oxide with an initial concentration of pure ^{233}U-oxide, chosen to ensure the wanted initial value of the multiplication

coefficient k_0. The initial choice of the multiplication parameter is set high enough in order to make the best possible use of the current of the Accelerator, but low enough as to avoid that the machine in some circumstance may become critical. The main parameters of the EA are the ones listed in Table 4.1. Note that a real life situation may be slightly different since the Uranium fuel bred, for instance starting with spent fuel from a PWR (see paragraph 5.3) or coming from a previous cycle, will contain also some other isotopes, like ^{232}U, ^{234}U, etc. As amply discussed in paragraph 2.8, they are not such as to modify the general features of the results, which become more transparent by our simplifying assumption.

In order to simulate as closely as possible the real operating conditions of the EA, the programme can, during execution, change the current of the accelerator in order to ensure a constant power output. This is done introducing a sort of "software feedback" in which the beam current is adjusted for instance every 100 incident protons in such a way as to maintain constant the output power. The typical computer run covers of the order of some 2000 days of operation or a burn-up in excess of 100 GW $\times$ day/t. The integrated burn-up versus simulated time of operation is shown in Figure 5.1. The proton beam feed-back is the only control mechanism and control rods are absent.

In Figure 5.2a we display the accelerator current chosen by the programme as a function of the burn-up in order to produce a constant power of 1500 MW (Figure 5.2b). The variations of the current reflect the variation of the gain G (Figure 5.3), which in turn is primarily determined by the value of the multiplication coefficient k (Figure 5.4). The other two most relevant quantities are the (atomic) concentration of ^{233}U, normalised to ^{232}Th, averaged over the core (Figure 5.5) and the ^{233}Pa (breeding) concentration, normalised to ^{233}U (Figure 5.6). As is well known, this last concentration is closely proportional to the power density. By inspection of these figures, during burn-up we can distinguish two phases.

A first, relatively short initial phase in which a fraction of the initial ^{233}U is burnt and the breeding process based on the ^{233}Pa is setting on. During this period the multiplication coefficient, and hence the gain, is dropping typically by $\Delta k = -0.01$. This is normally handled by modulating the proton beam current automatically through the feed-back control system. Since the regime value of $k = 0.98$ has been set (see Table 4.1) the initial value of k at the cold initial start-up will be correspondingly higher, namely about $k_0 = 0.99$. In real life and provided such a number would be considered as too high, one can during this initial phase introduce for instance some small amounts of neutron absorbing, "burnable poison" materials which are quickly

transmuted and keep the value of k within the specified range. Alternatively the fuelling can be done in phases, installing inside the core a small fraction of fuel elements only after an initial period (≈ 10 GW $\times$ day/t) with the help of the refuelling machine. Note that storage space is provided inside the vessel for such elements.

This initial phase is followed by a regime phase in which the ^{233}U and the other isotopes tend exponentially to the breeding equilibrium and in which the Fission Fragments (FF) captures[38] grow roughly linearly with burn-up (Figure 5.7) and their effect on k is almost compensated by the increase in concentration of ^{233}U tending to the breeding equilibrium (Figure 2.5). One can adjust such a compensation numerology in such a way as to achieve an almost perfect cancellation over a long burn-up with a remarkably constant value of k and hence of the gain. But towards the end of the chosen burn-up the exponential growth of the ^{233}U concentration flattens out, while the FF growth remains essentially linear, thus causing a drop of the gain and a corresponding increase of the proton beam current required to maintain a constant power output. The maximum available current is set by the parameters of Table 4.1 and hence it determines the ultimate burn-up of the system without refuelling. This effect can be attenuated with more elaborate multiple refuelling schemes. In analogy to standard techniques of PWRs fresh batches of fuel are periodically introduced. Such schemes do not seem necessary in our case, since the single burn-up is long enough to reach the expected limit of the fuel elements due to radiation damage and gas pressure build-up.

The burn-up is not constant over the volume of the Core. Even if periodic, partial refuelling is not necessary, it may seem appropriate to shuffle the fuel elements locations every maybe ≈ 20 GW $\times$ day/t, namely about once a year, in order to uniformise the burn-up of the fuel load. This procedure can be performed without extracting fuel elements from the tank, using the fuel storage facility as a buffer location. If performed fast enough (for instance ≤ 10 days) as not to let a major fraction of the ^{233}Pa decay, it produces negligible effects on *k*. We have simulated this with our programme and found no real benefit for instance in extending the burn-up of the fuel. Consequently at this stage, we have concluded that this represents an additional complication with little or no advantage and we have therefore not applied this procedure to our simulations.

The relative power density distribution over the Core for unit fuel mass is shown in Table 5.1. Its radial (r) dependence is roughly linear, as expected because

[38] Of course only those elements for which cross sections are known are accounted for. We believe that the correction for the other elements is not very large.

of the value of k (see Figure 2.3b). The (z,r)-dependence is easily parametrized using as a universal parameter $\sqrt{r^2 + z^2}$ the distance from the approximate centre of the source ($r = z = 0$). This is why the z-dependence flattens out at larger radii. Likewise the concentration of ^{233}Pa in the various pixels of the core is directly proportional to the power density distribution. We have verified that the power distribution does not change appreciably during burn-up in the specified range, namely ≤ 100 GW × day/t.

Similar distributions can be generated for the Breeder. The concentration of bred ^{233}U rises approximately linearly with time. As already pointed out, such a Breeder is necessary since although the relative concentration of ^{233}U is growing with burn-up, its stockpile is in fact reduced because of the significant fraction of ^{232}Th which is burnt. The stockpiles of ^{233}U are shown in Figure 5.8. The total amount of ^{233}U is at the end of the burn-up slightly larger than at start-up. Note that the full amount of ^{233}Pa during fuel cool down will also transform itself into ^{233}U. Consequently, there is enough fissile material to start a new cycle at a convenient value of k_0.

The concentration of the main Actinides as a function of the burn-up is given in Figure 5.8. They are in good qualitative agreement with the simpler analytical calculations of Section 2.

The simulation programme has been used to explore successive fuel cycles. The simulated procedure is the following. After 100 GW × day/t the fuel is extracted from the Amplifier and chemically reprocessed. Uranium and Thorium isotopes are extracted and after a cool-down period of some 200 days to let primarily the ^{233}Pa decay into ^{233}U, these are used to manufacture new fuel elements, topped up with additional Thorium. Although some 12% of the ^{232}Th has been burnt, the stockpile of ^{233}U in the fuel has only slightly changed. We have reloaded in the EA exactly the initial concentration of ^{233}U. Since the separation is chemical, the new Uranium fuel will be made of several isotopes. The tiny quantities of ^{231}Pa (4.68 kg), of ^{237}Np (400 g) and of Plutonium [^{238}Pu (62 g) and ^{239}Pu (4.6 g)] are separated out and inserted again in the EA for an indefinite period of time until they are essentially incinerated.

The initial multiplication factor k_o of the renewed fuel is extremely close to the initial one and persists to be so over several fuel cycles, in agreement with the analytic description of Section 2.

Finally we have simulated the effects of power variations. As is well known, any major change of power requires that the ^{233}Pa can adjust itself to the new conditions. If the power output is suddenly increased (decreased) the value of k decreases (increases) with the characteristic decay time of the ^{233}Pa (39 days). It has been verified that the magnitude of this effect is in good agreement with the predictions of Section 2.

5.3 - Start-up Fuel cycle with "dirty" Plutonium. There are many ways to initiate the sub-critical operation of an EA. The most naive approach, but most impractical would consist in starting with a pure ThO_2 fuel. This method is most inefficient, since initially the multiplication factor *k* is hopelessly low and the power of the accelerator will be correspondingly huge. Fortunately large amounts of readily fissile material exist in the form of enriched ^{235}U or of "waste" trans-uranic elements from ordinary PWRs and either of them can be used as initial substitute for the ^{233}U.

We propose to use for the first fill a mixture of ThO_2 spiked with about 14% of "dirty Plutonium" from the discharge from a PWR, normally destined to Geologic Storage. Our scheme permits to start-up the EA at the nominal power and gain right from the beginning and smoothly evolve from the initial to the regime conditions essentially in one fuel cycle. At the end of the first cycle, most of the ^{239}Pu is burnt, converted with a high efficiency into ^{233}U. The higher actinides can then either follow their initial destiny of geologic storage, with a significant reduction in toxicity and reduced military proliferation risk or can be continuously incinerated in the successive cycles until they ultimately fission inside the EA.

The simulation programme has been used in order to simulate the burn up of the initial mixture of "dirty" Plutonium and of Thorium. The fuel is — as previously — made of mixed oxides. The concentrations at start-up and at the discharge are given in Table 5.2. Americium and Neptunium can be freely added to the mixture with little effects on the over-all performance. The concentration of Plutonium is chosen such as to produce a reasonable value of initial k_o. During operation, a large amount of breeding interactions occur in ^{232}Th with rapid production of ^{233}U, while the Plutonium isotopes are progressively burnt. We are witnessing a genuine transformation of Plutonium into ^{233}U (Figure 5.9).

The multiplication coefficient *k* (Figure 2.9) and therefore the EA gain is now the resultant of mutual interplay amongst three main processes, namely (1) disappearance of the Plutonium and higher Actinides (2) the formation of ^{233}U and

(3) the emergence of captures due to FFs. It is a fortunate circumstance that these three effects combined produce a value of the multiplication coefficient *k* which is almost constant, in spite of the large changes in concentrations, although not as constant as in the case of an EA operated with Th-U mixture. Note also that the fast drop of *k* during the early life of the cycle, due in the case of the Th-U mixture to the formation of the ^{233}Pa is essentially absent in our case, since the initial operation is dominated by the Plutonium. The variations of k are now sufficiently large to justify some compensatory measure, justified by the exceptional nature of the initial EA fuel generation and start-up. The easiest way is to play with the refuelling machine and introduce the fuel assemblies progressively in the EA.

Because of the "external" contribution of the Plutonium, the burn-up of this fuel load can be extended well beyond the one of the normal cycles and a value in the vicinity of 150 ÷ 200 GW × day/t is appropriate. In order to reach such a long burn-up, it may be necessary to exchange the fuel assemblies during operation, in order to uniformise the radiation damage on the pins. As already mentioned this operation is easily performed in a short time.

5.4 - Neutron Spectra and Estimates of the Radiation Damage. Neutron flux distribution can be easily calculated by the Montecarlo programme by adding the path length inside each "pixel". Its energy dependence is easily obtained by binning the accumulated path length according to energy. The results have been cross checked by a less accurate method in which a standard multi-group (reactor-like) calculation has been performed on the structure. The latter method does not take into complete account the sub-critical nature of the device, like for instance spallation neutrons. Since it is not an evolutionary programme, it does not take into account the variations of the chemical composition during burn-up. As anticipated, the high energy component of the spectrum due to the high energy beam is quickly attenuated by the (n,n') inelastic collisions in Lead (Figure 5.10). By the time the neutrons reach the closest structural element of the Fuel the spectrum has softened to the point of becoming similar to the one of Liquid Metal Fast Reactors[39] (LMFBRs) for which a considerable experience exists already. For instance the flux ≥ 100 keV (≥ 1.0 MeV) is in both cases 55% (10%) of the whole flux. Neutron damage for LMFBRs [64] has been studied in the past theoretically and experimentally, and a large experience up to high fluences has been accumulated. Testing and development of

[39] SuperPhénix (inner core).

materials for such reactors has arrived at fluences well within the range of the present design (see section 4.5).

Neutron irradiation in structural materials is an important design parameter and it determines their rate of replacement. The main physical and mechanical effects of the irradiation of metals are summarised in Table 5.3 [65]. In the case of fast neutrons, for fluences $\int\phi dt \leq 10^{22}$ cm^{-2} changes are usually undetectable. Structural modifications start to appear at larger fluences, eventually approaching saturation for very large irradiation. Effects on metals are relevant to our case and they are generally smaller at higher temperatures since recovery (annealing) of the Frenkel defects produced by irradiation is facilitated. After irradiation one generally observes an increase of the yield strength and, to a smaller extent, of the ultimate tensile strength. Hence, irradiation results in a decrease in ductility and an increase in the temperature characterising the transition from ductile to brittle fracture (NDT). This is an important effect in nuclear power systems.

There are several mechanisms by which irradiation may cause modifications besides direct heating. We shall mention two of them, namely creation of defects in the lattice and gas production. Particles of significant energy traversing the material collide both with electrons and nuclei, which in turn recoil inside the lattice generating lattice defects. The magnitude of the corresponding effects on properties such as elasticity, can be described in terms of an empirical parameter, the number of displaced atoms (DPA). Such DPA depends in turn on the total energy spent to cause displacements, E_a, and the (average) energy required to displace an atom from its lattice position, E_d:

$$DPA \propto \frac{E_a}{2E_d} \tag{1}$$

The denominator E_d is a purely empirical but universal parameter of the material and of which a wide range of values are available in the literature [66] [67]. The energy E_a depends on the spectrum and nature of the incident radiation and on the energy partition between electronic excitations and atomic recoils. We have used in our computer simulations the module HEATR of the nuclear data processing code system NJOY [68]. The partition function used was given by Robinson [69] based on the electronic screening theory of Lindhard [70]. HEATR calculates the damage energy production cross section, $\langle \sigma E_a \rangle$ (barn-keV). An estimate of the number of displacements per second in the metal is given by:

$$S\left[\frac{dpa}{s}\right] = \frac{\langle \sigma E_a \rangle}{\frac{2E_d}{\eta}} \phi \cdot 10^{-21} \tag{2}$$

where $\eta \approx 0.8$ is the collision efficiency factor and ϕ the particle flux (cm^{-2}s^{-1}).

Helium, hydrogen and other light gases are produced in structural materials by nuclear reactions process with α, p, T and so on in the final state. In the case of fast neutrons (n,α) and (n,p) reactions have significant cross sections. In conditions of large fluence, these locally generated gases may be in sufficient amount as to have a pronounced effect on the mechanical and dimensional properties of components, like for instance:

- The radiation induced swelling due to vacancy agglomeration (voids), in which the internally produced gas acts as a nucleating agent for voids, promoting their growth and stabilising them once they are formed.
- The high temperature embrittlement due to inert gas bubbles.
- The low temperature embrittlement due to defect clusters-vacancy or interstitial clusters.
- The "in-pile-creep" producing dimensional changes like swelling.

Swelling and "in-pile-creep" may cause some dimensional changes of the core components which may even affect the dynamics of the energy amplification.

We consider next in more detail the radiation damage in two main structural components namely (1) the beam window and (2) structure and cladding of the Fuel Core. Note that molten Lead is not a "structural material" and it is continuously recirculated from a very large mass. Paradoxically, radiation damage in the highest flux by the highest energy particles can be neglected, evidently with the exception of the beam window! Molten Lead acts as a "filter", moderating the most radiation damaging components of the spallation spectrum.

The rate of radiation damage in the beam window is comparable to the one in high-yield spallation sources under design and construction (see for instance SINQ [71]). The most severe effect is produced by the incoming proton beam. Effects due to the secondary neutrons produced by the cascade are small in comparison with the high energy charged particles. According to Eq. (2), the damage rate is given by:

$$S\left[\frac{dpa}{s}\right] = 3.18\times10^{-6}\,\frac{\langle\sigma E_a\rangle}{\frac{E_d}{\eta}D^2}\,I(mA)$$

where D is the beam diameter. Production yields of He and H can be obtained from cross sections and incident flux (current density):

$$P\left[\frac{appm}{s}\right] = 7.95\times10^{-3}\,\frac{\sigma}{D^2}\,I(mA)$$

Parameters for a proton energy of 800 MeV and several relevant materials are given in Table 5.4. Since cross sections change only very slowly with energy, these values are applicable to a wide interval of proton energies and in particular to our design.

The relevant parameters after 7000 hours at the nominal (see section 4.4) peak current density of 113 μA/cm^2 are about 200 dpa, 13150 He (appm), and 116,350 H (appm). With these numbers, because of embrittlement and swelling, in order to guarantee safety, the window should be replaced after about one year [53]. The periodic replacement of the proton window can be easily accomplished as a routine maintenance task.

It is however evident that some experimental work is required in order to ensure safe conditions of operation of this relatively new component which is the beam window. In particular we remark that the peak beam current density is inversely proportional to the square of the beam diameter. If required by these additional investigations, the beam size could be enlarged without major consequences in the rest of the system.

The irradiation effects on the Fuel Core region have been already mentioned. They must not limit the maximum burn-up due to FFs poisoning which has been set to be of the order of 100 GW × day/t. This corresponds to an integrated neutron fluence through the cladding of $\int \phi dt = 3.3 \times 10^{23}$ n/cm^2, averaged over the core. The most exposed pins will accumulate about twice such a fluence. Two structural components deserve consideration namely (1) the Fuel itself, a mixture of ceramic oxides and (2) the steel cladding of the fuel pins and other structural materials holding the pins together.

If Thorium is mixed with Uranium using Thorium-Uranium oxides, the irradiation experience available for these components indicates a small incidence on fuel swelling. However, more data needs to be collected to attain a high degree of confidence for long-term performance [53].

It is expected that our cladding material will experience conditions similar to those of an LMFBR at 600 ÷ 700 °C and neutron fluences above 0.1 MeV of about 10^{23} cm^{-2}. As already mentioned we must consider four major effects: (1) radiation hardening, (2) irradiation creep, (3) embrittlement and (4) swelling. Different alloys have been proposed and studied as cladding in these neutron environments: (i) stainless steels (304, 316, 321, 347, Incoloy 800); (ii) Nickel based alloys (Inconel 600, Inconel X750, Hastelloy X, Inconel 718, Inconel 625). Type 316 is the reference material for many LMFBR in-core cladding and structural applications.

In the design of the EA there are the added requirements of corrosion in molten Lead (see paragraph 4.3) and the necessity of keeping the activation stockpile to a minimum at long times. For these reasons we prefer to use instead low-activation

HT-9 steel [72]. Ferritic steels (e.g. HT-9) have demonstrated a high swelling resistance, a good stress-corrosion resistance, and a particularly high temperature strength which could increase significantly the fuel element lifetime. The rates of displacements and gas production in different material zones of interest are given in Table 5.5. Combining these with the data of ref. [72] it is expected a swell fraction of ≈ 1 % and a shift in the temperature characterising the transition from ductile to brittle fracture (DBTT) of about 30 °C at design fluence. Under these conditions, our design lifetime of approximately 5 years corresponds to an acceptable radiation damage level for the fuel cladding.

5.5 - Temperature distributions and coolant Flow. The temperatures reached by the different elements of the core are important parameters related with the safety of the EA. In particular, a safe operation requires the cladding and fuel temperatures to be well below the structural limits of the constituent materials.

The lead temperature distribution along any cooling pin channel can be estimated on the basis of the pin axial power density distribution. The internal temperature of the pin cladding can be calculated adding to the lead temperature the temperature increases from the lead to the outer part of the cladding and from there to the inner part. The fuel temperature is then obtained by adding to the internal cladding temperature the increment inside the fuel.

For the EA the linear power density axial distribution *(q′)* can be expressed as:

$$q'(z) = q'_{max}\left[1 - b(z - z_{mid})^2\right] \qquad (q' \equiv W/m) \qquad (1)$$

where z is the axial coordinate, q'_{max} is the maximum linear power density, reached in the middle of the pin ($z = z'_{mid}$), and b is a parameter given by the power distribution shape. Both q' and b are function of the pin radial position in the core. The temperature distribution of lead can be calculated by using the expression

$$\frac{dT(z)}{dz} = \frac{q'(z)}{f_a v \rho C_p} \qquad (2)$$

where T is the lead temperature and f_a, v, ρ and C_p are the lead flow area, velocity, density and specific heat respectively. In the approximation in which these quantities are kept constant (as an averaged values) the lead axial temperature through the channel distribution is given by

$$T_{Lead}(z) = T_{Lead,in} + \frac{q'_{max}}{f_a v \rho C_p}\left[z - \frac{b}{3}\left(z - z_{mid}\right)^3 - \frac{b}{3}z_{mid}^3\right] \qquad (3)$$

The heat flow between the cladding and the lead surface is described by the Newton law of convection

$$T_{out\,clad}(z) = T_{Lead}(z) + \frac{q''(z)}{h}$$

where q'' is the surface power density distribution and h is the local heat transfer coefficient which can be calculated as a function of the Nusselt number

$$Nu = 4.82 + 0.0185 \times \left(\frac{v \rho C_p d_e}{k_L} \right)^{0.827} \quad ; \quad h = \frac{Nu.k_L}{d_e}$$

d_e is the effective diameter, defined in section 4.7, and k_L is the lead thermal conductivity. By using for the surface power density (q'') the same z behaviour for the linear power density, the temperature increase between the lead and the outer surface of the cladding can be obtained,

$$T_{out\,clad}(z) = T_{Lead,\,in} + \frac{q'_{max}}{fav\rho C_p}\left[z - \frac{b}{3}\left(z - z_{mid}\right)^3 - \frac{b}{3} z_{mid}^3 \right] + \frac{q''_{max}\left[1 - b\left(z - z_{mid}\right)^2\right]}{h} \qquad (4)$$

A similar calculation allows to get the temperature difference between the outer and inner parts of the cladding, which depends on the HT-9 thermal conductivity k_c and the cladding thickness e, according to the following expression

$$T_{inn\,clad}(z) = T_{out\,clad}(z) + \frac{e}{k_c} q''_{max}\left[1 - b\left(z - z_{mid}\right)^2\right]$$

The temperature increase inside the fuel, without considering the axial pin heat transfer, can be written as a function of the radius and the fuel length:

$$T_{inn\,fuel}(r,z) = T_{out\,fuel}(z) + \frac{q'''(z)}{4\bar{k}_{ThO_2}}\left(r_1^2 - r^2\right) \qquad r_2 \le r \le r_1$$

where $q'''(z) = W \rho_{ThO_2}\ \ (W/m^3)$.

$$T_{out\,fuel}(z) = T_{inn\,clad}(z) + \frac{q''_{max}}{\bar{k}_{ThO_2}}\left[1 - b\left(z - z_{mid}\right)^2\right]$$

r being the radial position and r_1, r_2 the fuel pellet radius and the inner void radius respectively. $\bar{k}_{ThO_2}$ is the temperature averaged Thorium oxide thermal conductivity.

The calculations were performed with a simulation programme [73]. The results, which are in excellent agreement with the full thermal-hydraulic code COBRA [55], give a maximum cladding and fuel temperature of 707 °C and 2250 °C, well below 1470 °C and 3220 °C, which are the HT-9 and ThO_2 melting temperatures respectively.

As described in section 4.7 the EA cooling is achieved by convective pumping. The pressure difference generated in the lead loop is sufficient to extract the heat from the core. For a fixed ΔT in the core, a variable pitch value is used in order to adjust the coolant speed through the core to the pin power density. In practice, however, the pitch value is quantified and there is a residual radial dependence of ΔT. This effect is particularly important if the breeder is to be included in the same coolant loop and if its pitch value is not drastically different from that of the fuel, since its power density is very low. A simple method of cancelling this residual dependence is to decrease the pressure at the entry of the bundles such as to get the same ΔT than for the hottest channel, for which the pressure decrease is set to zero. For the other channels this extra pressure drop increases when the power density decreases. This implies a tuning of the coolant flow rate as a function of the bundle radial position.

The calculations were done by a simulation programme using the expressions already described in section 4.7. The results, pressure drop inserted and lead velocity distribution, are shown in Figures 5.11a and b. Finally, the speed map at the exit of the core has been used as input in a simulation of the coolant flow. As observed in Figure 5.12, the speed gently homogenises along the path through the lead column.

The convection start-up has been simulated using a computational model based on the following expression

$$l_f \rho \frac{\partial v}{\partial t} = \Delta P_{Column} + \Delta P_{Core} - \sum \Delta P_i$$

where l_f, is the fuel length, ΔP_{Column}, ΔP_{Core} are the pressure induced by the lead in the column and in the core and ΔP_i are the pressure terms losses due to friction and changes in flow area, as defined in section 4.7

The lead outlet core temperature T_{out} has been obtained as:

$$T_{out} = T_{in} + \frac{q}{\rho f_a v C_p}$$

where T_{in} is the lead inlet core temperature.

The equation was solved by time steps and for each time ΔP_{Column} and ΔP_{Core} have been estimated by averaging, with the appropriate weights, the temperatures of the lead in the column and in the core with the temperatures of the lead leaving and entering the core respectively. In the model the time of heating the fuel has been neglected and the heat transmission to lead was supposed instantaneous.

The results show that it is possible to reach the operating power conditions in a few minutes without overheating the Lead leaving the core beyond the nominal operating temperatures (Table 5.6). For start-up times below 2 minutes the lead is overheated, for instance by about ≈ 20 °C if the start-up is done in 1 minute or by ≈ 100 °C if it is done in 30 s. Also, after an instantaneous shut down and without considering the residual heating, the inertia of the coolant is such as to maintain the lead speed in ≈ 8% of its steady state value after 5 minutes, and ≈ 3% after 15 minutes.

5.6 - Safety and Control of Fast Transients. The safety of multiplying systems depends to a large extent on fast transients caused by accidental reactivity insertions. To study the power changes in accelerator driven systems a kinetic model dealing with fast transients as a function of reactivity insertion, Doppler feedback and the intensity of an external neutron source, was developed and programmed.

A kinetic model is given by the diffusion equation, in one energy group. This equation relates the change in time of the neutron density with the physical constants of the system, specially the reactivity, and has to consider the prompt and delayed neutron production rates [74]:

$$\frac{\partial N}{\partial t} = \left(\frac{1-\beta}{1-\rho(\$)\beta} - 1 \right) \frac{N}{\Lambda} + \sum_{i=1}^{6} \lambda_i C_i + S(t) \tag{1}$$

$$\frac{\partial C_i}{\partial t} = \frac{\beta_i}{1-\rho(\$)\beta} \frac{N}{\Lambda} - \lambda_i C_i \tag{2}$$

where N is the neutron density, β_i, β are the delayed neutron fraction of the i-th delayed precursor group and the total delayed neutron fraction respectively, λ_i and C_i are the decay constant and the concentration of the i-th delayed precursor group respectively, $\rho(\$)$ is the total reactivity, expressed in dollars, Λ is the averaged prompt-neutron lifetime and $S(t)$ is the external source term.

For a sub-critical device, fed by a spallation neutron source, the source term may be expressed as [75]:

$$S(t) = -\frac{\rho_0 \, n_{sp}}{\Lambda} \tag{3}$$

where $\rho_0 < 0$ is the total reactivity in the steady state and n_{sp} is the number of spallation neutrons density per source proton. At the steady state the external source term is kept constant. Establishing the k_0, effective multiplication factor, at this steady state, the n_{sp} value is expressed as:

$$n_{sp} = \frac{1}{1-\rho_0(\$)\beta} N_0$$

$$S(t) = (1-k_0)\frac{N_0}{\Lambda}$$

Here N_0 is the neutron density at the steady state.

The coupled equations (1) and (2) are solved by a numerical method described later. The general features of the program include time dependence of the total reactivity, prompt neutron generation time and time size step, and a maximum of six delayed neutron precursors groups. In addition, the total stored energy is also calculated by integrating the reactor power from $t = 0$ to the time of interest.

The total reactivity of the sub critical device is then a sum of four terms:

$$\rho(t) = \rho_0 + \rho_{ext}(t) + \rho_{Doppler}(t) + \rho_{Mod.density}(t) \qquad (4)$$

$$\rho_{Doppler} = \frac{\alpha(\$/{}^0C)}{c_p} \times P(t) \times t$$

$$\rho_{Mod.density} = \alpha'(\$/g\,cm^{-3}) \times (Dens.(T_{\mathrm{mod.}}(t)) - Dens_{\mathrm{mod.},0})$$

where $\rho_{ext}(t)$ is the external reactivity inserted, simulating an accident. It is time dependent, usually represented by a linear or quadratic ramp; $\rho_{Doppler}$ is the reactivity decrease due to the fuel temperature increase ($\alpha < 0$) and P(t) is the power density. The reference fuel temperature is the one at the steady state. This effect is very fast, it is therefore the main stability feedback of an external reactivity insertion accident which would rise at high speed. The rapid fuel answer is due to the direct relationship between the power density change with the reactivity increase and the fuel temperature variation; $\rho_{Mod.density}$ is the reactivity decrease ($\alpha' < 0$) due to the moderator density change, which is a moderator temperature function. This negative reactivity evolves at a lower speed because of the thermal inertia of the moderator. Hence, this effect is less important than the one mentioned above.

The last equations, necessary to complete the cycle, are the power density and neutron density relationships, and the temperature changes due to a power density variation. The first one is given as

$$P(t)\ (W/g) = \frac{\varepsilon \Sigma_f N(t) v}{Fuel\,density}$$

where $\varepsilon = 3.044 \cdot 10^{-11}$ *Joule (190 MeV/fission)*, v is the averaged neutron speed. Once the averaged power density at the steady state is known (P_0) and also the neutron density (N_0) is fixed, it is not necessary to calculate the neutron group constants (Σ_f, v)

$$P(t) = P_0 \frac{N(t)}{N_0} \qquad (5)$$

The reactivity reduction by the Doppler coefficient is calculated as a heat generation coefficient [74]. Let ρ_0 represent the initial reactivity increase resulting from a step change. If $\alpha(=-d\rho/dT)$ is the negative of the temperature coefficient of reactivity, i.e., α is a positive quantity, the reactivity resulting from a temperature increase T is given by

$$\rho = \rho_0 - \alpha T$$

Suppose the time scale of the power excursion is such that the heat loss from the system is insignificant. The increase in thermal energy E will then be related to T by

$$E = CT$$

where C is the heat capacity, i.e., mass × specific heat, of the system. Hence,

$$\rho = \rho_0 - \frac{\alpha}{C}E = \rho_0 - \gamma E, \qquad (6)$$

where $\gamma = \alpha/C = -d\rho/dE$ is the negative of the energy coefficient of reactivity. The reactor power P is equal to the time rate of energy change, i.e., dE/dt; it is obtained by differentiating equation (6) with respect to time, so that

$$P = \frac{dE}{dt} = -\frac{1}{\gamma}\frac{d\rho}{dt}.$$

It follows, therefore, that

$$\frac{d\rho}{dt} = -\gamma P. \qquad (7)$$

The coupled equations (1) and (2) were integrated by discrete time steps. It is important to note that the time step has to be of the same order of magnitude as the prompt-neutron average lifetime. Three types of unprotected reactivity accidents have been considered.

- A slow reactivity ramp insertion: the reactivity increases at a rate of *170 $/s* for a period of *15 ms* (this corresponds to a control rod withdrawal speed of *0.55 cm/ms* in the case of a reactor). After this time the reactivity is kept constant.
- A fast reactivity ramp insertion: the reactivity increases at a rate of *250 $/s* for a period of *15 ms* (*0.81 cm/ms*).
- A thermal run-off of the accelerator, due to a variation in the proton beam intensity. The new source term is:

  $$S'(t) = S(t)\frac{I_{new}}{I_0}$$

  where I_0 is the nominal beam intensity and I_{new} is the accidental new proton current, increased by a factor 2.

The analysis of this problem allows a comparison with transient calculations obtained for a critical reactor (Figure 5.13). It gives a first indication of the mitigating effect of using a sub critical accelerator driven system. The parameters used for the

Energy Amplifier transient study, extracted from references [76] [77], are indicated in Table 5.7.

Figures 5.14(a-d) show the power, fuel average temperature and reactivity change in a critical reactor (lead cooled) and in the Fast Energy Amplifier subjected to a slow reactivity insertion. The important reactivity effects all occur within one second.

- The power excursion curve which corresponds to a critical reactor oscillates and has two distinct peaks in a short time interval. Super prompt criticality produces these peaks (Figure 5.14b). The power rises rapidly during the period of super prompt criticality and reaches its peak, *100* times nominal after *7 ms*, at the time when the Doppler effect reduces the reactivity to values below super prompt limit. However, the fuel average temperature continues to rise rapidly during *15 ms* (due to the thermal inertia of the fuel), until the Doppler counter-reactivity has fully established itself. By this time, the average temperature of the fuel has increased by *50 %* ($\overline{T}_{fuel} \approx 1250\ ^0C$), assuming that the heat loss from the fuel is insignificant during the power excursion. The integrated power, after *20 ms*, measured from the start of the ramp is ≈ 0.8 full power seconds.
- In the case of the Fast Energy Amplifier operated at $k = 0.98$, the power increases only by *42 %* after *15 ms* and after *20 ms* the power decreases almost proportionally with the neutron source strength. If on the other hand the neutron source is maintained (the accelerator is not shut-off), the power remains almost constant in this time range. The total energy released during the excursion is much less than for a critical reactor (*0.025* full power seconds after *20 ms*). The average temperature of the fuel rises gradually but at a much lower rate. After *20 ms*, the fuel average temperature has increased by *8%*. Note, that in this case the Doppler reactivity feedback is almost negligible and very much delayed (appears only after *23 ms*). The long time constant of the response implies that the heat loss from the fuel cannot be neglected anymore. In fact, there is sufficient time (of the order of a few seconds, as estimated by the convection studies described in *section 5.5*) for the natural convection mechanism to safely adapt itself to the new operating conditions without occurring any fuel damage.

The next examples illustrated in Figures 5.15(a-d) and 5.16(a-d) deal with a fast reactivity ramp insertion and a thermal run-off of the accelerator, respectively. Compared to the previous case, the power peak values are higher. The power and temperature changes are faster, and so is the response (fuel Doppler reactivity

feedback). The integrated power, i.e. the total energy released during the excursion, is slightly larger.

An interesting result of this analysis is the fact that the Fast Energy Amplifier responds much more benignly to a sudden reactivity insertion than a critical reactor. Indeed, no power excursions leading to high power levels are possible for positive reactivity additions which are of the order of the sub criticality and similarly for a thermal run-off of the accelerator. More importantly, even if the spallation source is still active (the accelerator is not shut-off), the relative slow power changes induced could be passively controlled by means of natural convection alone (massive coolant response) thus avoiding any meltdown of the sub-critical core.

5.7- Compositions at Discharge. The evolution programme computes the full composition of the elements of the EA during operation. The composition at discharge is therefore directly obtained, with the proviso however that the beam is made of discrete pulses separated in time. Appropriate corrections have to be introduced if short-lived components, with lifetime shorter than the proton repetition rate (typically $5\times10^3 \div 3\times10^4$ s) have to be exactly estimated. In the case of the Fuel discharge also an appropriated, averaged mixture of elements substitutes the actual fine structure of the fuel pins and of the lead coolant. Therefore, the discharge composition will include also the small amount of new elements produced in the closely surrounding Lead.

The discharge composition of the Fuel after 110 GW × day/t corresponding to approximately 5 years in the standard operating conditions are listed in Table 5.8. We have listed only those elements which have a 1/e lifetime longer than 10 days and an amount larger then 100 mg. The relative scarcity of trans-uranic elements reflects the conditions of the first Fuel cycle. The evolution of the Actinides with fuel cycle has been amply discussed in section 2.9 to which we refer for further details. The FF mass composition is substantially different from the one of an ordinary PWR for two main reasons, namely (1) the fission yields for ^{233}U and ^{235}U are quite different and (2) incineration of some of the FFs is quite strong for thermal spectrum and it is quite small in our case. We have listed in Table 5.8 the ratio of mass yields for the same thermal energy produced by the EA and a PWR after 33 GW day/t and initial enrichment of the ^{235}U to 3.3%. Some of the elements show a ratio very different from 1.

The activation of the Fuel cladding material (HT-9) leads mainly to about 0.2 kg of ^{54}Mn (1.24 y), 1.72 kg of ^{55}Fe (3.95 y), 0.234 kg of ^{185}W (108.6 d) and 2.52 kg of ^{187}Re (6.30×10^{10}y), the last two elements due to the very small content of just 162.6 kg of W in the steel alloy. Other radioactive elements like ^{60}Co, ^{51}Cr, ^{59}Fe, etc. are present in traces at the level of ≤ 1 g.

The Lead coolant within the core volume accumulates over 5 years of operation about 20.3 kg of rather inoffensive ^{205}Pb (2.2×10^7 y), K-capture at 0.065 MeV, no γ i.e. ν-emission), some 45 g of ^{202}Pb (7.5×10^4 y) and very small traces of ^{194}Hg (751.9 y), ^{204}Tl (5.47 y),^{208}Bi (5.32×10^5y) and ^{210}Po (200 d). The very small amount of ^{194}Hg is in contrast with the much larger production rate of the same isotope in the Spallation target (see next paragraph). Its absence evidences the sharp confinement of the spallation processes in the target region, away from the fuel core. Radioactive isotopes in the coolant are rapidly mixed in the bulk of the coolant, about 10^4 tons, leading to very small relative concentrations[40], in many instances measured in units of parts per billion. The fate of these impurities is to a major extent unpredictable and specific experiments are required.

The discharge from the Breeder has to a major extent the same general features as the one from the Fuel, with the exception of the much smaller number of FFs and the smaller neutron flux.

The Lead coolant surrounding the Core and Breeder volumes, with the exception of the spallation region which will be discussed separately, is relatively unaffected by the neutron flux (paragraph 4.2). Two unstable Lead isotopes are present, the long lived ^{205}Pb with 43.71 kg and the short lived (4.7 h) ^{209}Pb with traces at the level of 1 g. Its modest activation is related to the lower energy and flux in the region immediately surrounding the core. Even smaller is the activation of the containment vessel, dominated by ^{55}Fe (3.95 y) and ^{59}Fe (64.35 d), with 400 g and 1 g respectively.

The Actinide composition is also radically different from the one, for instance, of a PWR and its consequences need some consideration. The main differences are:

(1) the presence of several Protactinium isotopes. At the design power level, the stockpiles of ^{233}Pa is of 53.25 kg in the Core and of 5.60 kg in the Breeder. This relatively short lived element is the source of a substantial amount of decay

[40] 1 kg of dissolved material corresponds to 0.1 ppm in relative mass. Many radioactive impurities which amount typically to ≈ 1 g, once diluted in the bulk of the coolant, represent a concentration of 10^{-10} by weight in the coolant.

heat, 2.99 MW (2.70 MW in the Fuel Core) immediately after shut-off and decaying with the characteristic 1/e time of 38.99 days. Since the ^{233}Pa concentration is proportional to the power produced during steady operation, its decay heat represents a constant fraction of this last quantity, initially 0.2 % of the design power. In view of its relatively long decay constant, the contribution of ^{233}Pa is comparable to the decay heat produced by the FFs and it must be taken into account (Figure 5.17). The breeding transformation is accompanied by intense γ-emission. More specifically we have calculated the time dependence of the γ-spectra produced by Actinides of Table 5.8. In Figure 5.18 we give the time dependence of the γ-activity of the Fuel weighted proportionally to energy over the spectrum, namely the number of 1 MeV equivalent γ's produced per second. As one can see, the dominant contribution comes from ^{233}Pa, at least during the early times. A corresponding cooling time of about one year is strongly recommended, which also insures that the major fraction of ^{233}Pa has decayed into useful ^{233}U. With these provisos, the presence of ^{233}Pa should not introduce additional, specific problems. Other Protactinium Isotopes are some 4.47 kg (including the 0.15 kg in the Breeder) of the long-lived ^{231}Pa (4.74×10^4 y), amply discussed in paragraphs 2.8 ÷ 2.10 and traces (≤ 1 g) of the short-lived ^{232}Pa (1.89 d) and ^{234}Pa (9.69 h). The long-lived isotope ^{231}Pa primarily produced by fast neutrons through the (n,2n) reaction on the main element ^{232}Th followed by β-decay, constitutes a considerable source of radio-toxicity and it must be incinerated, re-injecting it inside the subsequent Fuel Loads, as discussed in paragraph 2.10. Fortunately the cross section for neutron capture, leading to ^{232}U is quite large and equilibrium between production and decay is reached already at the end of the first cycle. This means that a net stockpile of the order of 5 kg of ^{231}Pa will persist during the whole lifetime of the EA plant as balance between production and incineration.

(2)The presence of a specific composition of Uranium isotopes, evolving toward an asymptotic distribution. A relative novelty is the presence of a substantial amount (1.46 kg) of the long lived isotope ^{232}U (99.6 y) produced by fast neutrons and the (n,2n) reaction on the main fissile material ^{233}U. As in the case of ^{231}Pa, the concentration of ^{232}U reaches practically its asymptotic limit already at the end of the first fuel cycle. As already pointed out, the presence of such an isotope, which has a decay chain prolific of high energy γ-rays is a major inconvenience if some of the Uranium fuel were to be diverted to military applications. The γ-ray activity of the Fuel is of primary importance also during reprocessing and new fuel preparation. We show in Figure 5.18 the number of 1 MeV equivalent γ's produced per second by the discharge fuel of an EA and

compared with the one of an ordinary PWR. This last curve has been normalised to the same electric energy produced in the EA. *As one can see, after the cooling down period of about one year needed to transform the ^{233}Pa, the γ-doses of the spent fuel of an EA are not substantially different than the one of an ordinary PWR.*

(3)The isotopic composition of the Uranium is a rapidly decreasing function of the atomic number. There is essentially no ^{238}U produced, since the previous element, ^{237}U is short lived (9.76 d) and it β-decays into ^{237}Np, which is the main gateway to the trans-uranic elements.

(4) A remarkable scarcity of trans-Uranic elements. Concentrations are fuel cycle dependent and values of Table 5.8. refer to the most favourable case of the first fuel cycle. The main production mechanism is neutron capture of the long-lived ^{237}Np producing ^{238}Np, which then quickly (3.06 d) decays into ^{238}Pu (127 y). The family of Plutonium isotopes with $A \geq 239$ becomes accessible by successive neutron captures. Even asymptotically, as shown in detail in paragraph 2.9, concentrations decrease rapidly with growing A, because of the competing fission channel at each step. Asymptotic concentrations are also many orders of magnitude lower than for instance in the case of a Uranium driven Reactor. Seven neutrons are needed for instance to transform ^{232}Th into ^{239}Pu, while a single neutron capture can achieve the same result starting from ^{238}U.

Amongst the unstable elements which require special consideration in the Table 5.8, there is a significant amount (14.5 g) of ^{14}C (8286 y) produced by n-capture reaction on the isotope ^{17}O, present in small amounts (1.84 kg) in the natural Oxygen of the ThO_2 and UO_2 in the Fuel and in the Breeder. The production of this isotope is however of importance since it is one of the main contributors to the radio-toxicity emitted in the environment during reprocessing. It is difficult to separate out such a small amount of Carbon with the methods proposed to reprocess the Fuel (see paragraph 6.2). The relevant neutron capture cross section for the process $^{17}O(n,\alpha)$ (averaged over the Fuel spectrum) has the relatively large value of 23.3 mbarn. An additional source of ^{14}C in the EA, not included in Table 5.8 could be due to the presence of N_2 impurities in the fuel, typically of the order of 10 ppm by weight (0.3 kg). The cross section for the relevant process $^{14}N(n,p)$ is of the order of 2 mbarn and its contribution for the integrated neutron fluence $\int\Phi dt = 3.3 \times 10^{23}$ n/cm^2 is then only 0.198 grams. Note that the total amount of chemical Carbon produced in the Fuel is 0.587 kg, mostly of ^{13}C. It is expected to be almost completely oxidised at the

fuel operating temperatures and therefore be mostly in the form of CO_2 at the time of reprocessing.

5.8 - Spallation Products. The spallation process produces a large amount of fragments. These fragments, which are generated primarily by high energy particles, have been properly taken into account in the FLUKA part of the simulation programme. The mass spectrum of the spallation fragments is strongly energy dependent. At low proton energies (≤ 40 MeV), the mass (A,Z) spectrum is peaked close to the father nucleus. At intermediate energies (≈ 400 MeV) a splitting similar to fission occurs, in which two fragments of roughly similar mass are formed. At very high energies, the spallation spectrum changes again and all (A,Z) are produced in a roughly flat distribution. This complex phenomenology is only approximately represented by FLUKA and the mass yield could be uncertain to up to a factor two.

In order to evidence them the spallation target region, namely the Lead volume to which the core is concentric has been considered as a different material. In our design however the whole coolant is mixed during operation. Hence in reality spallation products will diffuse inside the whole EA volume.

As shown in Figure 5.18, the overall γ-activity of the spallation products is many orders of magnitude smaller than the one of the Fuel. Still it is sizeable and it must be considered carefully. We give in Table 5.9 the list of unstable elements with lifetime larger than 10 days. As already mentioned this corresponds to very small concentrations (1 g = 0.1 ppb) and therefore it is difficult to predict what will be their actual fate without additional experiments.

Qualitatively we can say that several elements will come out in the form of gas or vapours and accumulate in the (inert) gas inside the vessel[41]. This is definitely the case of (1) some Tritium and the noble gases ^{39}Ar (389 y), ^{42}Ar (47.6 y),^{81}Kr (3.3×10^6 y), ^{85}Kr (15.5 y),^{127}Xe (52.6 d), which are produced at the modest total rate of about few g/year, (2) traces (≤ 1 g) of some elements which have a significant vapour tension at the operating temperature of the EA, namely ^{36}Cl (4.3×10^6 y), ^{73}As (116 d), ^{125}Sb(4.0 y), ^{125}I (86 d), ^{134}Cs (2.98 y) and the main elements which are 15.25 g of ^{202}Tl (17.68 d), 386 g of ^{204}Tl (5.5 y), 415.9 g of ^{194}Hg (751.9 y) and 6.2 g of ^{203}Hg (67 d).

---

[41] Note that the quoted values for the masses are the values at discharge after 5 years of continuous operation. If continuously extracted, the total amount of the short-lived elements is correspondingly larger.

Others will remain in solution inside the coolant. There is a large number of elements which will form with Lead inter-metallic compounds. Some elements will combine chemically with Lead (S, Se and Te) and remain dissolved. We note that ^{210}Po (200 d) belongs to the same series but its precise chemistry is unknown. There are several elements which will remain metallic but have a large solubility in Lead and therefore should be retained. Finally some elements have a very high melting point and presumably will also remain trapped inside the coolant.

During operation some of the spallation products may be "incinerated" by the neutron bombardment. The programme records the secondary interactions of all the materials of the spallation target and therefore the effect is taken into account in Table 5.9. The effects of these secondary interactions are negligibly small, since the concentrations are insufficient to produce a sizeable interaction probability.

Table 5.1- Power density distribution, in units of averaged power, over the Core. Data are for an average power density ρ = 52.76 W/g of mixed fuel oxide.

Radial	(Bottom)←		← Segmentation along fuel pins →							→(Top)	Average
↓Segm.↓	1	2	3	4	5	6	7	8	9	10	over pin
Fuel section											
5	1.42	1.74	2.15	2.43	2.62	2.62	2.41	2.10	1.70	1.40	2.06
6	1.28	1.58	1.88	2.18	2.35	2.33	2.14	1.88	1.54	1.24	1.84
7	1.20	1.47	1.77	1.99	2.12	2.11	1.99	1.74	1.45	1.16	1.70
8	1.12	1.36	1.66	1.84	1.97	1.97	1.86	1.63	1.35	1.10	1.59
9	1.05	1.29	1.52	1.71	1.79	1.81	1.70	1.54	1.28	1.02	1.47
10	0.97	1.20	1.45	1.58	1.67	1.69	1.57	1.43	1.18	0.96	1.37
11	0.91	1.12	1.32	1.47	1.53	1.54	1.46	1.30	1.10	0.90	1.27
12	0.82	1.01	1.19	1.33	1.40	1.42	1.32	1.20	1.01	0.82	1.15
13	0.74	0.91	1.07	1.19	1.26	1.25	1.20	1.08	0.91	0.74	1.04
14	0.66	0.82	0.97	1.07	1.11	1.12	1.06	0.95	0.80	0.66	0.92
15	0.60	0.71	0.83	0.92	0.95	0.96	0.92	0.84	0.69	0.58	0.80
16	0.51	0.60	0.70	0.77	0.81	0.80	0.78	0.70	0.59	0.50	0.68
17	0.44	0.49	0.56	0.62	0.65	0.66	0.63	0.57	0.49	0.42	0.55
18	0.38	0.40	0.46	0.50	0.52	0.52	0.51	0.46	0.40	0.37	0.45
Breeder section: Power proportional to burn-up. Values for 100 GW × day/t											
19	0.07	0.07	0.09	0.10	0.11	0.11	0.09	0.09	0.07	0.07	0.09
20	0.07	0.08	0.07	0.08	0.09	0.09	0.09	0.08	0.07	0.07	0.08

Table 5.2 - (Dirty) Plutonium into ^{233}U conversion: stockpiles at start-up and at discharge. The Plutonium isotopic concentrations correspond to the discharge after 33 GW × day/t of a standard PWR with initial ^{235}U enrichment to 3.3%.

Nuclide	Mass at start-up (kg)	Mass at discharge (kg)	Difference(kg)
^{238}Pu	67.98	39.49	-28.49
^{239}Pu	1636.0	323.0	-1313.0
^{240}Pu	671.6	527.0	-144.6
^{241}Pu	314.9	78.3	-236.6
^{242}Pu	109.9	105.4	-4.5
All Plutonium's	2800.38	1073.1	**-1727.19**
^{233}U	0.0	1809	**+1809**

Table 5.3 - General effects of neutron irradiation on metals

Irradiation increases	Irradiation decreases
Length (growth)	Ductility
Volume (swelling)	Stress-rupture strength
Yield strength (usually)	Density
Ultimate tensile strength	Fracture toughness
NDT temperature	Thermal conductivity
Hardness	Yield strength
Creep rate	Corrosion resistance
	Strain hardening rate

Table 5.4 - Parameters relevant to a proton energy of 800 MeV (extracted from reference [71])

Material	(σE_a) [*barn-keV*]	E_d [*eV*]	σ_{He} [*barn*]	σ_H [*barn*]
^{63}Al		40	0.21	0.86
Steel	300	40	0.32	2.52
Cu	330	30	0.40	2.58
Mo	900	58	0.58	4.00
W	1430	65	0.58	5.13

Table 5.5 - Displacements and gas production rates in the Energy Amplifier

Region	Fluence/y	dpa/y	He [appm]/y	H [appm]/y
Inner Core	1.1x 10^{23}	25	2.0	40
Outer Core	6.5x10^{22}	15	1.5	27
Breeder	2.3x10^{22}	3.5	0.2	3
Plenum	2.5x10^{22}	2.5	0.1	1
Main Vessel	9.7x10^{19}	0.001	--	--

Table 5.6 - Simulation of convection start-up and shut-down (hottest fuel channel)

Steady conditions:		
q^{st}		102 W/g
T_{in}^{st}		400°C
T_{out}^{st}		649 °C
v^{st}		2.02 m/s
Start-up[42]: *Power Density, quadratic for* $(0 < t < at_1^*)$, *exponential for* $at_1 < t < t_1$, *constant* $= q^{st}$ *for* $_1 < t$		
T_{max}	$649 + 439\ e^{-0.051t_1}$	$10 < t_1 < 120$
T_{max}	≈ 649	$t_1 > 120$
Time in which the Lead T_{max} *is reached, in seconds:*		
$t\ (T_{max})$	$0.43\ t_1$	$10 < t_1 < 120$
$t\ (T_{max})$	$\approx t_1$	$t_1 > 120$
Shut-down: *Power Density for* $t < 0, q = q^{st}$; *for* $t > 0, q = q^{st}$		
$v(t)$ (m/s)		$v\ (t) = \dfrac{v^{st}}{(1+0.2t^{0.725})}$
T_{out}(t) (°C)		$T_{out}(t) = T_{in}^{st} + \dfrac{(T_{out}^{st} - T_{in}^{st})}{(1+0.4t^{0.76})}$

[42] *Steady conditions reached at* $t = t_1$, *in seconds*

[*] The results are for $\alpha = 0.35$ but they do not change significantly for other values giving a smooth time dependence.

Table 5.7 - Main kinetic parameters used for the Energy Amplifier transient study

Prompt neutron lifetime:	
$\Lambda =$	$2.9 \times 10^{-8}\ s$
Doppler effect coefficient:	
$\left(\frac{\Delta k}{\Delta T}\right)_{fuel}$	$-1.380 \times 10^{-5}\ {}^{\circ}C^{-1}$
$\left(\frac{\Delta \rho}{\Delta T}\right)_{fuel} = \frac{1}{k_0^2}\left(\frac{\Delta k}{\Delta T}\right)_{fuel}$	$-1.44 \times 10^{-5}\ {}^{\circ}C^{-1}$
Moderator density change coefficient:	
$\left(\frac{\Delta k}{\Delta Dens}\right)_{lead}$	$9.68 \times 10^{-7}\ m^3\ kg^{-1}$
$\left(\frac{\Delta \rho}{\Delta Dens}\right)_{lead} = \frac{1}{k_0^2}\left(\frac{\Delta k}{\Delta Dens}\right)_{lead}$	$1.01 \times 10^{-6}\ m^3\ kg^{-1}$
$Dens_{lead}(kg/m^3)$	$11149.7442 - 1.3594615 \times T_{lead}({}^{0}C)$
	$T_{lead} \in [400\ {}^{\circ}C,\ 900\ {}^{\circ}C]$
$\left(\frac{\Delta \rho}{\Delta T}\right)_{lead} = \left(\frac{\Delta \rho}{\Delta Dens}\right)_{lead}\left(\frac{\Delta Dens}{\Delta T}\right)_{lead}$	$-1.37 \times 10^{-6}\ {}^{\circ}C^{-1}$

Table 5.8 - Discharge of Core Volume at the end of the First Fuel Cycle.

	Mass (kg)	EA/ PWR	1/e Lifetime		Mass (kg)	EA/ PWR	1/e Lifetime
^{14}C	0.0145	—	8286. y	^{102}Rh	0.0007	—	299.3 d
^{49}V	0.0003	—	1.339 y	^{107}Pd	1.926	0.096	0.939E+07 y
^{51}Cr	0.0078	—	40.06 d	^{111}Ag	0.0063	0.152	10.77 d
^{53}Mn	0.004	—	0.540E+07 y	^{123}Sn	0.1047	2.645	186.8 d
^{54}Mn	0.2019	—	1.237 y	^{125}Sn	0.0149	1.435	13.94 d
^{55}Fe	1.717	—	3.948 y	^{126}Sn	4.236	1.734	0.144E+06 y
^{59}Fe	0.0033	—	64.35 d	^{124}Sb	0.0084	1.087	87.05 d
^{60}Co	0.0006	—	7.622 y	^{125}Sb	1.127	0.889	3.988 y
^{70}Zn	0.006	—	0.723E+15 y	^{126}Sb	0.0026	2.253	18.02 d
^{79}Se	0.9983	1.916	0.94E+06 y	^{129}I	27.28	1.722	0.227E+08 y
^{85}Kr	21.64	10.160	15.55 y	^{131}I	0.2924	0.458	11.63 d
^{86}Rb	0.0088	4.261	26.94 d	^{134}Cs	6.062	0.546	2.982 y
^{87}Rb	46.52	2.157	0.687E+11 y	^{135}Cs	115.9	4.505	0.332E+07 y
^{89}Sr	2.402	1.127	73.07 d	^{136}Cs	0.1134	2.103	19.03 d
^{90}Sr	74.76	1.578	41.62 y	^{137}Cs	118.5	1.109	43.52 y
^{88}Y	0.0006	—	154.2 d	^{140}Ba	0.8585	0.470	18.44 d
^{91}Y	3.313	0.991	84.61 d	^{137}La	0.0135	—	0.867E+05 y
^{93}Zr	88.34	1.387	0.221E+07 y	^{138}La	0.0040	—	0.151E+12 y
^{95}Zr	3.537	0.623	92.57 d	^{139}Ce	0.0023	—	199.0 d
^{94}Nb	0.0011	—	0.293E+05 y	^{141}Ce	2.5330	0.575	47.00 d
^{95}Nb	2.026	0.649	50.57 d	^{144}Ce	17.300	0.515	1.129 y
^{97}Tc	0.0003	—	0.376E+07 y	^{143}Pr	0.9254	0.547	19.62 d
^{98}Tc	0.0014	—	0.607E+07 y	^{147}Nd	0.2539	0.401	15.88 d
^{99}Tc	56.08	0.827	0.305E+06 y	^{146}Pm	0.0010	—	7.996 y
^{103}Ru	0.708	0.176	56.77 d	^{147}Pm	15.410	1.315	3.793 y
^{106}Ru	1.147	0.074	1.480 y	^{147}Sm	12.010	2.551	0.153E+12 y
				^{151}Sm	4.7700	0.568	130.1 y

Table 5.8(cont.) - Discharge of Core Volume at the end of the First Fuel Cycle.

	Mass (kg)	EA/ PWR	1/e Lifetime			Mass (kg)	EA/ PWR	1/e Lifetime	
^{152}Eu	0.0324	12.843	19.58	y	^{194}Hg	0.0026	—	751.9	y
^{154}Eu	0.6074	0.164	12.43	y	^{203}Hg	0.0001	—	67.40	d
^{155}Eu	0.4376	0.290	6.767	y					
^{156}Eu	0.0046	0.012	21.96	d	^{204}Tl	0.0049	—	5.466	y
^{160}Tb	0.0028	0.300	104.5	d	^{202}Pb	0.0455	—	0.759E+05	y
					^{205}Pb	20.300	—	0.221E+08	y
^{185}W	0.2344	—	108.6	d					
					^{208}Bi	0.0011	—	0.532E+06	y
^{187}Re	2.5220	—	0.629E+11	y					
					^{210}Po	0.0055	—	200.1	d

Table 5.8(cont.). - Actinides of Core Volume at the end of the First Fuel Cycle.

Element	Mass (kg)	1/e Lifetime		Element	Mass (kg)	1/e Lifetime	
^{228}Th	0.0213	2.766	y	^{232}U	1.4270	99.63	y
^{230}Th	0.2352	0.1090E+06	y	^{233}U	2463.00[43]	0.2302E+06	y
^{232}Th	20850.0[44]	0.2032E+11	y	^{234}U	260.40	0.3543E+06	y
^{234}Th	0.0059	34.85	d	^{235}U	24.0800	0.1018E+10	y
				^{236}U	2.7860	0.3387E+08	y
^{231}Pa	4.3120	0.4737E+05	y				
^{233}Pa	53.2500	38.99	d	^{237}Np	0.2889	0.3094E+07	y
				^{238}Pu	0.0712	126.9	y
				^{239}Pu	0.0003	0.3486E+05	y

[43]Initially 24,230 kg. Difference due to burn-up

[44]Initially 2635 kg. Difference (172 kg) to be compensated by the Breeder

Table 5.9 - Products at Discharge produced in the Spallation Target Volume.

	Mass (g)	1/e Lifetime	Vapour [boil. T]
^{3}H	1.435	17.83 y	*Gaseous* [-252°C]
^{35}S	0.009	126.5 d	*Gaseous* [445 °C]
^{36}Cl	0.204	0.435E+6 y	*Bound +)* [- 34°C]
^{39}Ar	0.336	389.0 y	*Gaseous*
^{42}Ar	0.336	47.57 y	*Gaseous* [-186°C]
^{45}Ca	0.007	236.9 d	*Intermet* 0.2 Torr
^{49}V	0.072	1.339 y	*Solid* [3409°C]
^{53}Mn	0.387	0.540E+7 y	*Solid(*)* 10^{-5} Torr
^{59}Fe	0.049	64.35 d	*Solid(*)*
^{60}Fe	0.586	0.216E+7 y	*Solid(*)* [2862°C]
^{56}Co	0.029	111.7 d	*Solid(*)*
^{57}Co	0.065	1.077 y	*Solid(*)*
^{58}Co	0.002	102.4 d	*Solid(*)*
^{60}Co	1.084	7.622 y	*Solid(*)* [2928°C]
^{59}Ni	0.253	0.109E+6 y	*Solid(*)*
^{63}Ni	2.134	144.7 y	*Solid(*)* [2914°C]
^{65}Zn	0.004	353.2 d	*Volatile*
^{70}Zn	2.424	0.723E+15y	*Volatile* 40 Torr
^{68}Ge	0.032	1.073 y	*Solid*
^{71}Ge	0.079	16.53 d	*Solid* [2834°C]
^{73}As	0.329	116.1 d	*Gaseous* [615 °C]
^{75}Se	0.184	173.2 d	*Intermet*
^{79}Se	2.03	0.939E+6 y	*Intermet* [685 °C]
^{81}Kr	5.777	0.331E+6 y	*Gaseous*
^{85}Kr	4.326	15.55 y	*Gaseous* [-153 °C]

	Mass (g)	1/e Lifetime	Vapour [boil. T]
^{83}Rb	0.036	124.6 d	*Gaseous*
^{86}Rb	0.181	26.94 d	*Gaseous* [688 °C]
^{85}Sr	0.264	93.76 d	*Intermet*
^{89}Sr	0.21	73.07 d	*Intermet*
^{90}Sr	3.88	41.62 y	*Intermet* 0.40 Torr
^{88}Y	0.247	154.2 d	*Solid*
^{91}Y	0.318	84.61 d	*Solid* [3338°C]
^{88}Zr	0.581	120.6 d	*Solid(*)*
^{93}Zr	6.426	0.221E+7 y	*Solid(*)*
^{95}Zr	0.46	92.57 d	*Solid(*)* [4409°C]
^{91}Nb	4.139	983.3 y	*Solid*
^{92}Nb	0.496	0.501E+8 y	*Solid*
^{94}Nb	1.13	0.293E+5 y	*Solid*
^{95}Nb	1.187	50.57 d	*Solid* [4744°C]
^{93}Mo	4.726	5784. y	*Solid* [4639°C]
^{97}Tc	1.896	0.376E+7 y	*Solid*
^{99}Tc	8.333	0.305E+6 y	*Solid* [4265°C]
^{103}Ru	0.182	56.77 d	*Solid*
^{106}Ru	1.069	1.480 y	*Solid* [4150°C]
^{101}Rh	4.32	4.772 y	*Solid*
^{102}Rh	0.244	299.3 d	*Solid* [3697°C]
^{107}Pd	5.207	0.939E+7 y	*Solid* [2964°C]
^{105}Ag	0.108	59.71 d	*Solid ?* $5\ 10^{-6}$ To
^{109}Cd	1.627	1.833 y	*Volatile* 200 Torr
^{113}Sn	0.427	166.4 d	*Solid(*)*
^{123}Sn	0.206	186.8 d	*Solid(*)*
^{126}Sn	0.622	0.144E+6 y	*Solid(*)* $3\ 10^{-8}$ To

+) Lead Cloride, $PbCl_2$, b.p. 950 °C

(*) Dissolved in the Molten Lead

Table 5.9(cont.) - Products at Discharge produced in the Spallation Target Volume.

	Mass (g)	1/e Lifetime	Vapour [boil. T]
^{124}Sb	0.043	87.05 d	*Volatile*
^{125}Sb	0.404	3.988 y	*Volatile*
		[1585°C]	0.5 Torr
^{121}Te	0.008	24.26 d	*Intermet*
			-)
^{125}I	0.014	85.90 d	*Gaseous*
			[184°C]
^{127}Xe	0.37	52.63 d	*Gaseous*
			[-108°C]
^{131}Cs	0.003	14.01 d	*Gaseous*
^{134}Cs	0.282	2.982 y	*Gaseous*
			[671°C]
^{131}Ba	0.001	17.06 d	*Intermet*
^{133}Ba	0.396	15.21 y	*Intermet*
			$2\ 10^{-2}$ To
^{137}La	2.653	0.867E+5 y	*Solid*
			[3464°C]
^{139}Ce	0.722	199.0 d	*Solid*
^{141}Ce	0.002	47.00 d	*Solid*
			[3443°C]
^{143}Pm	1.1	1.050 y	*Solid*
^{145}Pm	0.419	25.59 y	*Solid*
^{146}Pm	0.205	7.996 y	*Solid*
			[3520°C]
^{145}Sm	1.064	1.347 y	*Intermet*
^{146}Sm	0.406	0.148E+9 y	*Intermet*
^{151}Sm	2.492	130.1 y	*Intermet*
			$2\ 10^{-4}$ To
^{149}Eu	0.001	134.6 d	*Intermet*
^{150}Eu	0.76	51.77 y	*Intermet*
^{154}Eu	0.932	12.43 y	*Intermet*
			$8\ 10^{-3}$ To
^{151}Gd	0.05	179.3 d	*Solid*
			[3273°C]
^{160}Tb	0.214	104.5 d	*Solid*
			[3230°C]
^{159}Dy	0.021	208.8 d	*Solid*
			[2587°C]

	Mass (g)	1/e Lifetime	Vapour [boil. T]
^{173}Lu	0.908	1.981 y	*Solid*
			[3402°C]
^{172}Hf	0.288	2.704 y	*Solid*
^{175}Hf	0.029	101.2 d	*Solid*
			[4603°C]
^{179}Ta	2.467	2.588 y	*Solid*
^{182}Ta	1.025	165.5 d	*Solid*
			[5458°C]
^{181}W	1.621	175.3 d	*Solid*
			[5555°C]
^{183}Re	3.267	101.2 d	*Solid*
^{187}Re	1.829	0.629E+11y	*Solid*
			[5596°C]
^{185}Os	8.957	135.3 d	*Solid*
			[5012°C]
^{189}Ir	3.362	19.09 d	*Solid*
			[4428°C]
^{188}Pt	1.515	14.75 d	*Solid*
^{190}Pt	196.2	0.94E+12 y	*Solid*
^{193}Pt	307.4	72.30 y	*Solid*
			[3827°C]
^{195}Au	109.5	269.1 d	*Solid*
			[2857°C]
^{194}Hg	415.9	751.9 y	*Gaseous*
^{203}Hg	6.252	67.40 d	*Gaseous*
			[357°C]
^{202}Tl	15.25	17.68 d	*Volatile ?*
^{204}Tl	386	5.466 y	*Volatile ?*
			$6\ 10^{-2}$ To
^{202}Pb	2071	0.759E+5 y	*Dissolved*
^{205}Pb	11960	0.221E+8 y	*Dissolved*
			30 Torr
^{205}Bi	4.299	22.14 d	*Eutectic*
^{207}Bi	69.79	45.62 y	*Eutectic*
^{208}Bi	14.63	0.532E+6 y	*Eutectic*
^{210}Po	0.995	200.1 d	*Volatile*
		(boils at 254 °C)	

-) Lead Telluride, PbTe, m.p. 917 °C

Figure Captions.

Figure 5.1 Integrated burn-up versus simulated time of operation for an initial ^{233}U filling and pre-set regime at $k \approx 0.98$. Related parameters of the EA are given in Table 4.1.

Figure 5.2a Accelerator current chosen by the programme as a function of the burn-up in order to produce a constant power of 1500 MW. Related parameters of the EA are given in Table 4.1.

Figure 5.2b Resulting EA power output as a function of burn-up with appropriate variation of accelerator.

Figure 5.3 Energetic gain G of the EA as a function of the burn-up. Same conditions as Figure 5.1.

Figure 5.4 Multiplication coefficient k of the EA as a function of the burn-up: (a) linear time scale, (b) logarithmic time scale. Same conditions as Figure 5.1.

Figure 5.5 Atomic concentration of ^{233}U, normalised to ^{232}Th, averaged over the core (Breeding Ratio) as a function of the burn-up. Same conditions as Figure 5.1.

Figure 5.6 Atomic concentration of ^{233}Pa, normalised to ^{233}U, averaged over the core as a function of the burn-up. Same conditions as Figure 5.1.

Figure 5.7 Fraction of all neutrons captured by Fission Fragment products, as a function of the burn-up. Same conditions as Figure 5.1.

Figure 5.8 Concentration of the main Actinides as a function of the burn-up. Same conditions as Figure 5.1.

Figure 5.9 Stockpile of Plutonium and Americium isotopes as a function of the burn-up, for an initial fuel made of "dirty" Plutonium (see Table 5.2) and native Thorium. The concentration of produced ^{233}U is also shown.

Figure 5.10 Neutron flux spectrum in the different material regions of the F-EA. The breeder and the Fuel have similar distributions with fine resolution due to the resonant structure of the material cross sections.

Figure 5.11a Pressure drop inserted as a function of the radial position. As a reference the total pressure drop due to the Lead column is also displayed.

Figure 5.11b Lead velocity distribution as a function of the radial position.

Figure 5.12 Velocity map of Lead in the column above the Core.

Figure 5.13 LMFBR power excursion benchmark (as defined in a comparative NEACRP exercise) assuming a rod ejection accident.

Figure 5.14 Comparison of power excursions in a critical reactor (lead cooled) with the Fast Energy Amplifier for an accidental reactivity insertion of 170 \$/s for 15 ms.

Figure 5.15 Comparison of power excursions in a critical reactor (lead cooled) with the Fast Energy Amplifier for an accidental reactivity insertion of 255 \$/s for 15 ms.

Figure 5.16 Power excursion and reactivity behaviour during a beam run-off in the Fast Energy Amplifier.

Figure 5.17 Effect of ^{233}Pa on the decay heat of the Fast Energy Amplifier.

Figure 5.18 Time Evolution of the γ-activity of the fuel after discharge of the EA. The number of γ–rays is normalized according to their energy in MeV. The curve for the PWR has been calculated for the same energy delivered and a burn-up of 33 GW $\times$ day/t.

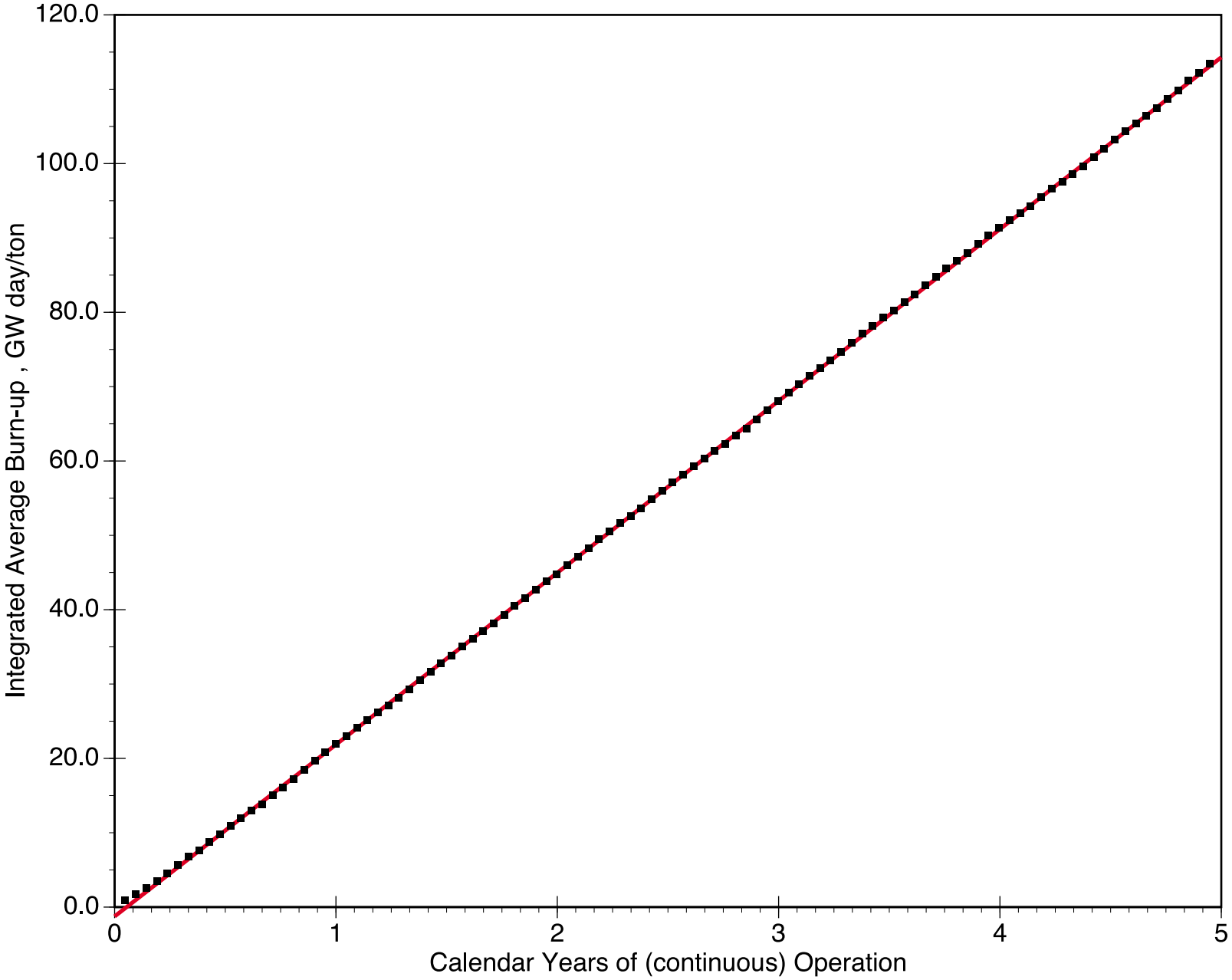
120.0
100.0
80.0
60.0
40.0
20.0
0.0
Integrated Average Burn-up , GW day/ton
0
1
2
3
4
5
Calendar Years of (continuous) Operation

Figure 5.1

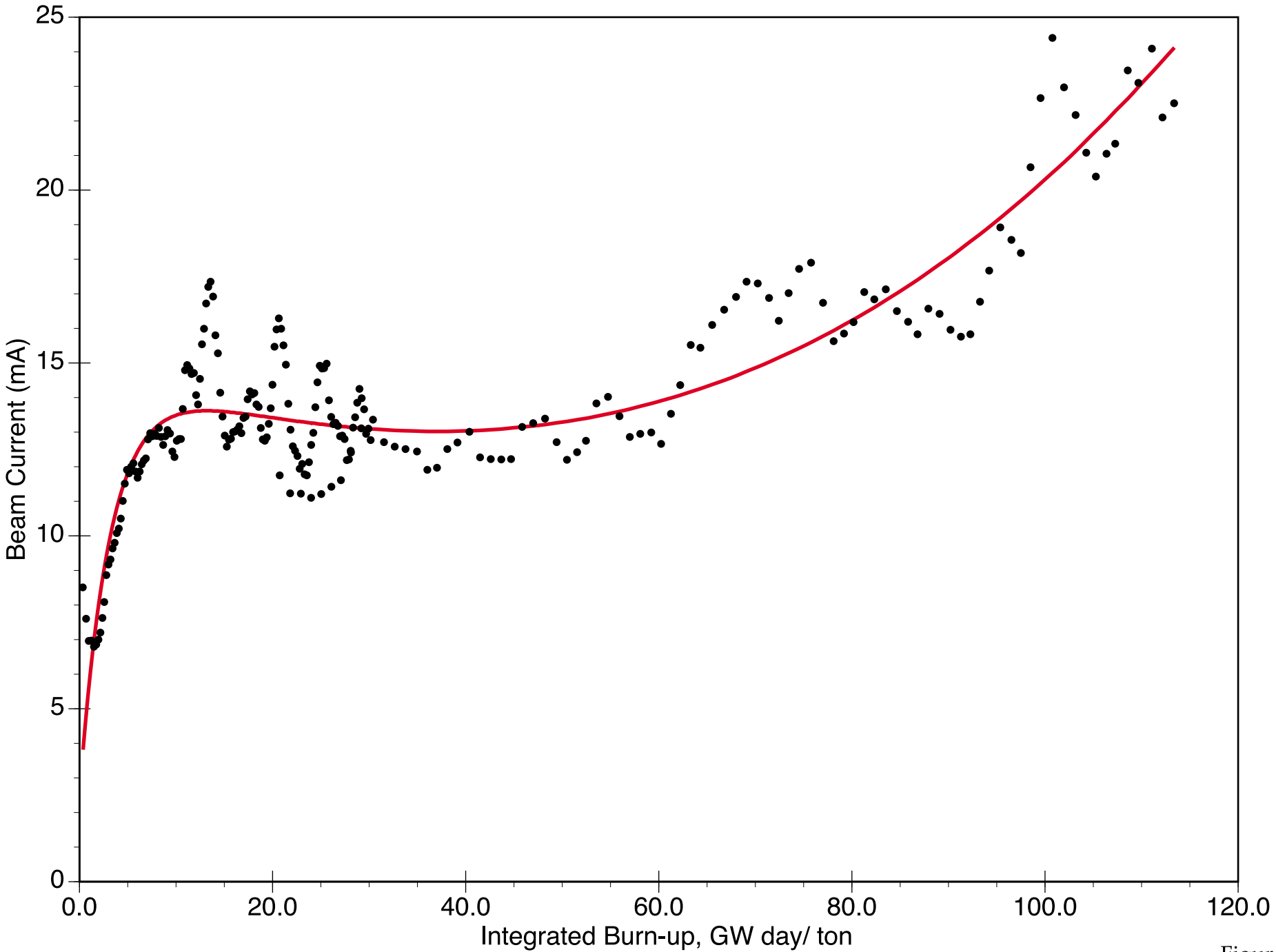
25
20
15
10
5
0
Beam Current (mA)
0.0
20.0
40.0
60.0
80.0
100.0
120.0
Integrated Burn-up, GW day/ ton

Figure 5.2a

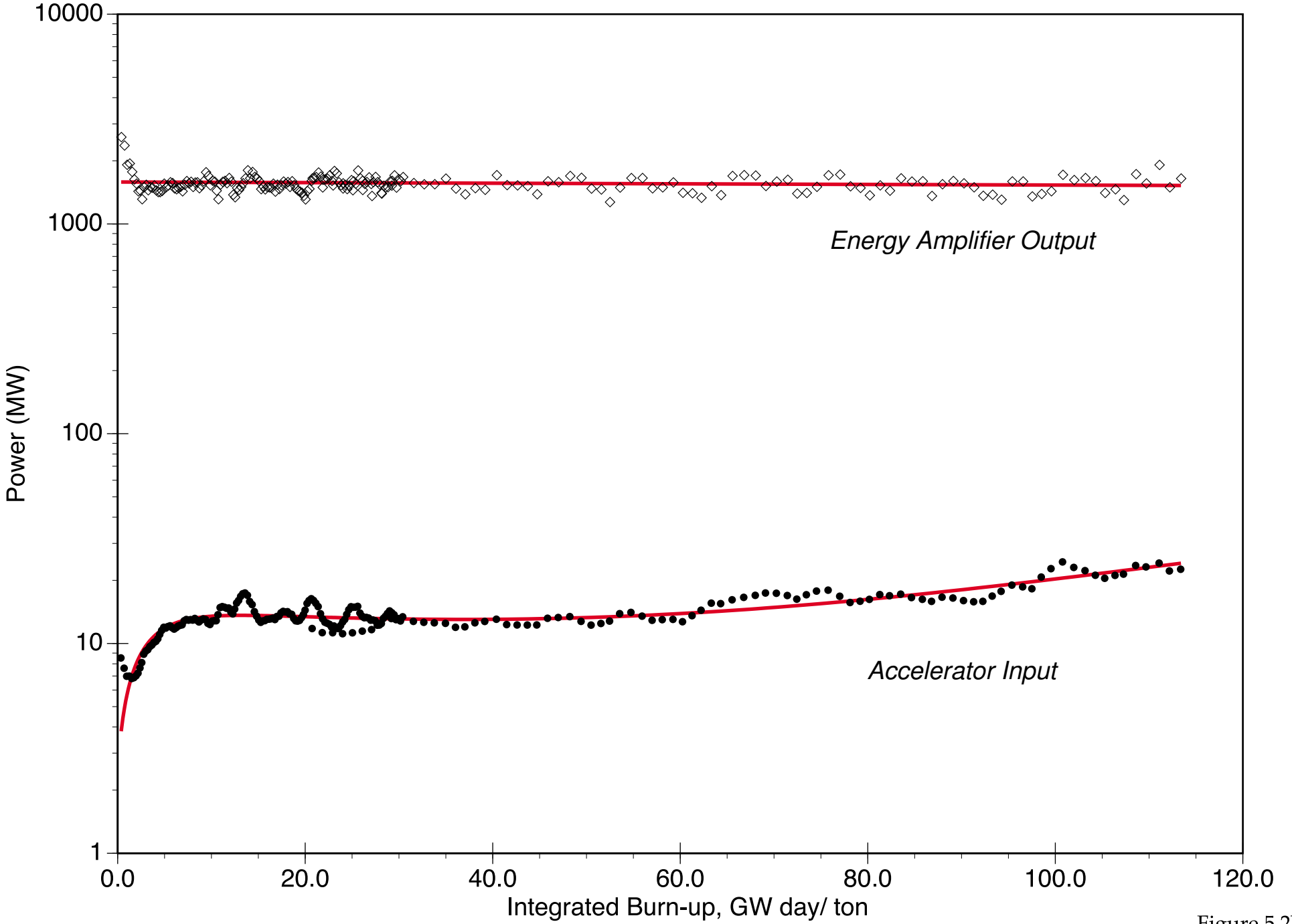
10000
1000
100
10
1
Power (MW)
Energy Amplifier Output
Accelerator Input
0.0
20.0
40.0
60.0
80.0
100.0
120.0
Integrated Burn-up, GW day/ ton

Figure 5.2b

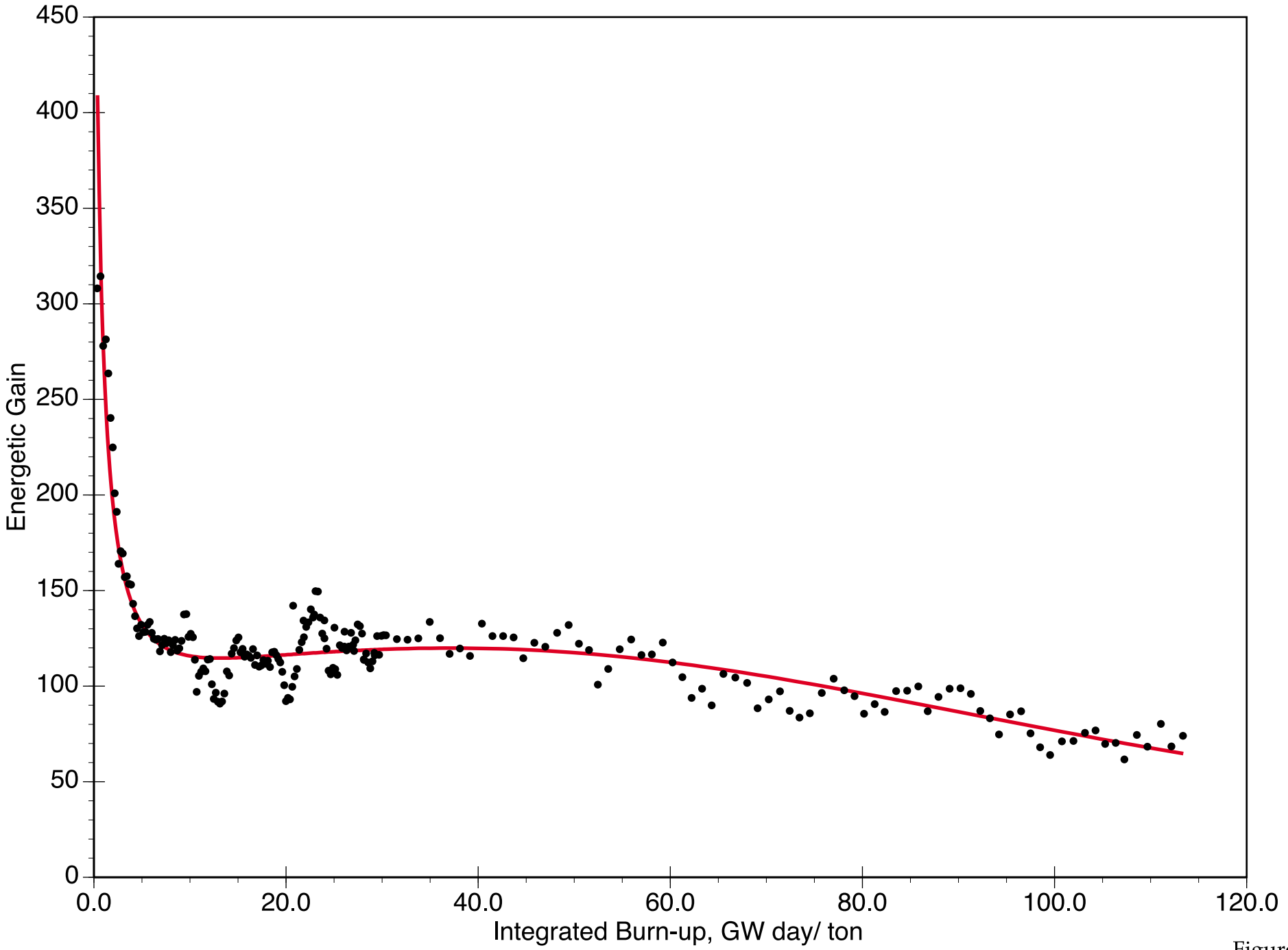
450
400
350
300
250
200
150
100
50
0
Energetic Gain
0.0
20.0
40.0
60.0
80.0
100.0
120.0
Integrated Burn-up, GW day/ ton

Figure 5.3

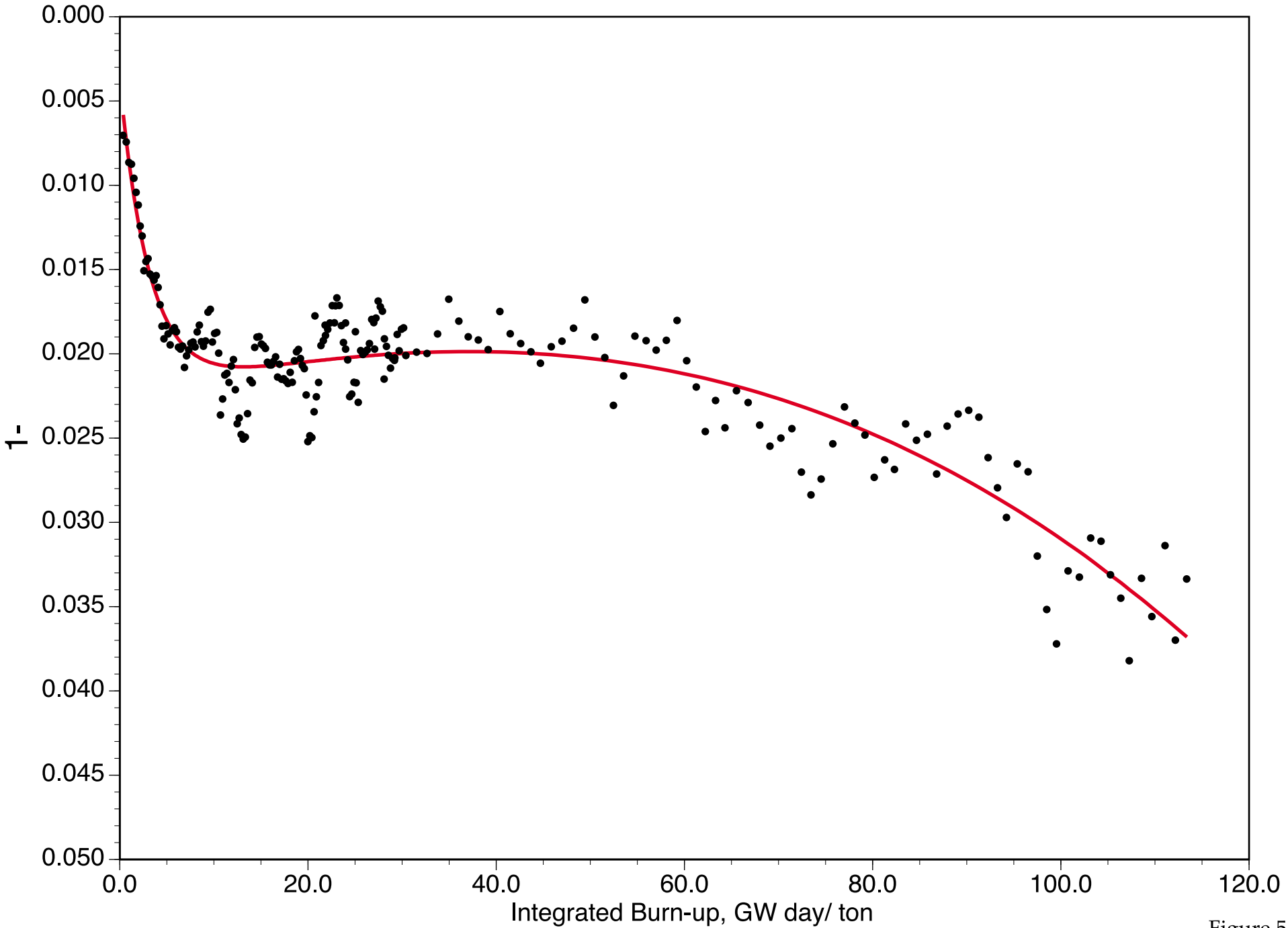
0.000
0.005
0.010
0.015
0.020
0.025
0.030
0.035
0.040
0.045
0.050
1-
0.0
20.0
40.0
60.0
80.0
100.0
120.0
Integrated Burn-up, GW day/ ton

Figure 5.4a

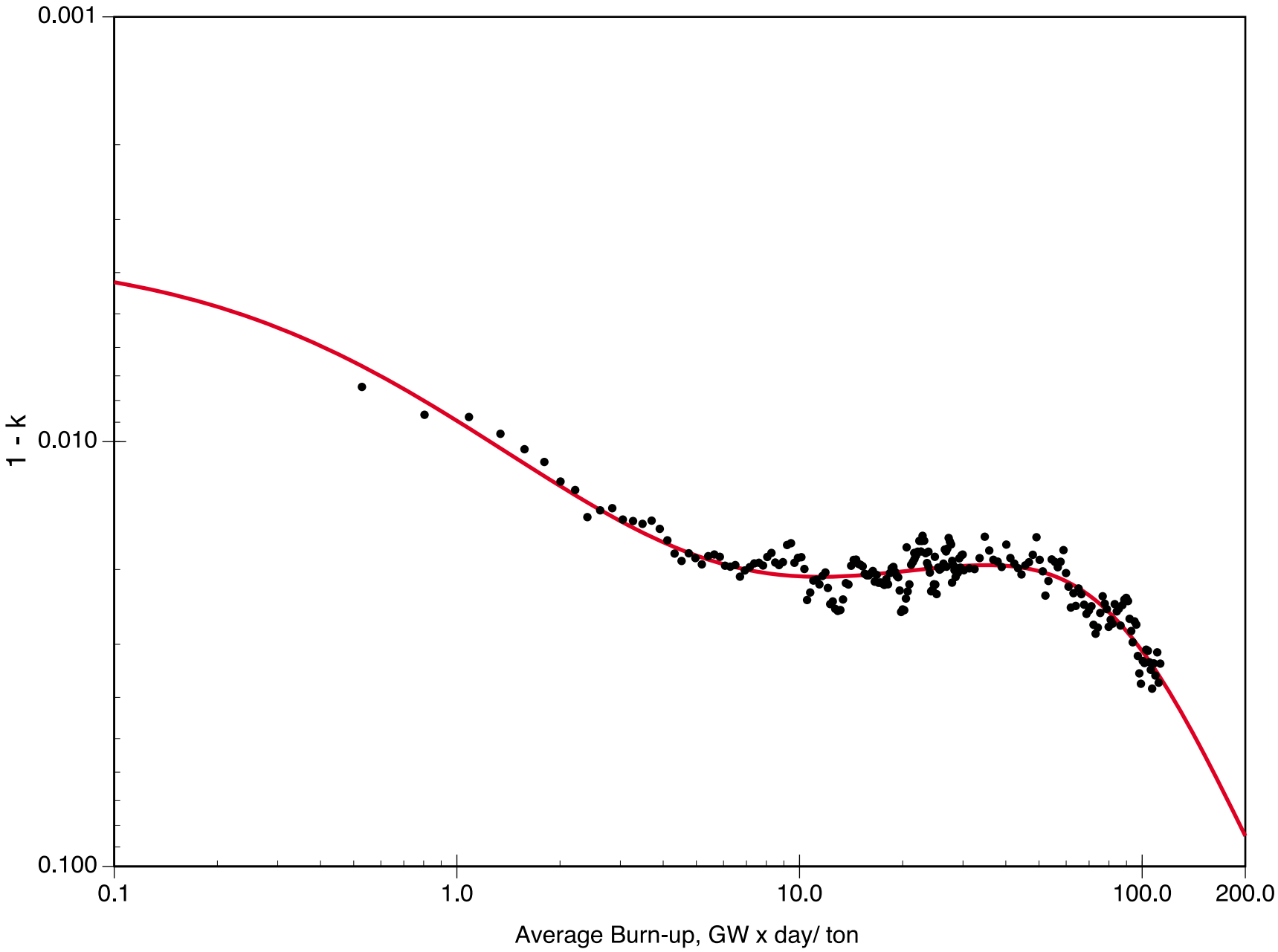
0.001
0.010
0.100
1 - k
0.1
1.0
10.0
100.0
200.0
Average Burn-up, GW x day/ ton

Figure 5.4b

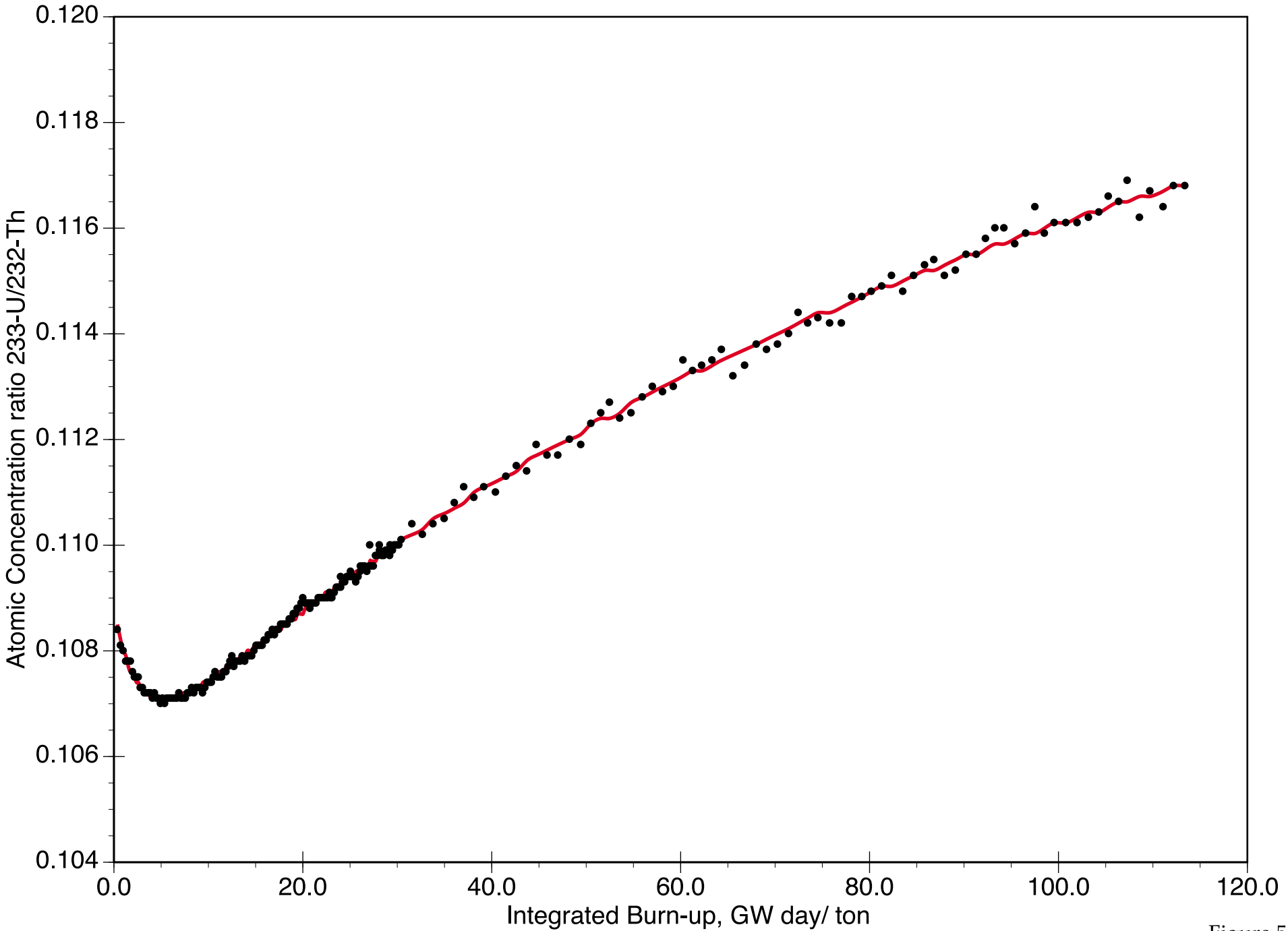
0.120
0.118
0.116
0.114
0.112
0.110
0.108
0.106
0.104
Atomic Concentration ratio 233-U/232-Th
0.0
20.0
40.0
60.0
80.0
100.0
120.0
Integrated Burn-up, GW day/ ton

Figure 5.5

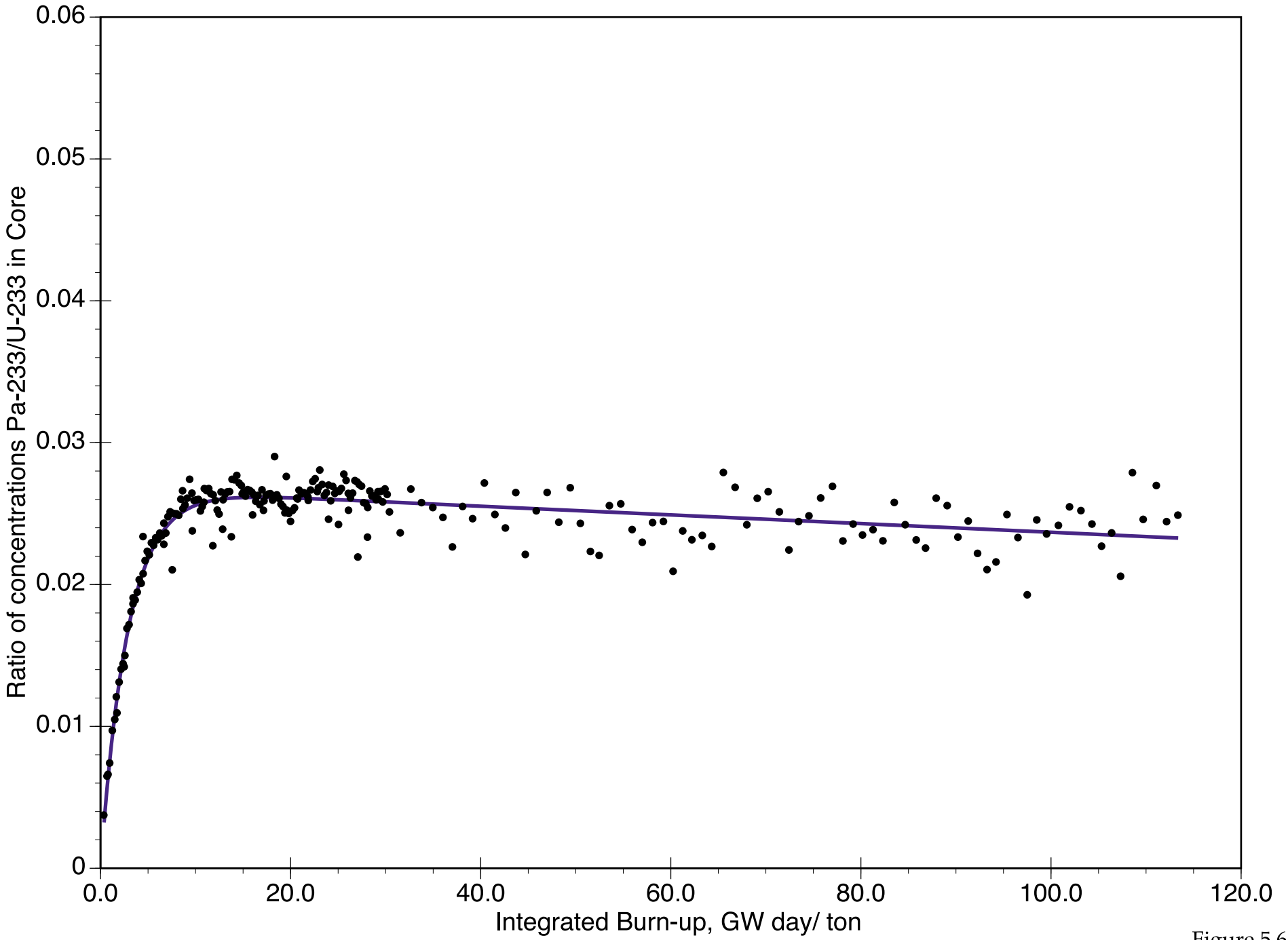
0.06
0.05
0.04
0.03
0.02
0.01
0
Ratio of concentrations Pa-233/U-233 in Core
0.0
20.0
40.0
60.0
80.0
100.0
120.0
Integrated Burn-up, GW day/ ton

Figure 5.6

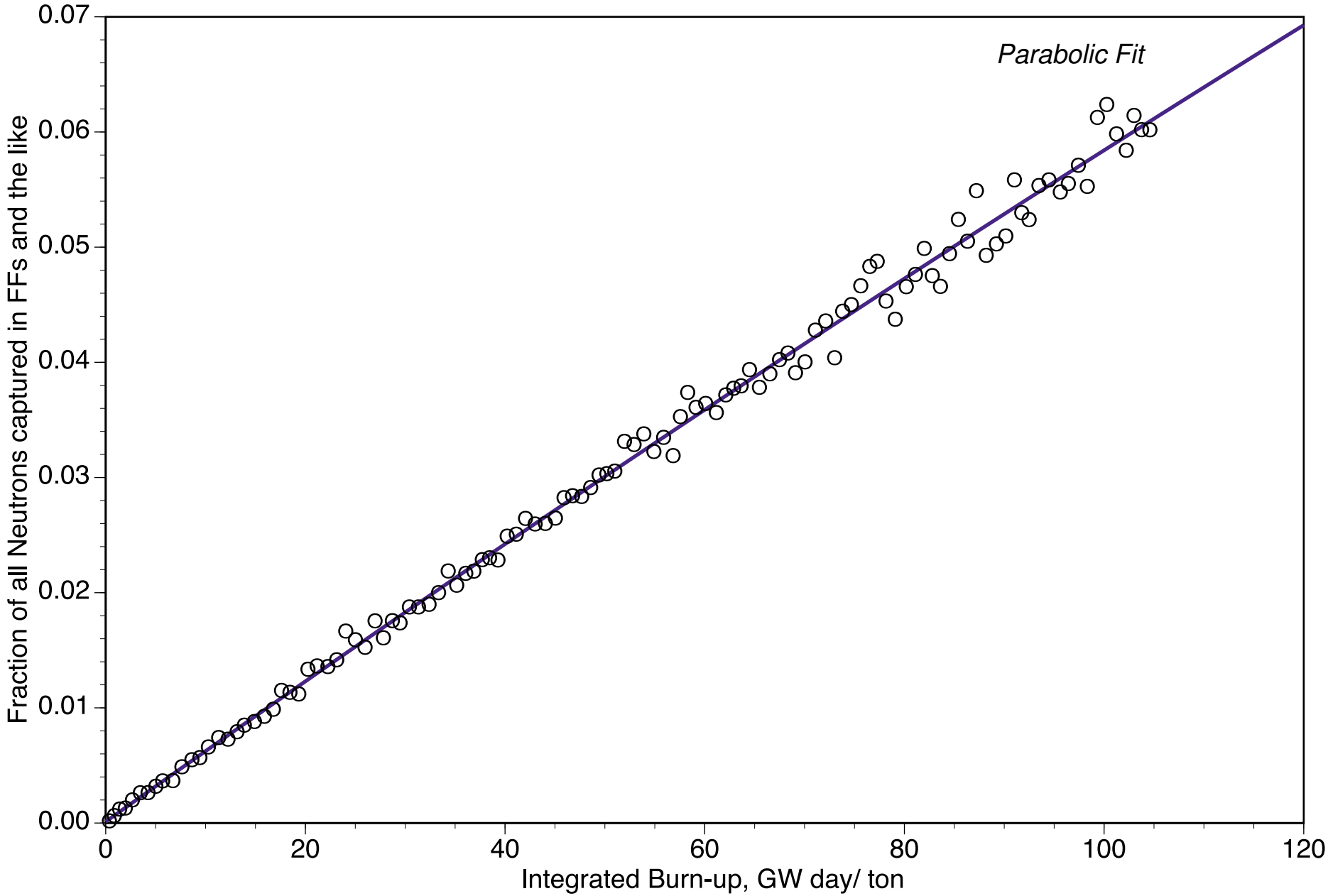
Parabolic Fit
Fraction of all Neutrons captured in FFs and the like
0.07
0.06
0.05
0.04
0.03
0.02
0.01
0.00
0
20
40
60
80
100
120
Integrated Burn-up, GW day/ ton

Figure 5.7

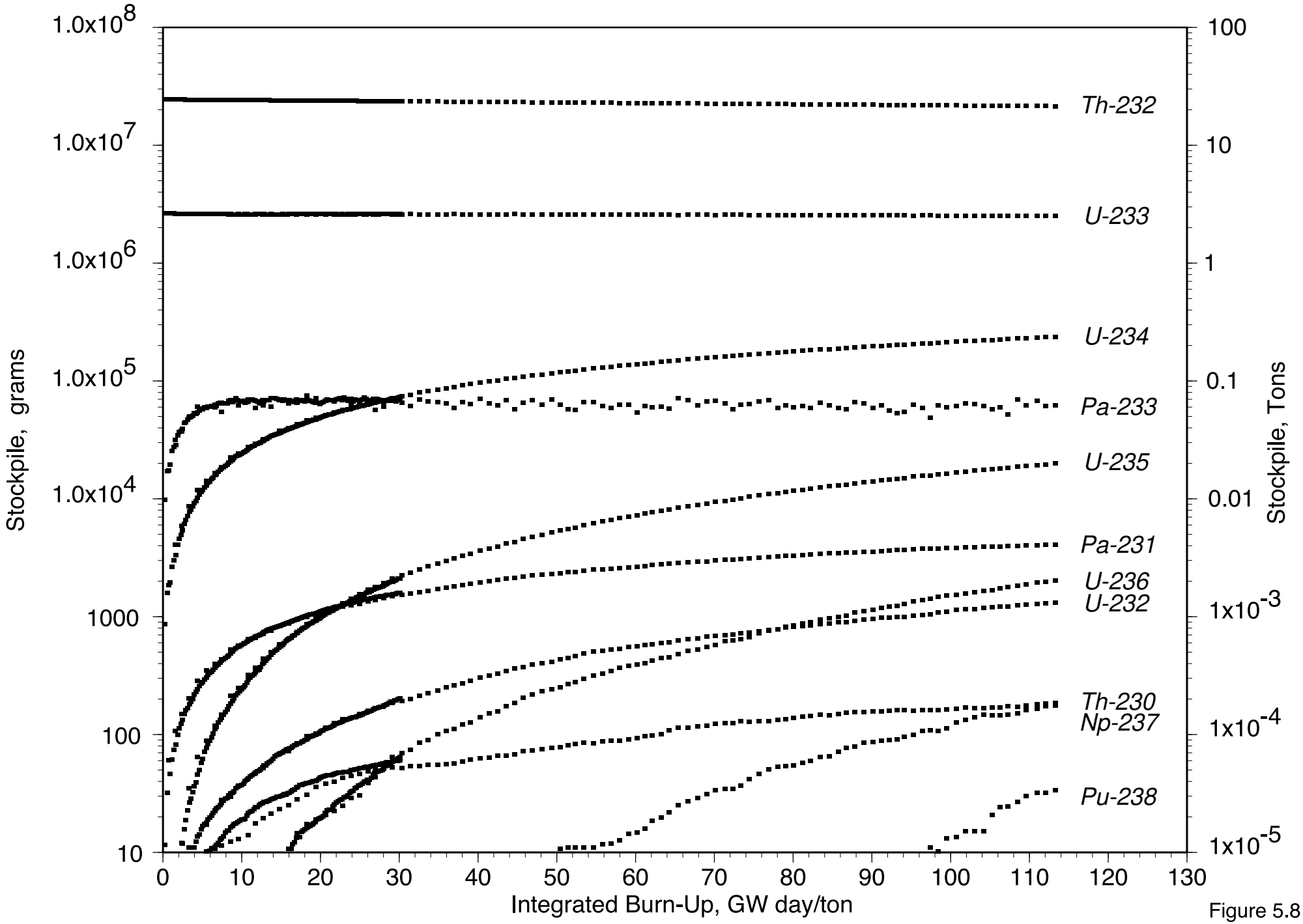
1.0x10^8
1.0x10^7
1.0x10^6
1.0x10^5
1.0x10^4
1000
100
10
Stockpile, grams
100
10
1
0.1
0.01
1x10^-3
1x10^-4
1x10^-5
Stockpile, Tons
Th-232
U-233
U-234
Pa-233
U-235
Pa-231
U-236
U-232
Th-230
Np-237
Pu-238
0
10
20
30
40
50
60
70
80
90
100
110
120
130
Integrated Burn-Up, GW day/ton

Figure 5.8

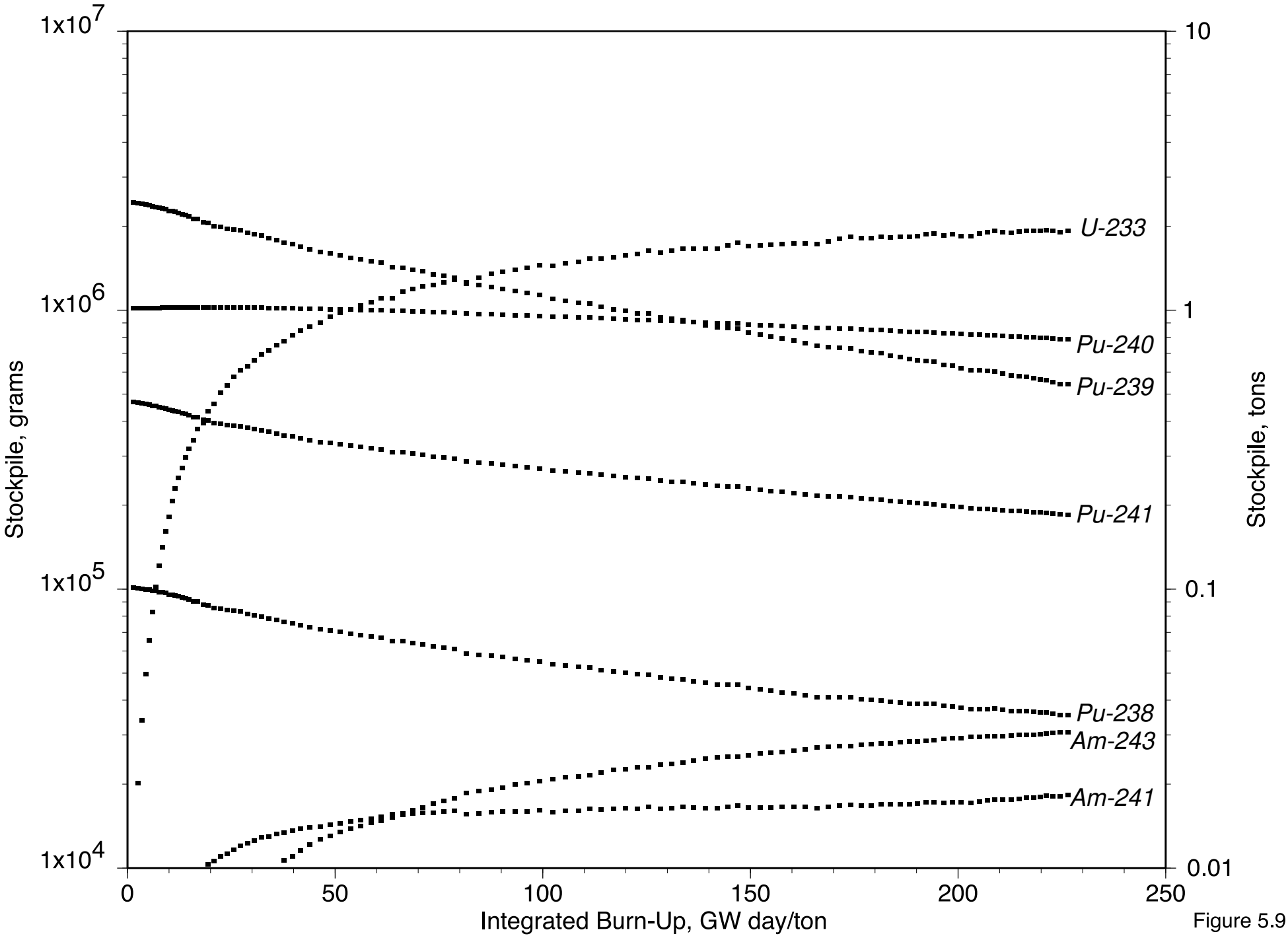
1x10^7
1x10^6
1x10^5
1x10^4
Stockpile, grams
10
1
0.1
0.01
Stockpile, tons
U-233
Pu-240
Pu-239
Pu-241
Pu-238
Am-243
Am-241
0
50
100
150
200
250
Integrated Burn-Up, GW day/ton

Figure 5.9

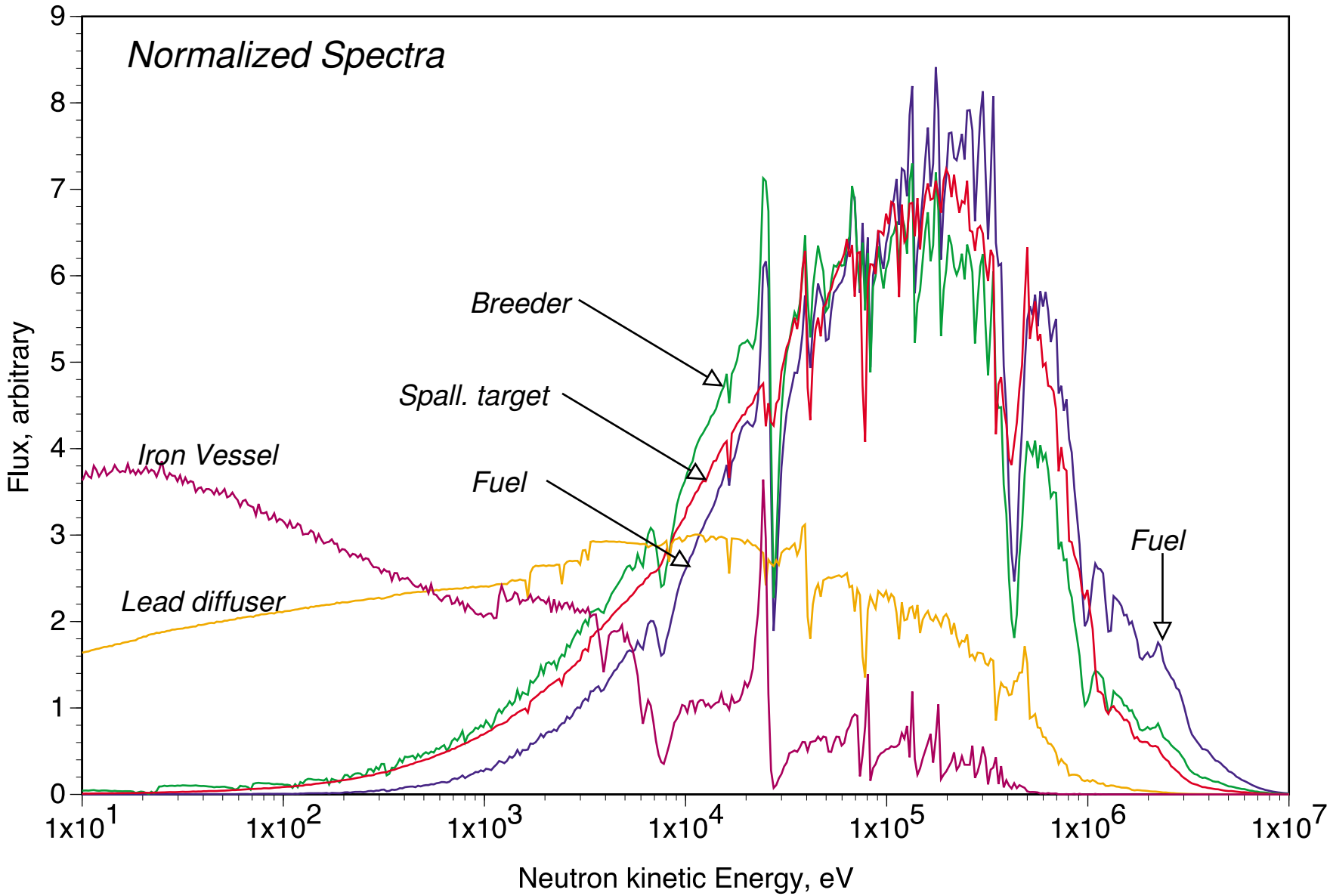
Normalized Spectra
Flux, arbitrary
Neutron kinetic Energy, eV
Breeder
Spall. target
Fuel
Iron Vessel
Lead diffuser
Fuel
0
1
2
3
4
5
6
7
8
9
1x10^1
1x10^2
1x10^3
1x10^4
1x10^5
1x10^6
1x10^7

Figure 5.10

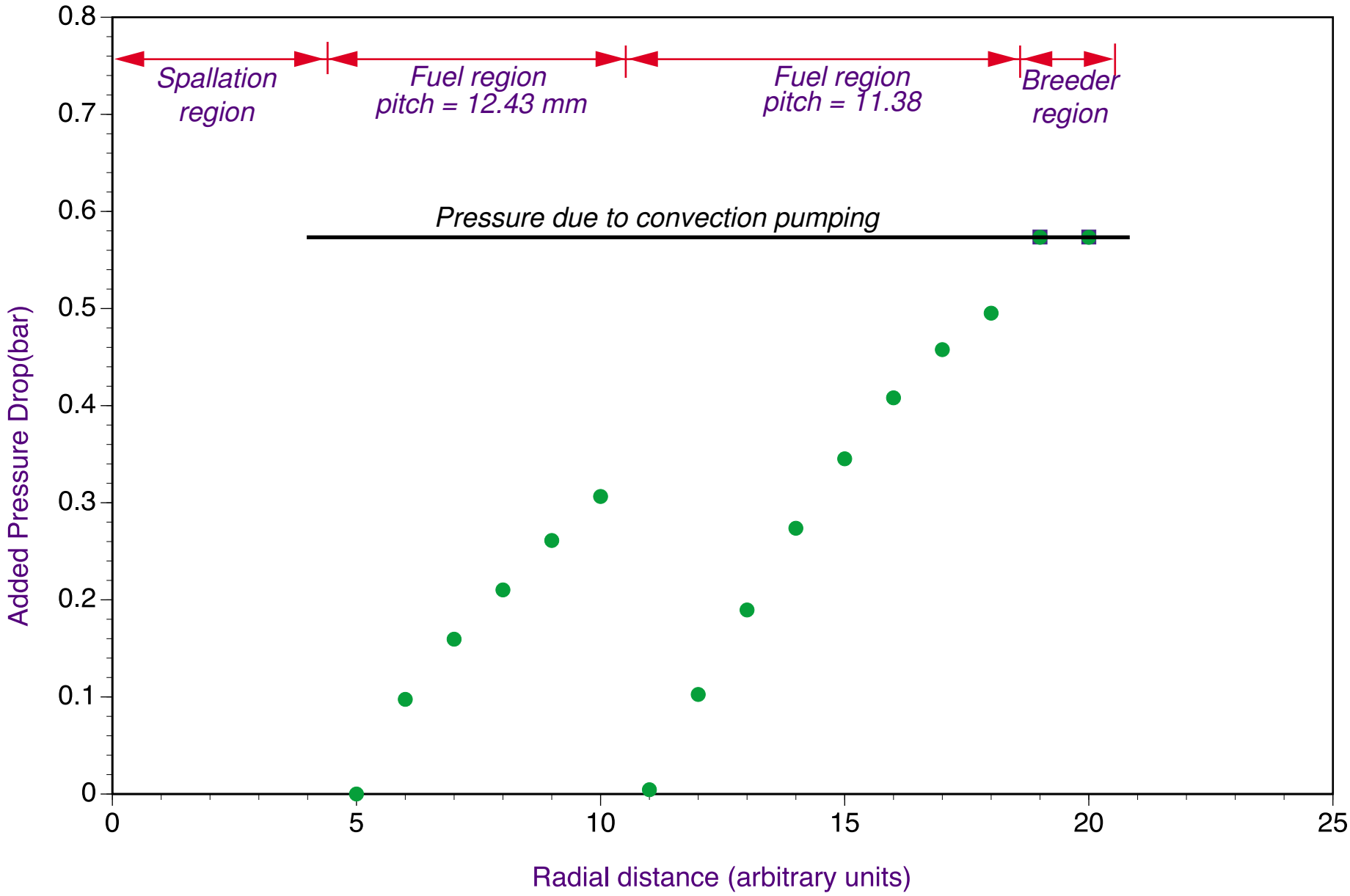
Spallation region
Fuel region pitch = 12.43 mm
Fuel region pitch = 11.38
Breeder region
Pressure due to convection pumping
Added Pressure Drop(bar)
Radial distance (arbitrary units)
0
0.1
0.2
0.3
0.4
0.5
0.6
0.7
0.8
0
5
10
15
20
25

Figure 5.11a

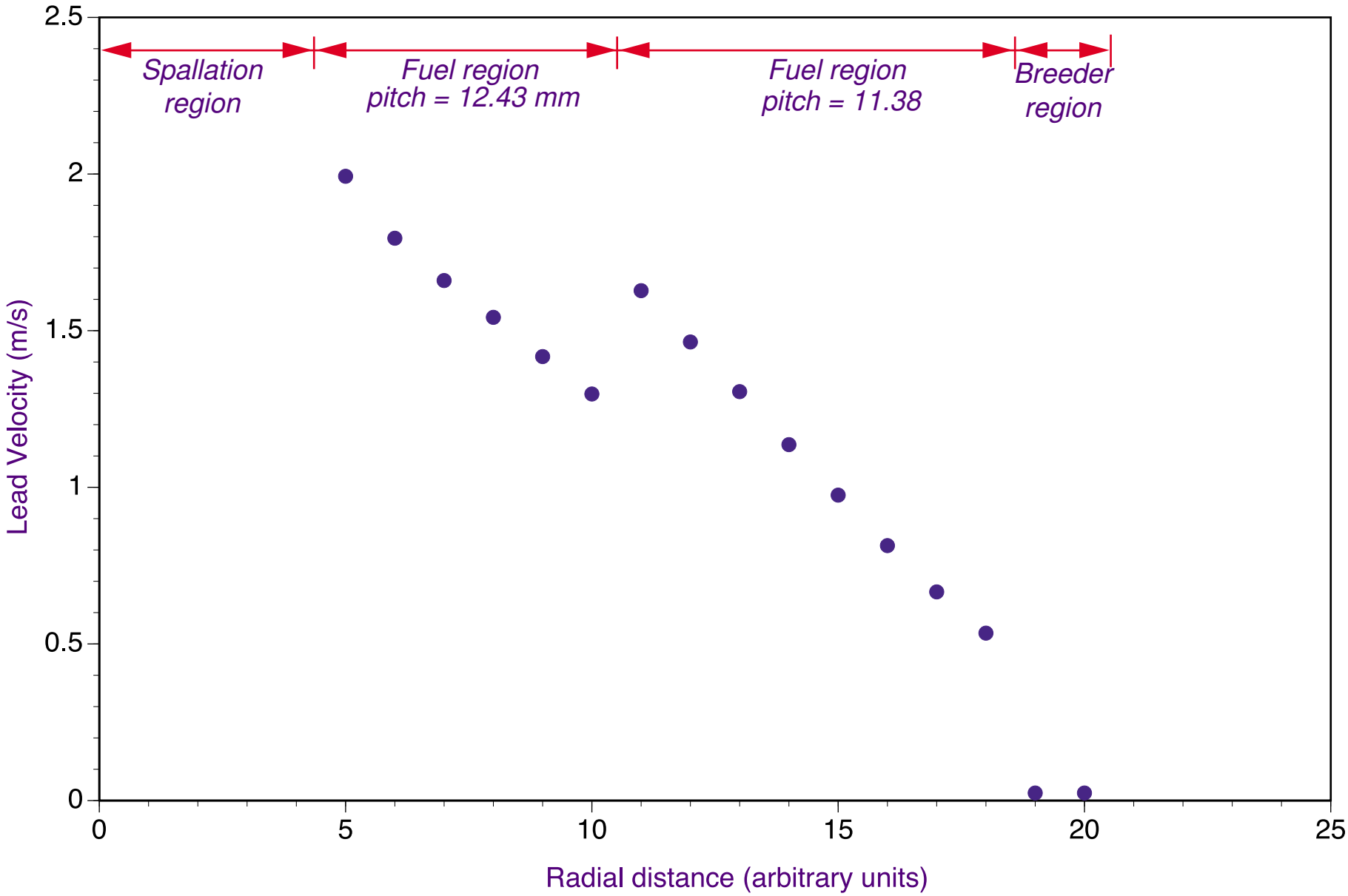
Spallation region
Fuel region pitch = 12.43 mm
Fuel region pitch = 11.38
Breeder region
Lead Velocity (m/s)
Radial distance (arbitrary units)
0
0.5
1
1.5
2
2.5
0
5
10
15
20
25

Figure 5.11b

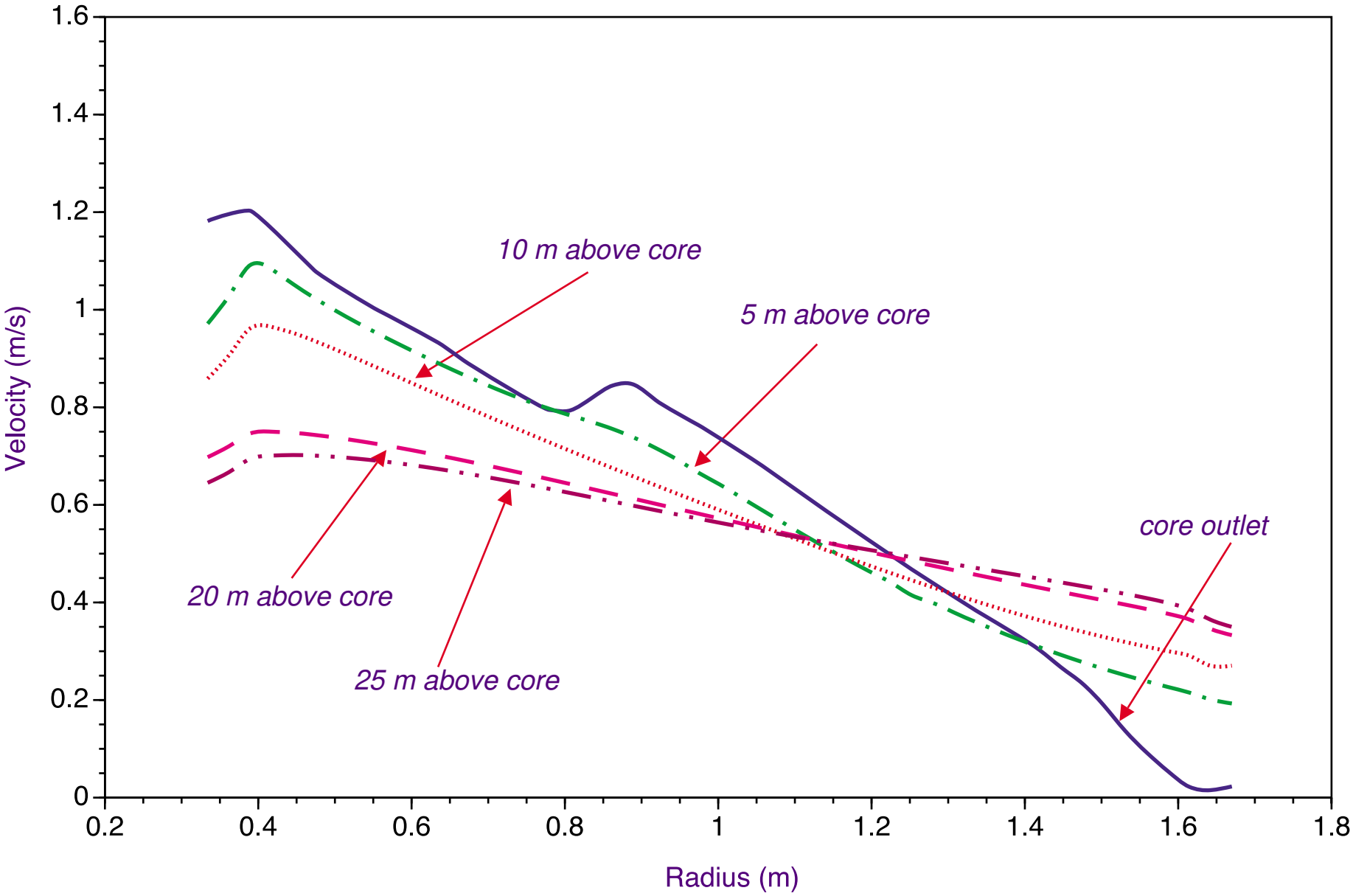
1.6
1.4
1.2
1
0.8
0.6
0.4
0.2
0
Velocity (m/s)
0.2
0.4
0.6
0.8
1
1.2
1.4
1.6
1.8
Radius (m)
10 m above core
5 m above core
core outlet
20 m above core
25 m above core

Figure 5.12

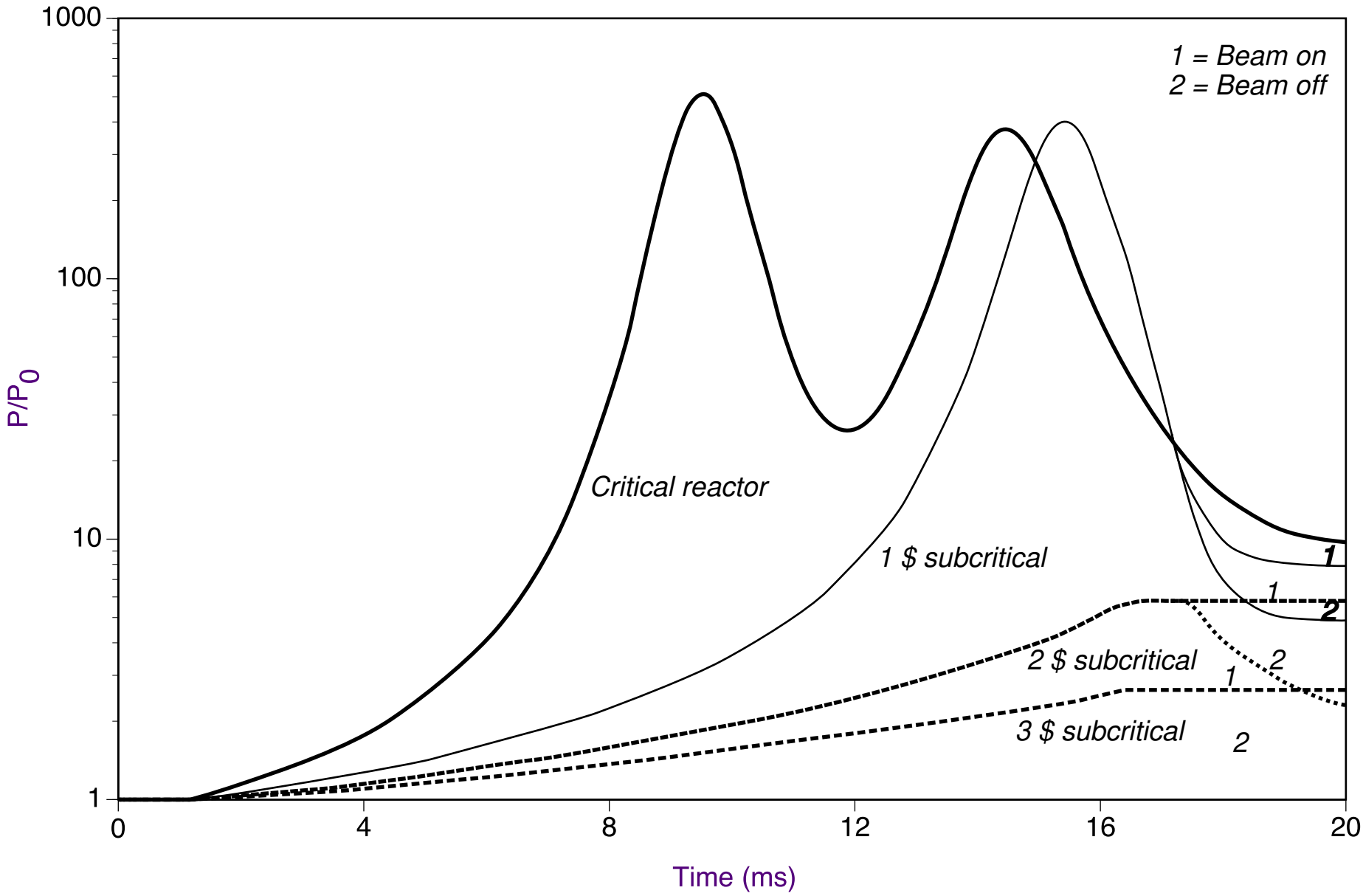
1000
100
10
1
P/P0
0
4
8
12
16
20
Time (ms)
1 = Beam on
2 = Beam off
Critical reactor
1 $ subcritical
2 $ subcritical
3 $ subcritical
1
2
1
2
1
2

Figure 5.13

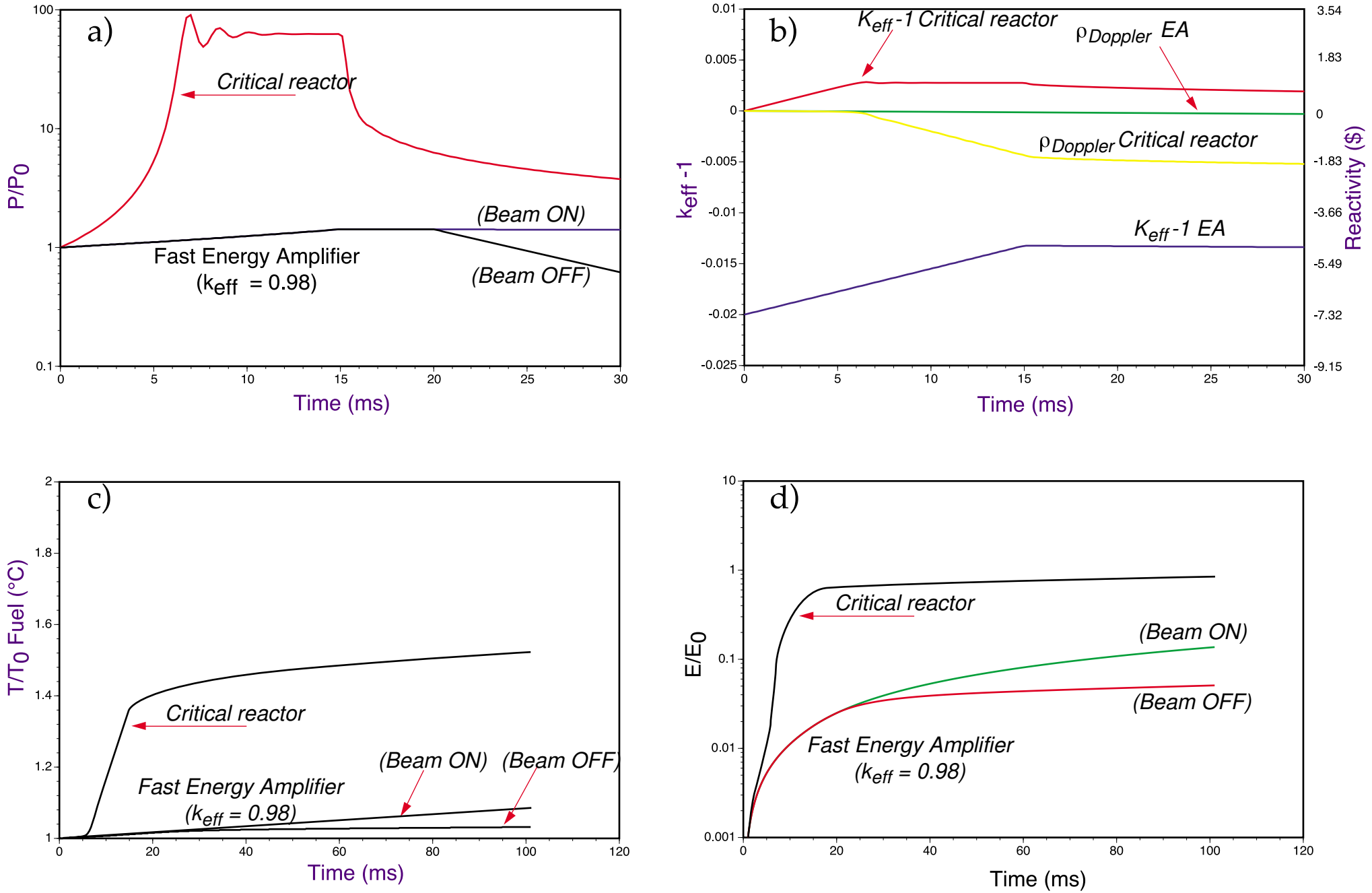
a)
Critical reactor
(Beam ON)
Fast Energy Amplifier
(keff = 0.98)
(Beam OFF)
P/P0
Time (ms)
b)
Keff -1 Critical reactor
ρDoppler EA
ρDoppler Critical reactor
Keff -1 EA
keff -1
Reactivity ($)
Time (ms)
c)
Critical reactor
(Beam ON)
(Beam OFF)
Fast Energy Amplifier
(keff = 0.98)
T/T0 Fuel (°C)
Time (ms)
d)
Critical reactor
(Beam ON)
(Beam OFF)
Fast Energy Amplifier
(keff = 0.98)
E/E0
Time (ms)

Figure 5.14

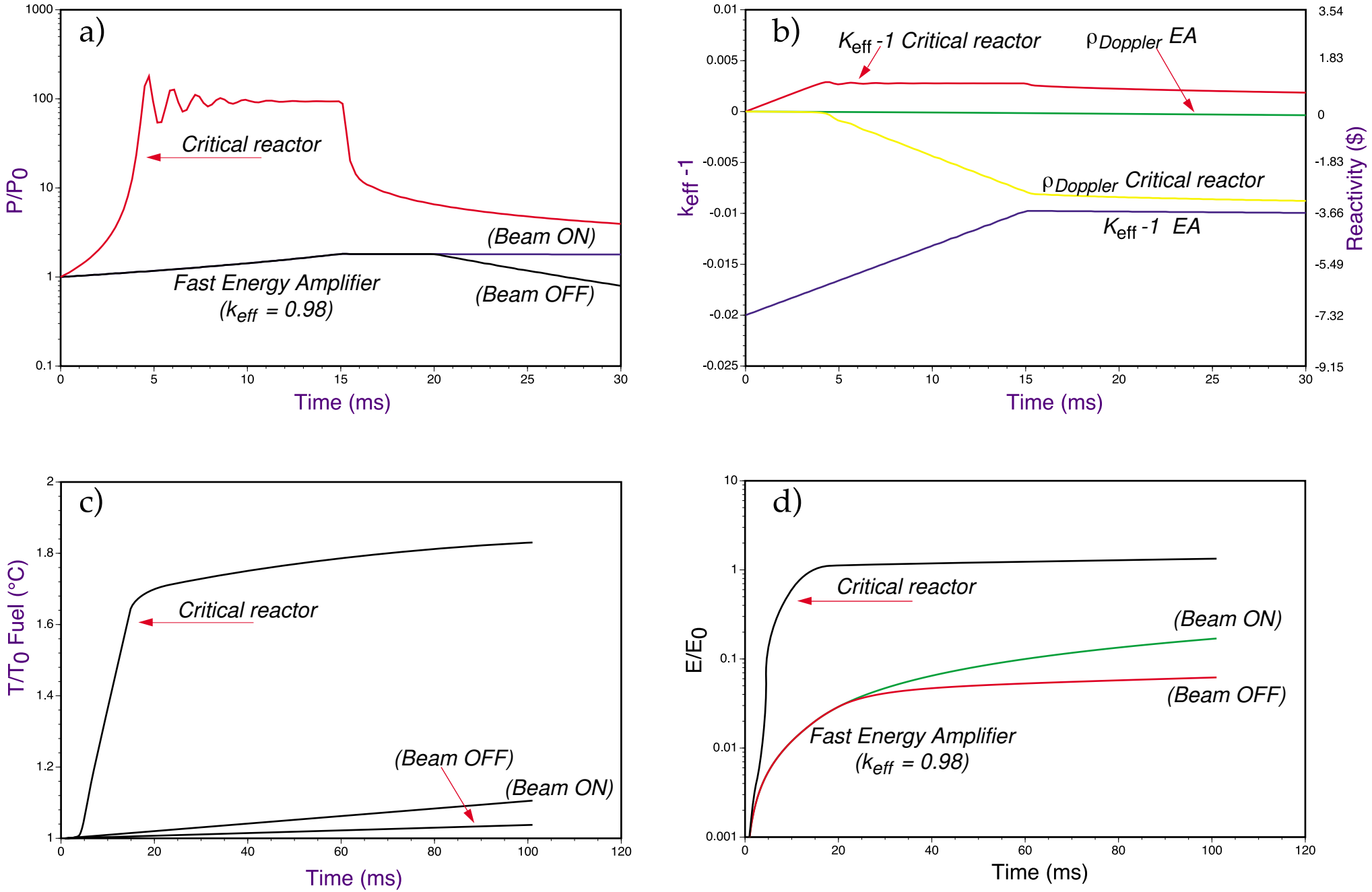
a)
P/P0
Critical reactor
(Beam ON)
Fast Energy Amplifier
(keff = 0.98)
(Beam OFF)
Time (ms)
b)
Keff -1 Critical reactor
ρDoppler EA
ρDoppler Critical reactor
Keff -1 EA
keff -1
Reactivity ($)
Time (ms)
c)
T/T0 Fuel (°C)
Critical reactor
(Beam OFF)
(Beam ON)
Time (ms)
d)
E/E0
Critical reactor
(Beam ON)
(Beam OFF)
Fast Energy Amplifier
(keff = 0.98)
Time (ms)

Figure 5.15

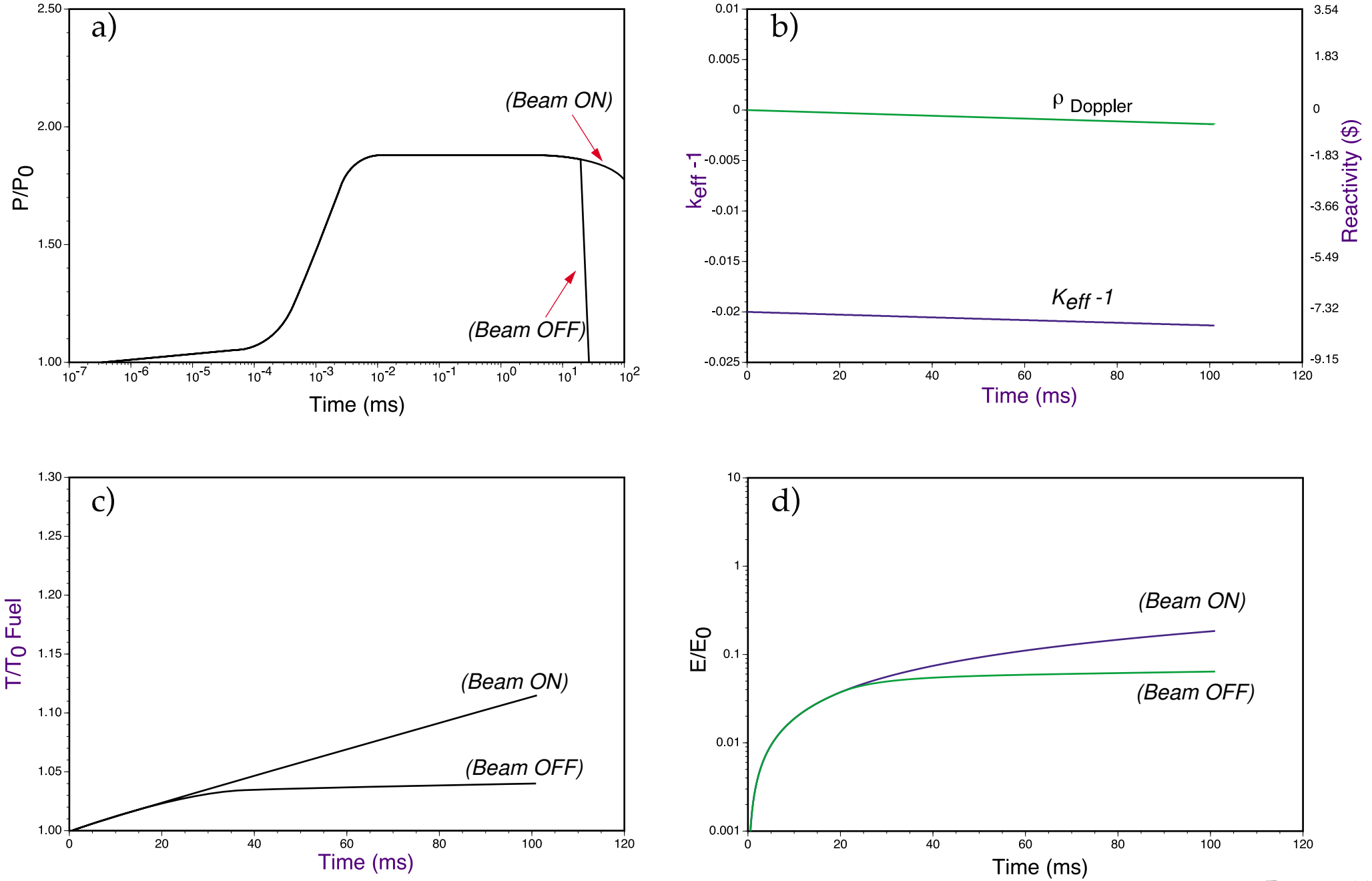
a)
P/P0
Time (ms)
(Beam ON)
(Beam OFF)
b)
keff -1
Reactivity ($)
ρ Doppler
Keff -1
Time (ms)
c)
T/T0 Fuel
(Beam ON)
(Beam OFF)
Time (ms)
d)
E/E0
(Beam ON)
(Beam OFF)
Time (ms)

Figure 5.16

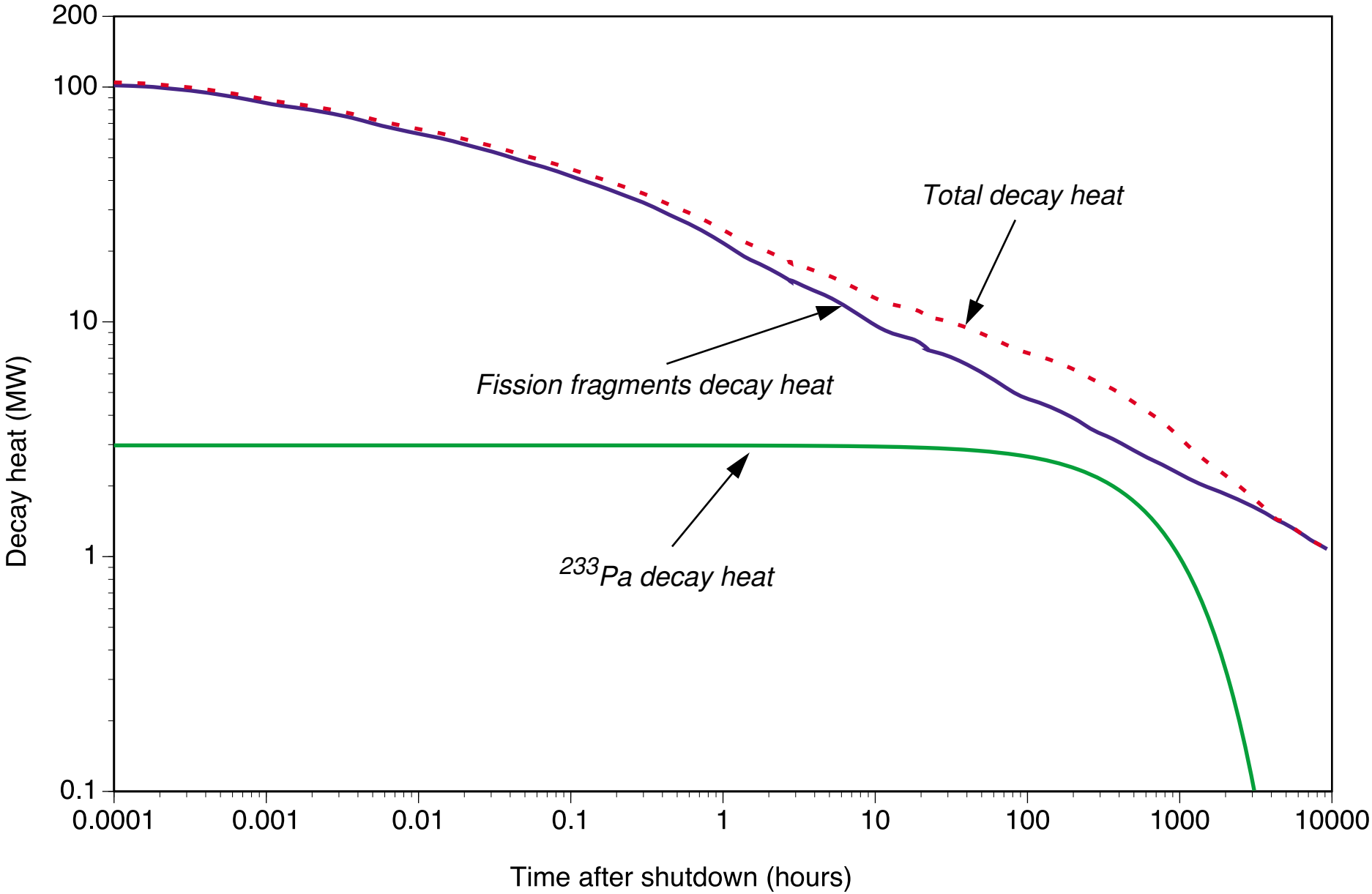
200
100
10
1
0.1
Decay heat (MW)
0.0001
0.001
0.01
0.1
1
10
100
1000
10000
Time after shutdown (hours)
Total decay heat
Fission fragments decay heat
233Pa decay heat

Figure 5.17

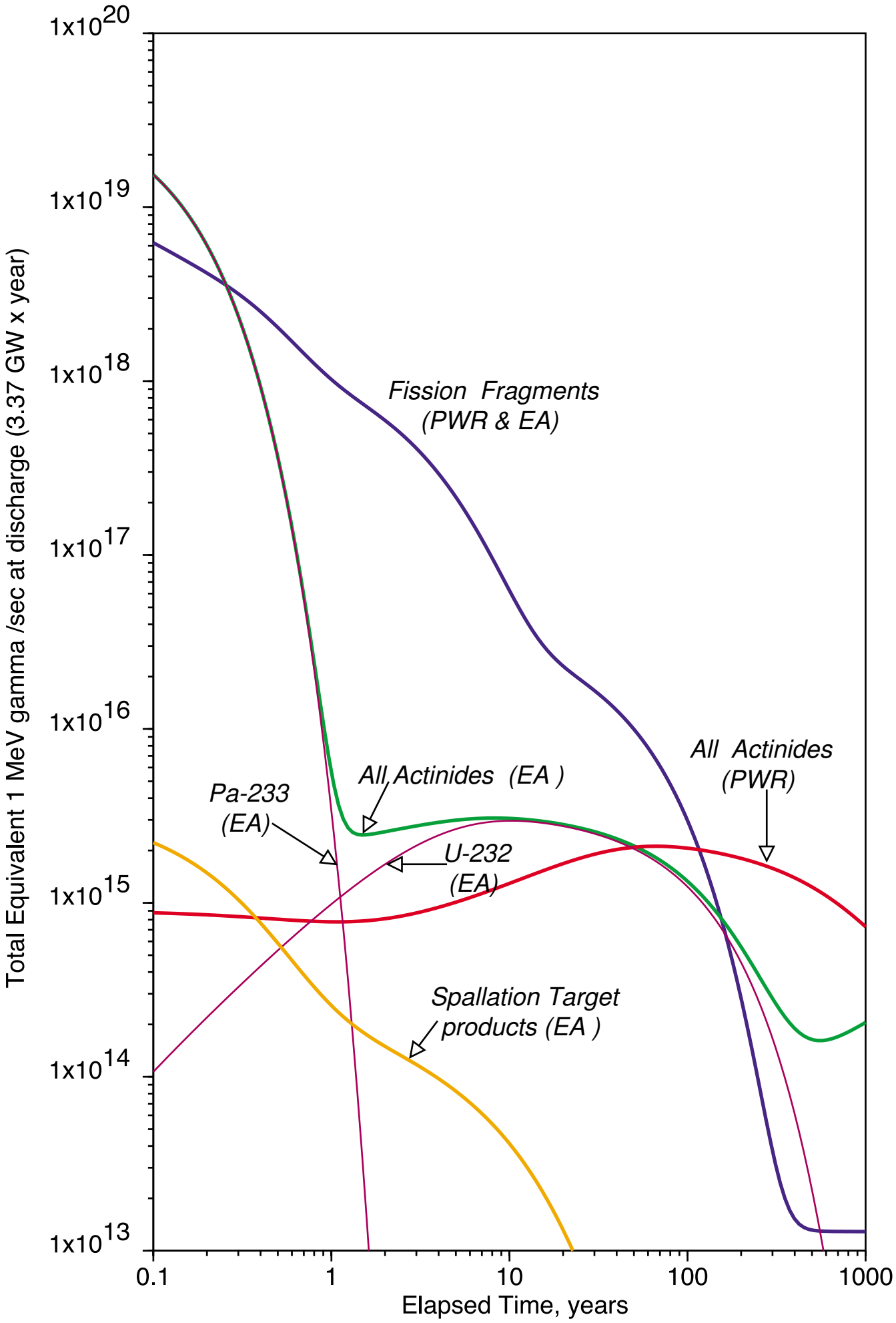
1x10^20
1x10^19
1x10^18
1x10^17
1x10^16
1x10^15
1x10^14
1x10^13
Total Equivalent 1 MeV gamma /sec at discharge (3.37 GW x year)
0.1
1
10
100
1000
Elapsed Time, years
Fission Fragments
(PWR & EA)
All Actinides (EA)
All Actinides
(PWR)
Pa-233
(EA)
U-232
(EA)
Spallation Target
products (EA)

Figure 5.18

6. — Closing the Fuel Cycle.

6.1 - General Considerations. There are significant, conceptual differences between what one means by "reprocessing" in the case of a PWR and an EA. In the case of a PWR, the primary purpose of reprocessing — if one excludes recovery of Plutonium for military applications — is the one of preparing for a more orderly, definitive repository of the radio-toxic products, separating for instance Actinides from FFs. Many conceptual designs have been proposed for the purpose of further healing the strong radio-toxicity of such individual products with nuclear transformations with the help of neutrons from Accelerators and Reactors. We shall mention as our reference case the project CAPRA [23] in which one intends to reduce the radio-toxicity of the Plutonium from spent fuels by about a factor 30 with the help of Fast-Breeders similar to SuperPhénix. In addition to producing a large amount of electric energy, one such device could process Plutonium and eventually Americium produced by about five ordinary PWRs.

In the case of the EA, at "replacement" time the fuel itself (Actinides) is still perfectly sound and it could continue to burn much further if it were not for the neutron absorption due to the accumulated FFs. Hence after a "reprocessing", which is in fact basically a "FF separation and disposal", the fuel can and should be used again. This is a fundamental difference with a PWR, where spent fuel is hardly more than waste material and for which reprocessing is arguable. In the case of an EA, fuel reprocessing could be better described as <u>fuel regeneration</u>. The purpose of such a procedure is

(1) to remove the poisoning FFs;
(2) to add the fraction of the Thorium fuel which has been burnt;
(3) to re-establish mechanical solidity to the fuel and the cladding which has been affected by the strong neutron flux.

In nuclear power generation, radioactive materials must be isolated at all times from the environment with an appropriate, multiple containment. The residual radio-toxicity is defined as the toxicity of products extracted from such a closed environment. Since the bulk of the Actinides are recycled inside the core for further use, the relevant toxicity is basically the one which is spilled out during the fuel regeneration process and the one of the elements which are deliberately removed, like for instance the one of the FFs which are not incinerated and of the sleeves which contain the fuel which are not reused. This is in contrast with an ordinary PWR — at

least if no incineration is performed — in which the totality of the radio-toxicity of the spent fuel constitutes "Waste" and it must be isolated from the environment by a Geologic Repository over millions of years.

6.2 - Strategy for the Spent Fuel. The main requirement of the reprocessing of the fuel from the EA is the one of generating a new fuel free of FFs. Therefore reprocessing is inevitable in our conception of the EA. In practice one must separate the Fuel into two different stock piles, the first destined to the next fuel load and the remainder which is usually called the high activity stream (HLW). The bulk of the Actinides are to be recycled into new fuel and they belong to the former stockpile. There is no need to worry about their long lasting consequences, since they will be burnt in the successive, cycles. The latter stockpile will contain all fission fragments and activity in the cladding plus the tiny fraction f of Actinides which is not separated by the reprocessing. They represent a considerable radio-toxicity, which will be handled either with natural decay or with active incineration of some specific radio-nuclides. Figure. 6.1 gives the ingestive radio-toxicity [31] of such a high activity stream assuming $f = 1.0\times10^{-4}$ (the choice of such a value will be clearer later on). The total radio-toxicity of a PWR initially loaded with 3.3% enriched Uranium and without reprocessing is also shown for comparison. Data are given for the fuel discharge after the first fill and for asymptotic fuel composition. The two distributions are very similar, since the fuel remaining radio-toxicity at long times is dominated by the ^{233}U contamination which is the same for all fillings. After a large drop over the first ≈ 500 years due to the decay of medium lifetime FFs (^{90}Sr-^{90}Y, ^{137}Cs), the ingestive radio-toxicity stabilises to a roughly constant level, dominated by the truly long lived FFs (^{129}I, ^{99}Tc, ^{126}Sn ^{135}Cs, ^{93}Zr and ^{79}Se) and to a lower extent by the residual fraction f of Actinides. After such a cooling-off time the residual radio-toxicity is comparable to the one of the ^{232}Th in the EA and about 5×10^{-5} times smaller than the one of a throw-away PWR of equivalent yield. The α-activity is very modest since it is dominated by the leaked fraction f of Actinides.

Inspection of Figure 6.1 suggests that the HLW should be stored for about 500 ÷ 700 years in what we call the "Secular Repository". Beyond such period, the residual radio-toxicity is considerably reduced as shown in Figure 6.2. The specific FFs contributing to radio-toxicity after 1000 years are listed in Table 6.1. It is possible to consider at this point the surviving radiation as Class A (10 CFR 61) for surface storage material even if the waste material will remain buried and provided it is diluted in ≥ 1000 $m^3/(GW_e \times year)$.

It is possible to further reduce the activity of the residual waste by extracting some or all the sensitive elements of Table 6.1 and "incinerating" them with neutrons in the EA. A more detailed paper on incineration is in preparation [78] and an experiment is in preparation at CERN [6], since most of the relevant cross sections are poorly known. Here we shall limit our considerations to the ones on general strategy. Three possible further steps are possible:

1) Technetium and Iodine are chemically extracted and incinerated. The first is a pure ^{99}Tc isotope and the second besides ^{129}I contains about 33% of stable isotopes which are kept in the incineration stream. The total mass to be incinerated is about 19 kg/($GW_e \times$ year), which is modest. The ingestive radio-toxicity of the remainder after 1000 years is reduced from 63.4 kSv to 16.2 kSv and the Class A dilution volume from 1194 m^3/($GW_e \times$ year) to 68 m^3/($GW_e \times$ year).
2) Procedure as point 1) but also Caesium is chemically extracted. The amount of Caesium is much larger, ≈ 100 kg/($GW_e \times$ year). In addition isotopic separation is necessary in order to separate the 34 kg/($GW_e \times$ year) of ^{135}Cs from the very radio-toxic (3.92×10^6 Sv) but shorter lived ^{137}Cs. This may be difficult, although a feasibility study has been carried out [79]. After incineration of ^{135}Cs, the ingestive radio-toxicity after 1000 years of the remainder is reduced to 6.3 kSv and the Class A dilution volume to 29 m^3/($GW_e \times$ year).
3) Procedure as point 2) but also Zirconium and Tin are chemically extracted. Both elements require isotopic separation. One of the other isotopes of Tin is radioactive and slightly toxic. In this way the only known long lived isotope left in the discharge is ^{79}Se (0.3 kg) which represents 0.745 kSv and the ridiculously small Class A dilution volume of 0.6 m^3/($GW_e \times$ year).

These procedures (Figure 6.3) will ensure that the radio-toxicity of the FFs in the "Secular Repository" is exhausted in less than 1000 years, which is a sufficiently short time to be absolutely confident that current technologies of vitrification and of containment can make the storage totally safe.

In addition to the FFs, in the High Level Stream there will be leaks of Actinides due to the imperfections of the reprocessing. These radio-nuclides are more worrisome since some of them are important α-emitters. The radio-toxicity and the α-activity in Ci for leaked fractions $f = 10^{-4}$ and $f = 2 \times 10^{-6}$ are displayed in Figure 6.4 and in Figure 6.5 respectively. The radio-toxicity has two maxima or "bumps", the first roughly for time span of the secular repository and a second for very long times, namely $10^5 \div 10^6$ years. The second maximum is due to ^{233}U and its descendants.

The first bump in the toxicity in the early fillings is due to ^{232}U and it grows substantially in the later fillings and in the asymptotic fuel composition because of the increased presence of ^{238}Pu and its descendants. The α-activity is instead always determined by the ^{232}U and its descendants at short times and by ^{233}U and its descendants at long times. The total α-activity of Actinides is about 10^5 Ci, for a fuel mass of the order of 22 tons, which corresponds to an average activity of about 5 mCi/g. Note that the activity of Thorium which is the largest mass is very small and that if Uranium's are separated out they will have a specific activity which is about ten times larger than the bulk of the spent fuel.

6.3 - Fuel reprocessing methods. In our case production of the lighter Neptunium and Plutonium isotopes is very low and higher actinides are nearly absent. However the (n,2n) reactions, more probable at high energies, increase the amount of highly toxic ^{231}Pa and ^{232}U.

The EA requires the recovery of the Uranium (^{233}U). However, it offers the opportunity of destroying the other Actinides by concentrating them, after each discharge, in a few dedicated fuel bars (targets) inserted somewhere in the bundles of ordinary fuel, where an incineration lifetime of years is at hand. The amount of leaking Actinides in the High activity Waste stream destined to the Secular repository must be a small fraction $f \leq 10^{-4}$ of the produced amount. If incineration of the long lived FFs is performed to alleviate the radio-toxicity of the stored products after 500 years, an even higher performance in separating power is advisable, $f \leq 2.0 \times 10^{-6}$. The efforts in order to attain such a figure is justified by the considerable benefit attained by the practical elimination of the "Geologic times Repository". We remark that such an incentive has been so far absent.

Two methods have been considered and appear suitable to our application: (1) aqueous methods, presently in use and (2) the newly developed pyro-electric method. We shall review both of them in succession.

Aqueous reprocessing methods have proven to be efficient, particularly for the separation of U and Th (99.5% and higher). The best known example is the THOREX process, based on solvent extraction through the use of tributyl phosphate (TBP), which extracts and separates the Thorium and Uranium. Other Actinides can also be extracted although their concentrations are so low that the extraction efficiency will be lower.

Figure 6.6 describes schematically the overall fuel cycle. The fuel rods should be stored for cooling at least for one year, to allow the ^{233}Pa to decay to ^{233}U. Fuel rods are then sheared and chopped. The gaseous fission products will be accumulated, with in particular attention for the ^{85}Kr and $^{14}CO_2$ which are destined to the secular repository. Dissolution should be made with a mixture of nitric acid (HNO_3) and hydrofluoric acid (HF) since ThO_2 is a very refractory ceramic material. The HF concentration should not be higher than 0.1 M and the addition of aluminium nitrate $Al(NO_3)_3$ as reagent could be needed in order to avoid corrosion of the stainless steel dissolver. Before carrying out the solvent extraction process from the obtained liquids they should be cleared of the remaining solids. The main components of the liquid will then be Thorium, Uranium, Fission Products, Protactinium and other trans-uranic Actinides.

The classic process to carry out the separation of Th and U from fission fragments is the acid THOREX. It uses TBP 30% v/v diluted with an organic solvent like dodecane. The partition of U from Th is done by washing the organic phase with diluted nitric acid. The U stream will also contain the very small amount of Pu and some contamination of Th and FF. The contamination of the Thorium stream will be mainly FF. The high active liquid waste stream will mainly contain FF, trans-uranic Actinides (^{231}Pa, ^{237}Np) and some residual contamination of Th and U. Further cycles for purification of Uranium and Thorium should be applied using TBP as extractant.

There is little information on the recovery of Pa and it will possibly require some additional studies. Tests carried out at Oak Ridge have shown [80] that Pa could be absorbed from solutions with high content of nitric acid by using various absorbents like unfired Vycor glass, silica gel or Zirconium phosphate. Its extraction should be done from the high level waste stream. Relative to the other Actinides its extraction will be less efficient since their concentration in the Highly Radioactive liquid Waste stream, although it can and should be increased, will nevertheless be very low.

The performance quoted in Figure 6.6 is above the current values according to standard experience on the THOREX process [13], [81], but appropriate tuning of the chemical parameters should allow higher efficiencies. The minimisation and ultimate disposal of High-Level radioactive Waste (HLW) generated from the reprocessing of spent fuel (THOREX) is an important part of the global nuclear fuel recycling strategy proposed in the framework of the Energy Amplifier Concept, as an alternative to classical disposal methods. The goal is twofold, (i) to recover from the

insoluble residue useful metals such us Ru, Rh and Pd; (ii) and to separate Actinides[45] and some of the LLFPs (Long-Lived Fission Products) for their further use (incineration) or disposal. We believe this can best be achieved with the method developed in the context of the IFR (Integral Fast Reactor) programme [82], where it is proposed to separate actinides[46] and FPs from HLW by dry process with pyro-chemical (or pyro-metallurgical) methods (Figure 6.7). However, the only process that has reached an industrial scale is, at least for the moment, the PUREX process (aqueous method) which has already been described in the previous paragraphs. All the other methods are still in the technical or laboratory development phase.

Figure 6.8 shows the flow diagram of the dry process for partitioning of Actinides [83]. This process consists of (i) denitration to obtain oxides, (ii) chlorination to oxide to chlorides, (iii) reductive extraction to reduce Actinides from molten chlorides in liquid cadmium by using lithium as reductant, and (iv) electro-refining to increase the purity of Actinides recovered. Both denitration and chlorination steps are pre-treatment processes prior to the application of the pyro-metallurgical process.

The principle of the reductive extraction with the subsequent step of electro-refining is schematically drawn in Figure 6.9. The electro-refiner is a steel vessel that is maintained at *775 K (500 ^{o}C)*. Liquid LiCl-KCl electrolyte in the electro-refiner contains about *2 mol%* of the Actinide chlorides. The Actinide solution (in liquid cadmium) is inserted into the electrolyte and connected to the positive pole of a dc power source (anode). The negative pole of the power source is connected to a cathode immersed in the same electrolyte. The cathodes are simple steel rods. About *80%* of the Actinide metals is electro-transported from the anode to the cathode rods, where it deposits as nearly pure metal along with a relatively small amount of rare earth fission products[47]. All the products are retorted to remove salt (and Cadmium from the Cadmium electrode). Ingots from the retort are blended to appropriate composition, and recast into special fuel pins. The fission products, with the exception of Tritium, Krypton and Xenon, accumulate in the electro-refiner during processing, and some noble metal fission products are removed with the anode after each batch of fuel has been processed. The three gases are released into the process

[45]In the F-EA, the Actinide residue consists mainly of Thorium, Protactinium, Uranium and a very small amount of TRUs, whereas in a PWR it is mostly TRUs.

[46] We expect this method can be extendedto the extraction of Thorium and Protactinium.

[47] In reprocessing F-EA fuel, the complete removal of fission products may not be necessary since their effect on the neutron economy is much less in a fast neutron spectrum than it is in a thermal spectrum.

cell which has an argon atmosphere. They are recovered at high concentrations by the cell gas purification system.

Several dozen batches of fuel are processed in a "campaign". At the end of a campaign, the salt in the electro-refiner is treated by a series of steps to remove active metal fission products, particulate noble metals, and any oxide or carbide impurities for incorporation in high-level waste forms. The salt and its associated Actinide chlorides are returned to the electro-refiner. The Actinide inventory in the electro-refiner amounts to about *20%* of the Actinide elements fed; this must be recovered to achieve more than *99.9%* overall Actinide recovery. A non-metal and a metal waste form will accommodate all of the high-level wastes. The non-metal waste form will contain Samarium, Europium and Yttrium; the halogens and chalogens; the alkali, and alkaline earth fission products; and a small amount of excess salt generated in the process. The Actinide content of that waste form will be exceptionally low (less than 1 part in 10^6 of the Actinides in the fuel that is processed). The only significant long-lived activity in this waste will be Se-79, I-129 and Cs-135: the total alpha activity should be less than *10 nCi.* g^{-1}. Metal wastes from the electro-refiner - noble metals, cladding hulls and salt filter elements - will be combined with any process scrap such as broken electrodes and the rare earths from the salt purification process in the metal waste form. The metal waste form will have a very low Actinide content, because of the effective Actinide recovery in the pyro-metallurgical process, but its Actinide level will not be quite as low as that of the non-metal waste form. This whole process can be made continuous, and thus can take place in a matter of only a few hours.

Pyro-processing offers a simple, compact means for closure of the fuel cycle, with anticipated high decontamination factor *(> 99.9%)*, minimal production of high-level radioactive waste, and significant reductions in fuel cycle costs. In addition, mainly from the weapons proliferation viewpoint, it offers an advantage over the PUREX and/or TRUEX methods, in that there is only partial removal of the fission products. Even though the process is based on the use of a metallic fuel alloy with nominal composition U-20Pu-10Zr, we believe it can be readily adapted to the EA fuel cycle without much efforts.

The final content of the HLW stream coming from the EA fuel reprocessing is mainly FFs, with only traces of Actinides. The volume generated is about 5 m^3 per ton of fuel. The following step is to concentrate the aqueous raffinate and to transfer it to an intermediate storage of the reprocessing plant. The volume of the concentrate will be about 1 m^3/t. of fuel and the usual intermediate storage are tanks of suitable

stainless steel such as to minimise the acid waste corrosion. To prevent the highly active liquid from boiling a redundant cooling system is required. Then, the concentrate is cooled for a period of about 10 years in order to reduce the heat generation by more than an order of magnitude before proceeding to waste solidification. Among the fission fragments, excluding the short lived and stable elements, there are a few elements which are medium lived (30 years, ^{90}Sr, ^{90}Y, ^{137}Cs, etc.) and some others (^{99}Tc, ^{135}Cs, ^{129}I, etc.) which are long lived (Table 6.1). Since Actinides are essentially absent from the HLW concentrates the policy we proposed to follow is to store in man-watched, secular repositories for several centuries the medium lived, in order to isolate them from the biosphere and to promote a vigorous research and development of methods for incinerating the bulk of the long lived FFs. The EA is an efficient tool to incinerate these wastes at the price of fraction of the neutron flux [6], but alternatively dedicated burners can be used.

In parallel with the R&D on incinerators, development on solvent extraction methods of long lived FF, which in some cases may additionally require isotopic separation, should be promoted, the goal being to virtually eliminate the need for Geological Repositories.

After the concentrates will be cooled down for the 10 years period and the long-lived FF extraction applied for later incineration the wastes will be solidified by using well known techniques. For instance by calcination and vitrification. The first step allows to get waste oxides and in the second step glasses are obtained by melting the waste oxides together with additives such as SiO_2, B_2O_3, Al_2O_3, P_2O_5, Na_2O, and CaO. Borosilicate glass is the most studied solidification product but others like phosphate glass, glass ceramic, etc. are also used. When the solidification process is finished the wastes are ready for disposal in the appropriate secular repositories.

6.4 - Spallation induced Radio-nuclides. In addition to the radioactive waste produced in the Fuel and in a minor extent in the Breeder, substantial amounts of radio-nuclides are produced by the spallation target. As pointed out they divide roughly into two batches, those which remain inside the molten Lead and those which are either gases or volatile and which can be found in the neutral filling gas of the main vessel. These last compounds are collected from the gas and stored in an appropriate way in order to avoid leaks in the biosphere (paragraph 5.8). The relative ingestive radio-toxicity of the various components of the Spallation target are given in Figure 6.10. Following Table 5.9 spallation products at 700 °C can be broadly divided into three different categories namely (1) gases or vapours in which

the contribution of ^{194}Hg (751.9 y, 123 g/(GW$_e$ × year)) is largely dominant in size and duration; (2) volatiles which, after a few years, are essentially dominated by to ^{204}Tl (5.466 y, 114 g/(GW$_e$ × year)), (3) inter-metallic combinations (alloys) with the molten Lead which at short times, shows a leading contribution from ^{90}Sr and, at longer times by ^{202}Pb (7.59×10^4 y, 614 g/(GW$_e$ × year)). The radio-toxicity of the spallation products is by no mean negligible: at early times it is about 10^{-3} of the total radio-toxicity produced. At the end of the Secular repository time for FFs, the effects of ^{194}Hg exceed all other contributions until about 2,000 years. There is no major difficulty in extending safely and economically the storage of about 2.3 kg/(GW$_e$ × year) of Mercury collected as vapours from the top main Vessel up to about 2000 years. Note that at least in the present design, the molten Lead of the Target region is directly mixed with the big volume (≈ 1000 m^3) which constitute the main coolant. Therefore at least the elements which remain inside the liquid are largely dispersed. They will follow the fate of the Lead at the time of final decommissioning of the installation.

We finally remark the existence of another lead isotope, ^{205}Pb (2.21×10^7y) which is abundantly produced by neutron capture of ^{204}Pb, namely 3.54 kg/(GW$_e$ × year) in the target region and 23.15 kg/(GW$_e$ × year) in total, and fortunately it is also rather inoffensive, since it is very long lived and it decays by K-conversion with an energy release of 51 keV mostly in the form of neutrinos.

6.5 - Radio-toxicity emitted in the Environment. Nuclear power production is based on the concept that pollutants and toxic materials are retained within the plant and in total isolation from the biosphere. The limited mass of such products makes it possible to achieve such a goal. Mining process however cannot retain all products and a significant amount of radiation is emitted in the biosphere during preparation of the fuel. Likewise in the reprocessing of the spent fuel some radioactive elements are currently re-emitted in the biosphere. Finally the ultimate storage of such materials (geologic repository) have raised some question on the ability of isolating them from the biosphere for times which largely exceed what can be considered an experience based retention. The EA concept strongly reduces such environmental impacts, when compared to the present reactor technology. We examine these points in turn.

(1)- *Mining.* Thorium is largely present in the Earth's crust, but in small concentrations. In addition several minerals exist, which have an excellent concentration of Thorium and which can be exploited economically. The

primary choice is the monazite, which is a phosphate of Cerium and other lantanides, containing a variable amount of Thorium and Uranium in a solid mixture. Usually the Thorium concentration is of the order of 10% but some mineral may reach as much as 20% by weight. Uranium minerals are usually much less rich, its concentration being in the best cases of the order of 0.2%. Incidentally one can remark that the solubility of Thorium is 1000 times smaller than the one of Uranium. Taking into account that Thorium burnt in the EA has an energetic yield which is 250 times larger than one of natural Uranium destined to PWRs, we conclude that the relative mining effort is reduced by a factor of the order $250 \times 50 = 12500$ times for a given produced energy. Starting with mineral containing 10% of Thorium by weight we need to dig only 70 tons of mineral to produce $GW_e \times$ year. For comparison and for the same energy produced the standard PWR methodology would require $0.875\ 10^6$ ton of mineral. In the case of Coal, the mass of fuel (TEC) is $4.24\ 10^6$ ton.

A pure Thorium mineral out of which the totality of Thorium is extracted will produce tailings with a negligible radio-toxicity after some sixty years, since all descendants of ^{232}Th have short decay lifetimes. Their evolution is governed by the 5.7 year half-life of ^{228}Ra. Furthermore there will be no risk associated to Radon, since ^{220}Rn has a half-life of 55.6 seconds and it decays before escaping the minerals. As pointed out by Schapira [5] the situation in reality is somewhat more complex, mainly because the monazite, which is the primary source of Thorium is generally mixed with some Uranium contamination. Such a contamination is strongly source dependent, as shown in Table 6.2, taken from Ref. [5]. Assuming somewhat pessimistically that the Uranium content is about 10% of the one of Thorium and that the long lived toxicity and Radon contamination are primarily due to Uranium, we conclude that the radio-toxicity produced at the mine is in the case of an EA about 250 / (10% = 2500 times smaller than the one of today's PWR for a given energy produced.

The UNSCEAR report [7] has estimated that the level of exposure of individuals to mining for today's PWRs amounts to about 1.5 man Sv $(GW\ y)^{-1}$ as local and regional component and to 150 man Sv $(GW\ y)^{-1}$ as global component. We remark that according to the same report the production of electricity from Coal is estimated to result in a global collective dose of 20 man Sv $(GW\ y)^{-1}$. The practice of using coal ashes for production of concrete will add as much as 20,000 man Sv $(GW\ y)^{-1}$. Values relative to Thorium and its use in the EA for some possible mineral sources are listed in

Table 6.2. We conclude that the typical radiation exposure to public with the EA due to mineral mining for the same energy produced are much smaller than today's PWRs and also Coal burning, even if solid ashes are correctly handled.

The same report estimates the collective dose due to initial Uranium enrichment and fuel fabrication to as little as 0.003 man Sv $(GW\ y)^{-1}$. In the case of the EA it is expected to be at least 1/4 of such a number, since the burn-up is four times longer and there is no isotopic separation, The collective doses are negligible in both cases.

(2) -*EA Operation.* During the EA operation the fuel and the spallation target volumes are kept strictly sealed. Indeed also for proliferation protective measures it is recommended that such volume be opened only in occurrence with the re-fuelling, namely once every about five years and only by a specialised team. While the fuel is safely sealed, the Lead coolant produces a significant amount of radioactive products, some of which remain in the liquid phase, but others are either gaseous or volatile and are found in the neutral gas (Helium) with which the main Vessel is filled. These volatile compounds are summarised in Table 6.3, extracted from Table 5.9. Some of these are noble gases and Tritium which remain gaseous at room temperature. Other, mostly Mercury and Thallium can be condensed and preserved in the solid state. Some other elements will be collected by the Lead purifier. In view of its small amount involved we believe that the gaseous elements can be released in the atmosphere. The collective effective dose per unit energy release is given by the UNSCEAR report [7] and summarised in Table 6.4. It is assumed that gases are released every 6 months, without cool-down period. A short cool-down will dramatically reduce the effects of ^{127}Xe (52.63 d) and it is recommended. The total local and regional doses are 0.42 man Sv $(GW\ y)^{-1}$. The global doses, integrated over 10,000 years, following the convention of Ref. [7] are of 0.18 man Sv $(GW\ y)^{-1}$. Both values are dominated by the effects of Tritium.

The rest of the solid high activity waste from the spallation products (dominated by Mercury and Thallium) has a substantial ingestive radio-toxicity (Figure 6.10) and it should be carefully accumulated and destined to the repository.

(3)-*Fuel reprocessing* has to deal with the very large radioactivity of the spent fuel. Since the techniques are not different that those generally in use, we can

make direct use of the estimated collective doses of Ref. [7] (Table 6.5), taking into account the differences in stockpile of the radio-nuclides produced (see Table 5.8). It is however assumed that both ^{14}C and ^{85}Kr are extracted during reprocessing and sent to the repository for cool-down. Separation of ^{85}Kr can be performed cryogenically according to a well documented procedure [84]. Also ^{14}C once reduced in the form of CO_2 can be extracted on the same time by the same method.

The total doses to members of the public are summarised in Table 6.6. Total global dose truncated at 10,000 years is 0.6 man Sv $(GW\ y)^{-1}$, namely for the same energy produced about 0.003 of the one of an ordinary Reactors [7] — without counting occurred criticality and melt-down accidental releases, avoided by the EA, ($\approx$ 300 man Sv $(GW\ y)^{-1}$ — and about 0.03 of the alternative of Coal burning, even if solid ashes are correctly handled.

6.6 - Conclusions. Realistic schemes are possible in which the spent Fuel from the EA is "regenerated" for further uses. Separation of the fuel materials into two streams is performed, the Actinide stream destined to the fuel fabrication and the FFs stream which is destined to the Secular repository. After 500 years the radio-toxicity for unit energy produced of the EA is about 20,000 smaller than the one of a PWR with a "throw-away" cycle. Incineration with the help of neutrons of some of the critical, long lived radio-nuclides can strongly reduce the radio-toxicity of the waste beyond 500 years. If sufficiently diluted it could be also let "die away" without incineration since it can be made to satisfy the requirements for Class A repository. Note also that at that time the residual ingestive radio-toxicity is comparable with the one of the Thorium metal burnt in the EA.

An essential element in the clean disposal of the spent fuel is the small leakage of Actinides (mainly Uranium) into the FFs stream. A level of 100 ppm. or better is required. We believe that it is within the state of the art, eventually with a few improvements.

An important source of radio-toxicity are the spallation products due to the proton beam interacting with the molten Lead target. A specific element of concern is ^{194}Hg which is the main surviving source of toxicity of the EA in the period of time between 500 and 2000 years. It can either be preserved far from the biosphere that long or, alternatively, incinerated, following the fate of the Actinides inside the EA. Unfortunately the relevant cross sections are only poorly known but they should be measured soon [6].

An experimental test of the feasibility of incineration with neutrons in a Lead diffuser [6] is in preparation at CERN. Would it be successful it could offer the right technique in order to eliminate also the modest amount of long lived radio-toxic elements produced.

Likewise important is the total radioactivity doses to members of the public due to operation. Total global dose of the EA truncated at 10,000 years is estimated to be 0.6 man Sv $(GW\ y)^{-1}$, namely about 1/330 of the one of an ordinary Reactors for the same energy produced (200 man Sv $(GW\ y)^{-1}$)— without counting occurred criticality and melt-down accidental releases, avoided by the EA (≈ 300 man Sv $(GW\ y)^{-1}$) — and about 1/33 of the alternative of burning Coal (≈ 20 man Sv $(GW\ y)^{-1}$), even if solid ashes are correctly handled.

Table 6.1 - Fission fragments' activity after 1000 years of cool-down in the Secular Repository. Values are given for 1 $GW_e \times$ year.

Radio-Isotope	1/e Life years	Mass (kg)	Other Isotopes (kg)	Activity @ 1000 y (Ci)	Ingestive Toxicity (Sv) × 10^3	Dilution Class A (m^3)
^{129}I	2.27E+7	8.09	3.48	1.43	19.58	178.47
^{99}Tc	3.05E+5	16.61	—	284.29	27.67	947.65
^{126}Sn	1.44E+5	1.187	1.783	33.79	3.20	9.65
^{135}Cs	3.32E+6	34.12	66.77	39.32	9.87	39.32
^{93}Zr	2.21E+6	26.11	99.11	65.64	2.38	18.75
^{79}Se	9.40E+5	0.30	3.02	2.06	0.745	0.59

Table 6.2 - Uranium and Thorium content in percent [5] and levels of population exposure for typical Ores [7].

Source	UO_2	ThO_2	Ratio U/Th	Local Sv $(GW\ y)^{-1}$	Global Sv $(GW\ y)^{-1}$
Italy	15.64	11.34	1.38	8.28×10^{-3}	0.828
Sri Lanka	0.10	14.32	0.007	4.20×10^{-5}	4.2×10^{-3}
California	6.95	4.22	1.64	9.84×10^{-3}	0.984
India	0.29	9.80	0.029	1.74×10^{-4}	0.0174

Table 6.3 - Radio-nuclides emitted in the neutral gas inside the Vessel by the Spallation target and the molten Lead coolant (≈ 700 °C).

Gas at Room Temperature				
	Mass (g)	1/e Lifetime		Boils at °C
^{3}H	1.435	17.83	y	-252
^{39}Ar	0.336	389.0	y	-186
^{42}Ar	0.336	47.57	y	-186
^{81}Kr	5.777	0.331E+6	y	-153
^{85}Kr	4.326	15.55	y	-153
^{127}Xe	0.37 (675)[48]	52.63	d	-108

Solid at Room Temperature				
	Mass (g)	1/e Lifetime		Boils at °C
^{35}S	0.009	126.5	d	445
^{65}Zn	0.004	353.2	d	907
^{70}Zn	2.424	0.723E+15	y	907
^{73}As	0.329	116.1	d	615
				615
^{83}Rb	0.036	124.6	d	688
^{86}Rb	0.181	26.94	d	688
^{109}Cd	1.627	1.833	y	767
^{125}I	0.014	85.90	d	184
^{124}Sb	0.043	87.05	d	1585
^{125}Sb	0.404	3.988	y	1585
^{131}Cs	0.003	14.01	d	671
^{134}Cs	0.282	2.982	y	671
^{194}Hg	415.9	751.9	y	357
^{203}Hg	6.252	67.40	d	357
^{202}Tl	15.25	17.68	d	1473
^{204}Tl	386	5.466	y	1473
^{210}Po	0.995	200.1	d	254

[48] Total integrated production, without decay over 5 years

Table 6.4 - Normalised, collective effective dose from locally, regionally and globally dispersed radio-nuclei during operation over a period of 10,000 years.

	Normalised release (Tbq)	Collective dose per unit release (man SvTbq^{-1})[7]		Normalised collective Dose (man Sv (GW y)$^{-1}$)	
		Local & Regional[49]	Global[50]	Local & Regional	Global
^{3}H	521	0.0027	0.0012	0.418	0.185
^{14}C	—	0.40	85	—	—
^{39}Ar	0.430	$7.4\ 10^{-6}$	$5.0\ 10^{-4}$	$9.4\ 10^{-7}$	$6.38\ 10^{-5}$
^{42}Ar	3.268	$7.4\ 10^{-6}$	$6.1\ 10^{-5}$	$7.2\ 10^{-6}$	$5.91\ 10^{-5}$
^{81}Kr	0.004	$7.4\ 10^{-6}$	$1.8\ 10^{-2}$	$9.2\ 10^{-9}$	$2.24\ 10^{-5}$
^{85}Kr	63.6	$7.4\ 10^{-6}$	$2.0\ 10^{-5}$	$1.4\ 10^{-4}$	$3.77\ 10^{-4}$
^{127}Xe	3718.[51]	$7.4\ 10^{-6}$	$1.05\ 10^{-7}$	$8.2\ 10^{-3}$	$1.16\ 10^{-4}$
Totals	*4307*			*0.42*	*0.186*

Table 6.5 - Normalised released dose of airborne and liquid effluents of radio-nuclides during reprocessing of Fuel. Values have been normalised to current practices [7].

	Process (kg)	EA/ PWR	Normalised collective Dose (man Sv (GW y)$^{-1}$)		Comments
			Airborne Effluents	Liquid Effluents	
^{3}H	—	1.0	0.11	0.0012	assumed same as PWR
^{14}C	0.0145	9.2	(7.45)	—	Retained
^{85}Kr	21.64	10.16	(0.924)	—	Retained
^{129}I	27.28	1.722	0.430	—	standard practices
^{131}I	0.2924	0.458	$1.37\ 10^{-4}$	—	" "
^{137}Cs	118.5	1.109	0.0188	1.22	" "
^{90}Sr	74.76	1.578	—	0.205	" "
^{106}Ru	1.147	0.074	—	0.207	" "
Totals			*0.60*	*1.63*	

[49] For noble gases, values are taken to be the same as ^{85}Kr.

[50] For noble gases, values are taken to be the same ones as ^{85}Kr, for decay over 10,000 years.

[51] Periodic (every 6 months) release, without cool-down.

Table 6.6 - Summary of normalised, collective doses to members of the public from radio-nuclides released from the EA.

Source	Local and regional Doses (man Sv (GW y)$^{-1}$)	Global Doses (man Sv (GW y)$^{-1}$)
Mining[52], Milling, Fuel fabrication	$4.2\ 10^{-5} \div 9.8\ 10^{-3}$	$0.0042 \div 0.984$
EA operation	0.42	0.188
Reprocessing (Atmospheric)	0.60	0.1
Reprocessing (Aquatic)	1.63	0.1
Miscellanea[53]	0.1	0.05
Totals(variation over mining range)	*2.75 ÷ 2.76*	*0.44 ÷ 1.42*

[52] The dose range depends on the Uranium content in the Thorium mineral. We have taken extreme values of Table 6.1.

[53] This includes mainly Transportation, Fuel fabrication, Solid Waste disposal. Figures are taken from Ref. [7].

Figure Captions.

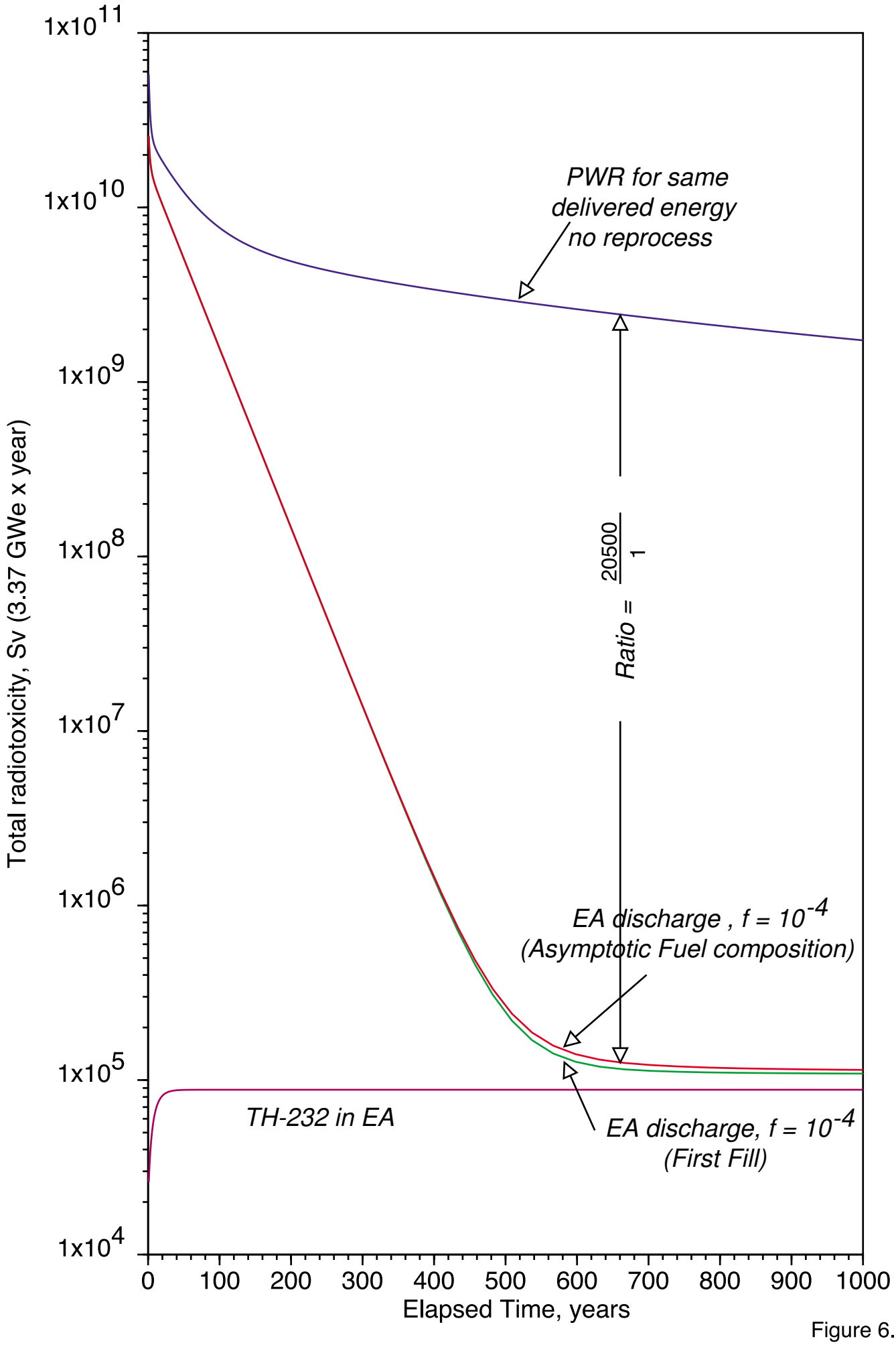
1x10^11
1x10^10
1x10^9
1x10^8
1x10^7
1x10^6
1x10^5
1x10^4
Total radiotoxicity, Sv (3.37 GWe x year)
0
100
200
300
400
500
600
700
800
900
1000
Elapsed Time, years
PWR for same
delivered energy
no reprocess
Ratio = 20500 / 1
EA discharge , f = 10^-4
(Asymptotic Fuel composition)
TH-232 in EA
EA discharge, f = 10^-4
(First Fill)

Figure 6.1

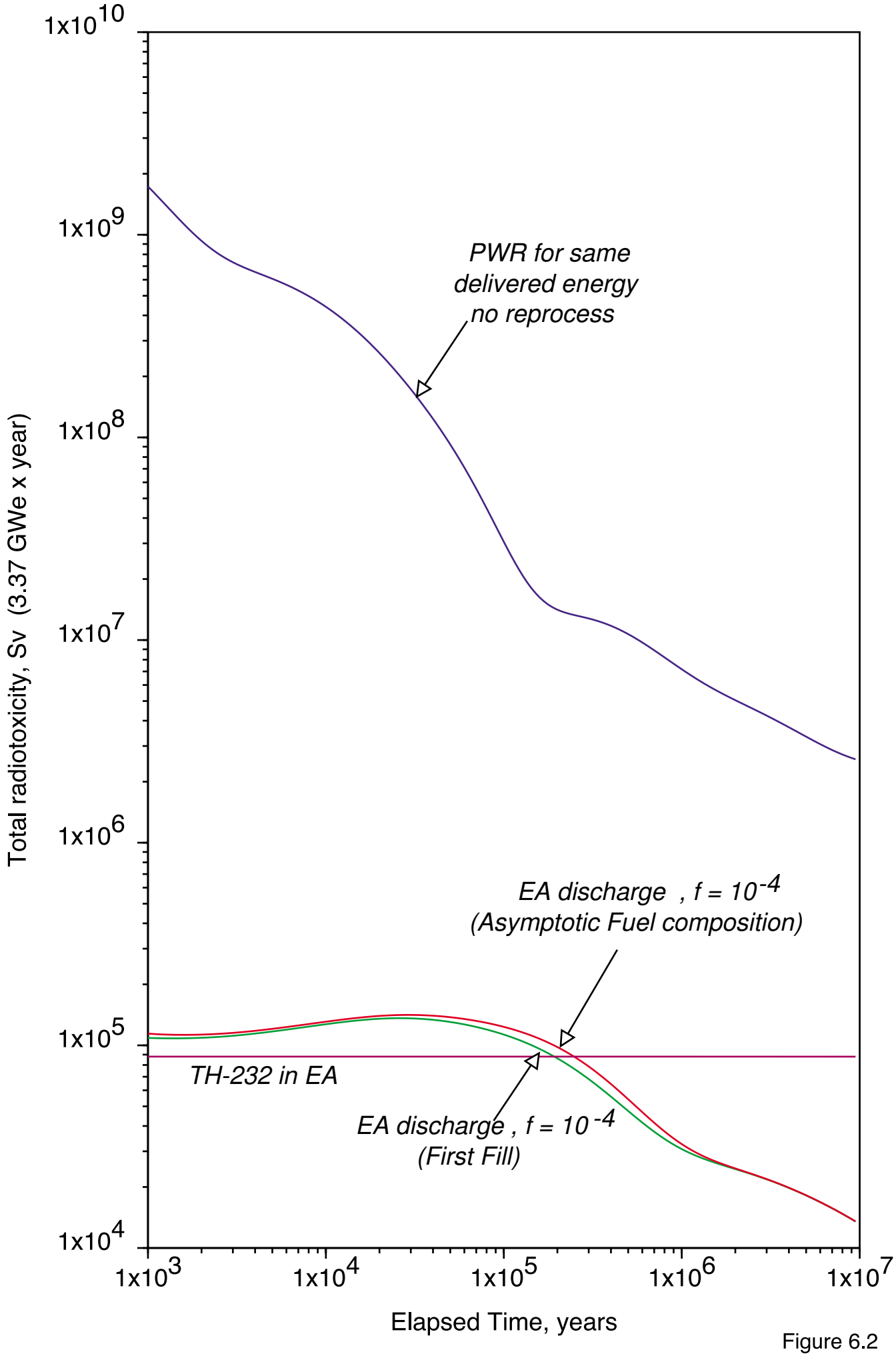
1x10^10
1x10^9
1x10^8
1x10^7
1x10^6
1x10^5
1x10^4
Total radiotoxicity, Sv (3.37 GWe x year)
PWR for same
delivered energy
no reprocess
EA discharge , f = 10^-4
(Asymptotic Fuel composition)
TH-232 in EA
EA discharge , f = 10^-4
(First Fill)
1x10^3
1x10^4
1x10^5
1x10^6
1x10^7
Elapsed Time, years

Figure 6.2

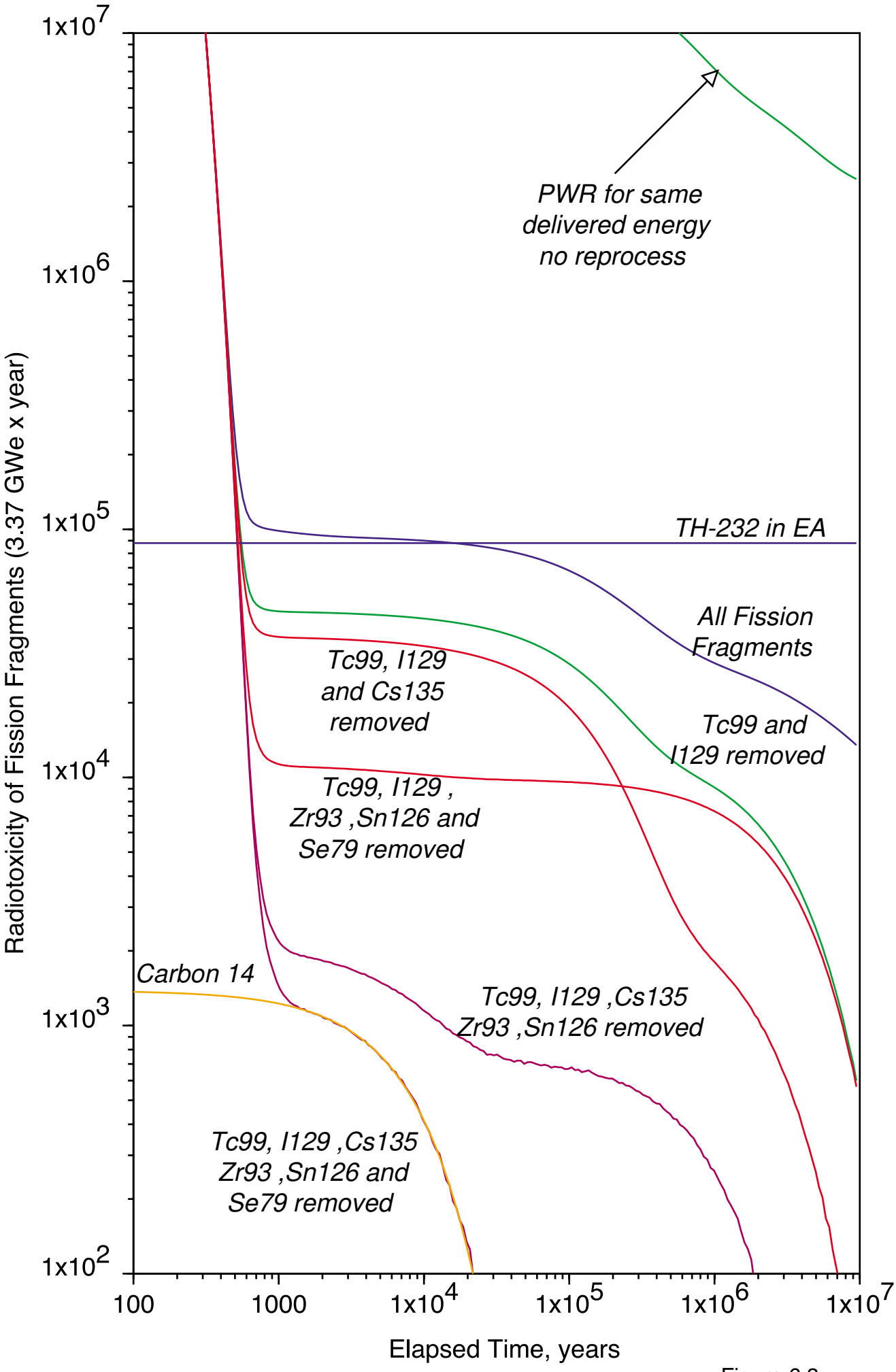
1x10^7
1x10^6
1x10^5
1x10^4
1x10^3
1x10^2
Radiotoxicity of Fission Fragments (3.37 GWe x year)
100
1000
1x10^4
1x10^5
1x10^6
1x10^7
Elapsed Time, years
PWR for same delivered energy no reprocess
TH-232 in EA
All Fission Fragments
Tc99, I129 and Cs135 removed
Tc99 and I129 removed
Tc99, I129 , Zr93 ,Sn126 and Se79 removed
Carbon 14
Tc99, I129 ,Cs135 Zr93 ,Sn126 removed
Tc99, I129 ,Cs135 Zr93 ,Sn126 and Se79 removed

Figure 6.3

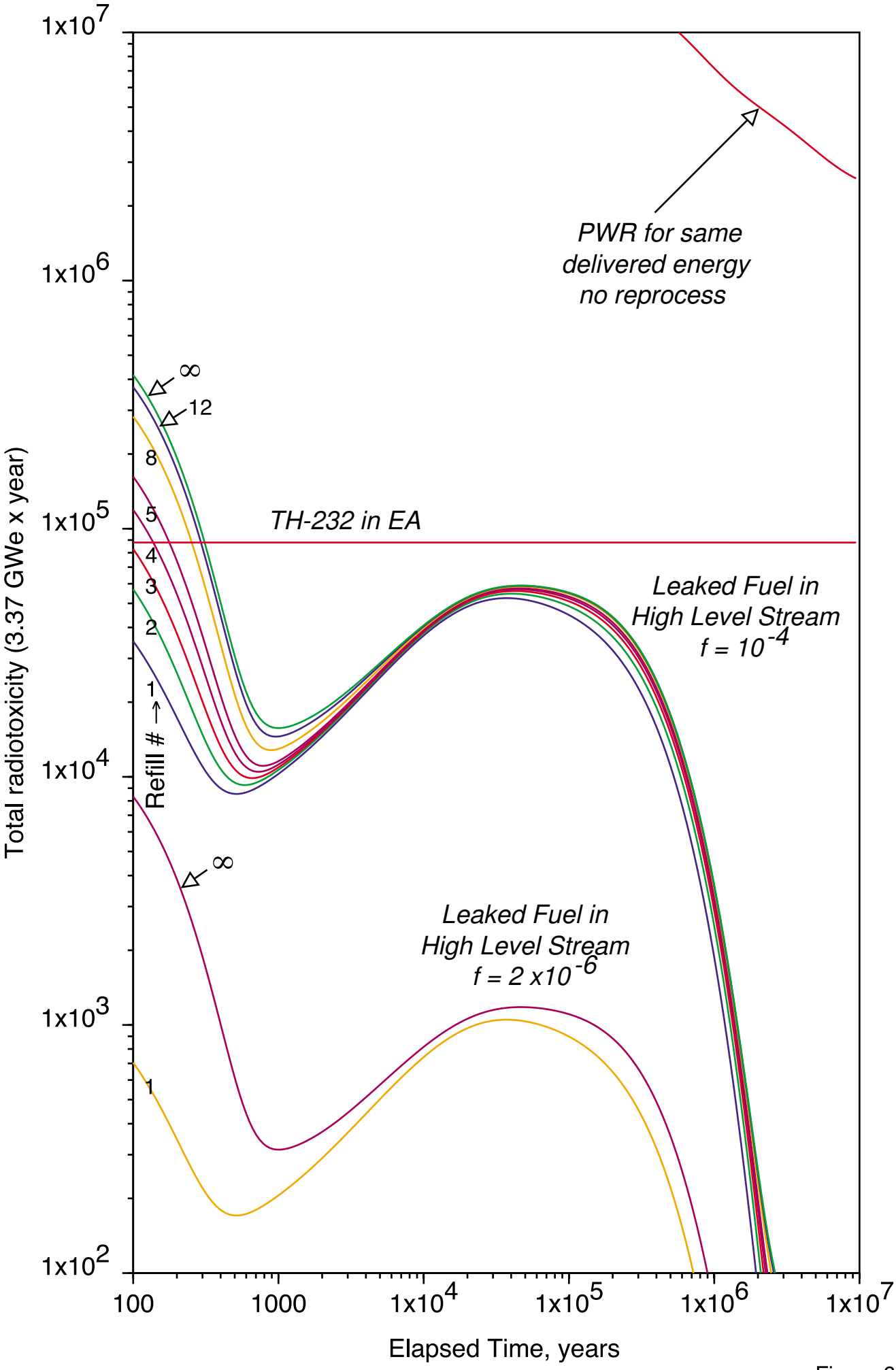
1x10^7
1x10^6
1x10^5
1x10^4
1x10^3
1x10^2
Total radiotoxicity (3.37 GWe x year)
100
1000
1x10^4
1x10^5
1x10^6
1x10^7
Elapsed Time, years
PWR for same
delivered energy
no reprocess
TH-232 in EA
Leaked Fuel in
High Level Stream
f = 10^-4
Leaked Fuel in
High Level Stream
f = 2 x10^-6
Refill # →
∞
12
8
5
4
3
2
1
∞
1

Figure 6.4

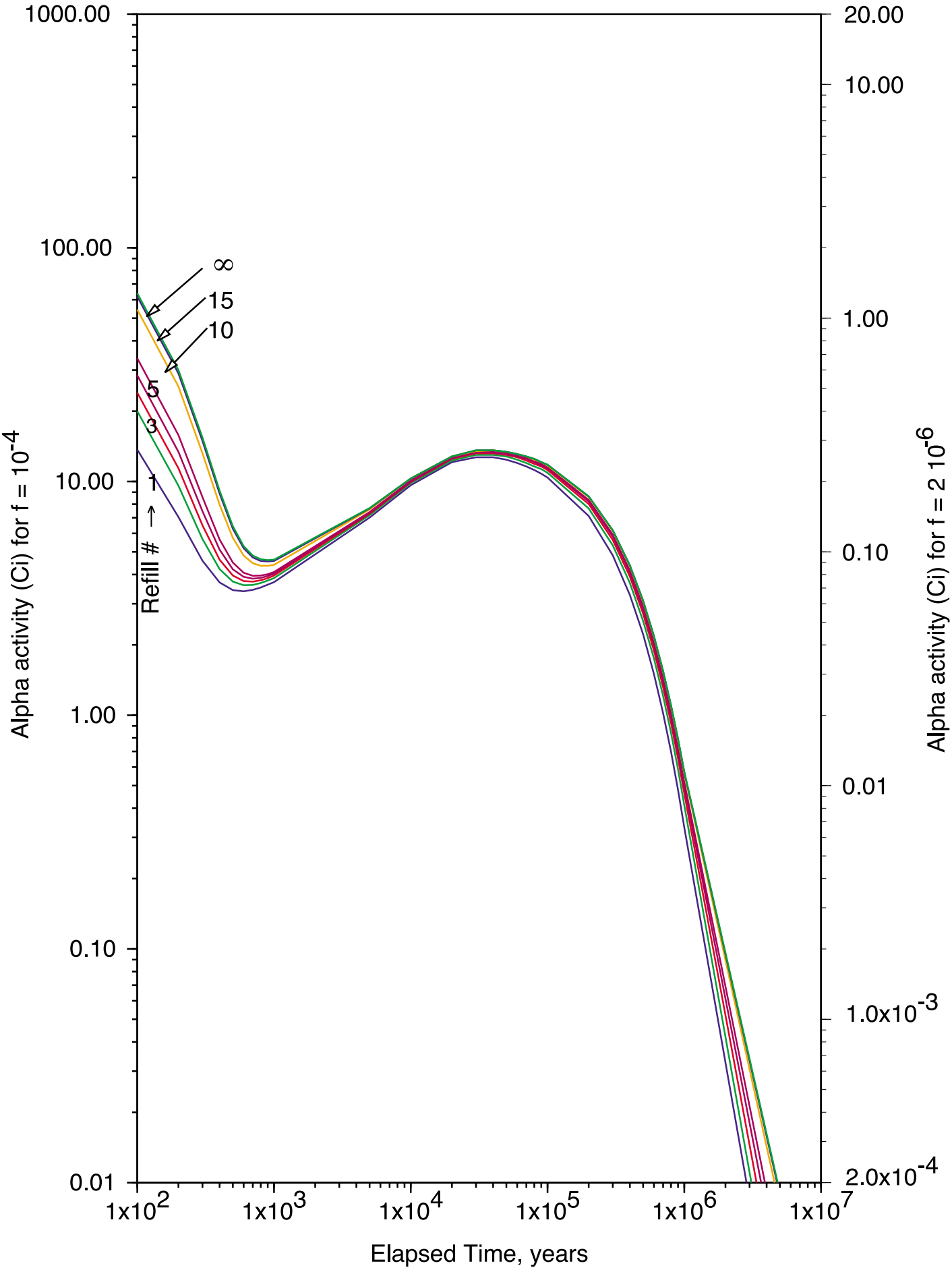
1000.00
100.00
10.00
1.00
0.10
0.01
20.00
10.00
1.00
0.10
0.01
1.0x10-3
2.0x10-4
Alpha activity (Ci) for f = 10-4
Alpha activity (Ci) for f = 2 10-6
Refill # →
1
3
5
10
15
∞
1x102
1x103
1x104
1x105
1x106
1x107
Elapsed Time, years

Figure 6.5

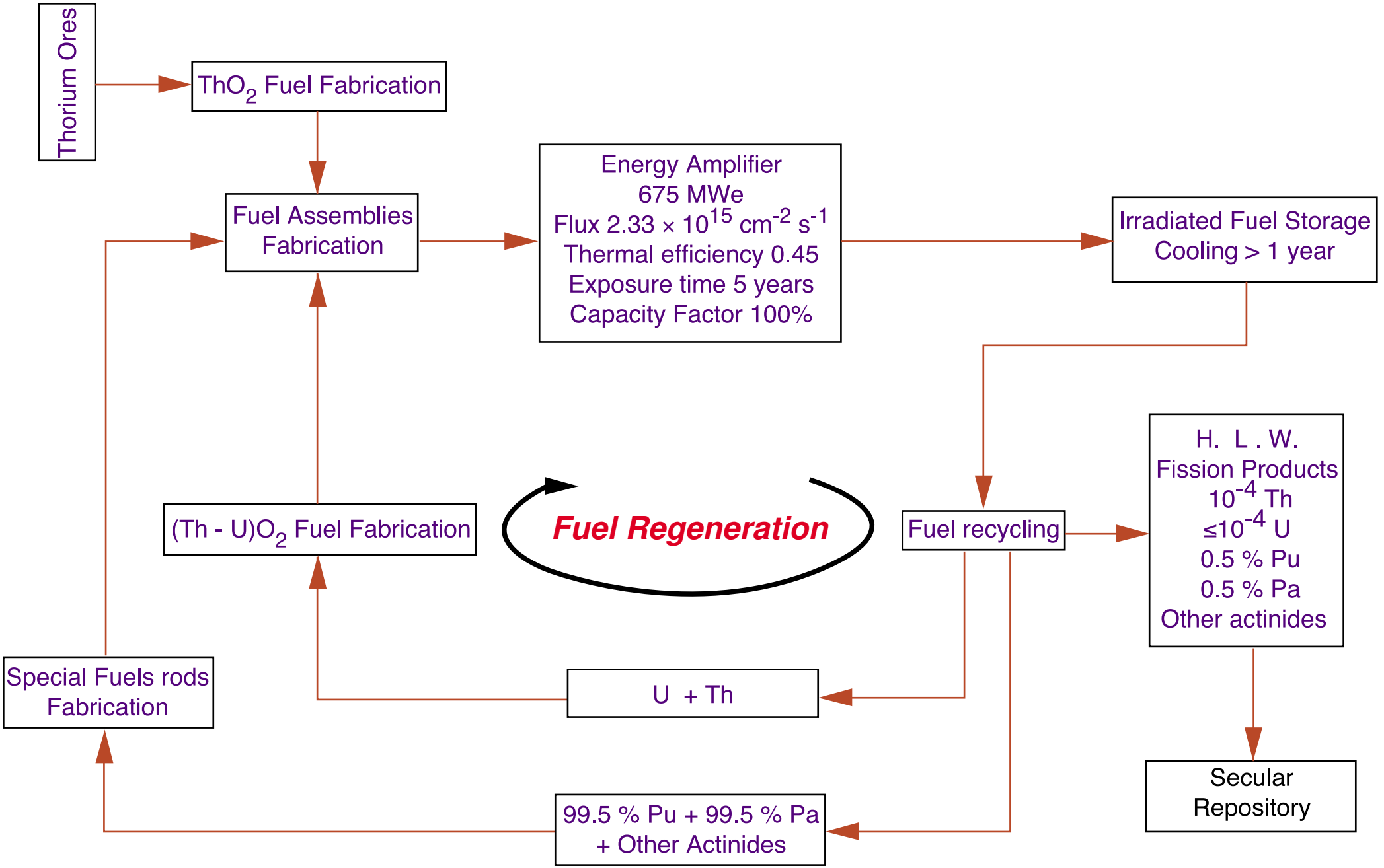
Thorium Ores
ThO_2 Fuel Fabrication
Fuel Assemblies Fabrication
Energy Amplifier
675 MWe
Flux 2.33×10^{15} cm^{-2} s^{-1}
Thermal efficiency 0.45
Exposure time 5 years
Capacity Factor 100%
Irradiated Fuel Storage
Cooling > 1 year
H. L . W.
Fission Products
10^{-4} Th
$\leq 10^{-4}$ U
0.5 % Pu
0.5 % Pa
Other actinides
Fuel recycling
Fuel Regeneration
$(Th - U)O_2$ Fuel Fabrication
Special Fuels rods Fabrication
U + Th
99.5 % Pu + 99.5 % Pa
+ Other Actinides
Secular Repository

Figure 6.6

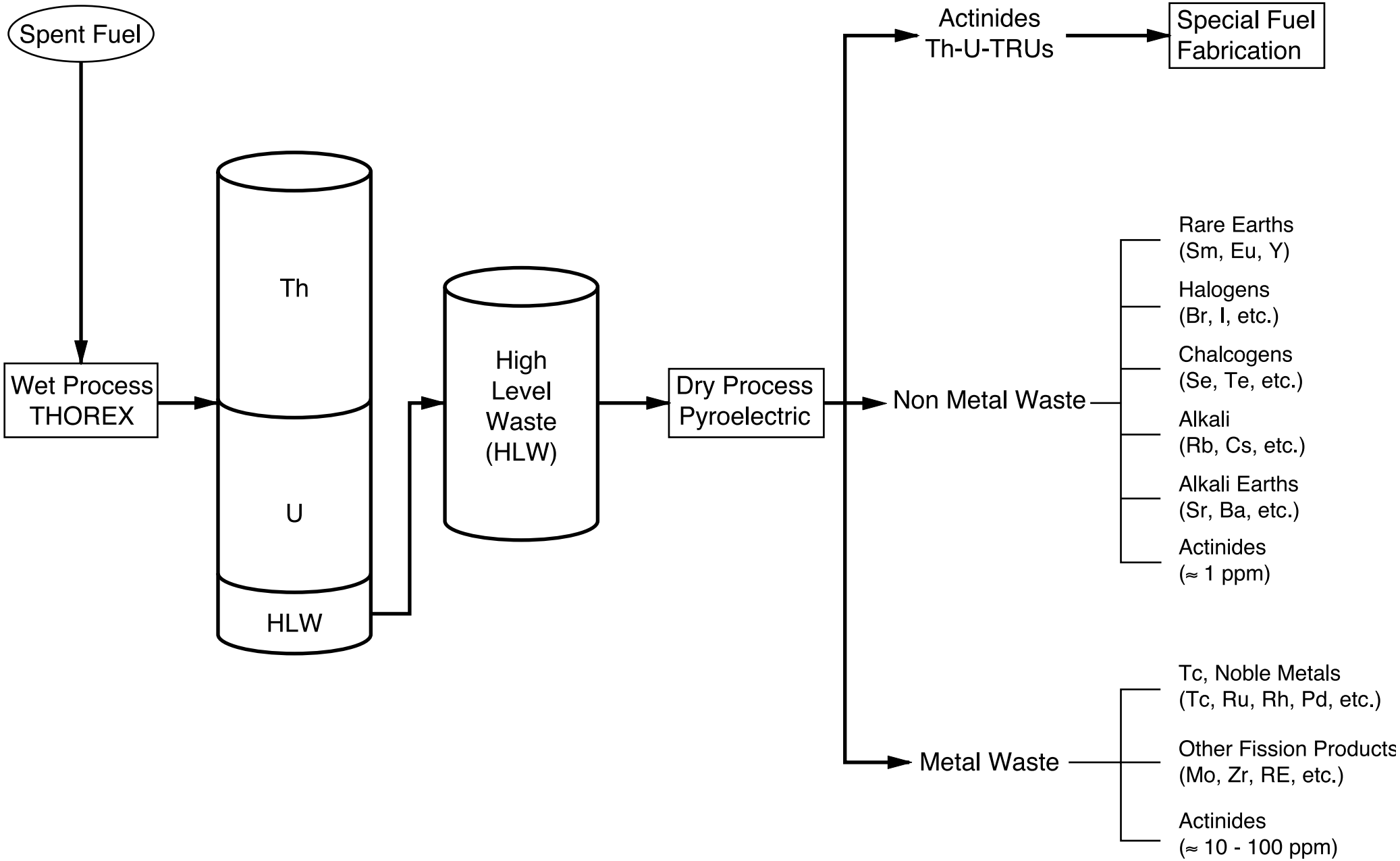
Spent Fuel
Wet Process
THOREX
Th
U
HLW
High
Level
Waste
(HLW)
Dry Process
Pyroelectric
Actinides
Th-U-TRUs
Special Fuel
Fabrication
Non Metal Waste
Rare Earths
(Sm, Eu, Y)
Halogens
(Br, I, etc.)
Chalcogens
(Se, Te, etc.)
Alkali
(Rb, Cs, etc.)
Alkali Earths
(Sr, Ba, etc.)
Actinides
(≈ 1 ppm)
Metal Waste
Tc, Noble Metals
(Tc, Ru, Rh, Pd, etc.)
Other Fission Products
(Mo, Zr, RE, etc.)
Actinides
(≈ 10 - 100 ppm)

Figure 6.7

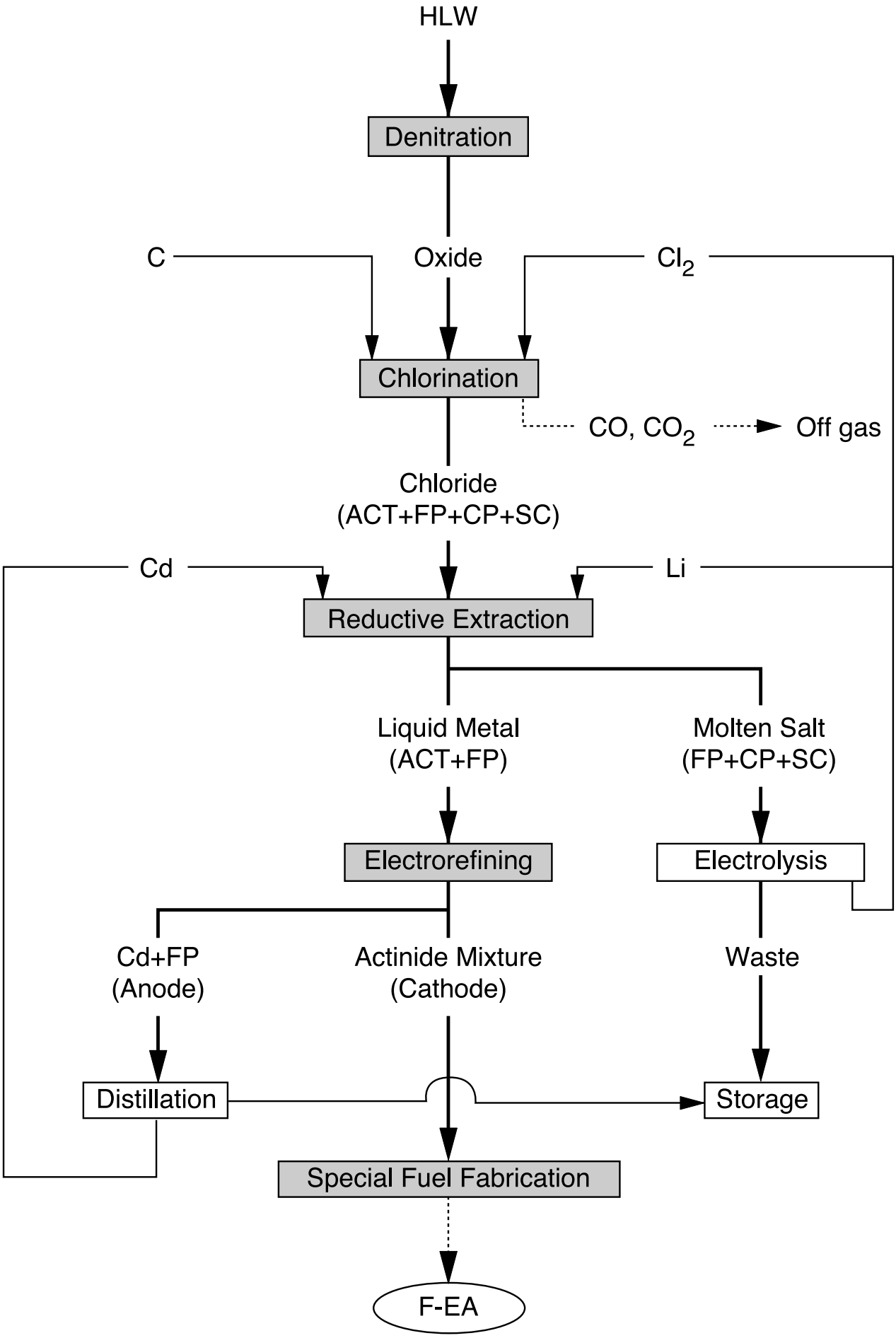
HLW
Denitration
C
Oxide
Cl_2
Chlorination
CO, CO_2
Off gas
Chloride
(ACT+FP+CP+SC)
Cd
Li
Reductive Extraction
Liquid Metal
(ACT+FP)
Molten Salt
(FP+CP+SC)
Electrorefining
Electrolysis
Cd+FP
(Anode)
Actinide Mixture
(Cathode)
Waste
Distillation
Storage
Special Fuel Fabrication
F-EA

Figure 6.8

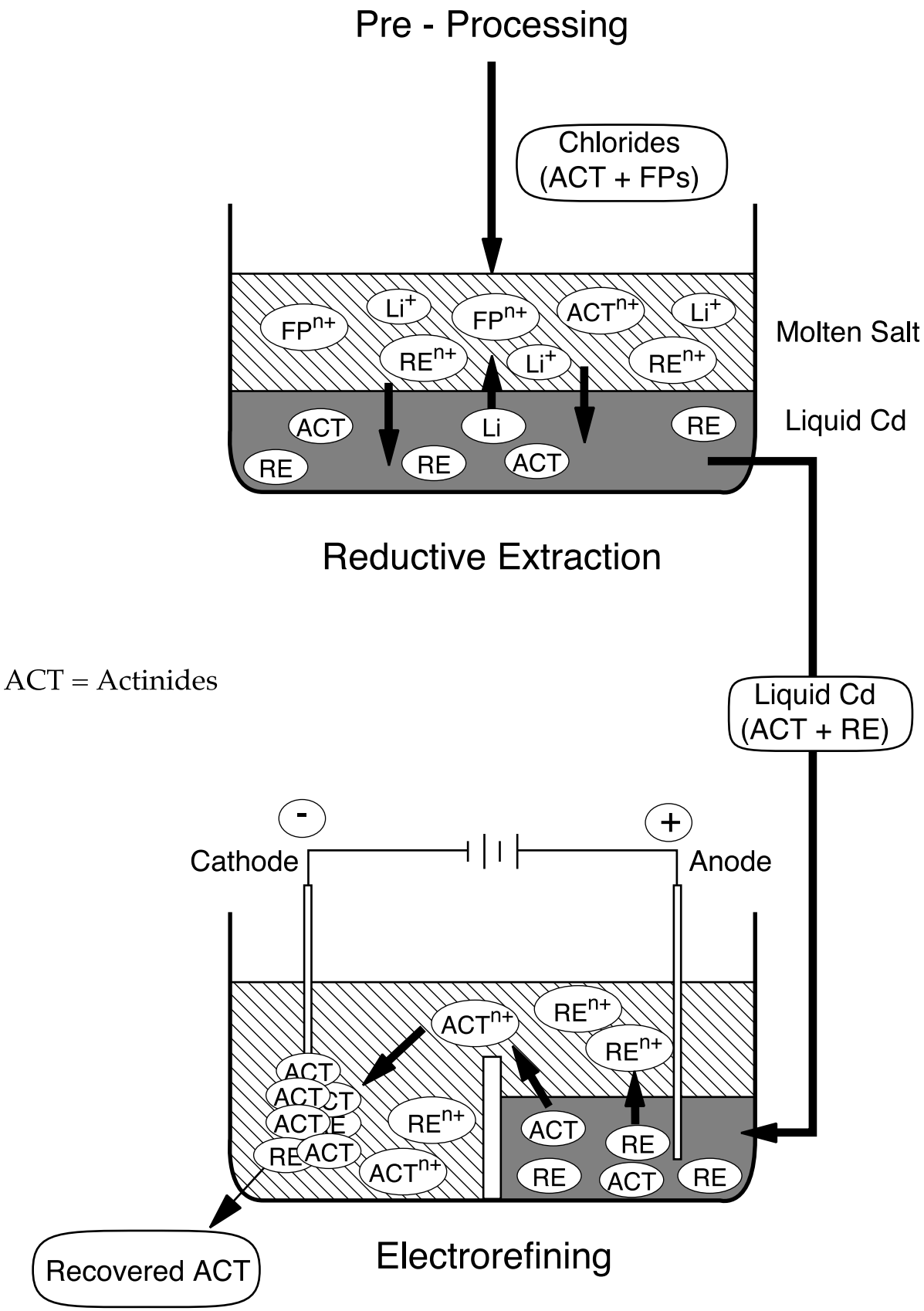
Pre - Processing
Chlorides
(ACT + FPs)
Molten Salt
Liquid Cd
Reductive Extraction
ACT = Actinides
Liquid Cd
(ACT + RE)
Cathode
Anode
Recovered ACT
Electrorefining

Figure 6.9

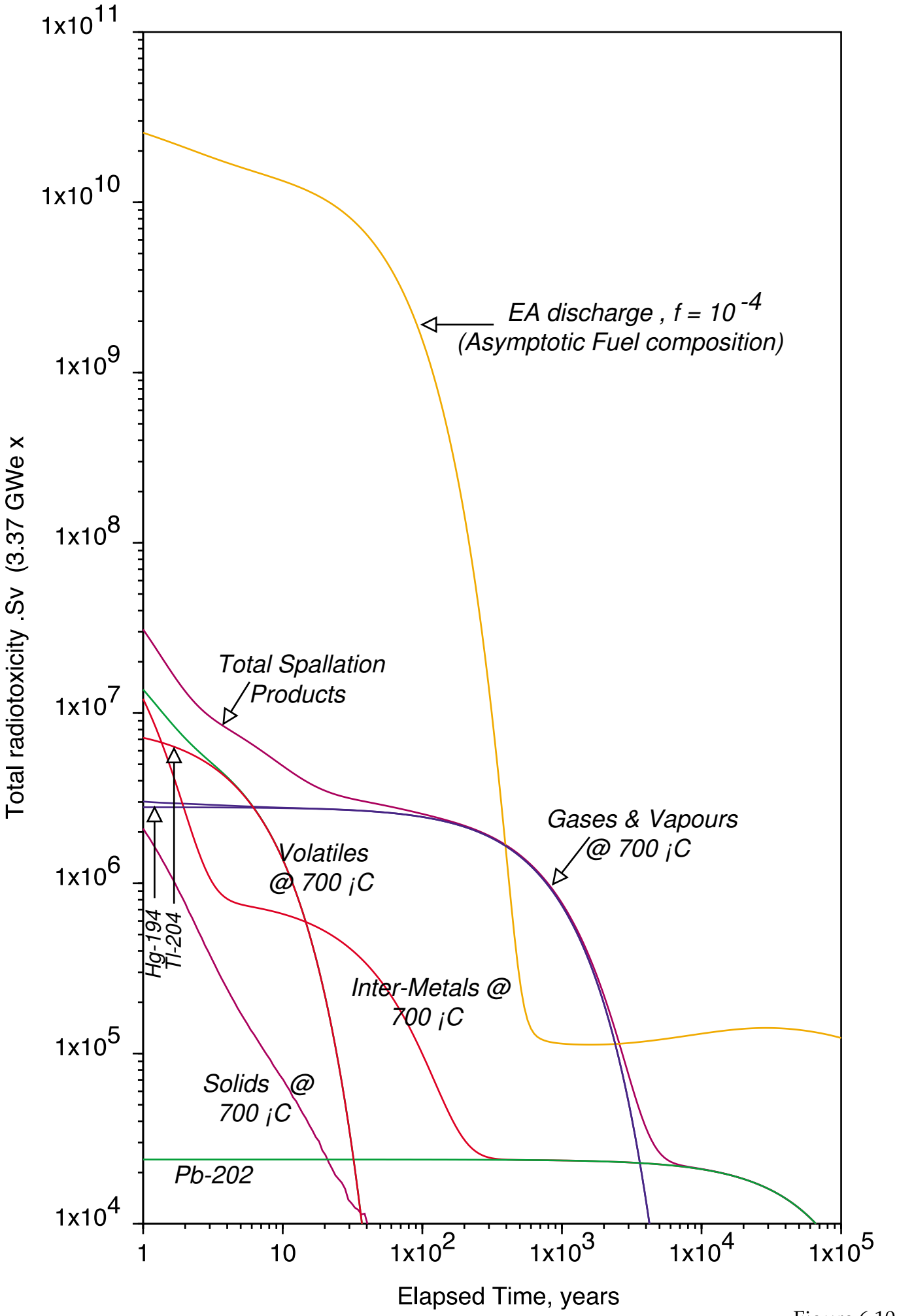
1x10^11
1x10^10
1x10^9
1x10^8
1x10^7
1x10^6
1x10^5
1x10^4
Total radiotoxicity .Sv (3.37 GWe x
EA discharge , f = 10^-4
(Asymptotic Fuel composition)
Total Spallation
Products
Gases & Vapours
@ 700 ¡C
Volatiles
@ 700 ¡C
Hg-194
Tl-204
Inter-Metals @
700 ¡C
Solids @
700 ¡C
Pb-202
1
10
1x10^2
1x10^3
1x10^4
1x10^5
Elapsed Time, years

Figure 6.10

Acknowledgements.

We would like to acknowledge the superb and dedicated work of **Susan Maio** and **F. Saldaña**, without whom this paper could not have become a reality. We would like to thank many of our CERN colleagues for frequent discussions of various aspects of the project and for their continuing and enthusiastic support. Stress analysis and hydrodynamic calculations have been performed with the help of **M. Battistin** and **A. Catinaccio**. **I. Goulas** has helped with programming. **M. Cobo**, **M. Embid** and **R. Fernandez** have diligently helped during their stay as summer students at CERN.

We have profited from (too) short, but illuminating visits of **E. Greenspan** (Univ. California at Berkeley), **V. Orlov** (RDIPE, Moscow), **H. Branover** (Ben Gurion University, Israel) and **K. Mileikowski**.

Many experts have helped us in different fields. We would like to thank in particular: **A. Ferrari** and **P. Sala** (University of Milan) for the code FLUKA; **J.P. Schapira** and **R. Meunier** (IN2P3) for their contributions to radio-toxicity and end-of-cycle aspects; **E. Gonzalez** and **A. Uriarte** (CIEMAT, Madrid); **R. Caro** and **A. Alonso** (Consejo de Seguridad Nuclear, Madrid); **M. Perlado**, **J. L. Sanz**, **E. Gallego** and **P.Trueba** (Universidad Politecnica, Madrid) and **A. Perez-Navarro** (Alfonso X El Sabio) for numerous and extended contributions pertinent to safety, radiation damage and end of cycle aspects; **H. Rief** (JRC, Ispra) for contributions to the question of reactivity insertions; **P. Gerontopoulos**, **J. Magill**, **M. Matzke**, **C. O'Carrol**, **K. Richter** and **J. Van Geel** (JRC Karlsruhe) for proliferation aspects; **D. Finon** and **Ph. Menanteau** (Institut d'Economie et de Politique de l'Energie, Grenoble), **M. Gigliarelli-Fiumi** (INFN, Frascati) and **M. A. Rodriguez-Borra** (SERCOBE, Madrid) for the economic and industrial aspects; **E. Sartori** (NEA), The International Dosimetry and Computation Group of NRPP (UK); **C. Dunford** and **S. Ganessan** (IAEA) and **G. Audi**, (CSNSM, Orsay), for their invaluable assistance in facilitating our access to relevant Data Banks.

The design of the accelerator has been made possible with the help of Laboratoire du Cyclotron, Centre Antoine Lacassagne. We thank its Director, **F. Demard**, and wish to acknowledge **J. M. Bergerot**, **A. Giusto**, **P. Montalant**, **J. F. Di Carlo**, **V. Rossin.** We had helpful discussions with **W. Joho**, **U. Schryber** and **P. Sigg** (PSI, Zurich) and **J. Pamela** (CEN, Cadarache). Last but not least, we would like to acknowledge the continuing support of the CERN Management (in particular of **H. Wenninger**), of the Sincrotrone Trieste (in particular **G. Viani**), and the DGXII of the European Commission, in particular its Director General, **P. Fasella** and **H.J. Allgeier**, **G. C. Caratti** and **W. Baltz**.

References.

[1] F. Carminati, C. Gelès, R. Klapisch, J.P. Revol, Ch. Roche, J.A Rubio and C. Rubbia, "An Energy Amplifier for Cleaner and Inexhaustible Nuclear Energy Production Driven by a Particle Beam Accelerator", CERN/AT/93-47 (ET) (1993).

[2] C. Rubbia et al., "A High Gain Energy Amplifier Operated with Fast Neutrons", Contribution to the Las Vegas Conference on Accelerator Driven Transmutation Technologies and Applications, 25-29 July 1994, to be published.

[3] S. Andriamonje et al., Physics Letters B 348 (1995) 697-709.

[4] C. Rubbia, "On the Feasibility of Fission Driven Hydrogen Production as Substitute for Natural Gas", CERN/AT/95-12 (ET) (1995).
I.T. Öztürk, A Hammache and E. Bilgen, Trans. IChemE, 241, 72A, (1994). and reference therein. The original process has been described in J.H. Norman et al. General Atomic Company Report, GA-A16713, 1982
S. Shimizu et al. "Iodine-Sulphur Process for Thermochemical Hydrogen Production", Proceedings of ICENES '93, H. Yashuda Editor, World Scientific, 1993

[5] S. Menard and J.P. Schapira, "Impact Radiologique à long terme de l'extraction du Thorium", IPNO-DRE 95-07, Orsay, France.

[6] S. Andriamonje et al., "Experimental Study of the Phenomology of Spallation Neutrons in a Large Lead Block", Proposal to the SPSLC, SPSLC/P291, May 1995.

[7] "Sources and Effects of Ionising Radiation", United Nations Scientific Committee on the Effects of Atomic Radiation, UNSCEAR 1993 Report to the General Assembly, with Scientific Annexes, New York, 1993.

[8] Th. Stammbach et al., "Potential of Cyclotron Based Accelerators for Energy Production and Transmutation", Contribution to the Las Vegas Conference on Accelerator Driven Transmutation Technologies and Applications, 25-29 July 1994, to be published.

[9] R.A. Jameson et al., "Accelerator-driven transmutation technology for energy-production and nuclear-waste treatment", 3rd EPAC, Berlin 1992, pp. 230-234.

[10] For a comprehensive description of these Projects, see for instance "Status of liquid metal fast reactor development", IAEA-TECDOC-791, March 1995.

[11] See for instance H. Alter, p. 2 in "Specialists' Meeting on Decay Heat removal and Natural Convection in LMFBRs", BNL (1985) and additional information in the same Proceedings.

[12] D. Geithoff, G. Mühling and K. Richter, "Performance of a Mixed Carbide Fuel Sub-Assembly in KNK II", in Proceedings of Global '93, 12-17 September, 1993, published by the American Nuclear Society, Inc., Vol. 2, p. 1173.

[13] L. Kuechler, L. Schäfer, B. Wojtech, "The Thorex Two-Stage Process for Re-Processing Thorium Reactor Fuel with High Burn-Up", Farbwerke Hoechst AG, Kerntechnik 13. No. 78, pp. 319-322 (1971).

[14] J.J. Laider et al, "Development of IFR Pyroprocessing Technology", in Proceedings of Global '93, 12-17 September, 1993, published by the American Nuclear Society, Inc., Vol. 2, p.1061 and also McPheeters et al, "Pyrochemical Methods for Actinide Recovery from LWR Spent Fuel", Vol. 2, p. 1094.

[15] C. Bowman et al., Nucl. Instr. Methods, A320, 336 (1992). More recent developments are to be found in the Proceedings of the International Conference on Accelerator-Driven Transmutation Technologies and Applications, Las Vegas, 25-29 July 1994.

[16] T. Takizuka et al., Specialist Meeting on Accelerator-driven Transmutation for Radwaste and other Applications (Stockholm, 24-28 June 1991).

[17] G. Van Tuyle et al., BNL Report 52279 (1991);
H. Takahashi, Fusion Technology 20 (1991) 657.
V.D. Kazaritsky et al., in Accelerators Applied to Nuclear Waste, 8th Journées Saturne, Report LNS/Ph/94-12.

[18] H. Takano et al, "A concept on self-completed fuel cycle based on Lead-cooled Nitride-fuel Fast Reactors", in Proceedings of ICENES-93, World Scientific.

[19] Proceedings of the First International Conference on Peaceful Uses of Atomic Energy (Geneva 1955) Vol 4.

[20] CRC Handbook of Chemistry and Physics, D.R. Lide Editor, CRC Press, 73rd Edition p. 4-29.

[21] F.H. Barthel and F.J. Dahlkamp, "Thorium Deposits and their Availability", IAEA TECDOC-650, Vienna, 1992, pp 104-115.

[22] K.S. Deffeyes and I.D. MacGregor, "World Uranium Resources", Scientific American, January 1980, pp. 50-66.

[23] J. Rouault et al., "Physics of Pu burning in Fast Reactors: Impact on Burner core design", Proc. ANS Topical Meeting on Advances in Reactor Physics, Knoxville, 11-15 April (1994).

[24] J. Sanz, J.M. Perlado, A.S. Perez and D. Guerra, J. of Nucl. Materials, 191-194, (1992), 1450.

[25] J. Perlado and J. Sanz, "Irradiation Effects and Activation in Structural Material", in "Nuclear Fusion by Inertial Confinement", edited by G. Verlarde, Y. Ronen and J.M. Martinez-Val, CRC Press (1993).

[26] J. Perlado, Private Communication.

[27] C. Rubbia, "An analytic approach to the Energy Amplifier", Internal Note CERN/AT/ET/Internal Note 94-036.
J.P. Revol, "Analytical Study of the Energy Amplifier Microscopic Physics", internal Note CERN/AT/ET/Internal Note 95-025.

[28] C. Rubbia, paper in preparation.

[29] S. Glasstone, Principles of Nuclear Reactor Engineering (D. Van Nostrand, New York, 1955).

[30] F. Carminati, "EET Code Collection User Guide", Internal Note, CERN/AT/ET/Internal Note 95-027, 16 March 1995.

[31] I. Goulas, J.P. Revol, "Further Update of Nuclear Data for the EET Group", Internal Note CERN/AT/ET/Internal Note 95-012, 26 April 1995 and "Corrections to the EET Nuclear Data Base", Internal Note CERN/AT/ET/Internal Note 95-026, 19 June 1995.

[32] F. Carminati, I. Goulas, Y. Kadi, "Proposal for transforming the evolution and MC program into a general purpose code", Internal Note CERN/AT/ET/Internal Note 95-020, 9 June 1995.

[33] H. Bateman, "The Solution of a System of Differential Equations Occurring in the Theory of Radioactive Transformations", Proc. Cambridge Phil. Soc. Vol. 15, p. 423, 1910.

[34] 1) MCNP: Judith F. Briesmeister, "MCNP™ - A General Montecarlo N-particle Transport Code", Los Alamos National Laboratory Report, LA-12625-M, November 1993.
2) TWODANT: R.E. Alcouffe, F.W. Brinkley Jr., D.R. Marr and R.D. O'Dell, "User's Guide for TWODANT: A Code Package for Two-Dimensional, Diffusion-Accelerated, Neutral-Particle Transport", Los Alamos National Laboratory Report, LA-10049-M, February 1990.

[35] J. Carson Mark, "Explosive Properties of Reactor-Grade Plutonium", Science & Global Security, 1993, Volume 4, pp. 111-128.

[36] J. Magill, C. O'Caroll, P. Gerontopoulos, K. Richter, J. Van Geel, "Advantages and Limitations of Thorium Fuelled Energy Amplifiers", Contribution to the Nuclear Society 5th Annual Conference on Nuclear Power and Industry, Obninsk, 7-11 November 1994.

[37] V. Orlov, Private Communication, November 1994.

[38] P. Bonnaure, P. Mandrillon, H. Rief, H. Takahashi, Actinide Transmutation by Spallation in the Light of Recent Cyclotron Development, ICENES 86, Madrid, July 1986.

[39] C. Rubbia, P. Mandrillon, N. Fiétier, "A High Intensity Accelerator for Driving the Energy Amplifier for Nuclear Energy Production", 4th EPAC, London 1994, pp. 270-272.

[40] Y. Jongen et al., "Extremely high intensity cyclotrons for radio-isotope production", Proc. of EPAC 1994, London.

[41] P. Mandrillon, "Injection into Cyclotrons", CERN Accelerator School, La Hulpe, Belgium, 2-6 May 1994

[42] "MAFIA, A Three-Dimensional Electromagnetic CAD System for Magnets, RF Structures and Transient Wake-Field Calculations", The MAFIA Collaboration, T. Weiland et al., Technische Hochschule Fachbereich 18, Fachgebiet Theorie Elecktromagnetischer Felder, 6100 Darmstadt, Germany.

[43] E. Branover, Private Communication.

[44] A.J. Romano, C.J. Klamut, D.H. Gurinsky, B.N.L. 811 (T 313), (1963).

[45] U.K. Bierman, B. Linch, W.M. Van de Wijgert, Patent No. 2516296, Neth., (1974).

[46] R.C. Asher, D. Davies, S.A. Beetham, Corrosion Science, 17, (1977), 545-557.

[47] F.R. Block, V. Schwich, Mater.Behav.Phys.Chem.Liq.Met.Syst., (1982), 253-264.

[48] H. Lengeler, "Proposal for Spallation Sources in Europe", EPAC '94, Proc. 4th European Particle Accelerator Conference, Vol. I, p. 249, 1994.

[49] *Shunk*, "Constitution of Binary Alloys", McGraw-Hill, 1969.

[50] A. Fassó et al, in "Intermediate Energy Nuclear Data: Models and Codes", Proceedings of a Specialists' Meeting, Issy les Moulineaux (France) 30 May-1-June 1994, p. 271, published by OECD, 1994, and references therein.
A. Fassó, A. Ferrari, J. Ranft, P.R. Sala, G.R. Stevenson and J.M. Zazula, Nuclear Instruments and Methods A, 332, 459 (1993), also, CERN Divisional Report CERN/TIS-RP/93-2/PP (1993).

[51] AA.VV., "STAR-CD Version 2.2 Manuals", Computational Dynamics.

[52] AA.VV., "ANSYS User's Manual, Version 5.0", Vol. I, II, III, IV, Swanson Analysis System, Inc. Huston.

[53] We would like to acknowledge the contribution from J.M. Perlado and J. Sanz. A part of their work is included in "Radiation Damage in Structural Materials", J.M. Perlado, J. Sanz, Instituto de Fusion Nuclear, Universidad Politecnica de Madrid (1995).

[54] S. Buono et al., "An Energy Amplifier System cooled by natural convection", Internal Note CERN/AT/ET/Internal Note 95-022, 21 August 1995.

[55] C.L. Wheeler, C.W. Stewart, R.J. Cena, D.S. Rowe and A.M. Sutey, "COBRA-IV-I: An Interim Version of COBRA for Thermal-Hydraulic Analysis of Rod Bundle Nuclear Fuel Elements and Cores", Battelle Pacific Northwest Laboratories Report, BNWL-1962, March 1976.

[56] H. Shibata et al., "On Problems to be solved for utilizing shock isolation system to NPP", Proc. SMIRT-10, Vol. E, Anaheim, August 1989.

[57] J.M. Kelly, "Aseismic Base Isolation: Review and Bibliography", Soil Dynamics and Earthquake Engineering, Vol. 5, No. 3, 1986.

[58] F.F. Tajirian, J.M. Kelly, I.D. Aiken, "Seismic Isolation for Advanced Nuclear Power Stations", to appear in Earthquake Spectra, Earthquake Engineering Research Institute (EERI), May 1990.

[59] F.F. Tajirian, M.R. Patel, "Response of Seismic Isolated Facilities: A Parametric Study of The ALMR", submitted to SMIRT 12, Stuttgart, Germany, August 1993.

[60] O. Gokcek et al., "Seismic Risk Reduction through Seismic Isolation", Proc. ANP '92, Tokyo, October 1992.

[61] J.M. Berkoe, "Modelling Passive Decay Heat Removal in Modular High Temperature Gas-cooled Reactor", Proceedings of the 5th FIDAP Users Conference, Chicago, Il, May 2-4, 1993.

[62] F. Carminati et al. "Analysis of 4th Week Data", Internal Note CERN/AT/ET/Internal Note 95-003, 17 January 1995.

[63] R. Chawla et al., "Fast Reactor Experiments with Thorium at the PROTEUS Facility, Paul Scherrer Institute Report, EIR-Bericht Nr. 444, November 1981.

[64] A.E. Waltar, and A.B. Reynolds, "Fast Breeder Reactors", Pergamon Press (1981).

[65] S. Glasstone, and A. Sesonske, in Nuclear Reactor Engineering: Reactor Design Basics. Vol. 1, Chapter 7, p. 242, Chapman & Hall, Fourth Edition (1994).

[66] T.A. Gabriel, J.D. Amburgy, and N.M. Greene, "Radiation Damage Calculations: Primary Knock-On Atom Spectra, Displacement Rates, and Gas Production Rates", Nucl. Sci. Eng. **61**, 21 (1976).

[67] D.G. Doran, "Neutron Displacement Cross Sections for Stainless Steel and Tantalum Based on a Lindhard Model", Nucl. Sci. Eng. **49**, 130 (1972).

[68] R.E. MacFarlane, D.W. Muir, and R.M. Boicourt, "The NJOY Nuclear Data Processing System, Volume I: User's Manual", Los Alamos National Laboratory Report, LA-9303-M (ENDF-324) (1982).

[69] M.T. Robinson, in Nuclear Fusion Reactors (British Nuclear Energy Society, London, 1970).

[70] J. Lindhard et al., Mat-Fys. Medd. **33** (1963).

[71] W.E. Fisher, "Target System Materials and Engineering Problems", in ICANS X, LA-UR-89-2920 (1988).

[72] J.M. Perlado et al., "Radiation Damage and Activation in the HT-9 Structure of ICF Reactors Using INPORT Protection", Ninth Topical Meeting on the Technology of Fusion Energy, Oak Brook (USA), October 1990. Fusion Technology, Vol. 19, 3, Part. 2A, 709 (1991).

[73] M. Cobo, M. Embid, R. Fernández, J. Gálvez, C. Rubbia, J. A. Rubio, “Study of the maximum cladding temperature reached in the Energy Amplifier”, Internal Note, CERN AT/EET 95-023, 21 August 1995.

[74] Samuel Glasstone & Alexander Sesonske, Nuclear Reactor Engineering. Reactor Design Basics. Vol. I, Chapter 5, p. 238-321 Chapman & Hall, Fourth Edition.

[75] H. Rief & H. Takahashi. "Safety and Control of Accelerator-Driven Subcritical Systems".

[76] Federico Goded & Vicente Serradell, Teoria de Reactores y Elementos de Ingenieria Nuclear. Tomo I. Publicaciones Cientificas de la Junta de Energia Nuclear. Tercera Edicion, 1975.

[77] Reactor Physics Constants, Argonne National Laboratory, United States Atomic Energy Commission, 1963.

[78] C. Rubbia, paper in preparation

[79] R. Meunier, "Faisabilité et Evaluation Exploratoires d'un Projet pour la Séparation Isotopique du Cesium Issu de la Fission", CSNSM, IN2P3-CNRS, Orsay, October 1994.

[80] A. Uriarte, "The Energy Amplifier, Considerations about the back-end of the Fuel Cycle", CIEMAT ITN/TR-05/II-95 and ITN/TR-13/II-95, 1995 (and references therein).

[81] J.T. Long, "Engineering for Nuclear Fuel Reprocessing", Gordon and Breach Science Publishers, 1967 (and references therein).

[82] J.P. Ackerman and T.R. Johnson, "New High-Level Waste Management Technology for the IFR Pyroprocessing Wastes", in Proceedings of Global '93, published by the American Nuclear Society, Inc., Vol. 2, p. 969.

[83] T. Hijikata et al., "Development of Pyrometallurgical Partitioning of Actinides from High-Level Radioactive Waste", in Proceedings of Global '93, published by the American Nuclear Society, Inc., Vol. 2, p. 1074.

[84] A. van Dalen et al., "Sea Disposal of Radioactive Krypton", European Applied and Research Reports, Nuclear Science and Technology Section, Vol. 4, 111-190, 1982.